ORNL/NUREG-19

PWR Blowdown Heat Transfer Separate-Effects Program Data Evaluation Report—System Response for Thermal-Hydraulic Test Facility Test Series 100

R. A. Hedrick
W. G. Craddick
K. G. Turnage
C. R. Hyman

Prepared for the U.S. Nuclear Regulatory Commission
Office of Nuclear Regulatory Research
Under Interagency Agreements ERDA 40-551-75 and 40-552-75

ORNL/NUREG-19
Dist. Category NRC-2

Contract No. W-7405-eng-26

Engineering Technology Division

PWR BLOWDOWN HEAT TRANSFER SEPARATE-EFFECTS PROGRAM DATA EVALUATION REPORT — SYSTEM RESPONSE FOR THERMAL-HYDRAULIC TEST FACILITY TEST SERIES 100

R. A. Hedrick
W. G. Craddick C. R. Hyman K. G. Turnage

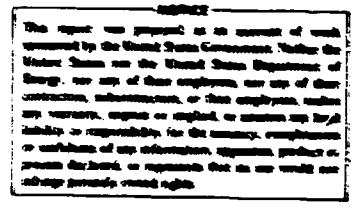

Manuscript Completed — October 21, 1977
Date Published — November 1977

Prepared for the
U.S. Nuclear Regulatory Commission
Office of Nuclear Regulatory Research
Under Interagency Agreements ERDA 40-551-75 and 40-552-75

Prepared by the
OAK RIDGE NATIONAL LABORATORY
Oak Ridge, Tennessee 37830
operated by
UNION CARBIDE CORPORATION
for the
DEPARTMENT OF ENERGY

BLANK PAGE

CONTENTS

LIST OF FIGURES

LIST OF TABLES

ACKNOWLEDGMENTS

The execution of a large experimental and analytical program always requires aid from a great many individuals whose contributions should be recognized. The dedicated efforts of the entire BDHT program staff are reflected in this report. The authors express their appreciation to the following personnel:

M. C. Adair
W. E. Baucum
R. E. Bohanan
V. D. Clemons
S. B. Cliff
C. E. Davis
E. D. Drennen
B. G. Eads
G. G. Fee
D. J. Fraysier
R. M. Flanders
C. A. Gifford
R. H. Greene
R. C. Hagar
R. E. Helms
P. A. Jallouk
A. F. Johnson
D. M. Leon
P. A. Moore
L. J. Ott
H. R. Payne
W. Ragan, Jr.
N. R. Raulston
J. L. Redford
M. J. Roberts
L. I. Schlemper
J. D. Sheppard
A. N. Smith
R. D. Stulting
R. E. Textor
D. G. Thomas
M. L. Walker
J. D. White
L. K. White
M. D. White
J. E. Wolfe

BLANK PAGE

PWR BLOWDOWN HEAT TRANSFER SEPARATE-EFFECTS PROGRAM DATA EVALUATION REPORT — SYSTEM RESPONSE FOR THERMAL-HYDRAULIC TEST FACILITY TEST SERIES 100

R. A. Hedrick
W. G. Craddick C. R. Hyman K. G. Turnage

ABSTRACT

Selected reduced instrument responses and analyses of the indicated phenomena are presented for Thermal-Hydraulic Test Facility (THTF) test series 100, which is part of the PWR Blowdown Heat Transfer Separate-Effects Program. The objective of the program is to investigate the thermal-hydraulic phenomena that govern the energy transfer and transport processes occurring during a postulated loss-of-coolant accident in a pressurized-water reactor system.

Comparisons are made between the trends indicated by the reduced instrument responses and the thermal-hydraulic transient simulator RELAP4/MOD5 (update 2) to aid in understanding the phenomenological sequences. The results of verification studies of RELAP's performance in prediction of the THTF data are presented.

1. INTRODUCTION

The ORNL Pressurized-Water Reactor (PWR) Blowdown Heat Transfer (BDHT) Program[1] is a separate-effects study of the relationships between the principal variables that can alter the rate of blowdown, the presence of flow reversals, time delay to critical heat flux (CHF), the rate at which dryout progresses, and similar time- and space-related functions that are important in loss-of-coolant accident (LOCA) analysis. Primary test results are obtained from the Thermal-Hydraulic Test Facility (THTF), a large nonnuclear pressurized-water loop incorporating a 49-rod electrically heated bundle in 7 × 7 geometry.

Test series 100, the first test series conducted in the THTF with bundle 1 in place,[2-7] was conducted from April 23 to August 19, 1976 (Table I.1). It was composed of six tests designed to provide baseline information on (1) the response of the test facility to full-scale operation and transient conditions, (2) the thermal-hydraulic parameters

Table 1.1. ORNL BDHT Separate-Effects Program test matrix – first 49-rod bundle

Variable	Test No.					
	100[a]	101	102	104	103	105
Rod power, kW/rod	0	30.5	122	122	122	122
Unpowered rods	0	0	0	0	0	0
Coolant mass flow rate						
kg m^{-2} hr^{-1} × 10^{-6}	12.7	12.3	12.1	12.3	12.3	12.2
lb_m hr^{-1} ft^{-2} × 10^{-6}	2.60	2.51	2.48	2.51	2.51	2.50
Break location (and area ratio where applicable)	In (0.5A) Out (0.5A)	Out	In (0.5A) Out (0.5A)	In (0.5A) Out (0.5A)	In (0.4A) Out (0.6A)	In (0.4A) Out (0.6A)
Nominal break size,[b] %	200	100	200	200	200	200
Time heater rod power on after blowdown initiation, sec		0	0	2	2	2 + power decay[c]
Coolant inlet temp.						
K	560	558	558	560	558	558
°F	549	545	545	548	545	545
Coolant outlet temp.						
K	559	573	608	607	607	607
°F	547	571	633	632	632	632
System pressure						
MPa	15.6	15.5	15.7	15.6	15.8	15.5
psig	2263	2245	2271	2263	2284	2253
Pump condition during blowdown	Off	Off	Off	Off	Off	Off
Sheath thermocouple upper set point						
Steady state		T_{max} + 50°F or 28 K →				
Transient		T_{max} + 50°F or 28 K		1350°F 1005 K	1350°F 1005 K	1450°F 1061 K
Schedule	4/23/76	5/27/76	6/18/76	7/8/76	8/4/76	8/19/76

[a] Isothermal test.

[b] A 200% break has a total break area A of 12.5 cm^2 (0.0135 ft^2).

[c] Heater rod power decayed with a 0.45-sec time constant for a total of six time constants.

necessary to provide input to the digital simulators, and (3) the sequence of events occurring during a blowdown in the THTF.

This report deals with thermal-hydraulic phenomena occurring in the THTF as a whole; the test section heat transfer will be analyzed in detail in a later report.[8] All RELAP calculations made for this report utilized the load module form of RELAP4/MOD5 (update 2).[9] For brevity, they will be referred to simply as RELAP calculations or predictions.

Experiments 100 through 105 are described and comparisons of predictions and measured data presented. It should be noted that attainment of the best possible agreement between all calculated and measured quantities was not the only goal. In some cases, closer agreement between predicted and experimental data could have been achieved by altering input parameters to compensate for inaccuracies inherent in the code. When RELAP is used before the modeled event has occurred, however, the user has no way of anticipating what compensation is needed. The RELAP modeling options used represent our best judgment of correct modeling techniques. The "minimum controls" option was specified, allowing complete freedom in choosing among available RELAP code options. (The overall performance of RELAP in loop hydraulics will be evaluated in a later section of this report.) The RELAP system model of the THTF (Fig. I.1), listed in Appendix A, was used in the analysis described in the sections on each test.[10] Other RELAP models will be described in the code verification section (Chap. VIII) and in Appendices B and C. For all cases, a trip was used to stop the calculations when the pressure in the pressurizer fell below 1.38 MN/m^2 (200 psia).

In any code verification study, the accuracy of experimental data being compared to calculations should be considered carefully. Temperature and absolute pressure measurements in the THTF closely approximate the actual phenomena as evidenced by concurrence of several instruments during blowdowns. Extensive calibrations of these instruments, which have small quoted errors in precision (Table I.2), were conducted. The output signals from pressure difference transducers (such as PdE-199, PdE-200, and PdE-30) have had excessive "ringing." Difficulties inherent in the measurement of two-phase mass flow rates, volumetric flow rates, and densities are well documented.[11,12] However, some special problems have been encountered with the THTF data for these tests. For example, uncertainties in the

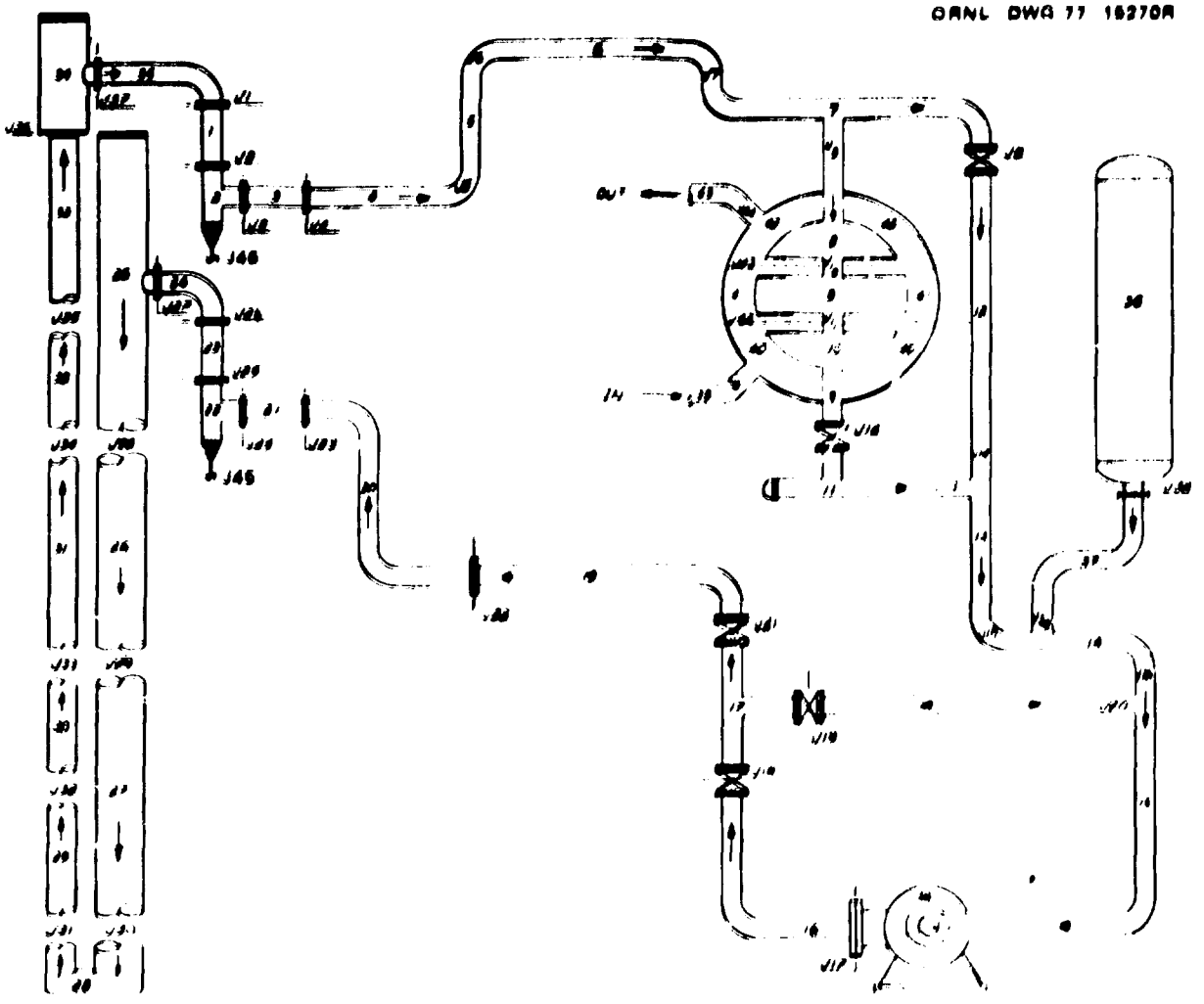

Fig. I.1. RELAP system model for THTF.

Table I.2. Precision of experimental measurements in the THTF for test series 100

System	Standard deviation
Pressure measurement	
Computer-Controlled Data Acquisition System (CCDAS)	0.185 MN/m^2 (26.8 psig)
Analog tape system	0.197 MN/m^2 (28.5 psig)
Pressure difference measurement	
CCDAS	
6.89-MN/m^2 (1000-psid) span	0.025 MN/m^2 (3.6 psid)
1.38-MN/m^2 (200-psid) span	0.005 MN/m^2 (0.72 psid)
0.34-MN/m^2 (50-psid) span	0.001 MN/m^2 (0.18 psid)
Analog tape system	
6.89-MN/m^2 (1000-psid) span	0.033 MN/m^2 (4.8 psid)
1.38-MN/m^2 (200-psid) span	0.007 MN/m^2 (0.95 psid)
0.34-MN/m^2 (50-psid) span	0.002 MN/m^2 (0.24 psid)
Temperature measurement	2.4 K (4.3°F)
Electric core power measurement	
Rod current	0.877 A
Rod voltage	0.304 V
Momentum flux measurement	
CCDAS	6793 $kg/m\text{-}sec^2$ (4565 $lb_m/ft\text{-}sec^2$)
Analog tape system	7661 $kg/m\text{-}sec^2$ (5148 $lb_m/ft\text{-}sec^2$)
Density measurement at 961 kg/m^3 (60 lb_m/ft^3)	12.9 kg/m^3 (0.81 lb_m/ft^3)

calibration of THTF turbine meters resulted in possible errors of over 0.00631 m^3/sec (100 gpm) at some locations for some tests (Table 1.3). Also, the inlet vertical turbine (FE-166) and the outlet horizontal turbine (FE-34) sometimes reversed polarity during tests 103, 104, and 105 when their signals were apparently affected by changes in the rod bundle power and/or vibrations.

Because of the inertia of turbine meter rotors used in the THTF and the delay in frequency-to-voltage conversion in the THTF flow monitors, output signals tend to lag the actual phenomena in the fast flow transients. Available knowledge about the dynamics of the rotors and the monitor electronics is being used to recover as much useful information as possible from the turbine meter signals. Two plots of turbine meter data which were processed using current reduction techniques will be presented in the RELAP data comparison section for test 105.

Calculated mass flow plots presented in this report[13] include both a homogeneous mass flow and a mass flow calculated by the Aya method.[14] The homogeneous mass flow is calculated from densitometer and turbine meter readings assuming no slip. This assumption is often inadequate in two-phase flow. The Aya method incorporates slip through the use of drag disk readings. Extensive efforts have been made to calibrate the THTF drag disks, but their effective range is quite large and thus during periods of low flow, the signal being measured is of the same order of magnitude as the uncertainty in the reading.

Errors in the single-beam densitometer readings may sometimes be due to the occurrence of stratified flow or other flow regimes where the average density along the beam is not representative of the average density in the spool piece.

In the THTF test section, the heater rods have a steel sheath separating the sheath thermocouples from the surface and thus their temperatures are not directly comparable to RELAP's predicted surface temperatures. A computer program entitled ORINC was written to calculate the transient surface temperatures and the surface heat fluxes so that such comparisons could be made.[15] ORINC uses data from calibration experiments and from the sheath thermocouples and power input monitors for the actual

Table I.3. Precision of flow measurements in the THTF for test series 100

Measurement system	Forward	Reverse
	All tests except test 101	
FE-19	+0.0009 m^3/sec (+13.97 gpm) −0.0002 m^3/sec (−2.90 gpm)	+0.0011 m^3/sec (+16.77 gpm) −0.0004 m^3/sec (−5.70 gpm)
FE-166	+0.0012 m^3/sec (+18.74 gpm) −0.0005 m^3/sec (−7.68 gpm)	+0.0010 m^3/sec (+16.15 gpm) −0.0003 m^3/sec (−5.09 gpm)
FE-216	+0.0048 m^3/sec (+75.59 gpm) −0.0041 m^3/sec (−64.52 gpm)	+0.0020 m^3/sec (+31.79 gpm) −0.0013 m^3/sec (−20.72 gpm)
FE-34	+0.0021 m^3/sec (+33.39 gpm) −0.0007 m^3/sec (−11.26 gpm)	+0.0124 m^3/sec (+197.11 gpm) −0.0110 m^3/sec (−174.97 gpm)
	Test 101	
FE-19	+0.0018 m^3/sec (+28.59 gpm) −0.0004 m^3/sec (−6.45 gpm)	+0.0022 m^3/sec (34.15 gpm) −0.0008 m^3/sec (−12.02 gpm)
FE-166	+0.0051 m^3/sec (+81.55 gpm) −0.0037 m^3/sec (−59.41 gpm)	+0.0034 m^3/sec (+53.43 gpm) −0.0020 m^3/sec (−31.29 gpm)
FE-216	+0.0101 m^3/sec (+159.35 gpm) −0.0087 m^3/sec (−137.21 gpm)	+0.0040 m^3/sec (63.35 gpm) −0.0026 m^3/sec (−41.21 gpm)
FE-34	+0.0021 m^3/sec (+33.39 gpm) −0.0007 m^3/sec (−11.26 gpm)	+0.0124 m^3/sec (+197.11 gpm) −0.0110 m^3/sec (−174.97 gpm)

blowdown. Azimuthal variations in the heat flux are not currently taken into account.

The purpose of this report is to provide analysis of the data obtained from this test series and to present comparisons of the reduced instrument responses and desired calculated quantities with those parameters predicted by the thermal-hydraulic transient simulator RELAP4/MOD5 (update 2). In areas where significant discrepancies were found between calculated and measured hydraulic quantities, efforts have been made to locate the sources of the errors. This report contains complete sections on each test and conclusions for the test series. Figures I.2 through I.5 show the test facility spatial positions and instrument locations referred to in each section.

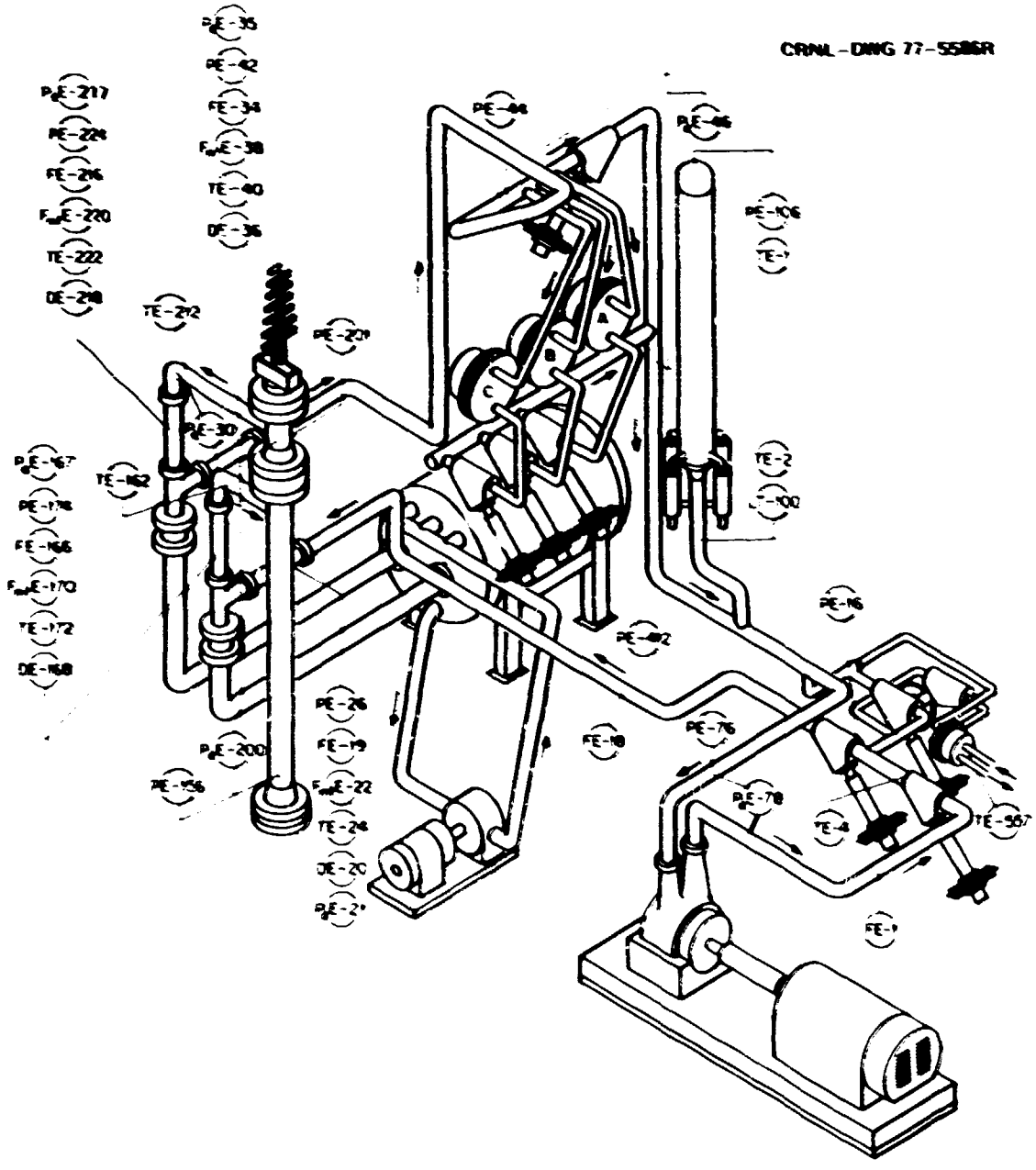

Fig. I.2. Thermal-Hydraulic Test Facility (THTF).

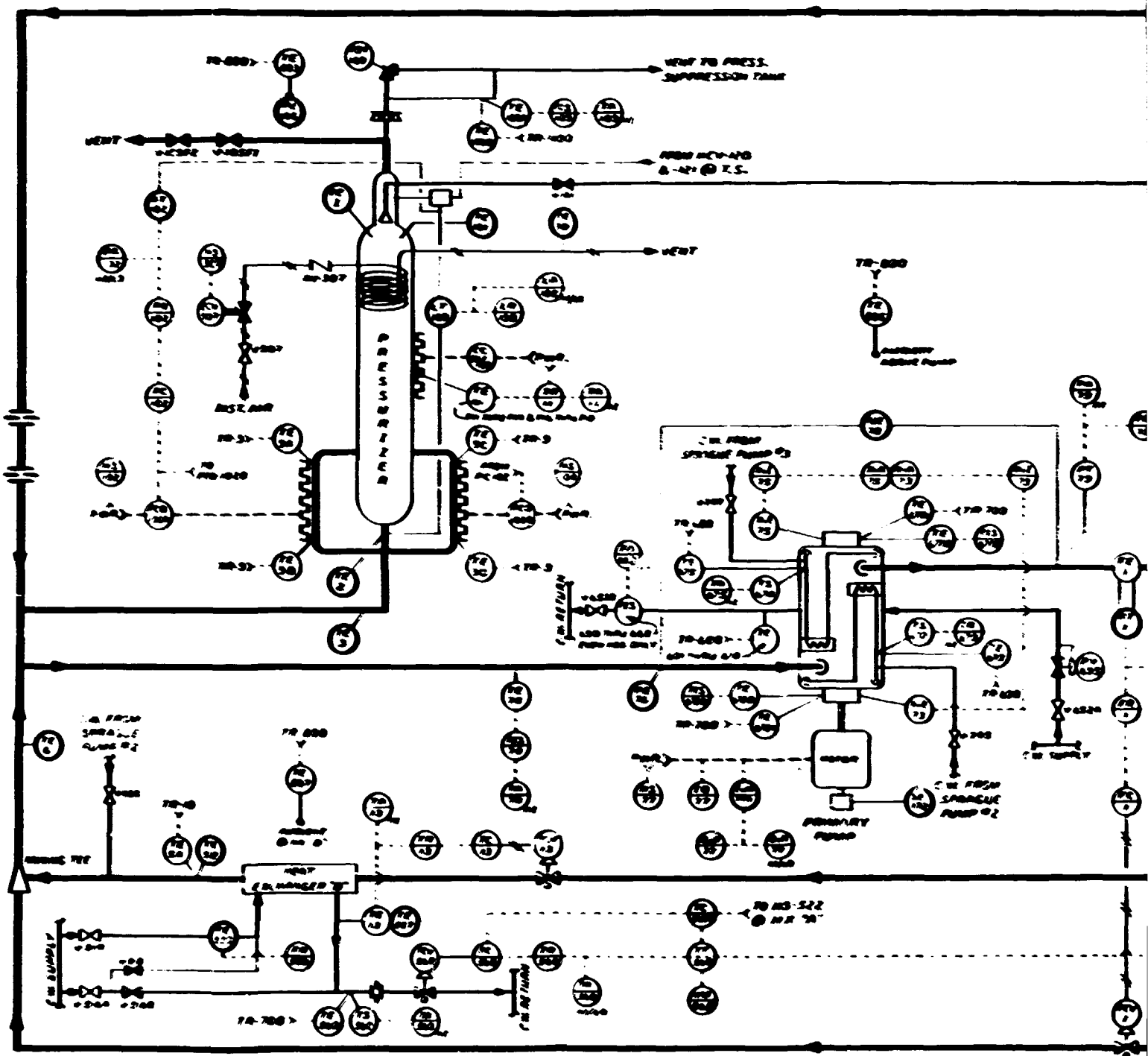

Fig. I.3. THTF instrumentation diagram.

BLANK PAGE

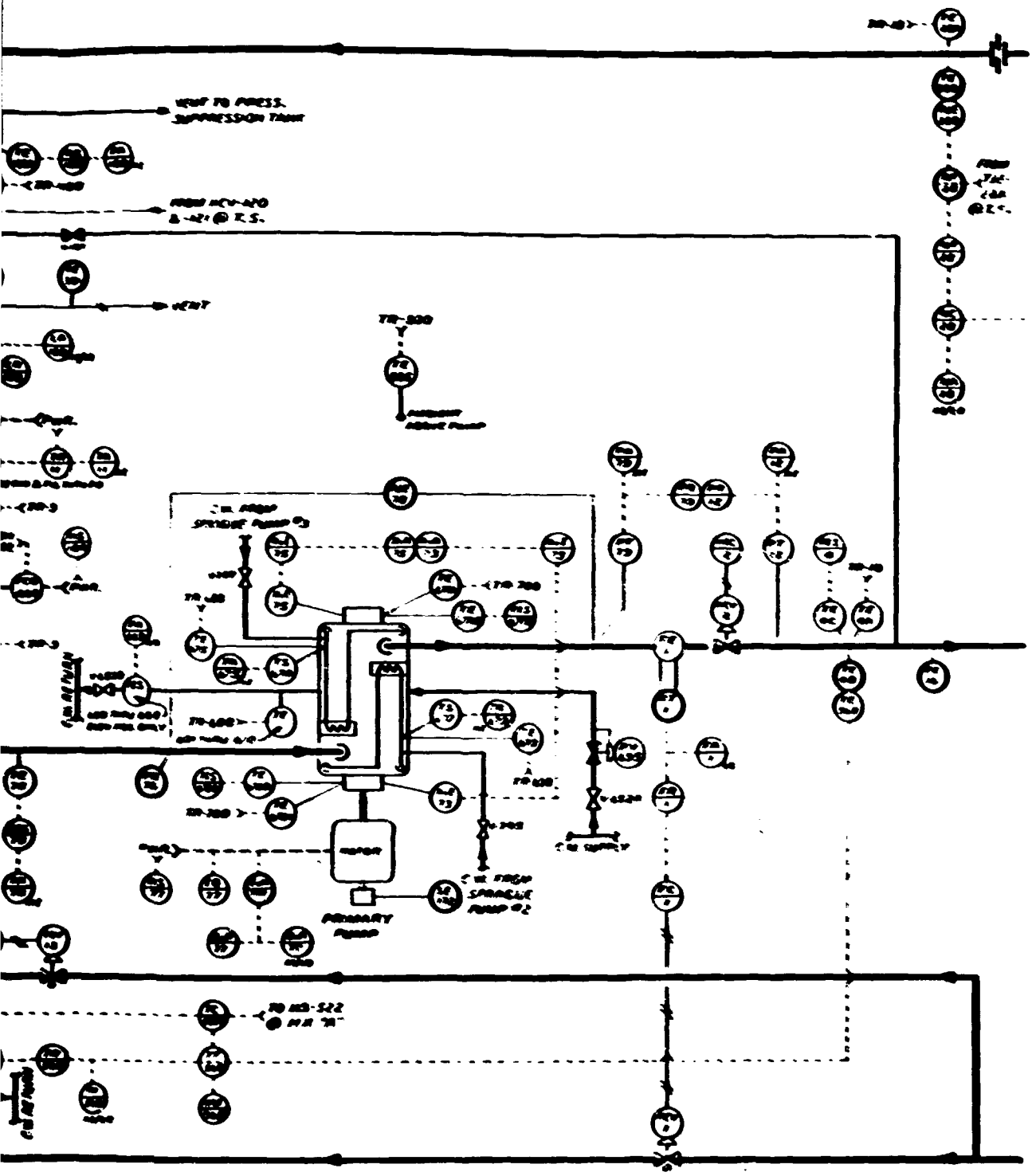

Fig. I.3. THTF instrumentation diagram.

BLANK PAGE

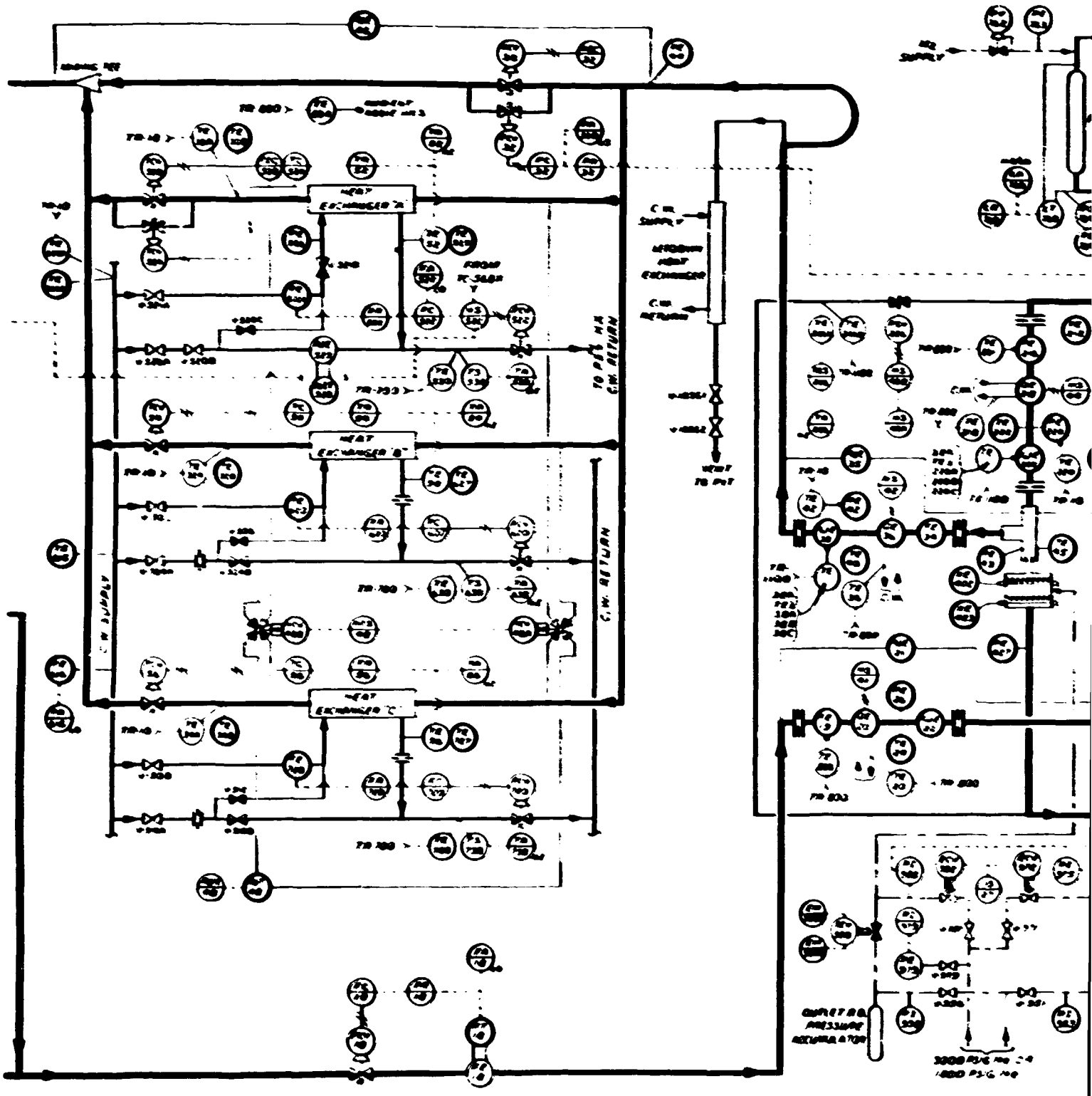
HEAT EXCHANGER A
HEAT EXCHANGER B
HEAT EXCHANGER C
C.W. SUPPLY
C.W. RETURN
TO PLANT C.W. RETURN

Fig

BLANK PAGE

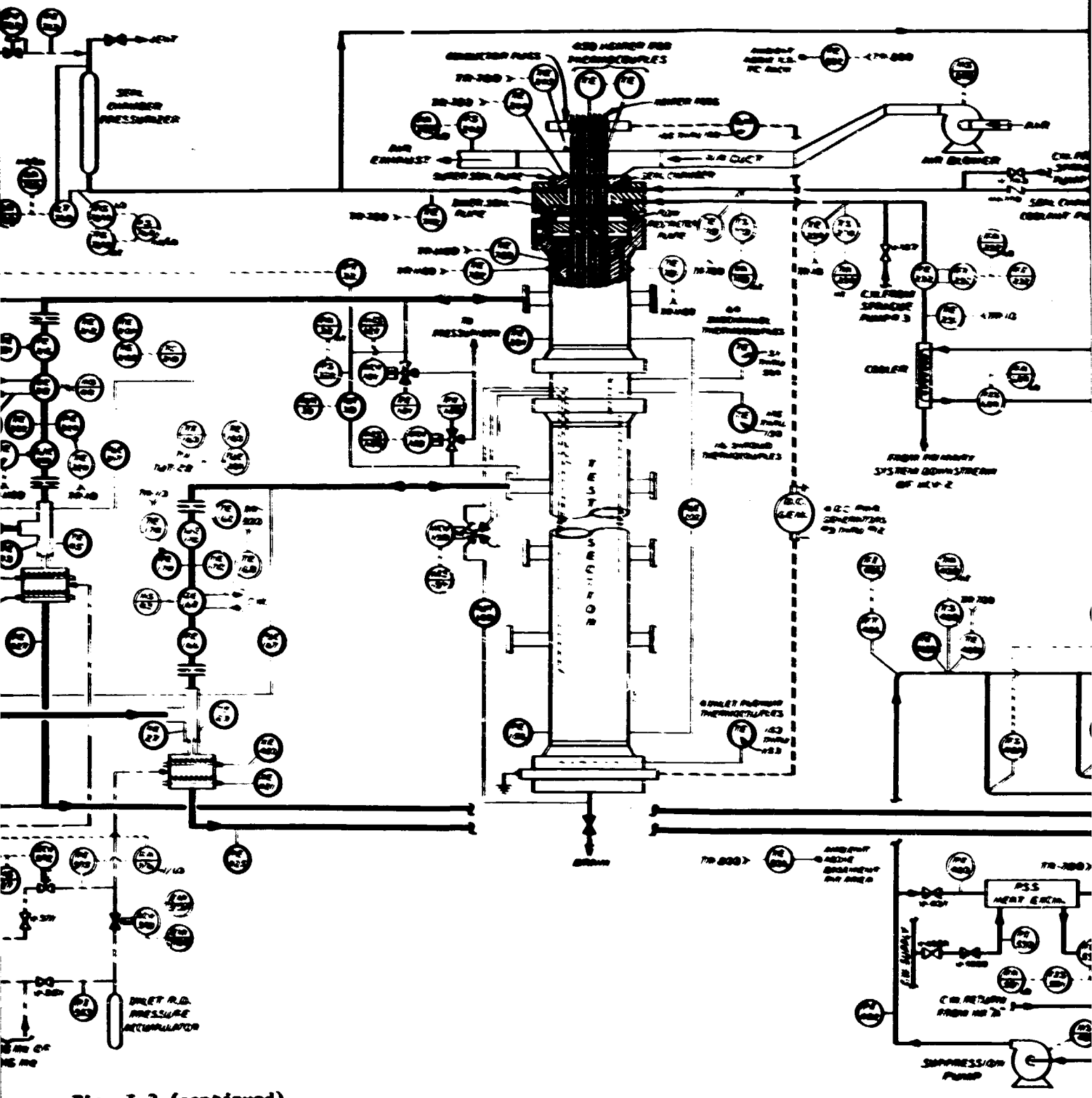

Fig. I.3 (continued)

BLANK PAGE

ORNL DWG 77 12968

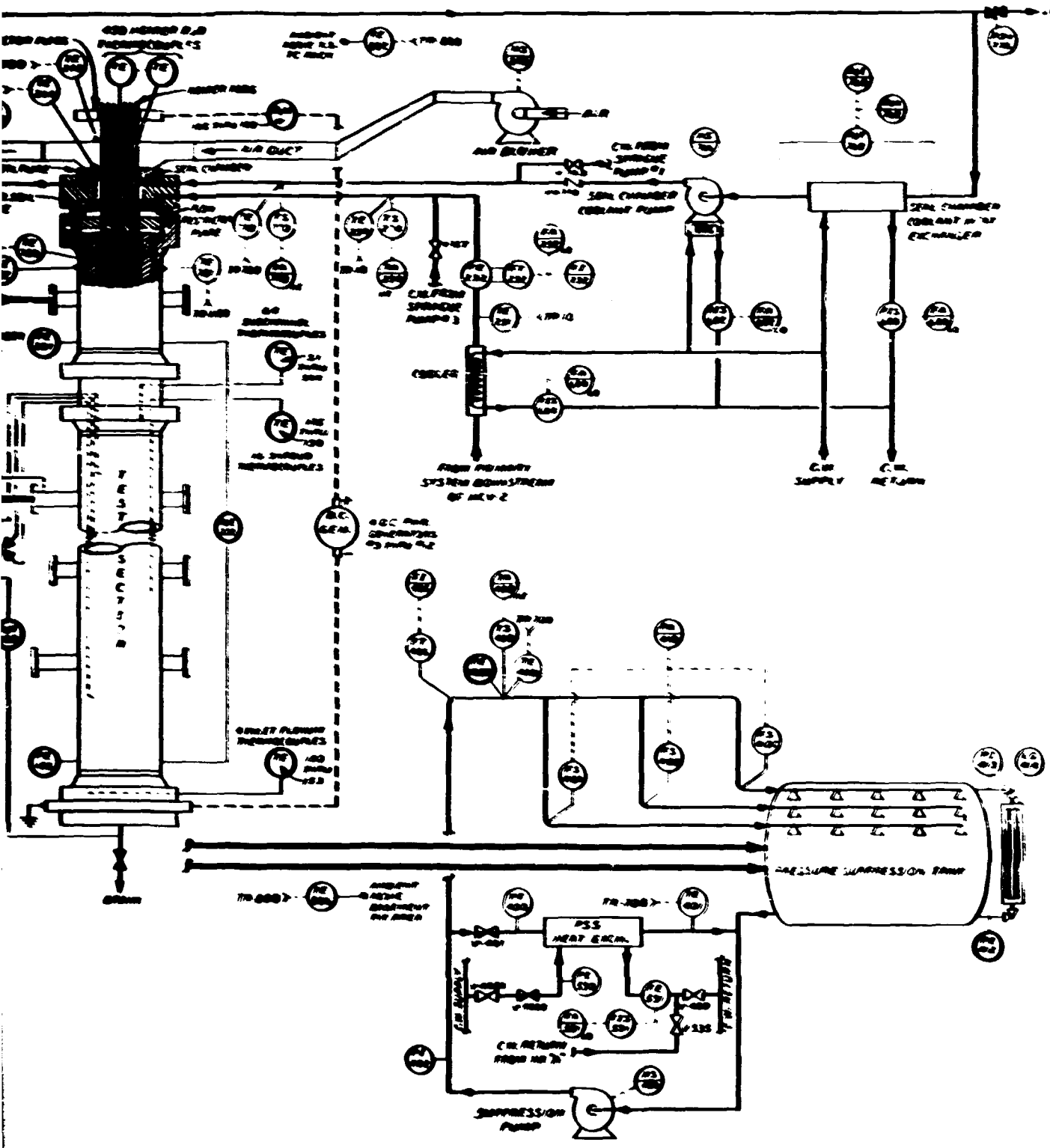

3

BLANK PAGE

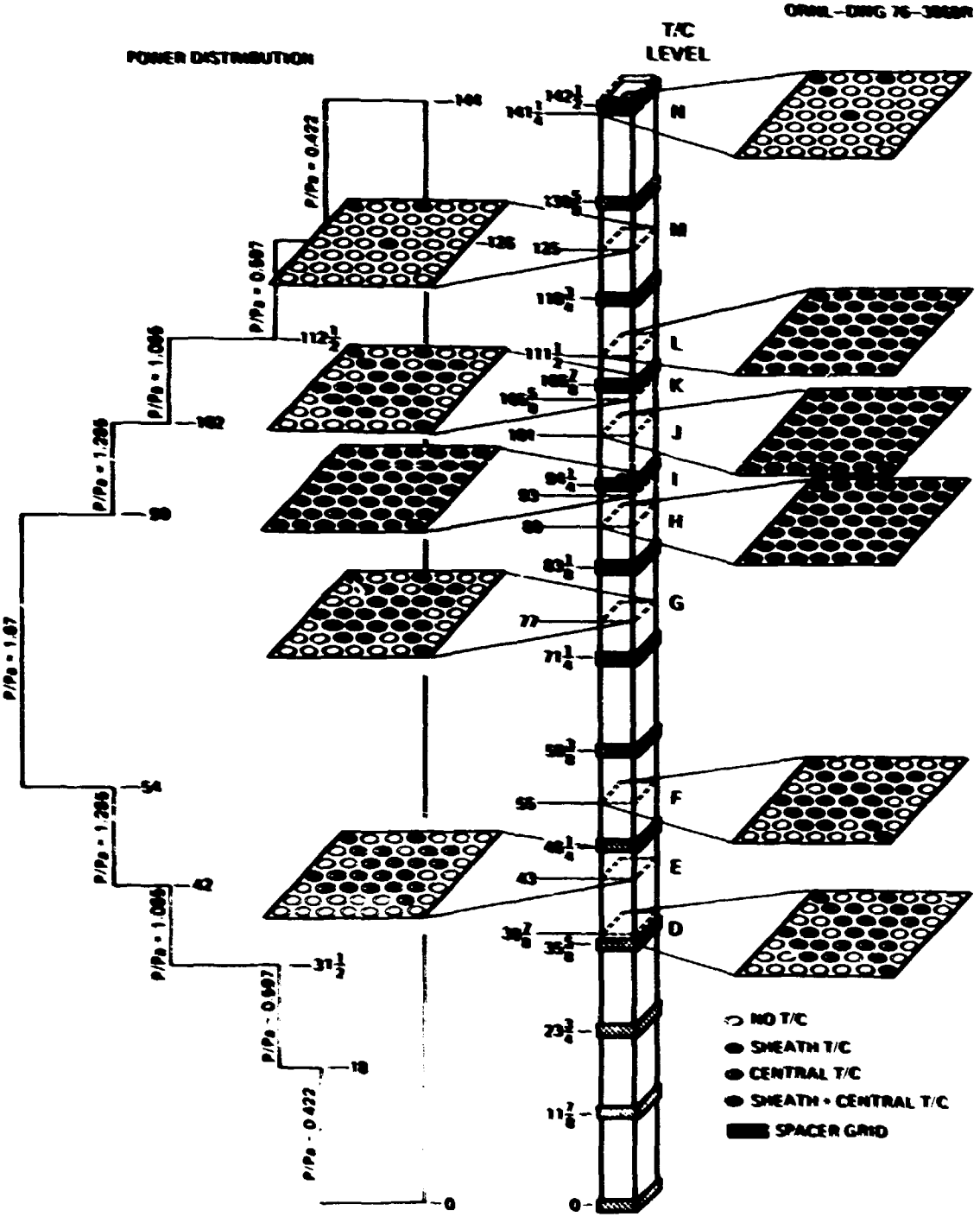

Fig. I.4. Location of thermocouples in THTF bundle 1.

ORNL-DWG 76-19894

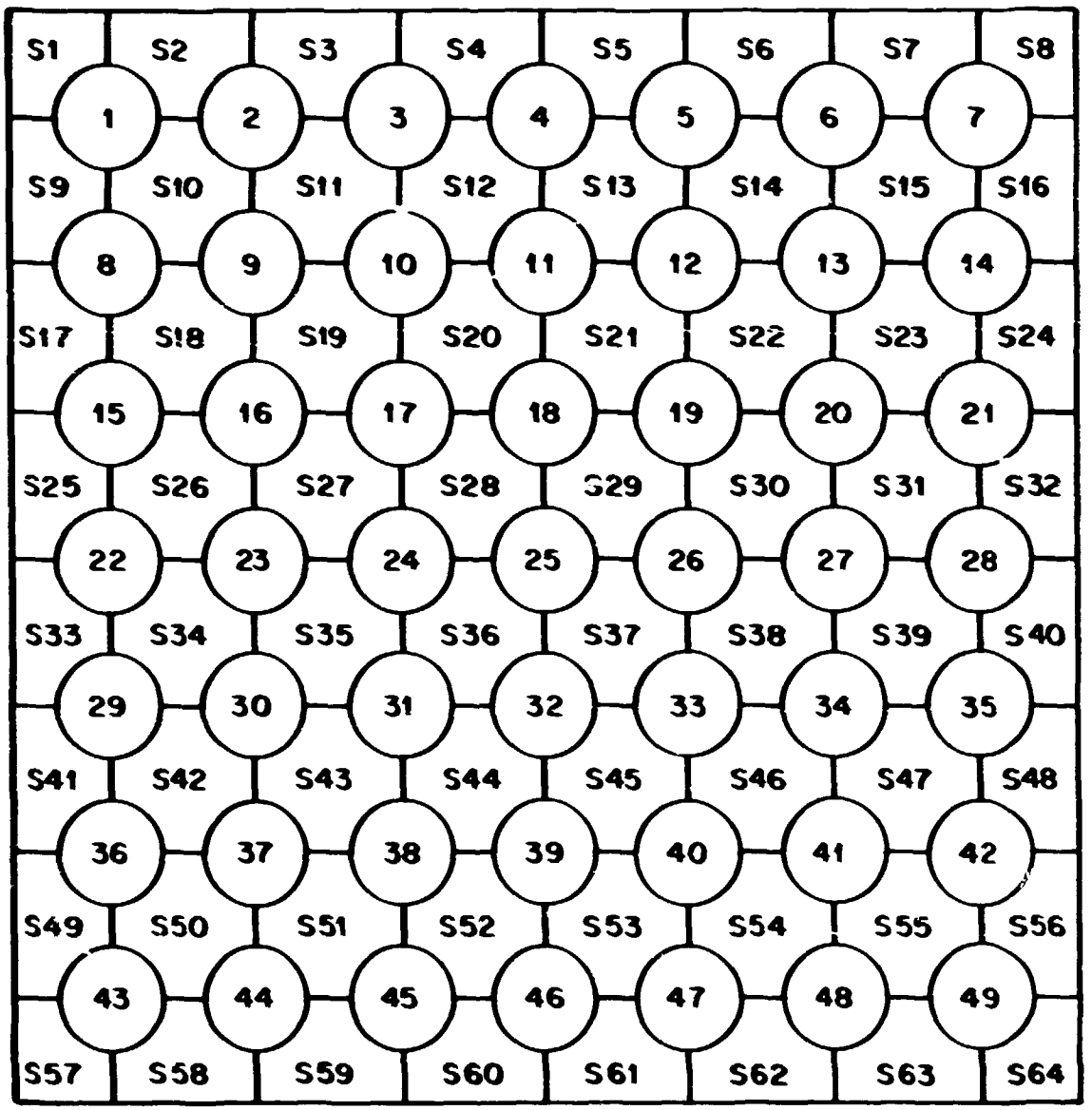

Fig. I.5. Identification of THTF heater rod and subchannel locations in bundles 1 and 2.

II. TEST 100

II.1. Description

Test 100,[2] the first blowdown test in the THTF with bundle 1 in place, was conducted on April 23, 1976. It provided data on the response of bundle 1 and the instrumented spool pieces (with flow-homogenizing screens installed) to a double-ended primary system rupture with equal break areas [6.27 cm^2 (0.0067 ft^2)] at the test section inlet and outlet. Although this was an isothermal test, the main heat exchanges were operated with primary side flows and the secondary sides drained and vented. The primary coolant pump was tripped coincident with break initiation. The THTF fluid conditions immediately preceding rupture are presented in Tables II.1 and II.2.

Test 100 provided operational verification of the data acquisition system and of the mechanical and electrical systems used to control the THTF. The test was isothermal to provide baseline hydraulic information on the response of the experimental facility without the large forcing function supplied by the electric core. As a result, the comparison of the data to RELAP's prediction of the hydraulic response and an evaluation of the techniques used to build the RELAP model were made easier.

II.2. Thermal Hydraulics

For test 100, the pressure traces at various locations around the loop had similar shapes but different magnitudes. The pressures in the horizontal outlet spool piece and the pressurizer appear in Figs. II.1 and II.2, respectively. From 0 to 2 sec, the RELAP predicted pressure is lower in the pressurizer when compared with the experimental data, but is higher in the spool piece. These data fit the general trend for this series; that is, the closer to the breaks, the greater the pressure resurgence. Between 2 and 2.5 sec, the experimental data show a small but obvious dip in the pressurizer pressure. This dip occurred because of extraneous signals on the data acquisition system and is not believed to represent a pressure phenomenon. From 2 to 3 sec, the experimentally measured pressure trace tends to flatten due to the effect of saturation

Table II.1. Desired vs actual prerupture conditions - test 109

Parameters	Desired[2]	Actual[3]
System pressure (PE-201)	15.513 MN/m² (2250 psig)	15.648 MN/m² (2269 psig)
Core power (EEE-9, EEE-10, EEE-11, EEE-12, EEE-9, EEE-10, EEE-11, EEE-12)	0	0
Voltage divar constant	0	0
Core volumetric flow rate (FE-139)	0.0265 m³/sec (420 gpm)	0.0289 m³/sec (458 gpm)
Test section inlet temperature (TE-162)	559.1 K (547°F)	560.9 K (550°F)
Test section outlet temperature (TE-212)	559.1 K (547°F)	559.8 K (548°F)
Pressurizer		
Pressure (PE-106A)	14.720 MN/m² (2135 psig)	14.872 MN/m² (2157 psig)
Mass liquid water (LI-100)	51.26 kg (113 lb_m)	77.10 kg (170.6 lb_m)
Coolant pump		
Speed (SE-22)	59.67 rps (3580 rpm)	60.30 rps (3621 rpm)
Pressure differential (P_dE-28)	4.447 MN/m² (644 psid)	4.576 MN/m² (655 psid)
Pressure between HCV-2 and FCV-10 (PE-16)	16.547 MN/m² (2400 psig)	17.320 MN/m² (2512 psig)
Pressure differential across main heat exchangers (P_dE-46)	-	0.476 MN/m² (69 psid)

[2]Desired prerupture conditions are based on programmatic requirements.

[3]Actual prerupture conditions are based on instrument signals recorded within 10 sec of primary system rupture.

[4]Not specified.

Table II.2. Prerupture primary coolant temperature and pressure distribution[2] - test 109

Location	Instrument	Temperature [K (°F)]	Pressure [MN/m² (psig)]
Vertical inlet spool piece	TE-172	560.4 (549)	
Vertical inlet spool piece	PE-174		15.789 (2290)
Test section inlet	TE-162	560.9 (550)	
Lower plenum	TE-150	559.3 (547)	
Lower plenum	PE-150		15.700 (2207)
Upper plenum	PE-208		15.685 (2283)
Test section outlet	TE-212	559.2 (545)	
Vertical outlet spool piece	TE-222	559.8 (548)	
Vertical outlet spool piece	PE-224		15.688 (2266)
Heat exchanger inlet header	PE-4A		15.350 (2226)
Mixed mean temperature downstream heat exchangers	TE-208	560.9 (550)	
Pressurizer surge line	TE-2	612.0 (642)	
Pressurizer	PE-106		14.874 (2157)
Primary pump suction	PE-26		14.930 (2166)
Between main control valves HCV-2, FCV-10	TE-48	557.6 (546)	
Between main control valves HCV-2, FCV-10	PE-16		17.322 (2512)

[2]Prerupture distribution is based on instrument signals recorded within 10 sec of primary system rupture.

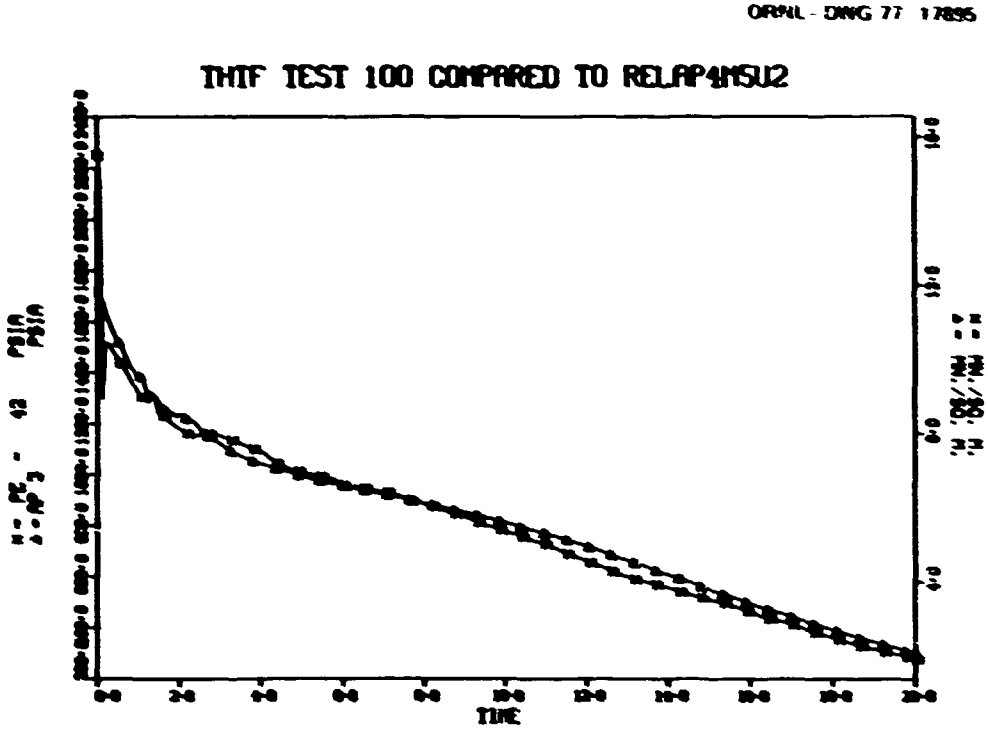

Fig. II.1. Horizontal outlet spool piece pressure.

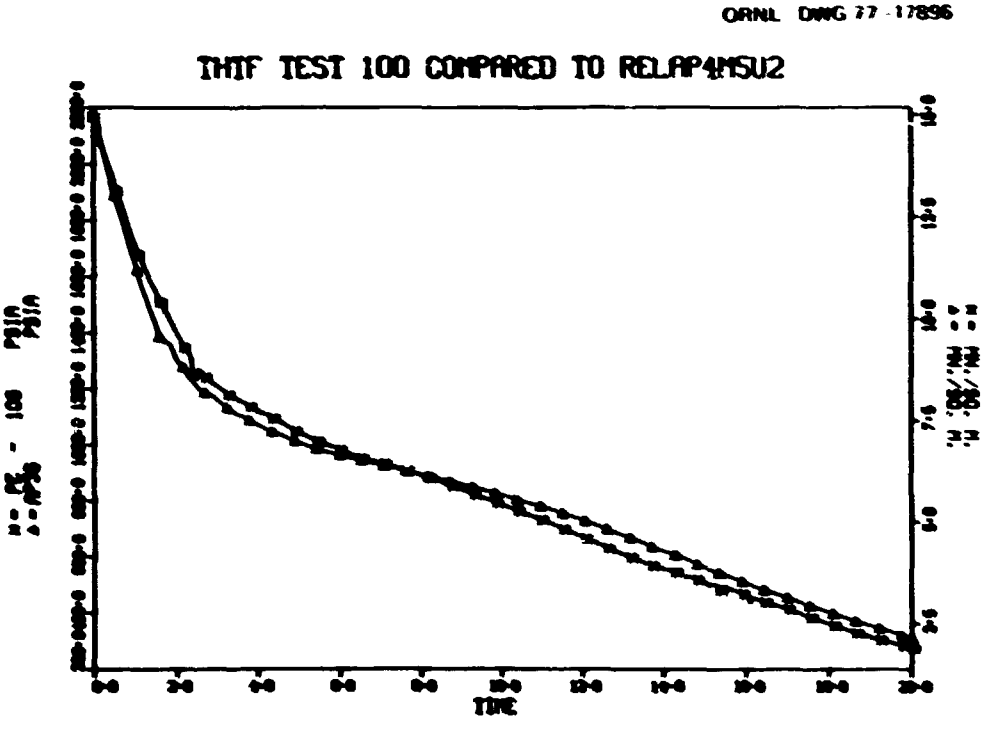

Fig. II.2. Pressurizer pressure.

on the sonic velocity and density of the fluid at the outlet break. At the saturation point, the sonic velocity and density decrease radically, lessening the magnitude of choked flow through the break. Saturation at the inlet break occurs at 5 sec but does not produce as much flattening of the pressure trace as the outlet saturation. For the first 6 sec, RELAP predicts too much depressurization in the pressurizer yet does not disagree appreciably with the experimental pressure at the spool piece. This "skewing" effect is reflected by the pressure difference across the main heat exchanger bypass valve (Fig. II.3). For the remainder of the transient, RELAP predicts pressures closely approximating those measured experimentally. The spool piece pressure comparison is typical of the pressures at other locations around the loop.

Comparisons of the calculated and measured loop temperatures are very similar to the pressure comparisons because the fluid is two-phase for the majority of the transient. Figure II.4, the horizontal outlet fluid temperature, indicates that a temperature rise occurs when pressurizer fluid arrives and that RELAP predicts this arrival too soon. Figure II.5 shows a similar RELAP temperature rise in the horizontal inlet

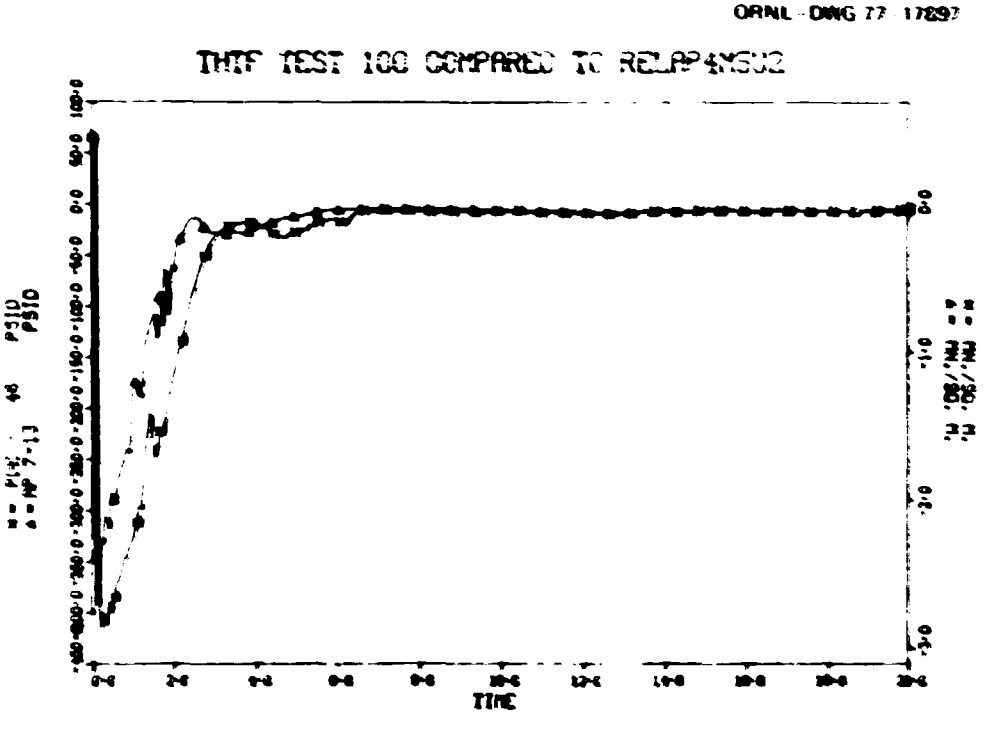

Fig. II.3. Main heat exchanger pressure difference.

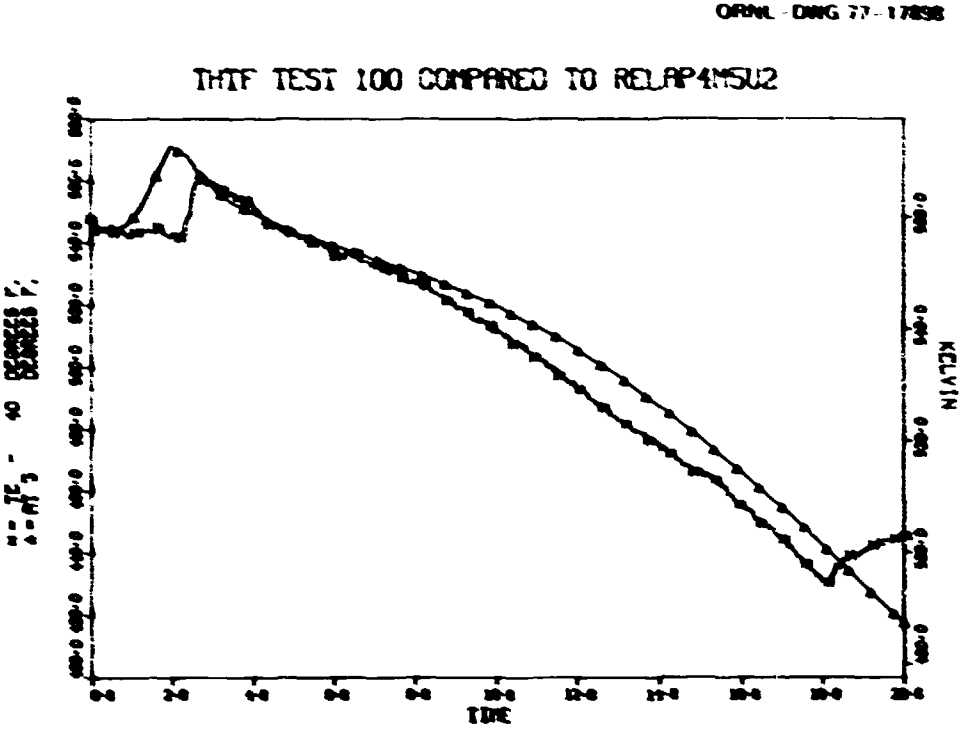

Fig. II.4. Horizontal outlet spool piece temperature.

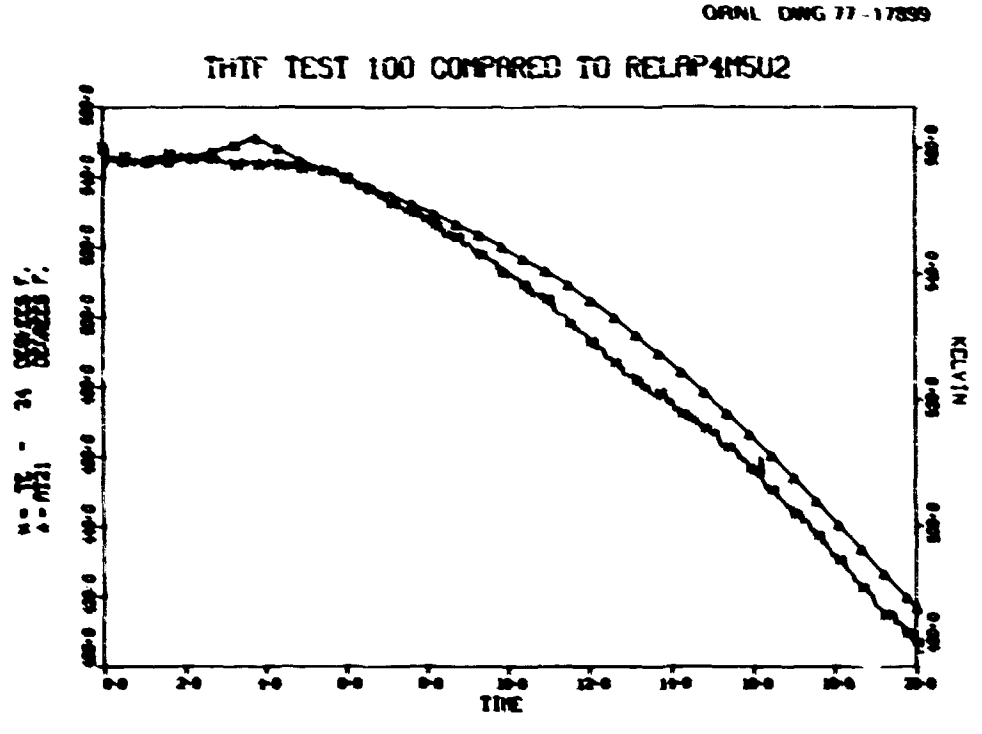

Fig. II.5. Horizontal inlet spool piece temperature.

spool piece but none in the experimental data. The experimental transport time of the leading edge of the pressurizer fluid to the horizontal outlet spool piece is approximately 2.5 sec. RELAP transfers some of the energy of the pressurizer fluid to that spool piece in approximately 1 sec. Another temperature rise is seen at the horizontal outlet late in the transient, which is indicative of heat transfer from hot metal in contact with the low-pressure fluid and subsequent dryout.

The densities at the outlet spool pieces are shown in Figs. II.6 and II.7. Because of the predicted temperature rise, the calculated densities of the subcooled fluid gradually decrease until saturation. The experimental data show no such decrease. The experimental saturation times are 2.8 and 2.5 sec for the vertical and horizontal outlet spool pieces, respectively. Note that since RELAP predicts the temperature rise too soon, it also predicts saturation too soon.

There is a sudden rise in the RELAP and experimental densities in the vertical outlet at approximately 4 and 6 sec, respectively (Fig. II.7).

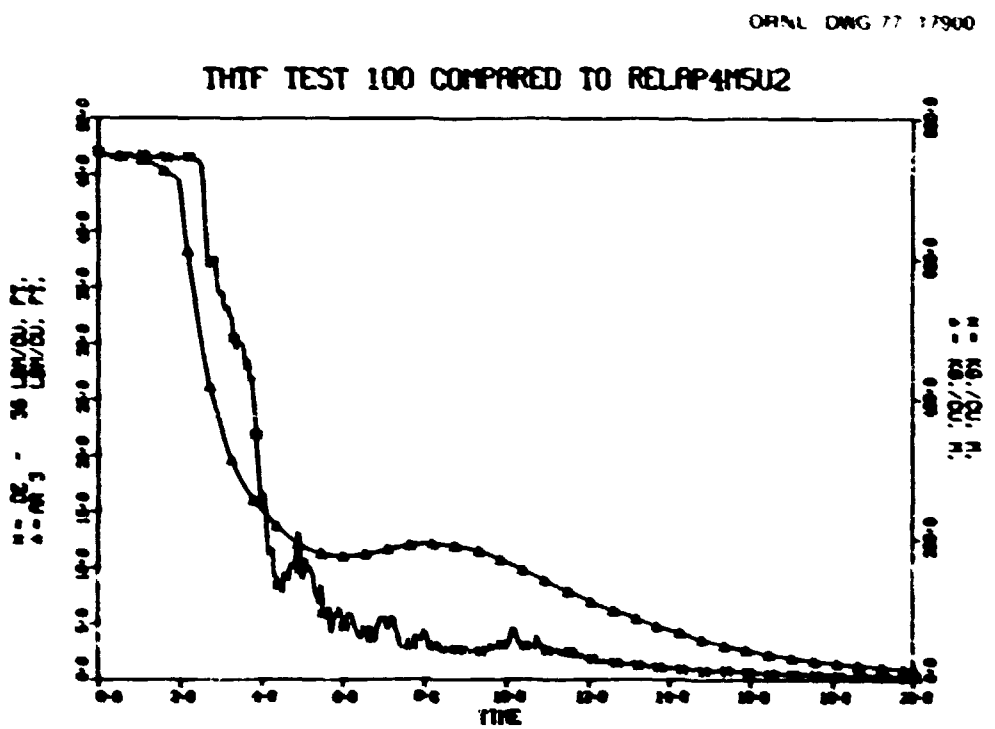

Fig. II.6. Horizontal outlet spool piece density.

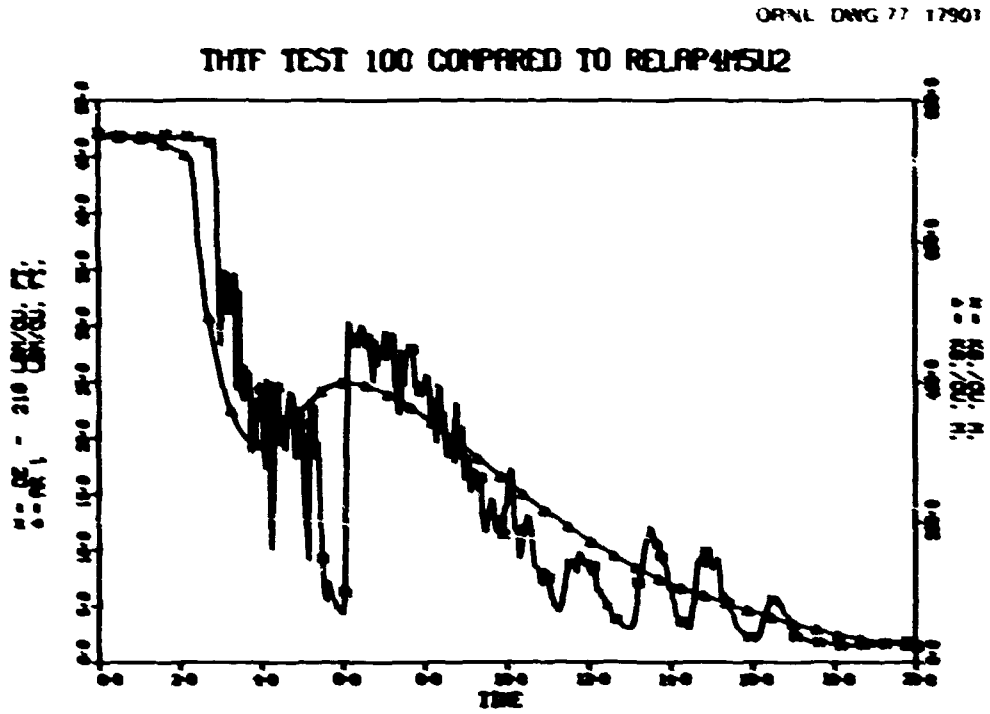

Fig. II.7. Vertical outlet spool piece density.

This rise is the result of a second flow reversal in the vertical outlet spool piece as seen in the volumetric flow measured by the vertical outlet turbine meter (Fig. II.8). It is clear that the flow direction reverses soon after the initiation of blowdown and continues to flow negatively until approximately 5 sec. Pressurizer fluid is indicated at the outlet at approximately 3 sec (Fig. II.4), allowing penetration of hot fluid into the upper part of the test section. The hot water appears to have traveled at least as far as the subchannel thermocouple region (Fig. II.9). The second flow reversal probably occurs as the last of the pressurizer fluid passes the outlet break. Therefore, the density rise in the vertical outlet spool piece denotes the passage of water which was in the test section prior to the injection of the hot pressurizer fluid. RELAP predicts this flow reversal and subsequent density rise too soon (Fig. II.7). The inlet spool piece density comparisons are not presented for this test because of densitometer failures.

The volumetric flows for the horizontal outlet and the vertical and horizontal inlets are presented in Figs. II.10 to II.12, respectively.

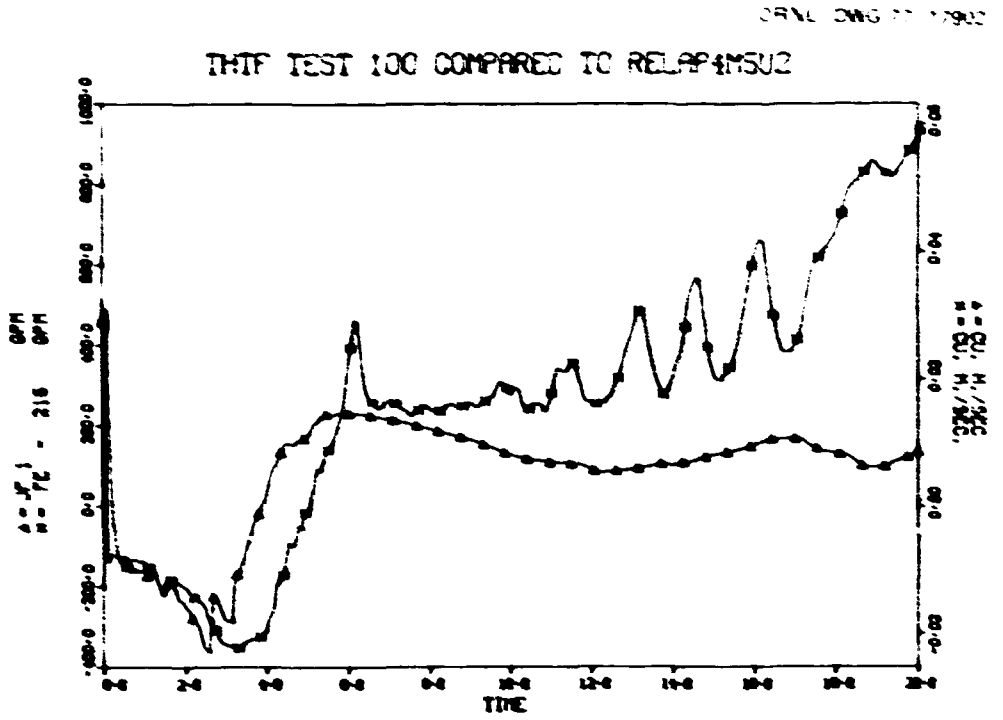

Fig. II.8. Vertical outlet spool piece volumetric flow.

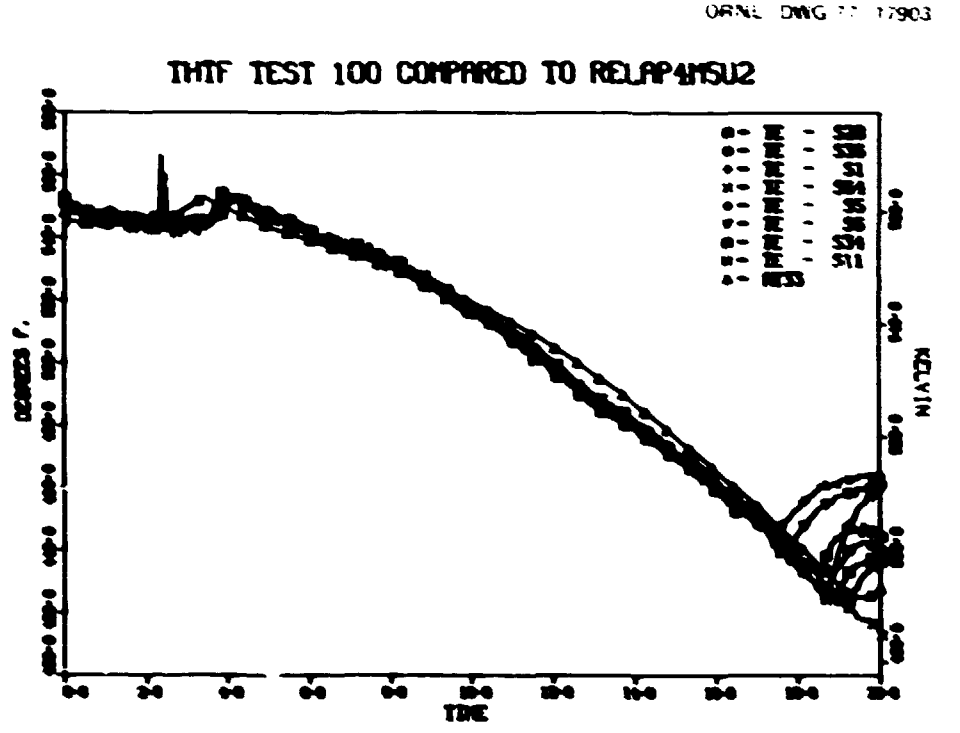

Fig. II.9. Test section subchannel temperatures.

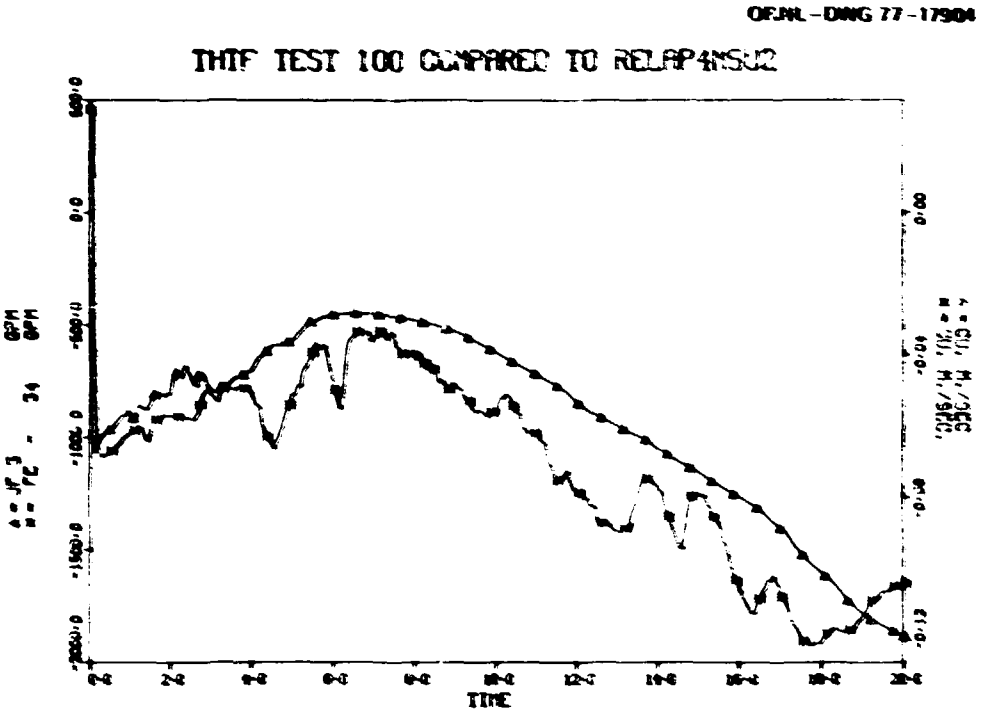

Fig. II.10. Horizontal outlet spool piece volumetric flow.

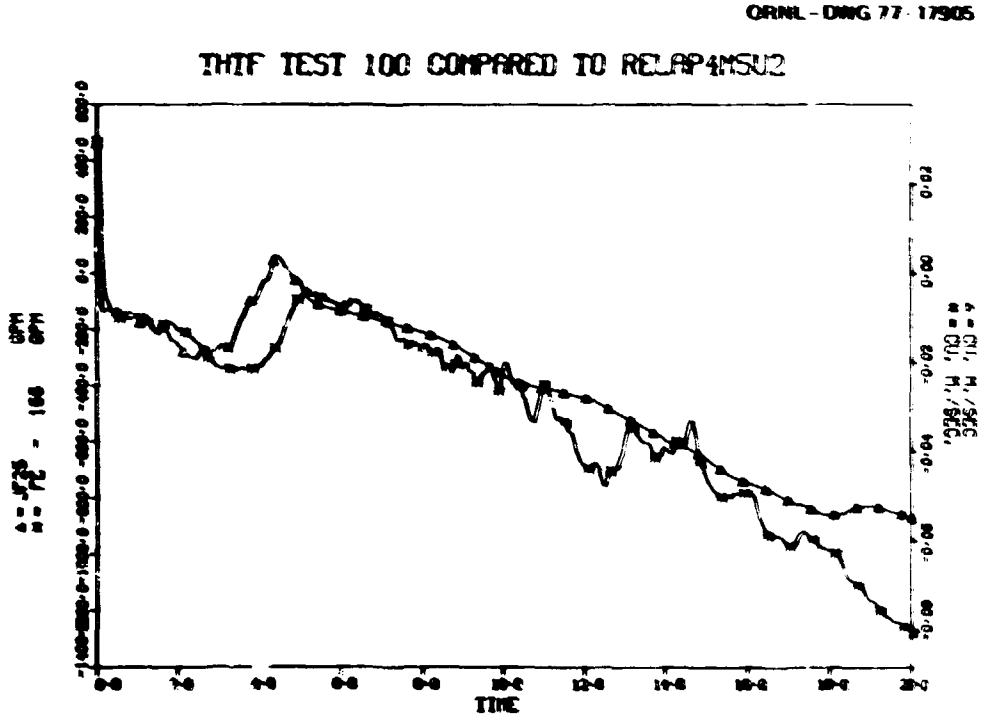

Fig. II.11. Vertical inlet spool piece volumetric flow.

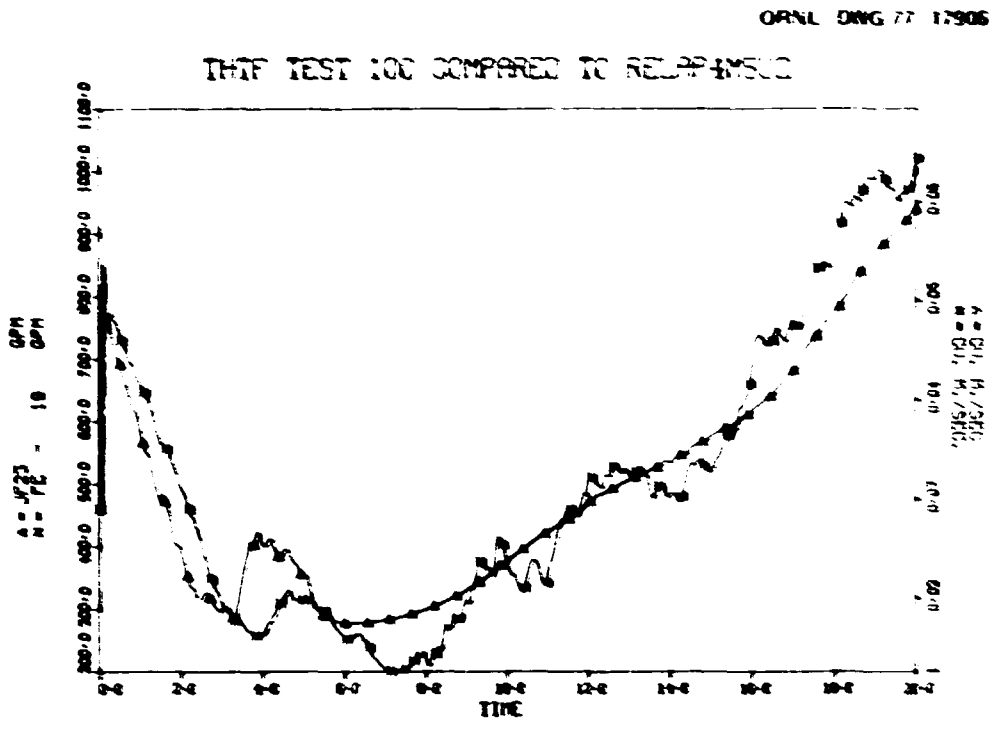

Fig. II.12. Horizontal inlet spool piece volumetric flow.

The horizontal outlet flow is negative for the duration of the transient (Fig. II.10), while the flow in the vertical inlet is strongly negative only for the first 4 sec (Fig. II.11). Because the pressurizer dominates the outlet break, there is negative flow in the vertical outlet and the flow at the vertical inlet is therefore much more negative than it would have been otherwise. During this period of time, the inlet break is being fed substantially through the vertical spool piece. After the second reversal at the vertical outlet, the negative flow at the vertical inlet is reduced (Fig. II.11). It is at this point that the flow at the horizontal inlet increases (Fig. II.12); however, this increased flow is short lived because of vertical inlet saturation at 5 sec (Fig. II.13). This saturation decreases the magnitudes of the flows coming from both the horizontal and the vertical inlets by decreasing the critical mass flow at the inlet break. Saturation at the horizontal inlet finally occurs at approximately 6 sec (Fig. II.5). The volumetric flows remain depressed until 7 sec, when there is an increase in both the horizontal and vertical inlet spool pieces.

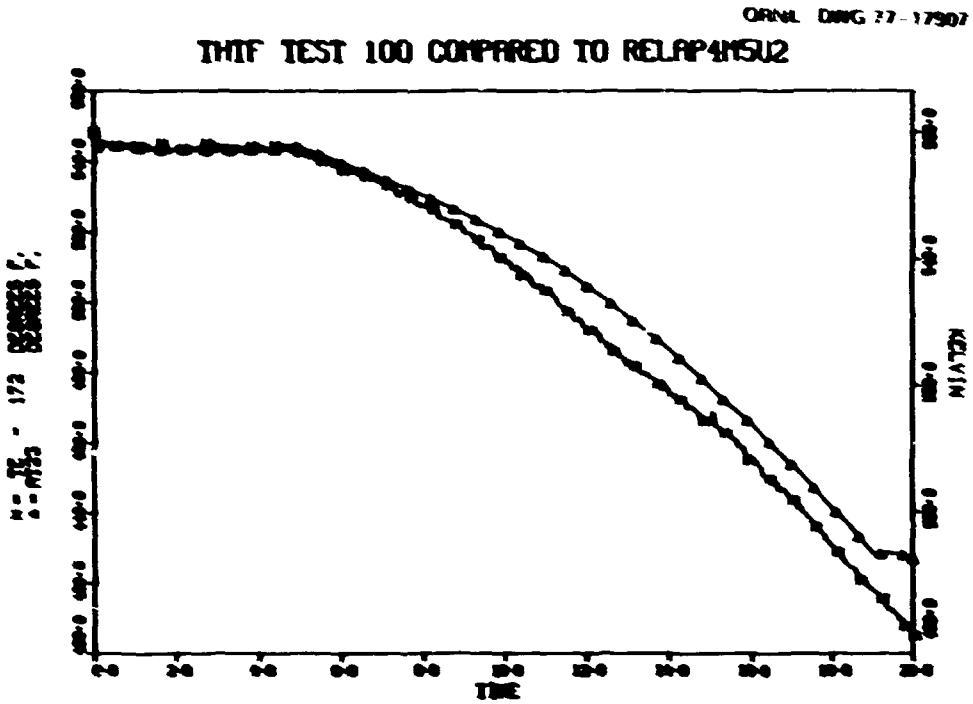

Fig. II.13. Vertical inlet spool piece temperature.

The mass flows for the horizontal and vertical outlets, presented in Figs. II.14 and II.15, respectively, show the same characteristics as the volumetric flows previously described. Note that, after approximately 10 sec, the volumetric flows increase as the mass flows decrease or remain the same. With decreasing densities around the loop, large velocities are generated from the existing pressure differentials, driving the volumetric flows upward.

Since test 100 was an isothermal test, the core fluid behavior is, in general, uninteresting. Comparisons of RELAP-predicted surface temperature with the surface temperature of a particular rod as calculated by ORINC (see Chapter 1) are presented in Figs. II.16 and II.17. Figure II.16 presents data from the upper end of the test section, where the effect of the pressurizer water is seen as a slight temperature rise at 5 sec. The flattening of the temperature trace late in the transient is due to dryout in the upper regions of the test section. Figure II.17 presents data from the lower end of the test section. The pressurizer water did not reach that level in the test section and therefore is not seen in the traces. Also, the dryout effect is less pronounced in that region.

ORNL DWG 77-17906

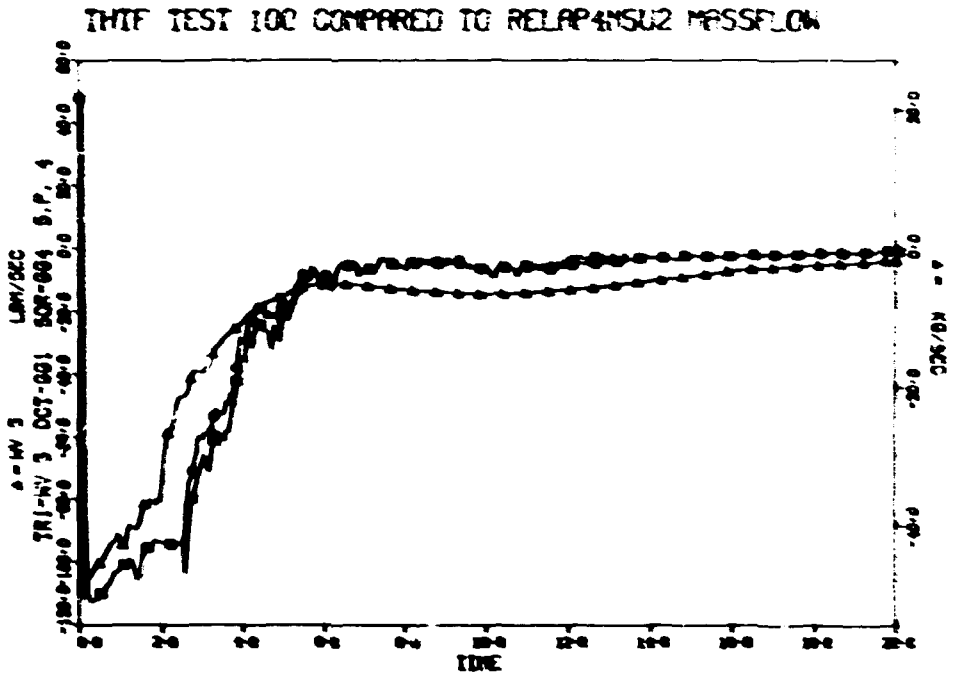

Fig. II.14. Horizontal outlet spool piece mass flow.

ORNL DWG 77-17909

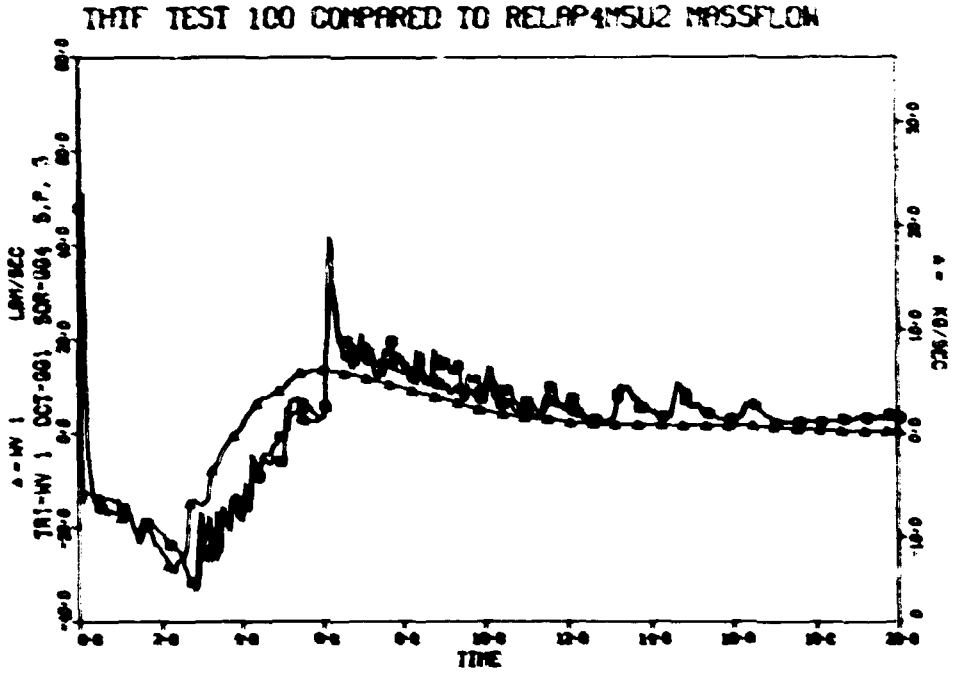

Fig. II.15. Vertical outlet spool piece mass flow.

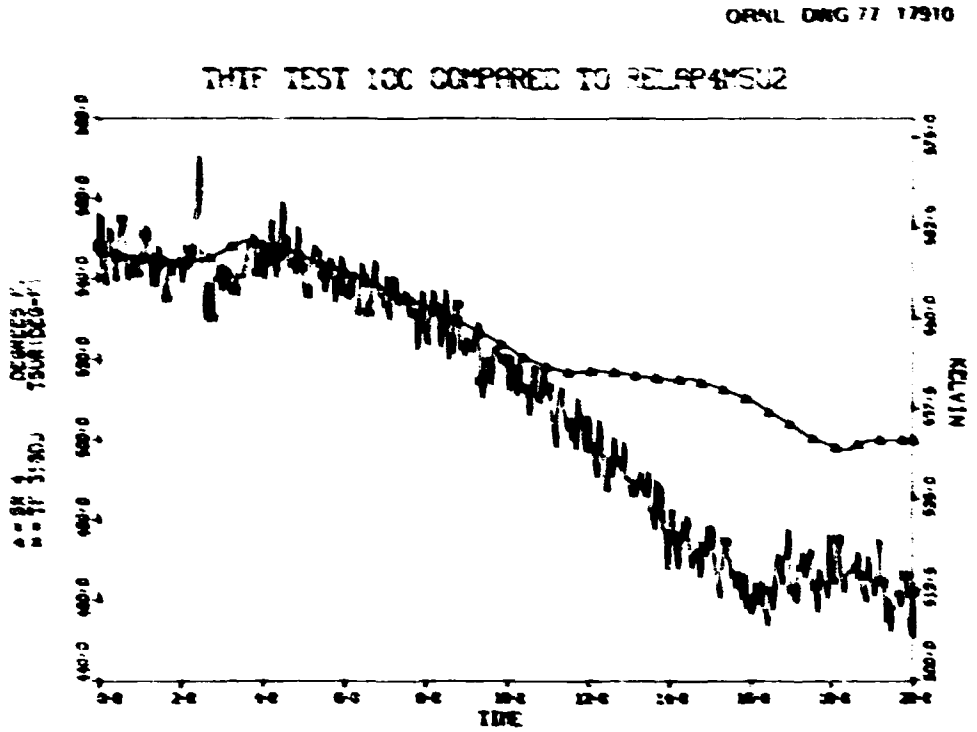

Fig. II.16. Surface temperature, rod 18, level J.

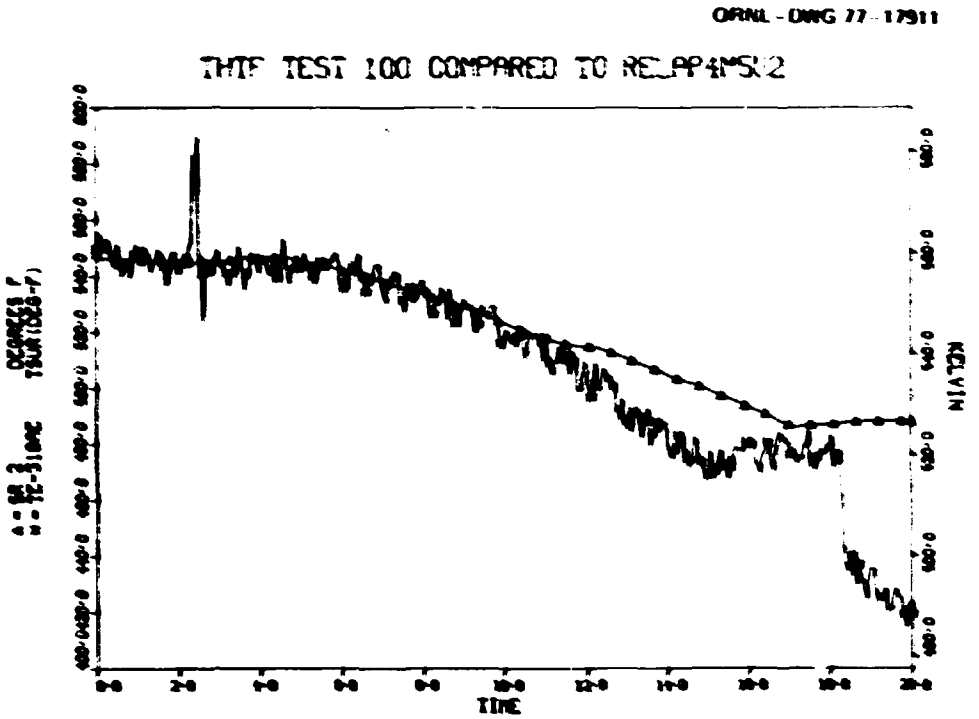

Fig. II.17. Surface temperature, rod 18, level E.

III. TEST 101

III.1. Description

Test 101, the second test conducted in the THTF with bundle 1 in place,[3] was conducted on May 27, 1976, to investigate the thermal-hydraulic response of bundle 1 and the main heat exchanger to powered conditions. The break configuration was an outlet break with an area of 6.27 cm^2 (0.0067 ft^2). This test was performed at 25% of full power with the electric core and primary coolant pump tripped and the closure of main heat exchanger secondary side valves initiated coincident with rupture. The THTF fluid conditions immediately preceding rupture are presented in Tables III.1 and III.2.

Test 101 provided operational verification of the mechanical and electrical systems used to control the THTF under powered conditions. The test had low rod power to provide an adequate safety margin during operational verification of the power circuits and safety trip systems of the THTF. The transient data provided an intermediate step in the evaluation of the RELAP models and their input parameters.

III.2. Thermal Hydraulics

Since test 101 had only an outlet break, the sequence of events differs from the other powered tests in the 100 series. The depressurization rate in this test was much slower because of the reduced total break area. A typical pressure plot is presented in Fig. III.1 for the vertical outlet. As noted previously, the pressurizer-induced pressure resurgence is greatest at the point of maximum depressurization. In test 101, this occurred at the outlet spool pieces. RELAP's calculated pressures for the spool pieces fall after too great a resurgence and become low compared to the experimental data. The crossover point in the calculated and experimentally measured pressures is between 1 and 2 sec. At approximately 3.5 sec, there is a flattening of the pressure trace in the experimental data. This effect corresponds to saturation at the horizontal outlet and is due to reduced critical flow through the outlet break.

Table III.1. Desired vs actual prerupture conditions — Test [illegible]

Parameters	Desired[a]	Actual[b]
System pressure (PE-201)	[illegible] MPa / [illegible] psig	[illegible] MPa / [illegible] psig
[illegible]	[illegible]	[illegible]
[illegible]	[illegible]	[illegible]
[illegible]	[illegible]	[illegible]
[illegible]	[illegible]	[illegible]
[illegible]	[illegible]	[illegible]
Pressurizer		
[illegible]	[illegible]	[illegible]
[illegible]	[illegible]	[illegible]
[illegible]		
[illegible]	[illegible]	[illegible]
[illegible]	[illegible]	[illegible]
[illegible]	[illegible]	[illegible]
[illegible]		[illegible]

[a][illegible]

[b][illegible]

[c][illegible]

Table III.2. Prerupture primary coolant temperature and pressure distribution[a] — test 201

Location	Instrument	Temperature K (°F)	Pressure MN/m² (psig)
Vertical inlet spool piece	TE-172	559.3 (547)	
Vertical inlet spool piece	PE-174		
Test section inlet	TE-162	568.2 (563)	
Lower plenum	TE-150	568.2 (563)	
Lower plenum	PE-156		15.472 (2229)
Upper plenum	PE-201		15.443 (2225)
Test section outlet	TE-212	572.0 (570)	
Vertical outlet spool piece	TE-222	572.5 (571)	
Vertical outlet spool piece	PE-224		15.427 (2223)
Heat exchanger inlet header	PE-44		15.408 (2220)
Mixed mean temperature downstream heat exchangers	TE-298	561.7 (551)	
Pressurizer surge line	TE-2	[illegible]	
Pressurizer	PE-106		15.300 (2204)
Primary pump suction	PE-76		15.219 (2192)
Between main control valves MCV-2, FCV-18	TE-48	555.9 (541)	
Between main control valves MCV-2, FCV-19	PE-16		[illegible]

[a]Prerupture distribution is based on instrument signals recorded within 10 sec of primary system rupture.

[b]Instrument failure.

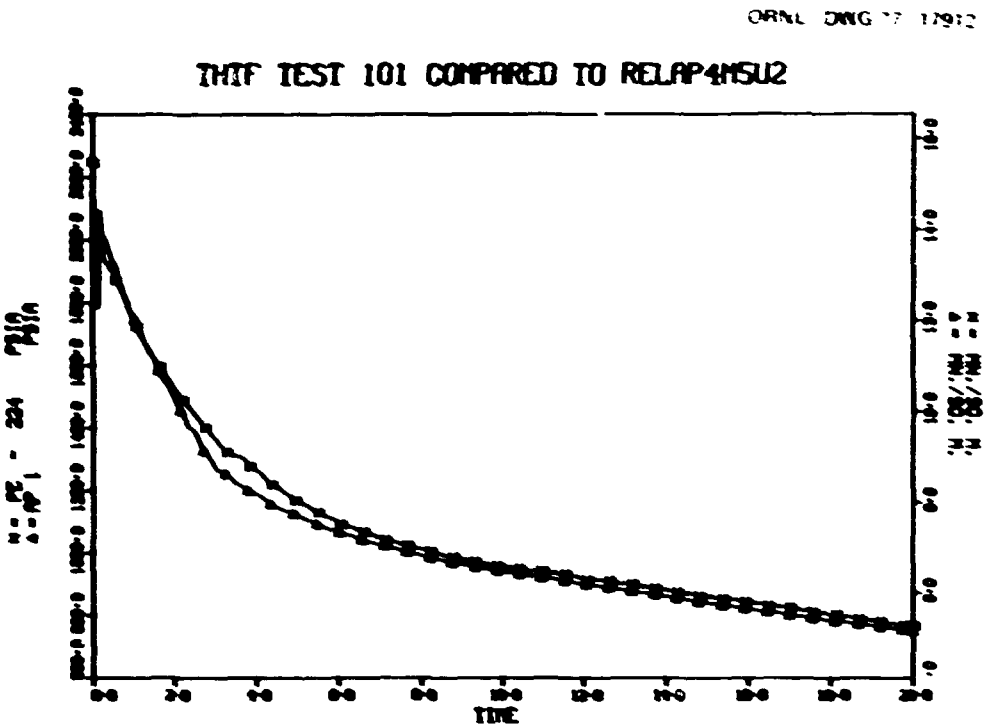

Fig. III.1. Vertical outlet spool piece pressure.

Differential pressure transducer P_dT-199 measured the pressure drop across the rod bundle during the transient (Fig. III.2). Since the test had only an outlet break, the flow in the test section was positive and had a positive pressure difference. The large oscillations in the experimental data early in the transient are due to the effect of "ringing" in the lines to the transducer.

The temperature at the horizontal outlet spool piece is presented in Fig. III.3. The sharp dip in the experimental data at 2.5 sec occurs as the leading edge of the subcooled water, initially between the heat exchangers and the pressurizer, reaches the horizontal outlet. The sharp rise in the data at 3 sec indicates the leading edge of the hot pressurizer fluid as it passes the horizontal outlet. This fluid induced saturation in that spool piece at approximately 3.3 sec. RELAP's prediction does not show this dramatic dip in the temperatures although it does predict a slightly lower temperature than the experimental data before the arrival of the cold fluid. Also, RELAP does not predict as high a temperature as the experimental data after the passage of the subcooled fluid. The fact

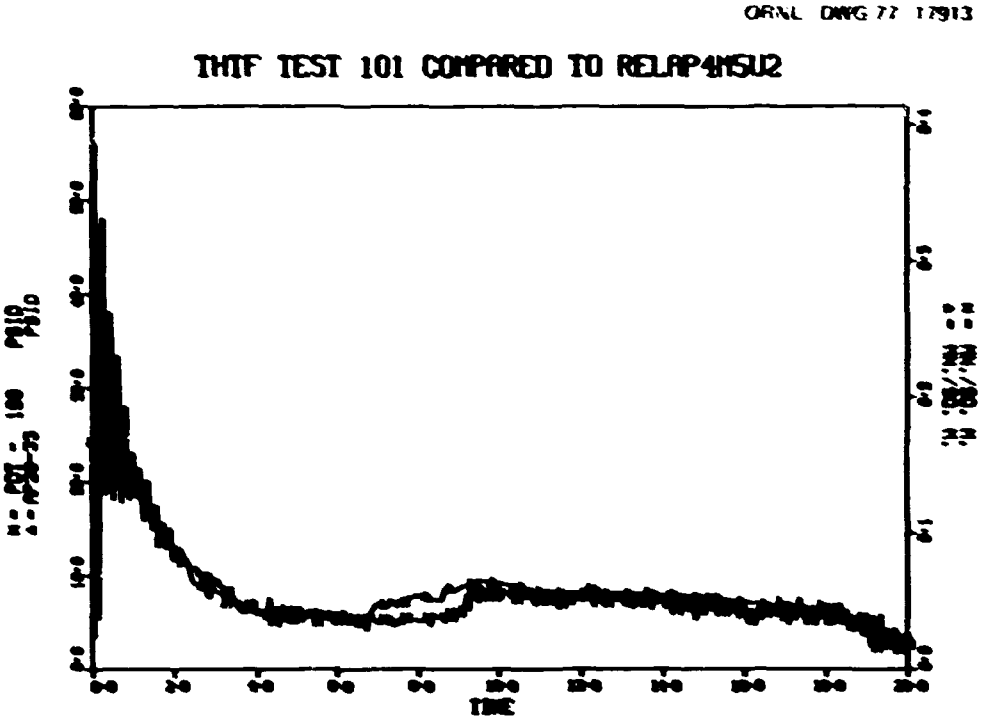

Fig. III.2. Rod bundle pressure difference.

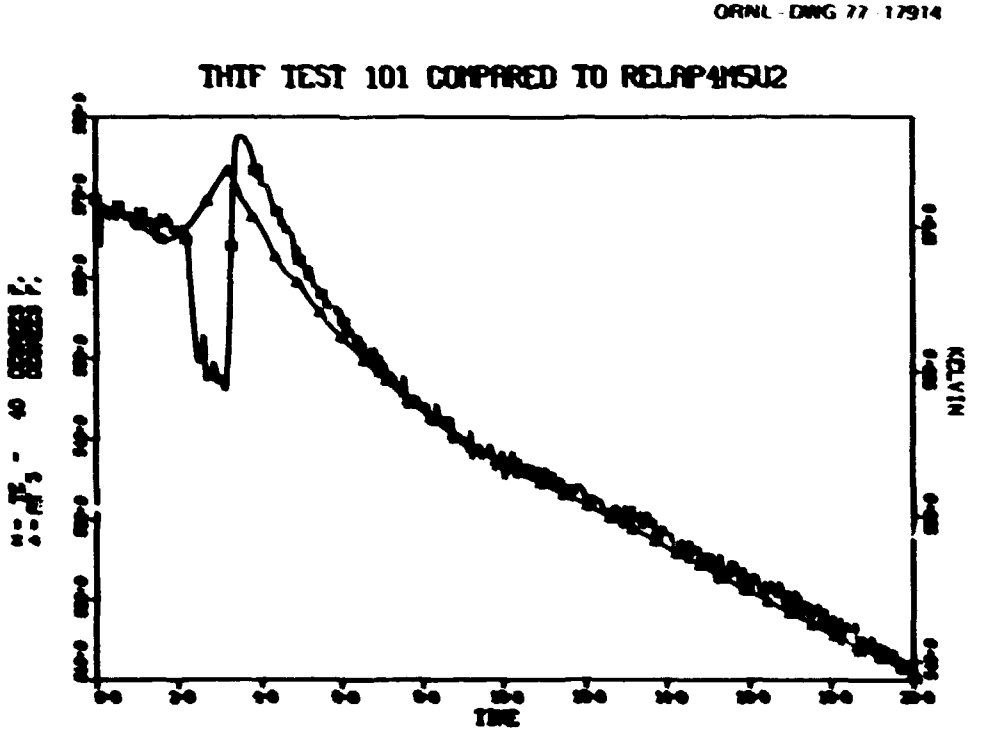

Fig. III.3. Horizontal outlet spool piece temperature.

that RELAP mixes fluid at sharp temperature interfaces explains why RELAP does not predict as cold or as hot a temperature as the data for the horizontal outlet spool piece. The vertical outlet temperature plot (Fig. III.4) shows a gradual temperature decrease before saturation at 6 sec. At the initiation of blowdown, the temperature of the fluid at the top and bottom of the core was 572 K (570°F) and 559 K (547°F), respectively. Because flow through the rod bundle is positive, the temperature of the subcooled fluid flowing at the vertical outlet will decrease before saturation. At 6 sec, saturation occurs and the temperature follows the saturation pressure for the rest of the transient.

The measured density for the horizontal outlet spool piece (Fig. III.5) shows the initial passage of the subcooled fluid between the heat exchanger and the pressurizer as a density rise at 2.5 sec. RELAP's calculation distributes this cold water so that no sharp density increase appears. Saturation occurs at 3.3 sec with the appearance of hot pressurizer fluid. Because of the smearing effect, the influence of RELAP's low pressures on time to saturation is negated. The low-pressure effect is seen in the vertical outlet density (Fig. III.6), where the RELAP-generated

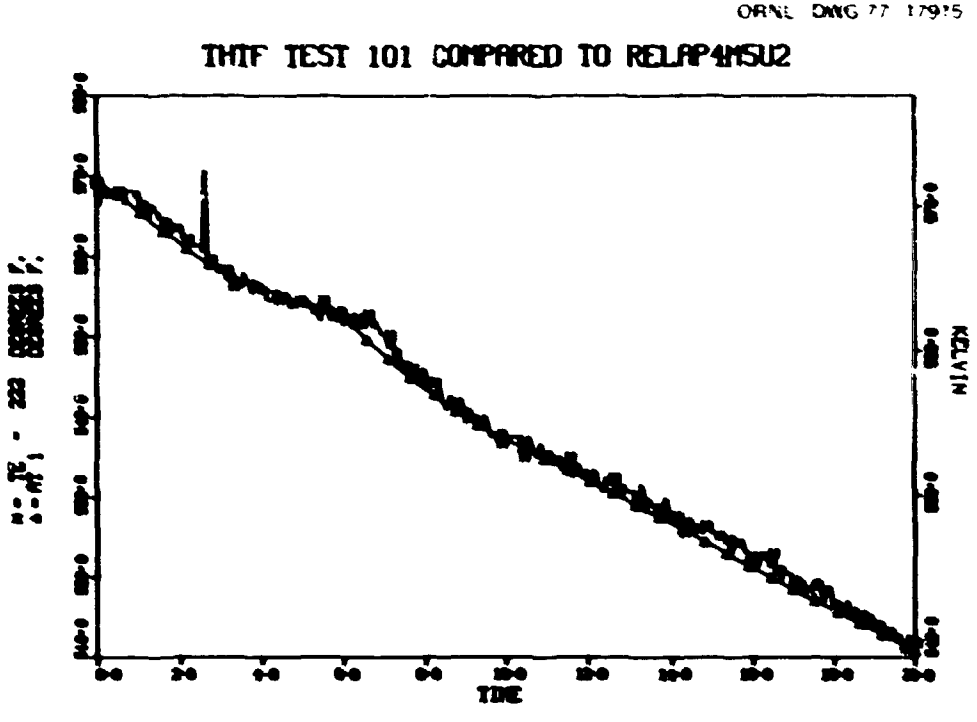

Fig. III.4. Vertical outlet spool piece temperature.

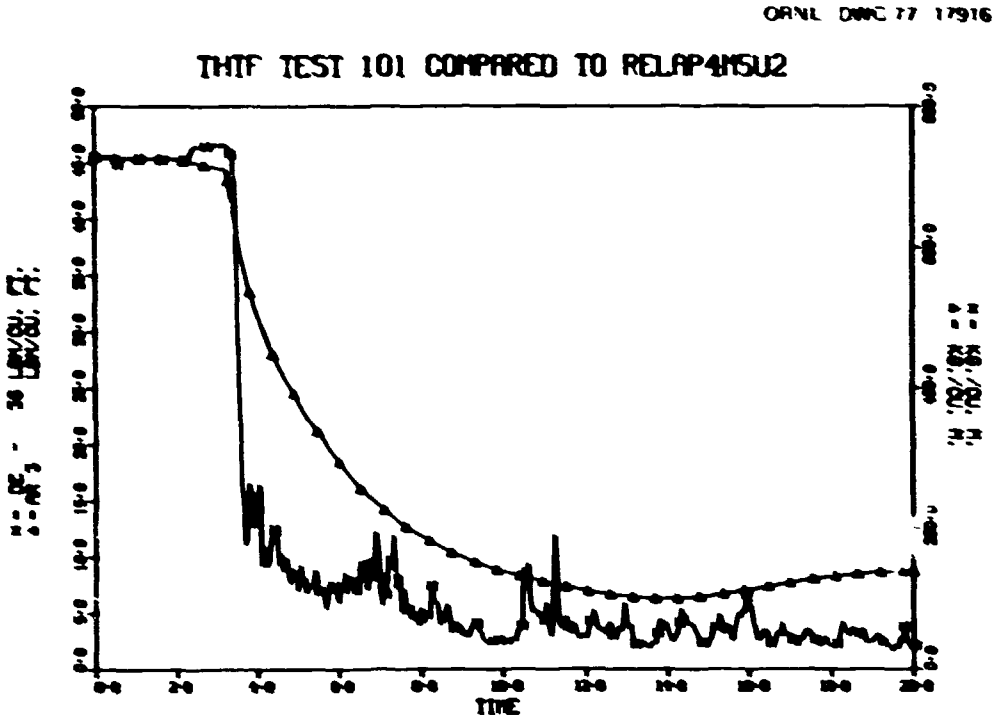

Fig. III.5. Horizontal outlet spool piece density.

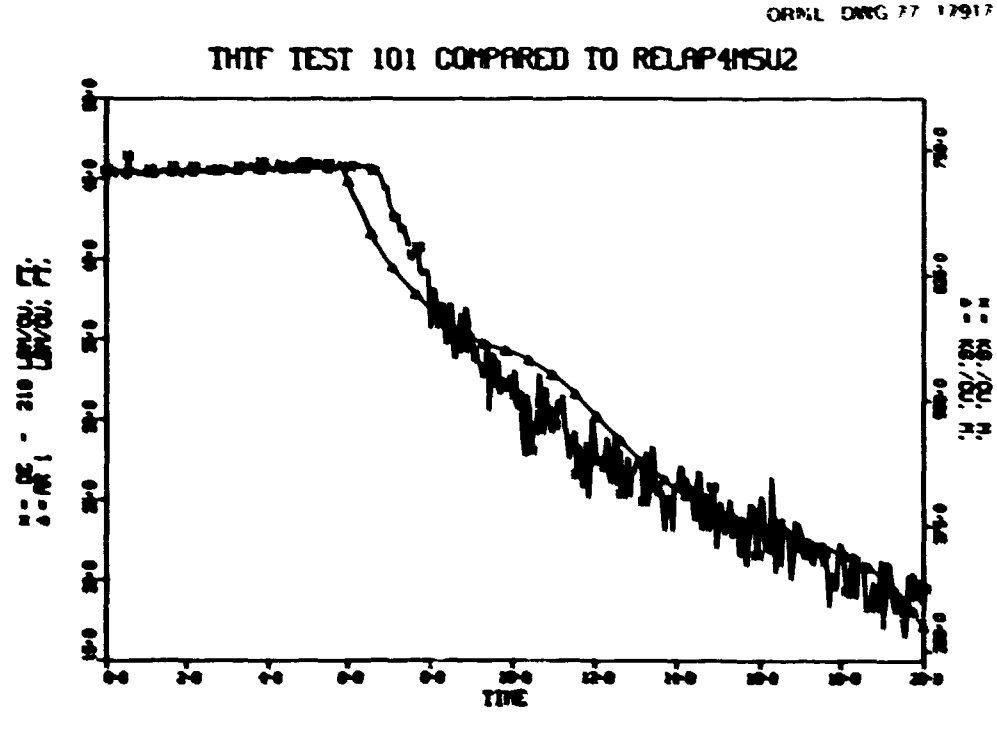

Fig. III.6. Vertical outlet spool piece density.

saturation point occurs almost 1 sec before the experimental data at 7 sec. The densities for the horizontal and vertical inlets are presented in Figs. III.7 and III.8, respectively. The saturation times at these spool pieces are about 10 sec, as indicated by the temperatures in each spool piece (Figs. III.9 and III.10). The reason for the apparent late saturation of the horizontal inlet as indicated by the density plot is believed to be stratification of flow in that spool piece. Low flow, which is conducive to stratification, existed in that spool piece at the time of saturation (Fig. III.11). Because of the orientation of the vertical spool piece, gravity-induced phase separation cannot occur without detection. The negative density in the horizontal inlet late in the transient (shown by the experimental data) is a result of inaccurate calibration of the instrument response.

The mass flows for the outlet spool pieces are presented in Figs. III.12 and III.13. The mass flow in the horizontal outlet is strongly negative for the first 3.5 sec. With the arrival of pressurizer water, saturation occurs and the critical flow out of the break is reduced. As

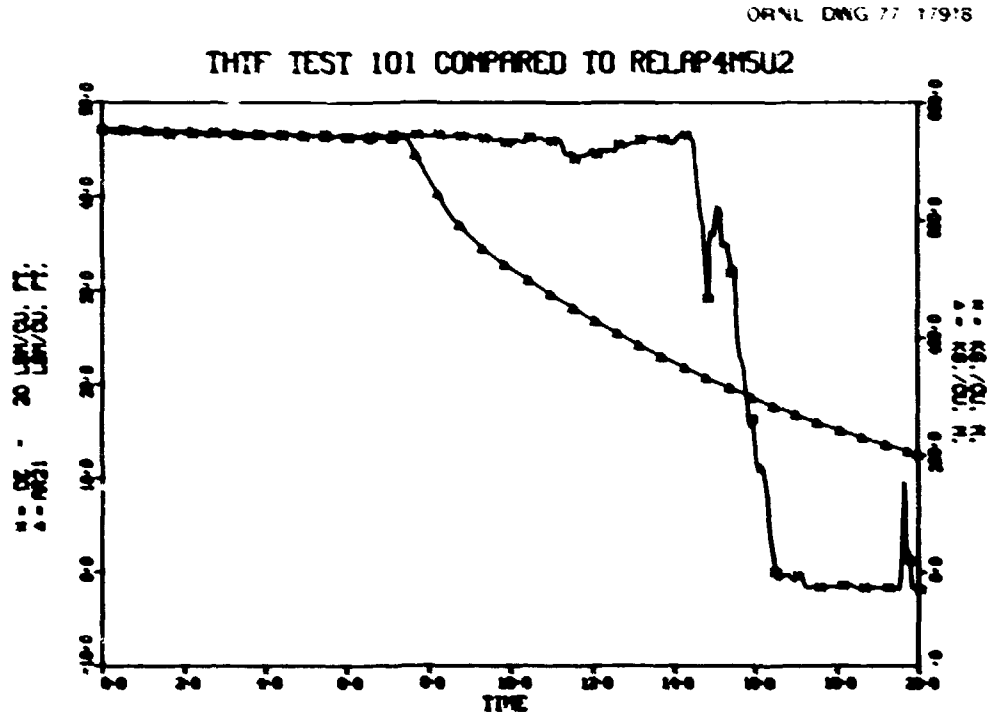

Fig. III.7. Horizontal inlet spool piece density.

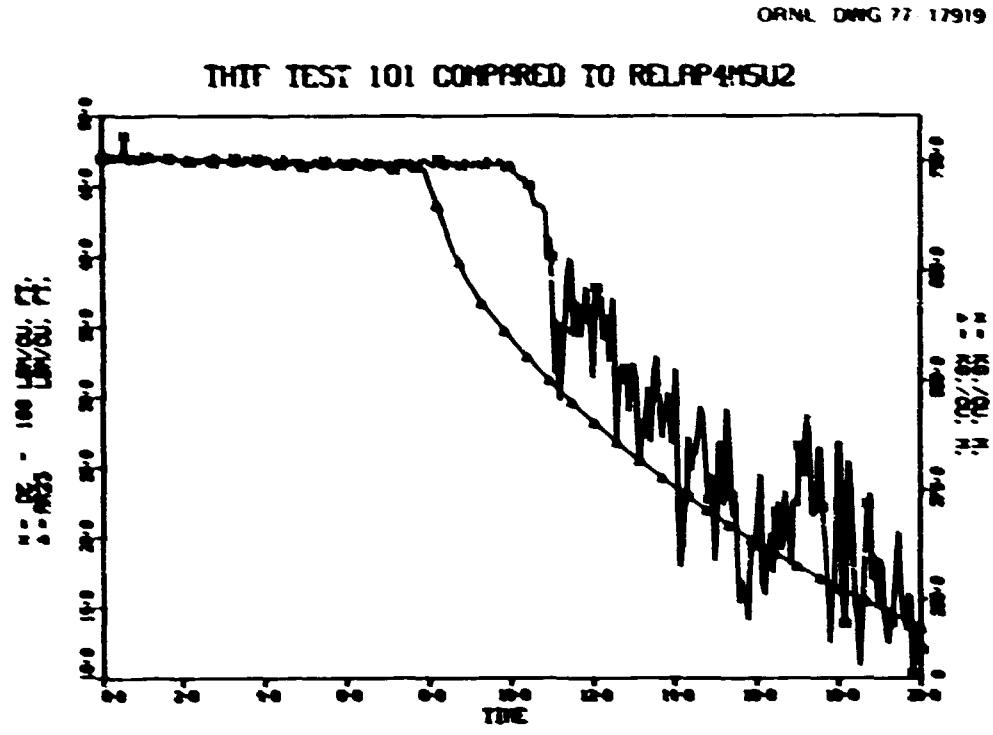

Fig. III.8. Vertical inlet spool piece density.

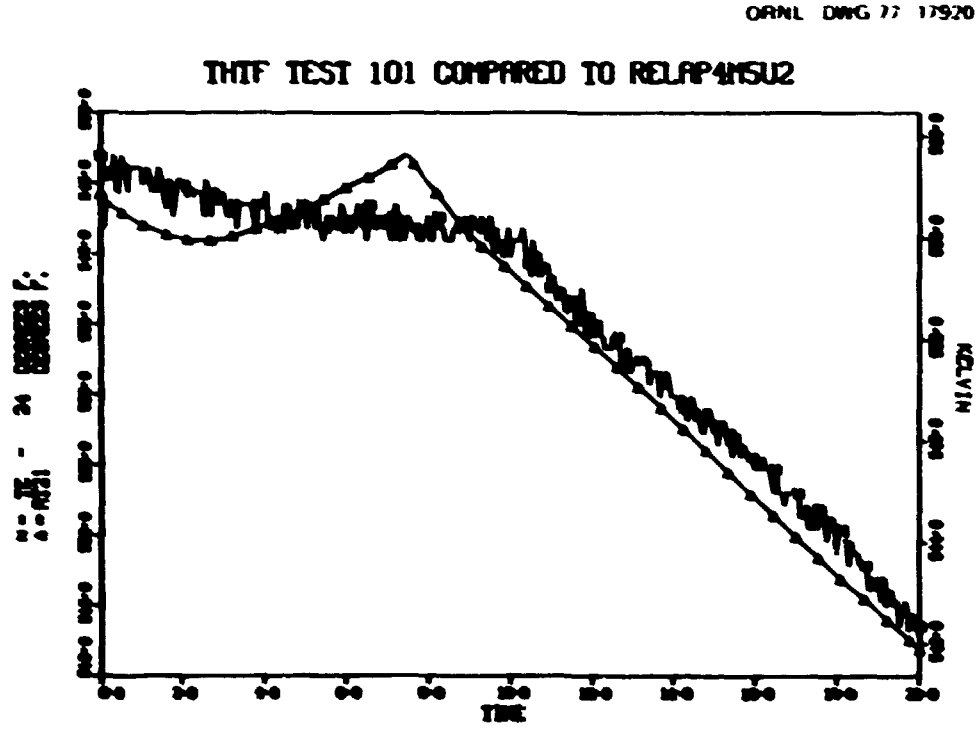

Fig. III.9. Horizontal inlet spool piece temperature.

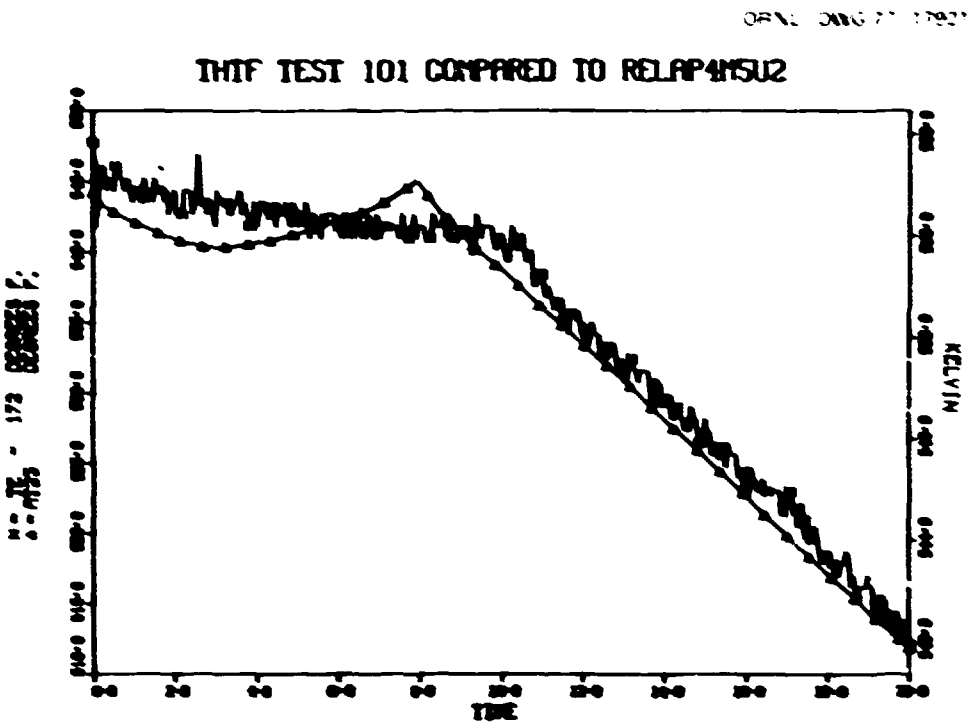

Fig. III.10. Vertical inlet spool piece temperature.

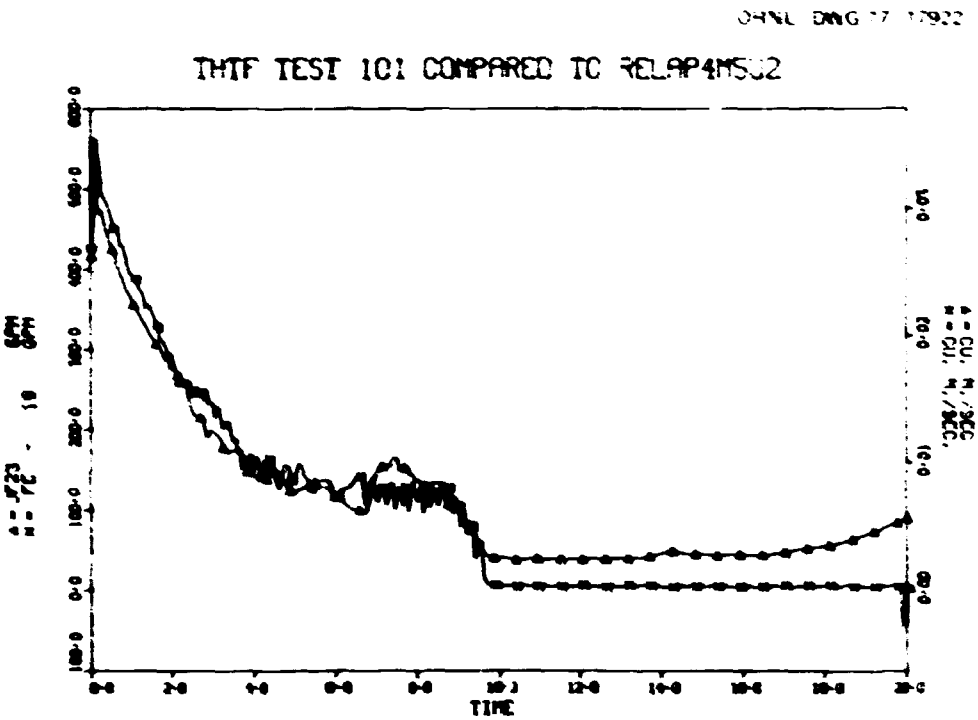

Fig. III.11. Horizontal inlet spool piece volumetric flow.

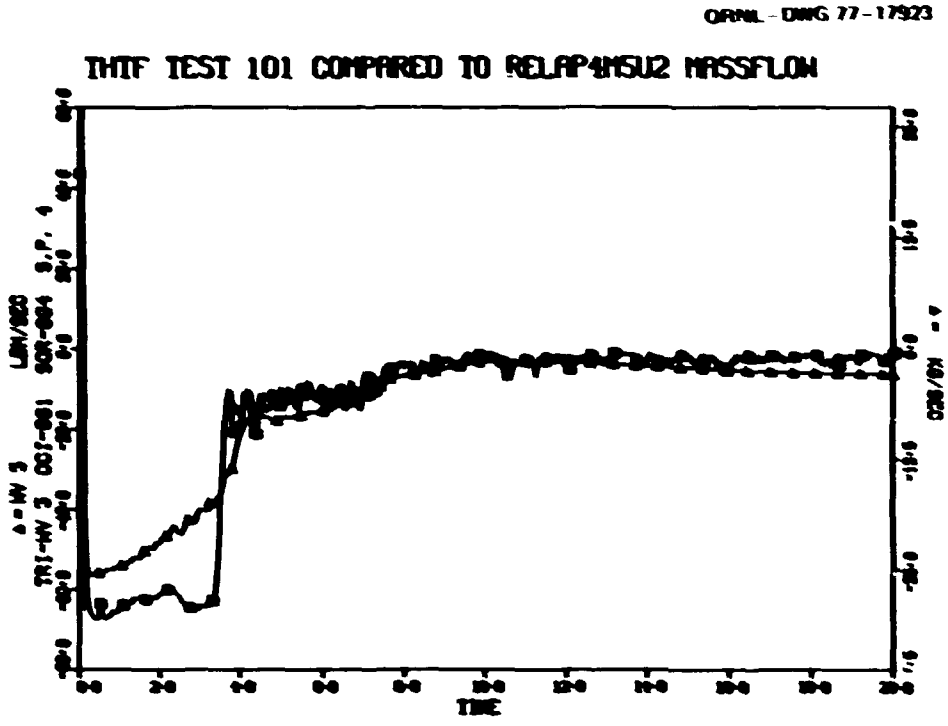

Fig. III.12. Horizontal outlet spool piece mass flow.

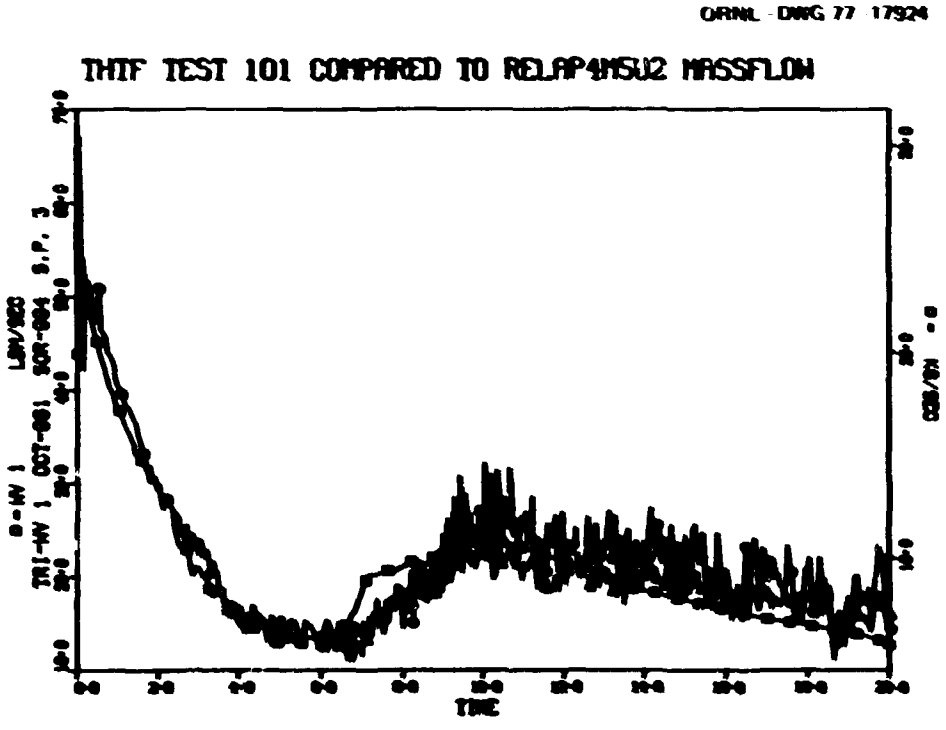

Fig. III.13. Vertical outlet spool piece mass flow.

a result, the horizontal outlet flow drops at 3.5 sec. At 7 sec, the flow decreases further toward zero. This is probably due to the depletion of hot pressurizer water, thus reducing its potential for driving flow out of the break. When this reduction of mass flow occurs at the horizontal outlet, the flow through the vertical outlet increases.

The response of the test section for test 101 will be analyzed in a subsequent report. However, some examples of RELAP's comparisons with the data will be presented here. In Fig. III.14, a plot of RELAP's surface temperatures for the second core slab is overlayed with the surface temperature of a heater rod at level E as calculated by ORINC (see Chapter I). Figure III.15 is a similar comparison for the same rod at the fourth core slab.

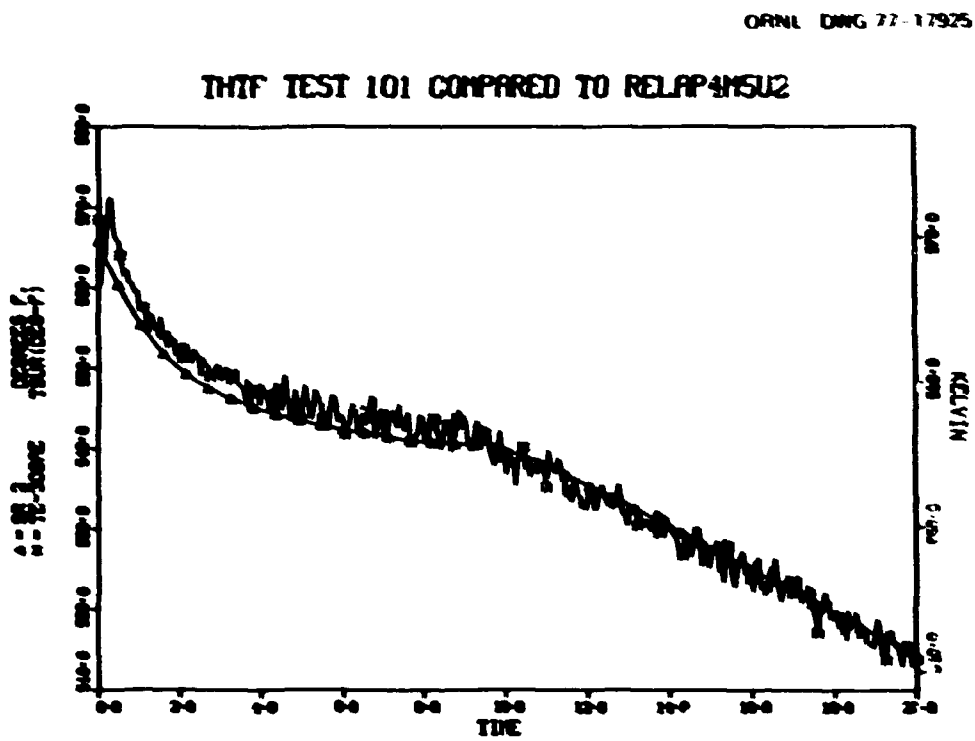

Fig. III.14. Surface temperature, rod 9, level E.

ORNL-DWG 77-17926

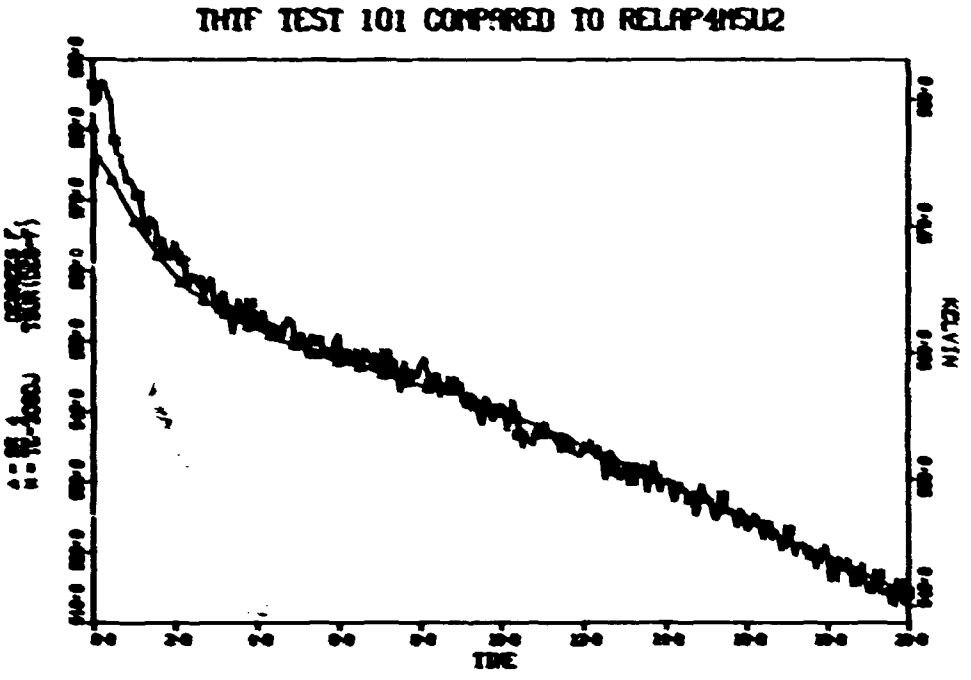

Fig. III.15. Surface temperature, rod 9, level J.

IV. TEST 102

IV.1. Description

Test 102, the third test in the THTF with bundle 1 in place,[4] was conducted on June 18, 1976, to investigate the thermal-hydraulic response of the THTF under full-power steady-state and blowdown conditions. This was the first full-power (122-kW/rod) test performed in the facility. The electric core and primary coolant pump were tripped, and closure of the main heat exchanger secondary side valves was initiated coincident with rupture. The THTF fluid conditions immediately preceding rupture are presented in Table IV.1 and IV.2.

Test 102 provided operational verification of the mechanical and electrical systems used to control the THTF under the full range of powered conditions. The steady-state data obtained during test 102 comprises the initial calibration data base for the electric core thermocouples and the flow instrumentation. In order to provide as much safety margin as possible and still obtain full-power verification of the data and safety systems, the electric core power was tripped coincident with rupture. The transient data, therefore, provides a baseline case for departure from nucleate boiling (DNB) and critical heat flux (CHF) comparisons with other tests in the series.

IV.2. Thermal Hydraulics

Test 102 was the first THTF blowdown experiment performed with full-power bundle and fluid conditions. Like tests 100 and 104, the break area was divided equally between the inlet and the outlet. The hydraulic transient in test 102 was similar to those for tests 103, 104, and 105, since initial fluid temperatures were nearly the same. The power to the rod bundle was tripped at 0.05 sec after rupture.

A typical spool piece pressure response is shown in Fig. IV.1. Starting from 47.5 MN/m^2 (2250 psig), the pressure drops to 43.6 MN/m^2 (1900 psig), which is the saturation pressure of the hot-leg fluid. The pressure rebounds slightly while the fluid in the pressurizer expands rapidly and

Table IV.1. Desired vs actual prerupture conditions - test 102

Parameters	Desired[1]	Actual[2]
System pressure (PE-201)	15.513 MN/m² (2250 psig)	15.513 MN/m² (2250 psig)
Core power (EIE-9, EIE-10, EIE-11, EIE-12, EIE-9, EIE-17, EIE-11, EIE-12)	3.678 MW	3.672 MW
Voltage decay constant	1	1
Core volumetric flow rate (FE-19)	1.1265 m³/sec (4270 gpm)	1.027 m³/sec (4274 gpm)
Test section inlet temperature (TE-142)	559.1 K (547°F)	559.2 K (547°F)
Test section outlet temperature (TE-222)	620.4 K (656°F)	607.1 K (633°F)
Pressurizer		
Pressure (PE-136)	14.896 MN/m² (2227 psig)	14.869 MN/m² (2217 psig)
Mass liquid water (LT-130)	52.24 kg (115 lb_m)	43.91 kg (96.72 lb_m)
Coolant pump		
Speed (SE-72)	59.67 rps (3580 rpm)	-
Pressure differential (P_dE-78)	4.423 MN/m² (644 psid)	4.442 MN/m² (644 psid)
Pressure between HCV-2 and FCV-18 (PE-16)	14.990 MN/m² (2465 psig)	14.692 MN/m² (2421 psig)
Pressure differential across main heat exchangers (P_dE-46)	0.159 MN/m² (23.0 psid)	0.407 MN/m² (59 psid)

[1]Desired prerupture conditions are based on programmatic requirements.

[2]Actual prerupture conditions are based on instrument signals recorded within 10 sec of primary system rupture.

[3]Instrument failed during test.

Table IV.2. Prerupture primary coolant temperature and pressure distribution[1] - test 102

Location	Instrument	Temperature [K (°F)]	Pressure [MN/m² (psig)]
Vertical inlet spool piece	TE-172	559.9 (548)	
Vertical inlet spool piece	PE-174		15.720 (2280)
Test section inlet	TE-142	558.2 (543)	
Lower plenum	TE-150	560.9 (550)	
Lower plenum	PE-156		15.679 (2274)
Upper plenum	PE-201		15.513 (2250)
Test section outlet	TE-212	607.0 (633)	
Vertical outlet spool piece	TE-222	606.5 (632)	
Vertical outlet spool piece	PE-224		15.417 (2236)
Heat exchanger inlet header	PE-44		15.203 (2205)
Mixed mean temperature downstream heat exchangers	TE-288	562.0 (552)	
Pressurizer surge line	TE-2	613.3 (649)	
Pressurizer	PE-106		14.989 (2174)
Primary pump suction	PE-76		14.906 (2162)
Between main control valves HCV-2, FCV-18	TE-48	558.3 (542)	
Between main control valves HCV-2, FCV-18	PE-16		14.692 (2421)

[1]Prerupture distribution is based on instrument signals recorded within 10 sec of primary system rupture.

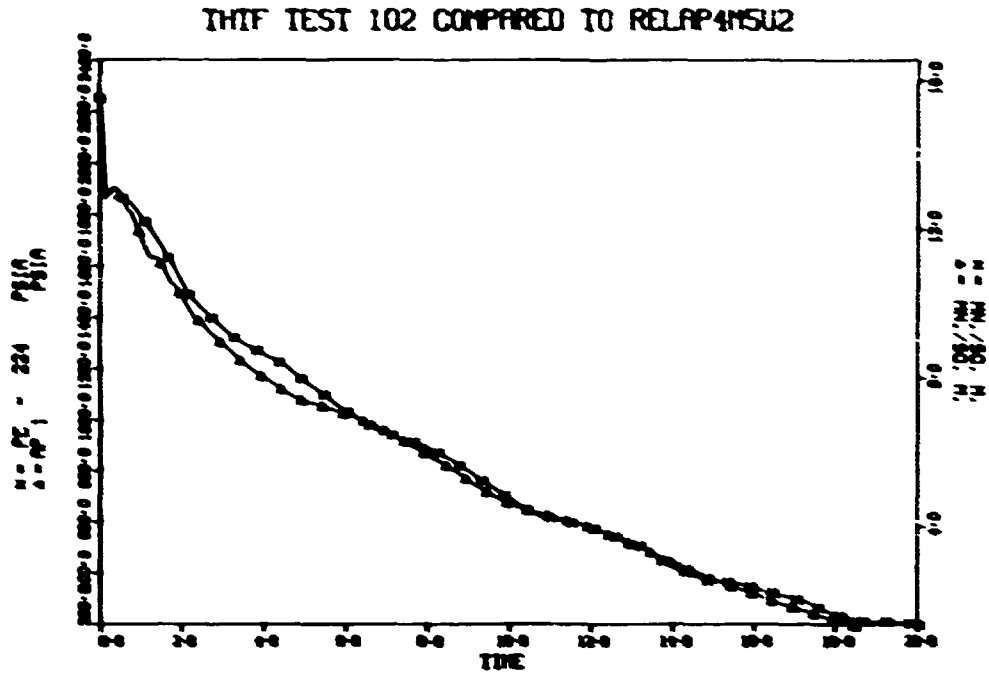

Fig. IV.1. Vertical outlet spool piece pressure.

cools. Water, which was initially between the heat exchanger outlet mixing tee and the pressurizer surge line, arrives at the outlet at 3 sec (Fig. IV.2). After passage of this "plug" of fluid, more rapid depressurization resumes at 4.5 sec. When fluid at the inlet horizontal spool piece flashes at 7 sec, the depressurization again slows; the predicted pressure shows the same effect beginning at 5 sec. Subsequent fluctuations in the pressure coincide with arrival of "plugs" of low-quality fluid at the outlet blowdown plenum from the horizontal outlet piping.

The calculated and measured pressure differentials across the main heat exchangers and their control valves are shown in Fig. IV.3. The difference quickly becomes negative as the front-side pressure drops below that of the back and flow reverses through the heat exchangers and bypass. Although several large fluctuations in this pressure difference were measured, they were not predicted by RELAP. These may correspond to smaller measured fluctuations occurring at the same times at the horizontal outlet spool piece turbine meter and densitometer (Fig. IV.2). Large pressure drops also occur across the flow-control valves downstream of the primary

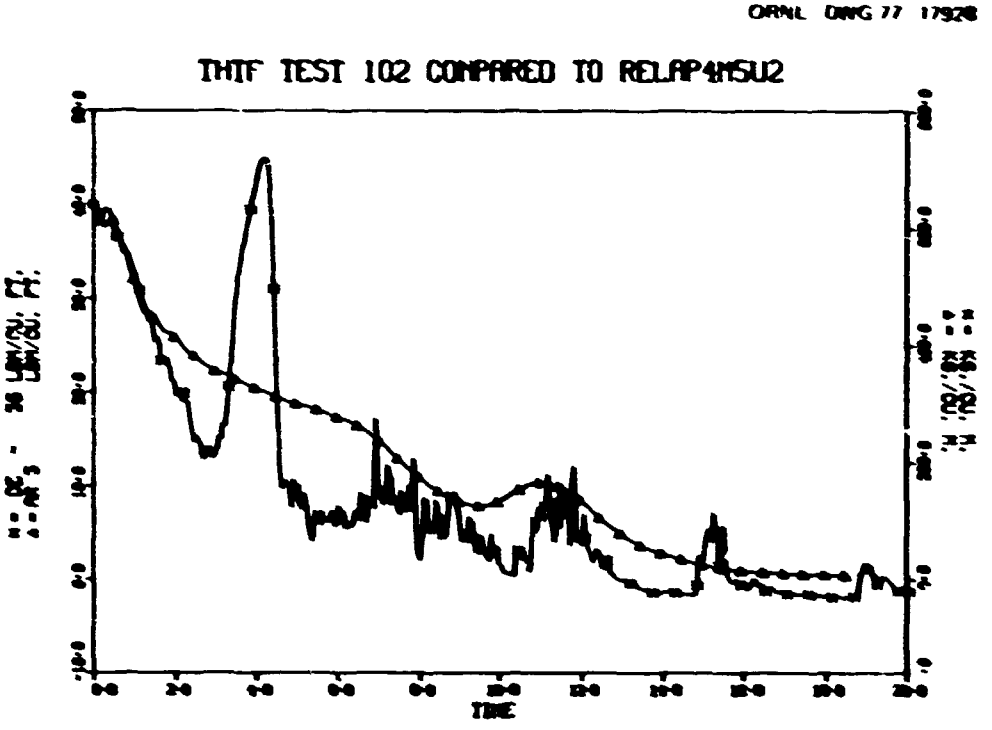

Fig. IV.2. Horizontal outlet spool piece density.

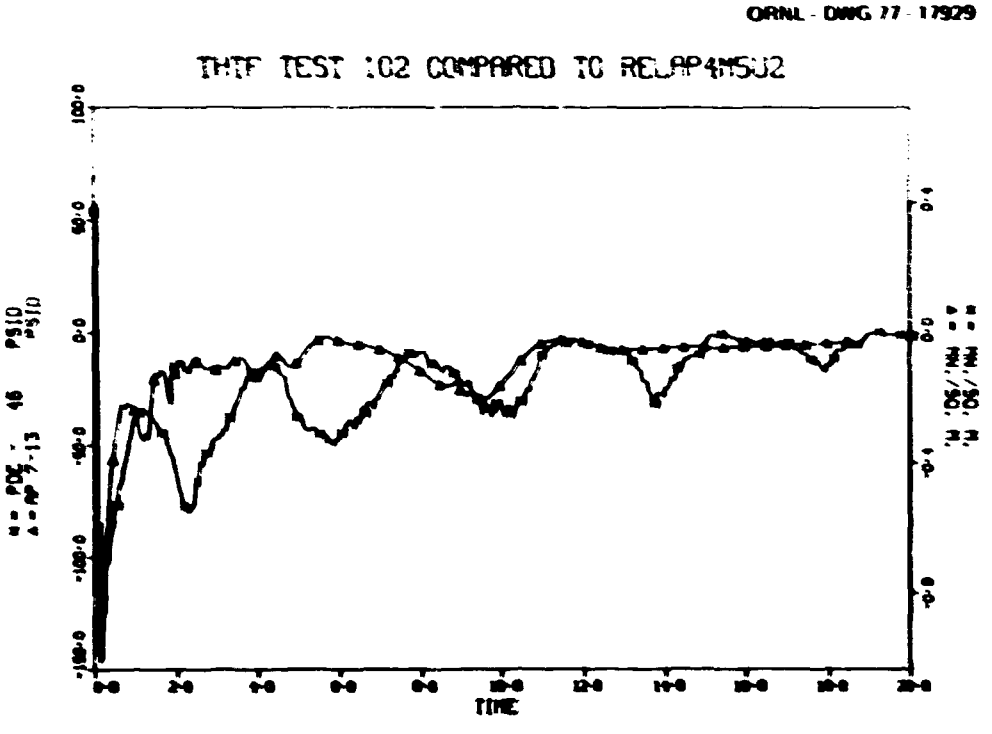

Fig. IV.3. Main heat exchanger pressure difference.

pump. The RELAP-calculated pressure between the two valves has the same relationship to the absolute pressure recorded there by PE-16 as it does elsewhere in the THTF. The recorded pressure difference across the rod bundle in test 102 (Fig. IV.4) indicates the driving forces which result in predominantly negative core flows for the first 5 sec and mostly positive core flows thereafter.

Except in a few cases, test section fluid temperatures decrease with system pressure because the fluid is saturated. Dryout was detected by most subchannel thermocouples at 18 to 20 sec; RELAP predicted the same effect at 15 sec (Fig. IV.5). Some core superheat is also predicted at 5.5 sec, but it was not measured.

Plots of heater rod surface temperatures for test 102 show a temperature rise occurring at the lower axial levels where hotter fluid passes levels initially in subcooled forced convection. Except for that early increase, most ORINC surface temperature curves are similar to depressurization curves. Typical traces appear in Figs. IV.6, IV.7, and IV.8 for levels E, G, and J, respectively. A temperature excursion suggesting

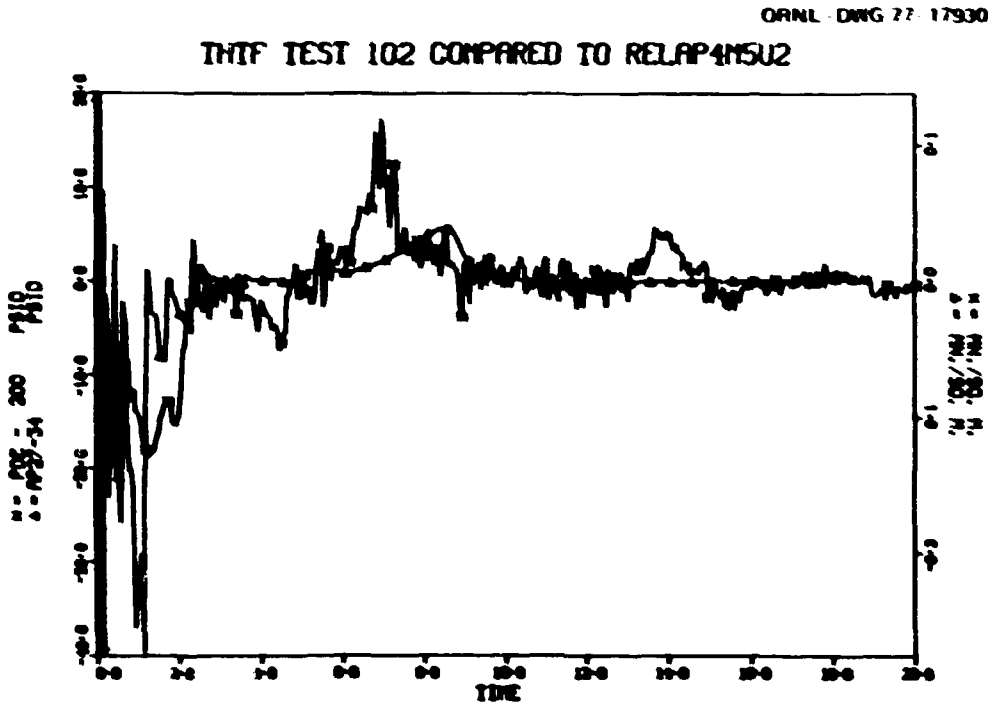

Fig. IV.4. Rod bundle pressure difference.

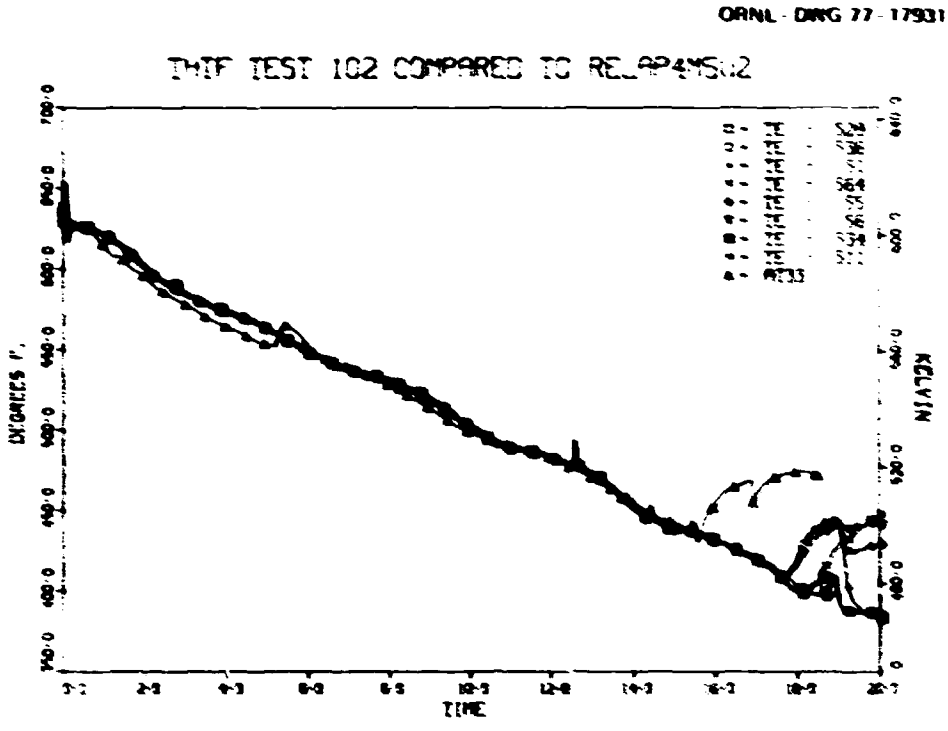

Fig. IV.5. Test section subchannel temperatures.

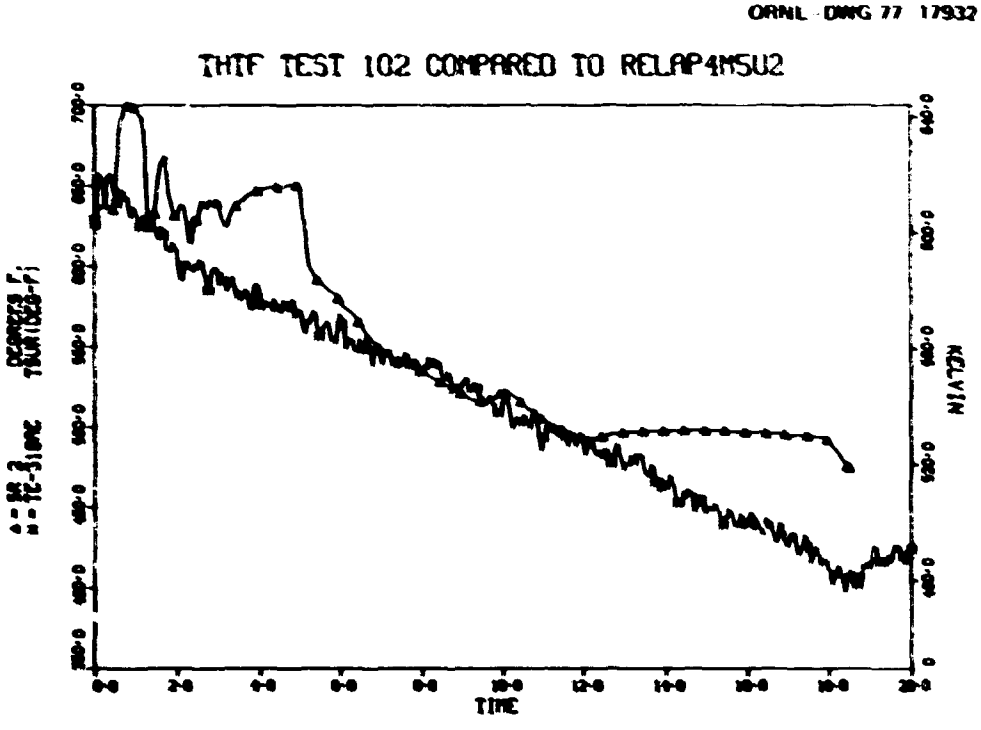

Fig. IV.6. Surface temperature, rod 18, level E.

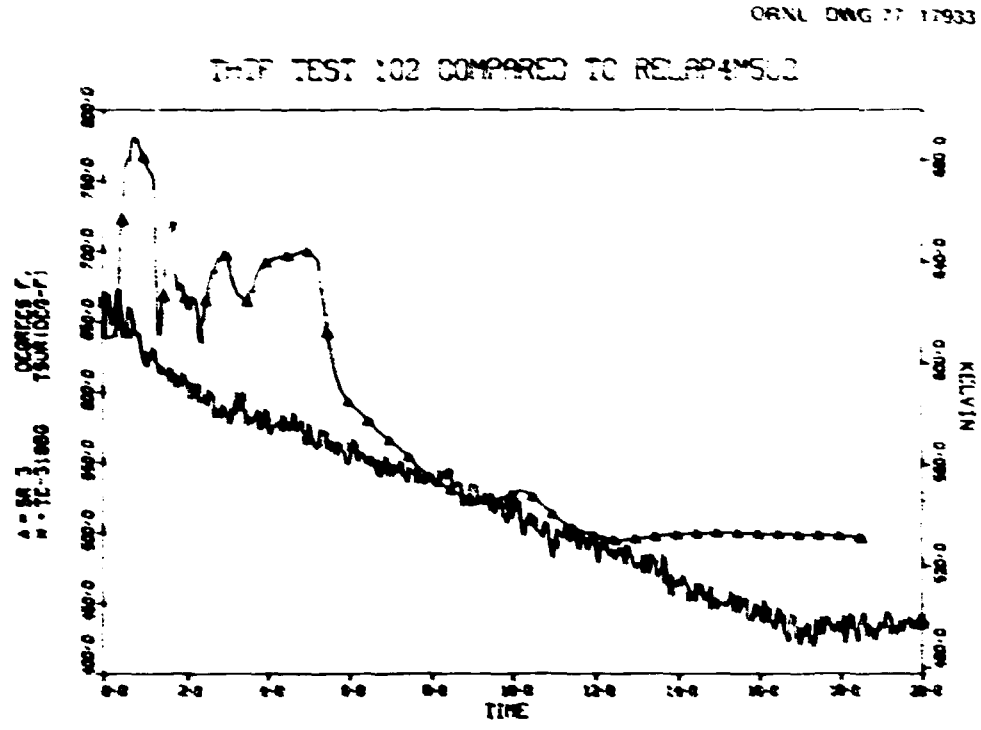

Fig. IV.7. Surface temperature, rod 18, level G.

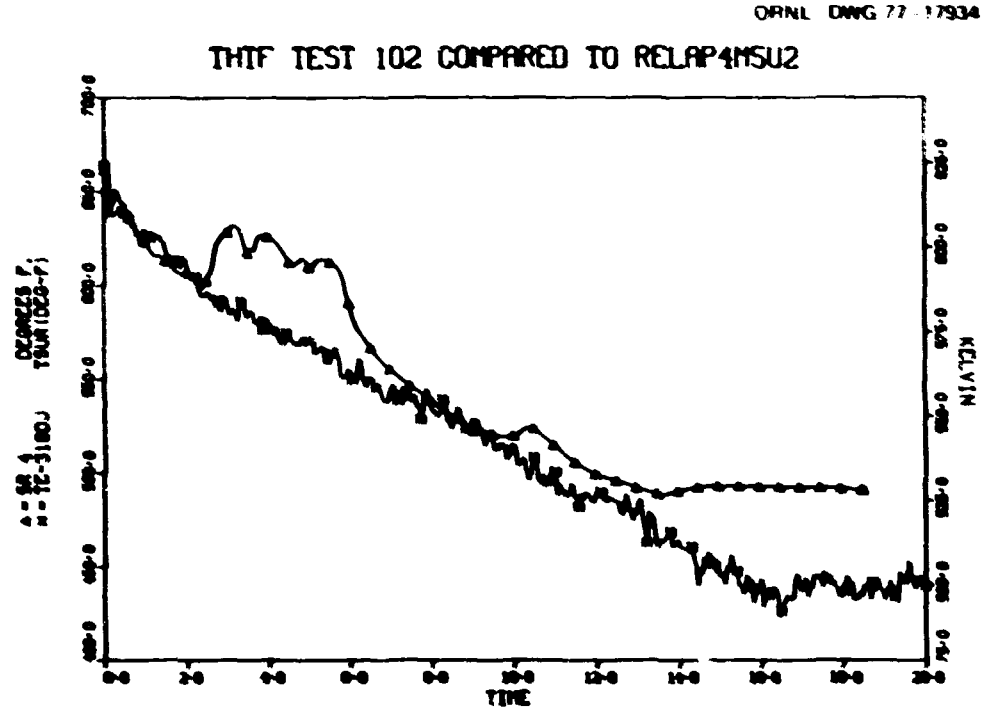

Fig. IV.8. Surface temperature, rod 18, level J.

departure from nucleate boiling was noted at level D at 0.5 sec (Fig. IV.9). RELAP calculations tend to overpredict surface temperatures for test 102, especially for the first 7 sec.

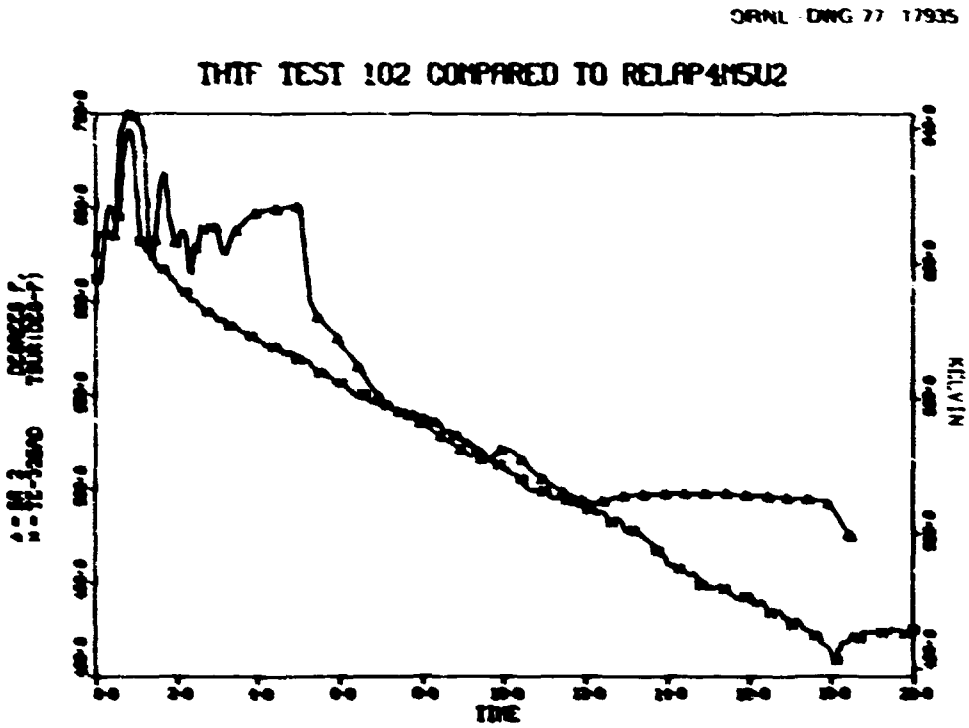

Fig. IV.9. Surface temperature, rod 25, level D.

V. TEST 103

V.1. Description

Test 103, the fifth test in the THTF with bundle 1 in place,[5] was conducted on August 5, 1976, to obtain hydraulic design information for test 105. It was a full-power (122-kW/rod) test with a 40% inlet–60% outlet break having a total area of 12.54 cm^2 (0.0135 ft^2). The electric core was maintained at full power for 2 sec into the transient. The primary coolant pump was tripped coincident with rupture, and closure of the main heat exchanger secondary side valves was initiated at power trip. The THTF fluid conditions immediately preceding rupture are presented in Tables V.1 and V.2.

Test 103 provided experimental verification of the RELAP prediction of spool piece flows with a 40% inlet–60% outlet break. This break configuration was predicted by RELAP to approximate most accurately the core flows of an NRC PWR double-ended guillotine break study. Test 105 was scheduled to approximate these supplied flows as closely as possible.

Test 103 provided the second CHF test for bundle 1. The different break ratio produced a time and spatial translation in the core thermal response. The extent of these translations provided data to compare with RELAP predictions.

V.2. Thermal Hydraulics

In test 103, the pressure as a function of time appears essentially the same throughout the loop, and the RELAP-predicted pressures have approximately the same relationship to the data throughout the loop. A representative comparison of RELAP-predicted pressure and the measured pressure (from the horizontal outlet spool piece) is presented in Fig. V.1. The resurgence in the pressure occurring very early in the transient is caused by the pressurizer. With the opening of the rupture disks, a rapid depressurization begins at the breaks and results in a depressurization wave propagating around the loop. When this wave reaches the surge line to the pressurizer, the pressurizer begins to discharge into the loop. This

Table V.1. Desired vs actual prerupture conditions - test 2A1

Parameters	Desired[1]	Actual
System pressure (PE-201)	15.513 MN/m² (2250 psig)	15.561 MN/m² (2257 psig)
Core power (EEE-4, EEE-10, EEE-11, EEE-12, EIE-4, EIE-10, EIE-11, EIE-12)	5.475 MW	5.475 MW
Voltage decay constant	2	2
Core volumetric flow rate (FE-14)	2.0265 m³/sec (4420 gpm)	2.027 m³/sec (4427 gpm)
Test section inlet temperature (TE-102)	559.3 K (547°F)	558.2 K (545°F)
Test section outlet temperature (TE-212)	591.4 K (depth°F)	606.3 K (632°F)
Pressurizer		
Pressure (PE-10a)	15.231 MN/m² (2180 psig)	15.30 MN/m² (2220 psig)
Mass liquid water (LT-100)	91.30 kg (201 lb_m)	88.94 kg (196.04 lb_m)
Coolant pump		
Speed (SE-7a)	54.67 rps (3280 rpm)	57.12 rps (3407 rpm)
Pressure differential (P_dE-7b)	4.413 MN/m² (640 psid)	4.473 MN/m² (649 psid)
Pressure between HCV-2 and FCV-18 (PE-19)	16.896 MN/m² (2465 psig)	16.927 MN/m² (2455 psig)
Pressure differential across main heat exchangers (P_dE-4a)	0.172 MN/m² (25 psid)	0.193 MN/m² (28 psid)

[1]Desired prerupture conditions are based on programmatic requirements.

Actual prerupture conditions are based on instrument signals recorded within 10 sec of primary system rupture.

Table V.2. Prerupture primary coolant temperature and pressure distribution - test 2A1

Location	Instrument	Temperature K (°F)	Pressure MN/m² (psig)[1]
Vertical inlet spool piece	TE-102	558.2 (545)	
Vertical inlet spool piece	PE-10a		15.496 (2248)
Test section inlet	TE-102	558.2 (545)	
Lower plenum	TE-150	560.4 (550)	
Lower plenum	PE-15a		15.755 (2285)
Upper plenum	PE-201		15.561 (2257)
Test section outlet	TE-212	606.5 (632)	
Vertical outlet spool piece	TE-212	606.5 (632)	
Vertical outlet spool piece	PE-12a		15.436 (2242)
Heat exchanger inlet header	PE-4a		15.496 (2248)
Mixed mean temperature downstream heat exchangers	TE-298	565.8 (557)	
Pressurizer surge line	TE-2	566.4 (560)	
Pressurizer	PE-10a		15.306 (2220)
Primary pump suction	PE-7a		15.279 (2216)
Between main control valves HCV-2, FCV-18	TE-48	536.5 (542)	
Between main control valves HCV-2, FCV-18	PE-18		16.927 (2455)

[1]Prerupture distribution is based on instrument signals recorded within 10 sec of primary system rupture.

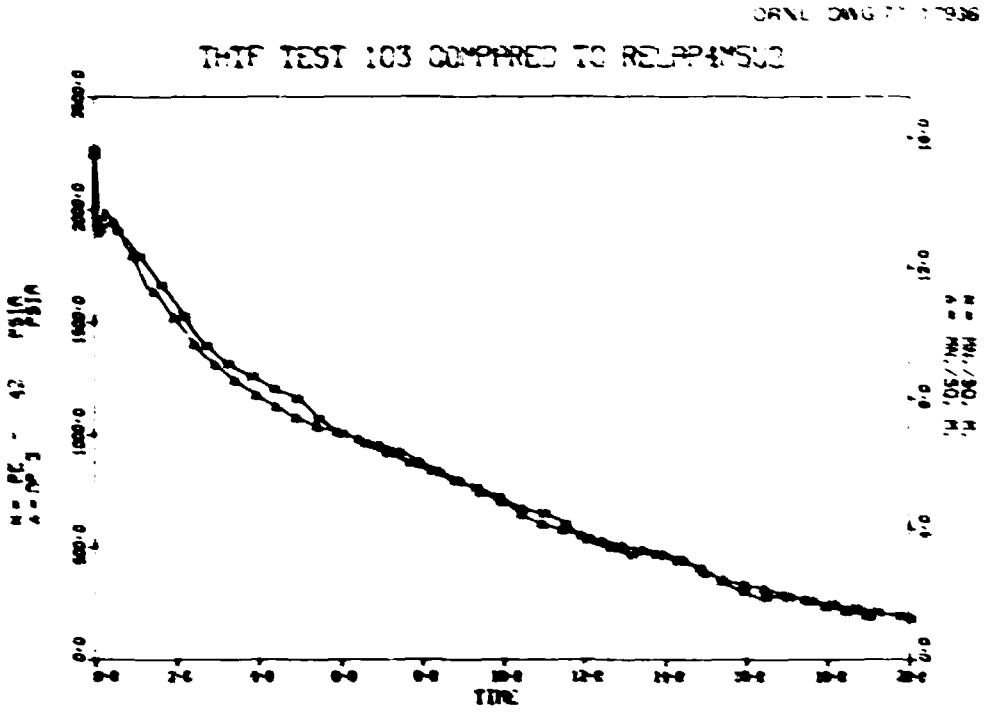

Fig. V.1. Horizontal outlet spool piece pressure.

discharge produces a repressurization wave which propagates back toward the breaks, resulting in a resurgence in the pressure. This resurgence is most evident at the spool pieces since they have undergone the greatest depressurization. RELAP predicts too small a drop in pressure and too high a resurgence throughout the loop except for the pressurizer itself, where no resurgence is predicted.

After the resurgence, RELAP's predicted pressure falls too low and remains too low for 6 sec, while the experimental data exhibit a marked decrease in the depressurization rate beginning at 3 sec. This coincides with the arrival at the outlet break of the water which was initially between the heat exchanger outlet and the pressurizer surge line. This water was subcooled, but by the time it arrived at the outlet break, the pressure had fallen to its saturation level, and the quality was very low or zero, as can be seen on the horizontal outlet spool piece densitometer (Fig V.2). Until the arrival of this "plug" of very low-quality water, the water being expelled through the break is of higher quality and has a relatively high volumetric flow. As the low-quality plug is being pushed

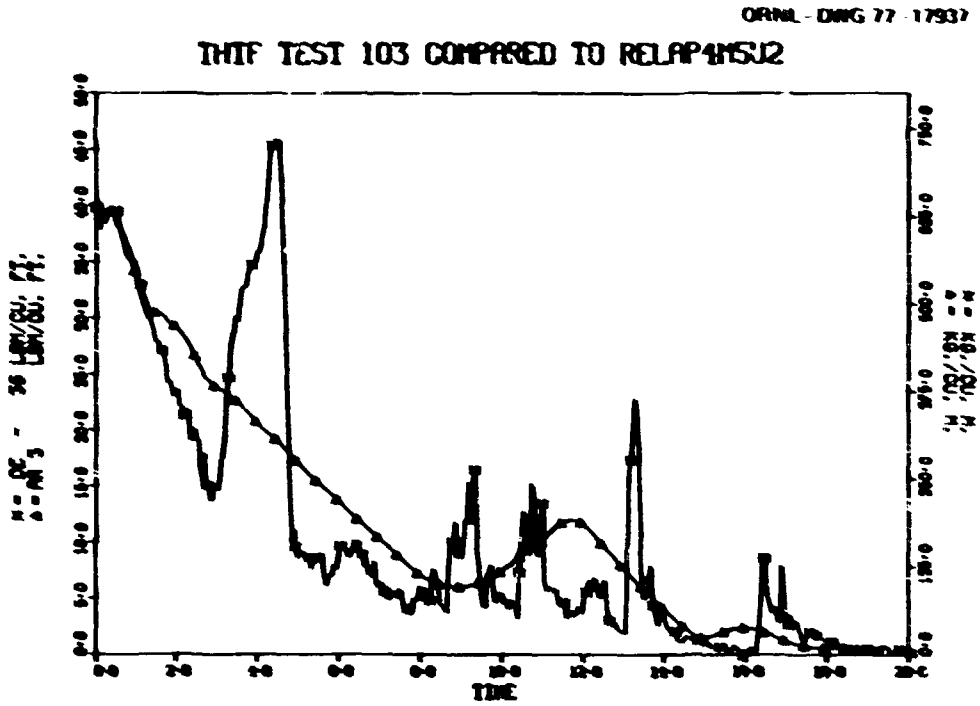

Fig. V.2. Horizontal outlet spool piece density.

toward the break, the expansion of the two-phase pressurizer water behind it allows the depressurization of the pressurizer fluid. When the plug arrives, the volumetric flow toward the outlet break decreases due to the higher density of the water. The higher density more than compensates for the increased mass flow from the break permitted by the lower enthalpy of the plug. Thus, the expansion of two-phase pressurizer fluid is slowed, causing a decrease in the depressurization rate throughout the loop. Higher volumetric flow, and correspondingly increased depressurization, resumes when the low-quality plug is expelled at 5 sec. RELAP does not exhibit this sharp slowing of depressurization.

Beyond 10 sec, both RELAP's prediction and the measured pressures have small, gentle fluctuations that coincide with their respective increases in density at the horizontal outlet spool piece. RELAP's prediction is in good agreement with the actual pressures after 6 sec. The fluid at the outlet break and adjoining spool pieces saturates immediately in test 103. Thus, the densities measured in the horizontal and vertical outlet spool pieces (Figs. V.2 and V.3, respectively) show an initial drop

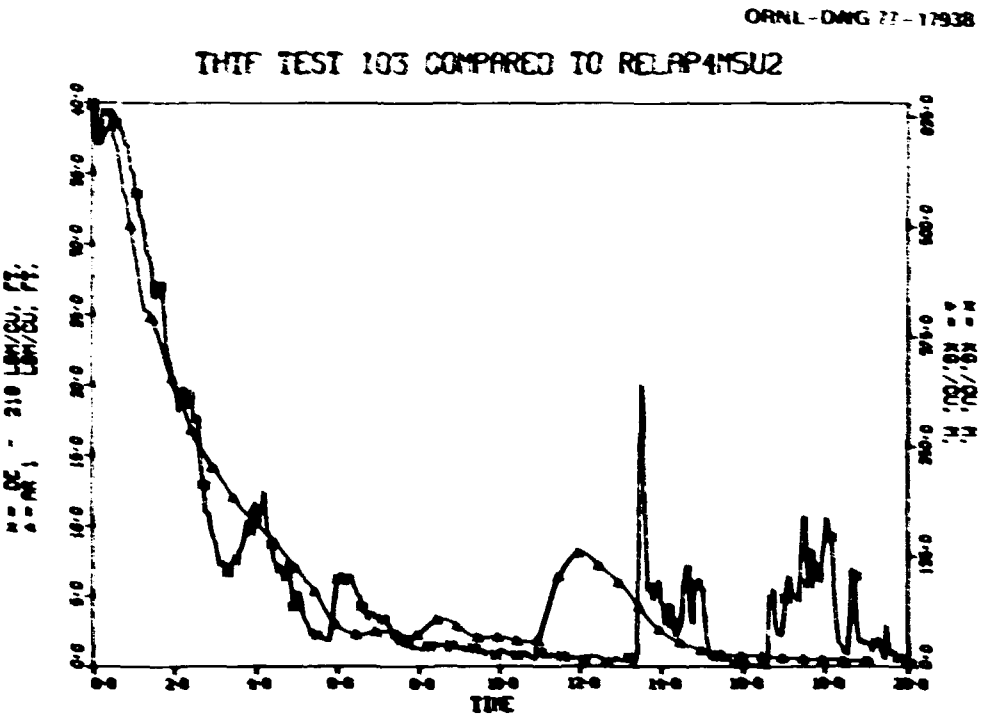

Fig. V.3. Vertical outlet spool piece density.

followed by a brief rise due to compression from the early pressure resurgence. (Note that the ordinates of these two graphs are different.) RELAP's predicted pressure resurgence, which was both early and too large, is clearly seen in the early density prediction for the vertical outlet spool piece. After the density increase, the densities begin to decrease with the depressurization. At the horizontal outlet spool piece, the data show the arrival (at about 3 sec) of the low-quality plug mentioned previously. The low-quality fluid has remained intact, causing large, sharp density changes. RELAP's prediction, however, indicates that this low-quality water has lost its integrity. It begins to arrive slightly after 1 sec and portions of it continue to arrive after 6 sec. Thus, RELAP's pressure prediction did not show the sharp decrease in the depressurization rate caused by the plug. This low-quality water surges upward into the vertical outlet spool piece, probably accounting for the rise in density observed at 4 sec. At this point, almost all the mass being discharged by the break consists of the low-quality fluid. A second smaller amount of low-quality fluid arrives at the horizontal and

vertical outlet spool pieces at 6 sec. The reason for this second density increase is uncertain. As with the first arrival of dense fluid, RELAP's prediction distributes the lower quality fluid. The late-transient density increases are believed to originate in the discharge of cold water from the heat exchangers; their appearance at the vertical outlet is again due to the passage of fluid upward from the break plenum. The largest of these occurs at 14 sec. RELAP's prediction mixes these later and separate arrivals of low-quality fluid into gradual density surges spread over time.

In contrast to the outlet, the inlet spool piece densitometers indicate late saturation (Figs. V.4 and V.5). The saturation of fluid at the vertical inlet occurs at 2 sec due to the arrival of hot fluid from the core. This can be seen by examining the temperature data (Fig. V.6). Although showing lower densities just before saturation, RELAP predicts saturation approximately 0.5 sec late. The horizontal inlet fluid saturates later, just before 7 sec, while RELAP's prediction of saturation is almost 2 sec early. Having noted that RELAP's pressure prediction is too

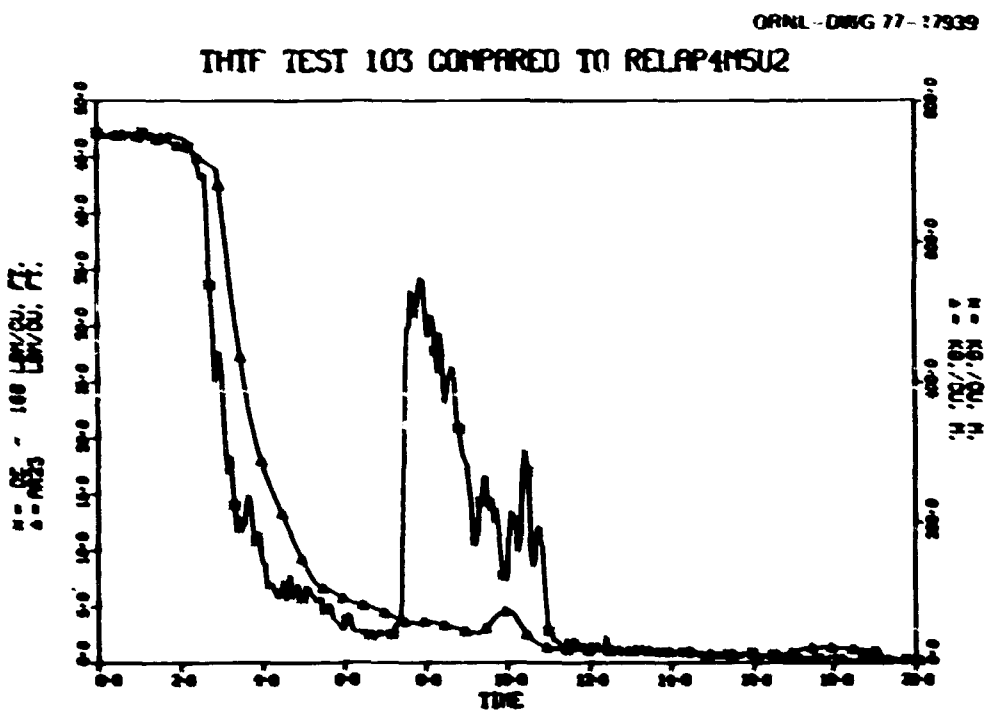

Fig. V.4. Vertical inlet spool piece density.

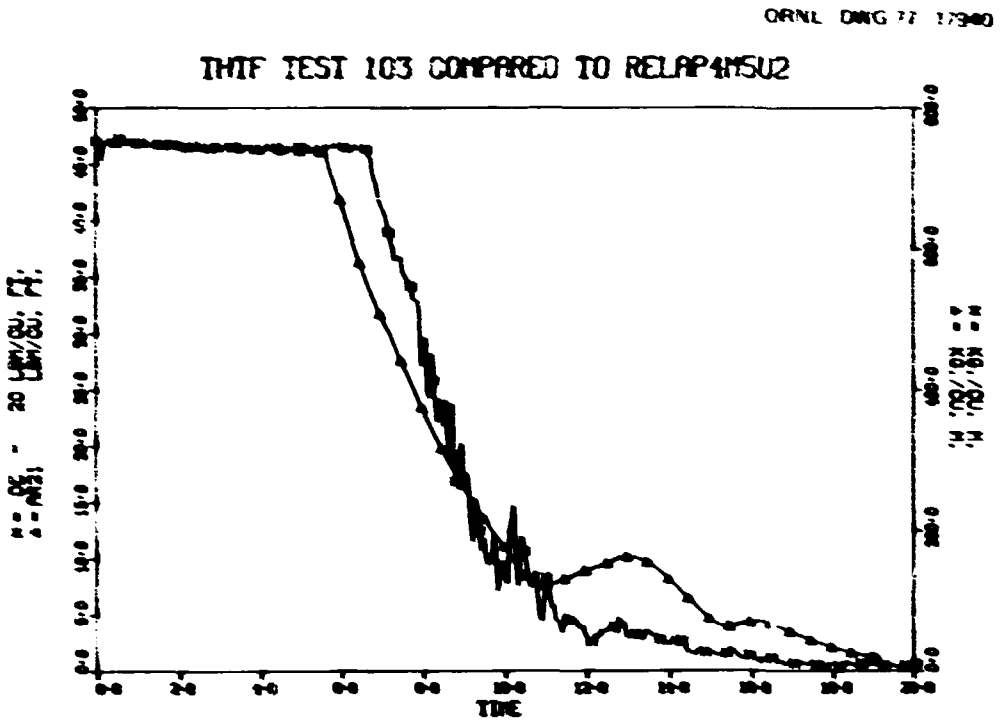

Fig. V.5. Horizontal inlet spool piece density.

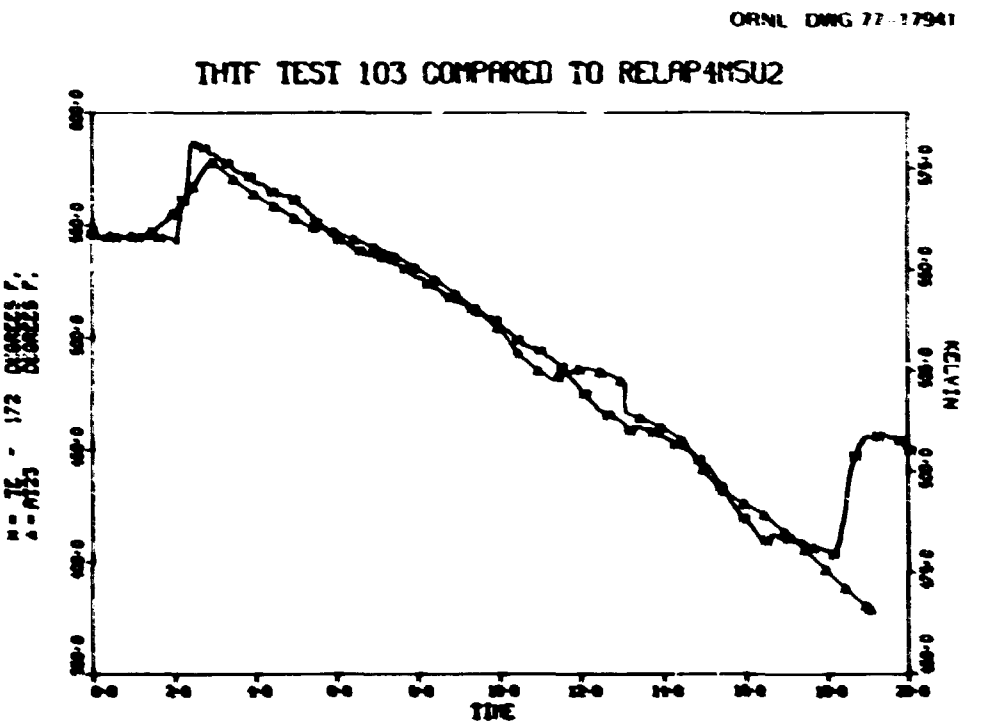

Fig. V.6. Vertical inlet spool piece temperature.

low, early saturation is not surprising. The vertical inlet density shows a sharp increase just after 7 sec, probably due to a flow reversal in the vertical piping at the break. As the mass capable of being discharged by the breaks decreases due to decreasing pressure, the horizontal inlet piping, which still contains subcooled fluid, begins to supply a larger percentage of the flow for the inlet break, much as the horizontal outlet piping does at the outlet break earlier in the transient. At the same time, the plug of subcooled fluid at the outlet break, which had prevented flow from the vertical outlet piping, has been discharged, so that flow toward the outlet break may resume. These factors together initiate a deceleration and eventual reversal of the flow in the vertical inlet piping. This begins at 5 sec, with the flow finally reversing near 7 sec. The saturation of the horizontal inlet fluid and its attendant increase in enthalpy contribute to this effect by further decreasing the flow which the inlet break can discharge. RELAP does not predict this density increase at the vertical inlet. Late in the transient, RELAP's density prediction for the horizontal inlet shows two gradual density increases not found in the experimental data.

Outside of the core, most fluid in the loop is two-phase throughout the transient. Thus, the predicted and measured temperatures show the same relationship as the predicted and measured pressures. The three temperature comparisons which prove informative are those for the vertical and horizontal inlet spool pieces and the vertical outlet spool piece (Figs. V.6 to V.8). The vertical inlet spool piece temperature (Fig. V.6) shows the arrival of hotter core fluid, causing saturation. This figure also shows why RELAP predicts saturation late; the arrival of hotter fluid is spread out over time, with part arriving early and a reduced amount arriving later. This effect lowers the temperature predicted by RELAP near the time of saturation, causing late saturation even though RELAP's predicted pressure is too low. After saturation, the temperatures at the vertical inlet reflect the pressure prediction until 18 sec, when a burst of superheated steam, not predicted by RELAP, arrives from the core. The horizontal inlet temperature comparison shows that RELAP predicts the arrival of hotter fluid from the pressurizer too soon, and this, combined with RELAP's low pressure prediction, causes early saturation.

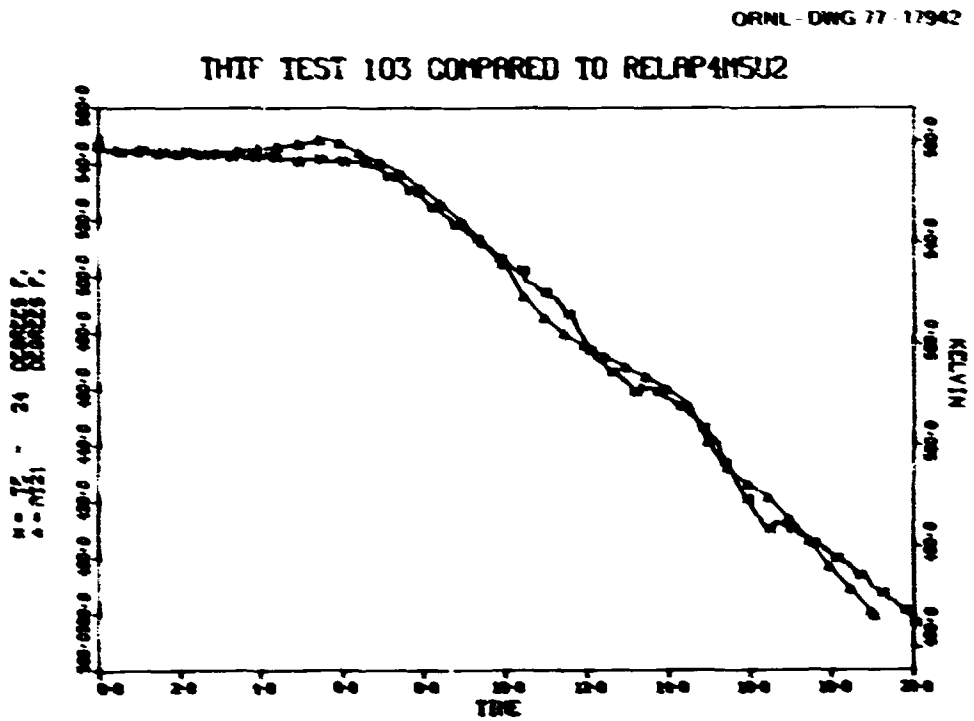

Fig. V.7. Horizontal inlet spool piece temperature.

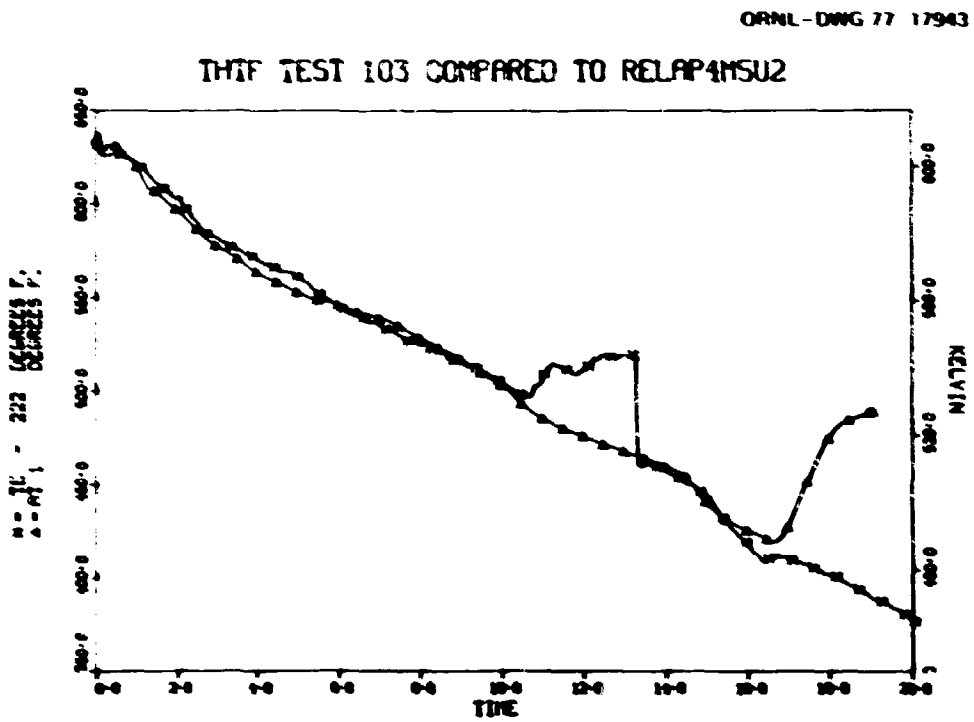

Fig. V.8. Vertical outlet spool piece temperature.

The vertical outlet spool piece temperature shows the arrival of superheated steam from the core at 10 sec. The return to saturation between 13 and 14 sec coincides with the largest late-transient density increase shown on the vertical outlet density plot (Fig. V.3).

The last portion of loop hydraulics to be examined is volumetric and mass flows. The flow data are useful in indicating trends and major shifts in the flow, but the magnitude is questionable (see Chapter I). The volumetric flow, both measured and predicted, is presented in Figs. V.9 to V.12. In test 103, the vertical inlet turbine meter signal incorrectly reversed polarity shortly after the blowdown began. Figure V.9 presents an inversion of the experimental readings taken; therefore, the first few tenths of a second must be ignored. RELAP's predicted volumetric flow is not in good agreement with the turbine meter data, but the significance of this is uncertain due to the possible errors in the turbine measurements. RELAP's prediction has most of the major characteristics of the data, although usually shifted in time and magnitude. Previously, the low-quality surge appearing on the vertical outlet density plot at 4 sec was stated to have originated in the horizontal outlet

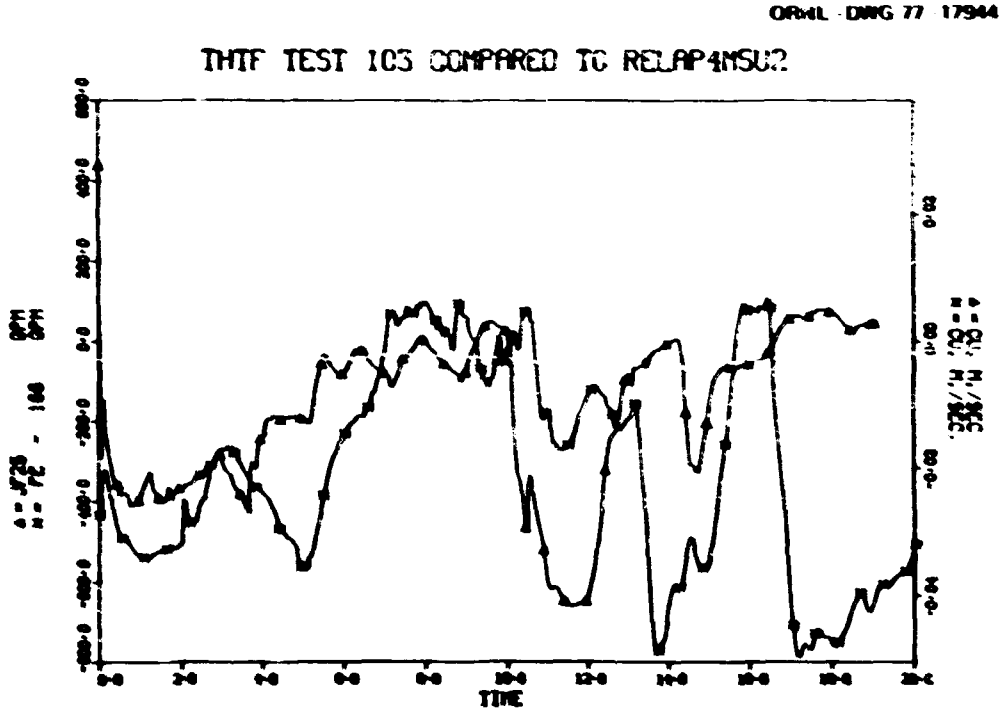

Fig. V.9. Vertical inlet spool piece volumetric flow (corrected).

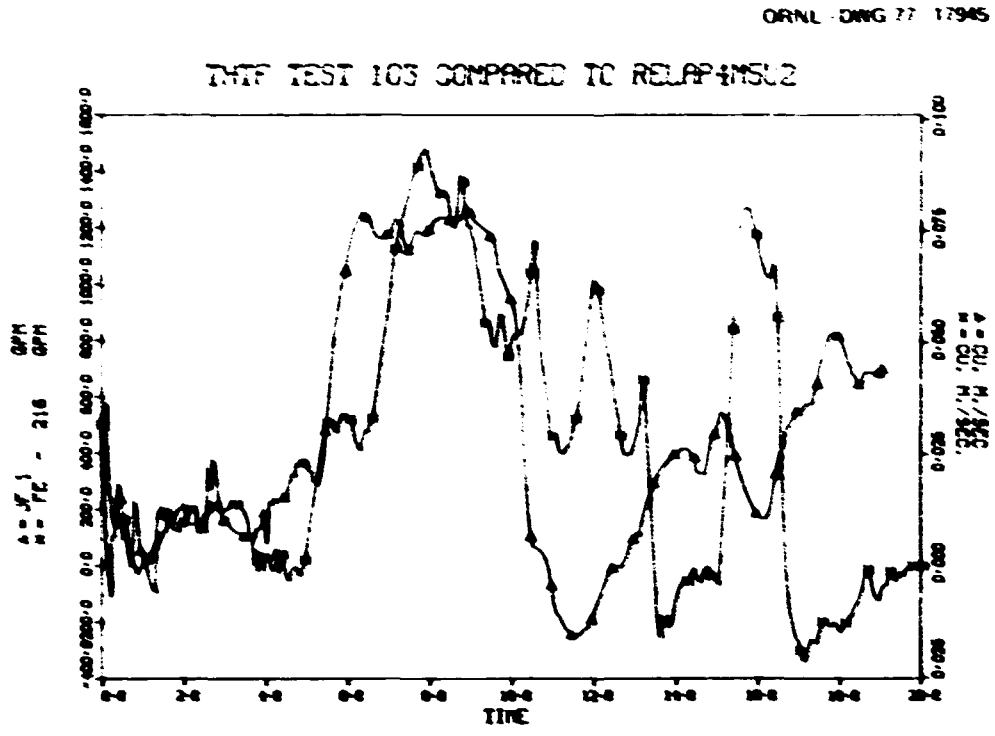

Fig. V.10. Vertical outlet spool piece volumetric flow.

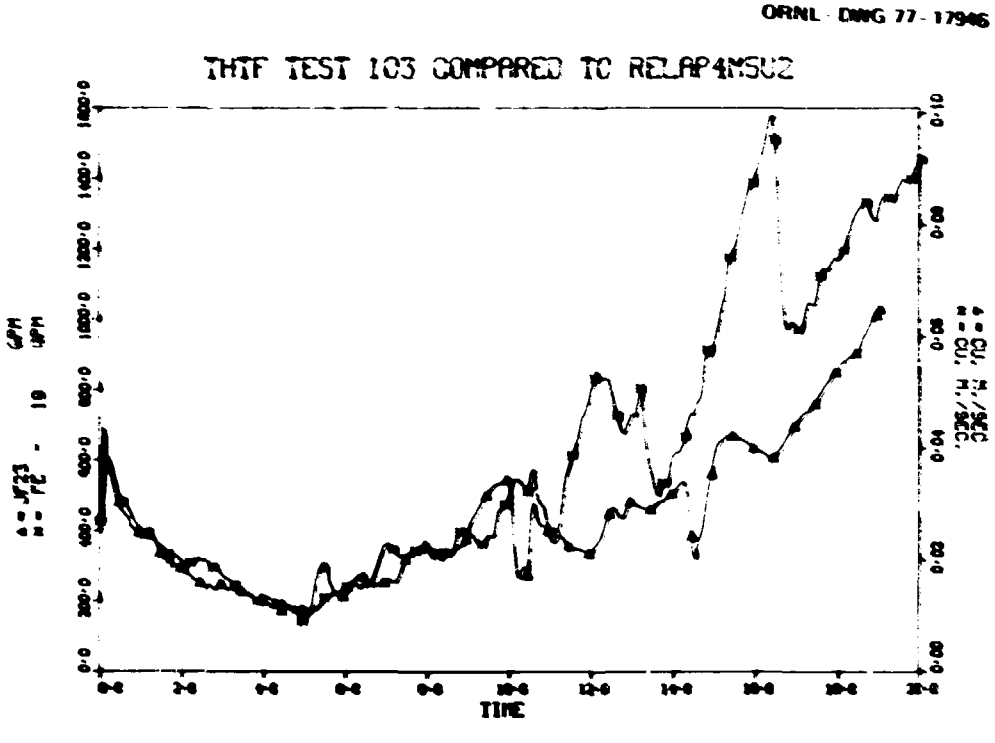

Fig. V.11. Horizontal inlet spool piece volumetric flow.

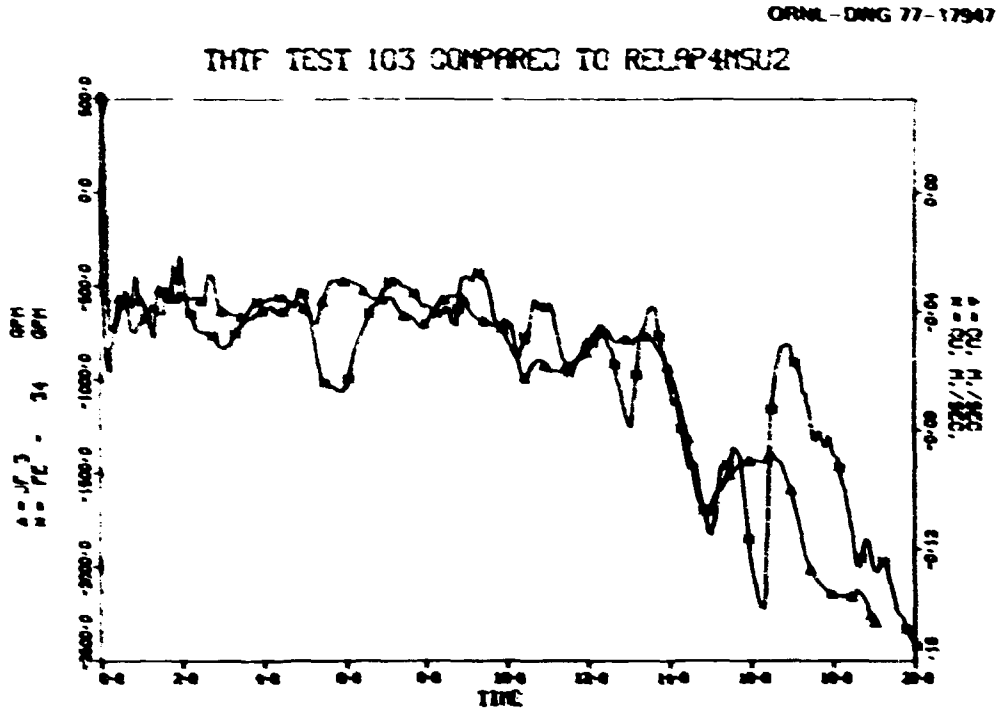

Fig. V.12. Horizontal outlet spool piece volumetric flow.

spool piece. This appears on the vertical outlet turbine meter as a drop from 200 gpm to near or below zero (Fig. V.10). The density increase at 14 sec appears on the turbine meter plot as a sharp reversal. It was also stated earlier that a flow reversal in the vertical inlet that began at 5 sec culminated in a low-quality surge from the horizontal inlet just after 7 sec. This reversal appears in the experimental data on the vertical inlet turbine meter plot. RELAP's prediction shows a marked decrease in the flow toward the break from just before 4 to 5 sec; thus, RELAP's decrease in flow anticipates the actual reversal by 1 or 2 sec. This reversal is also apparent in the vertical outlet turbine meter as a sharp resumption in flow toward the outlet break. RELAP predicts this flow increase too early by more than 1 sec.

The mass flow comparisons between RELAP's predictions and those calculated from experimental data are presented in Figs. V.13 to V.16. Both methods of calculating mass flow mentioned earlier are included; one, designated GG1, uses only the turbine meters and densitometers and assumes no slip; the other, designated GG4, uses the Aya method and includes the drag

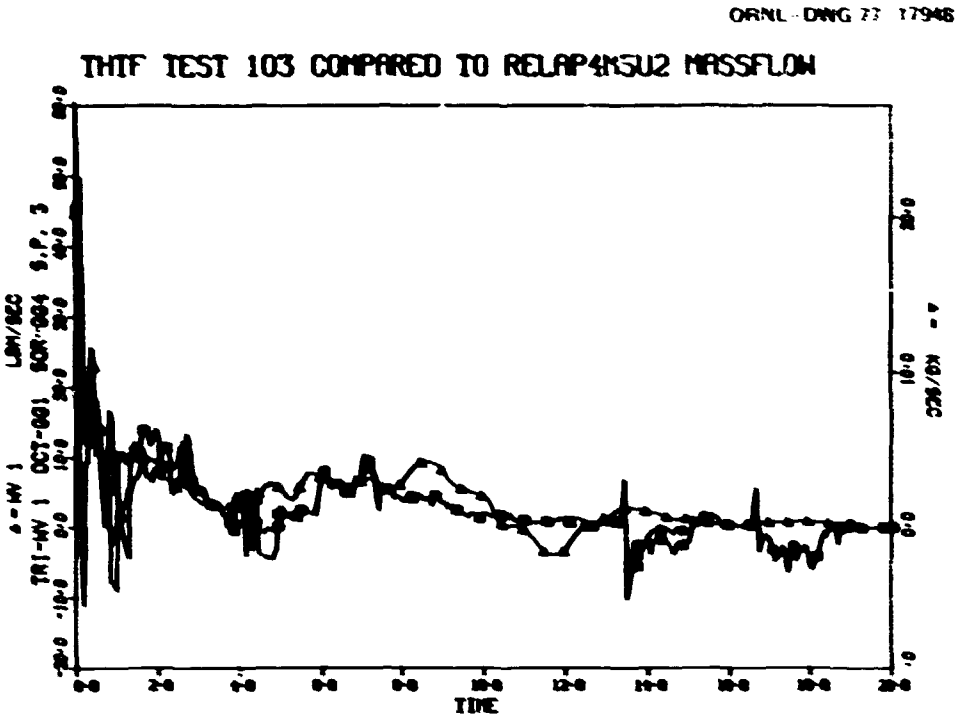

Fig. V.13. Vertical outlet spool piece mass flow.

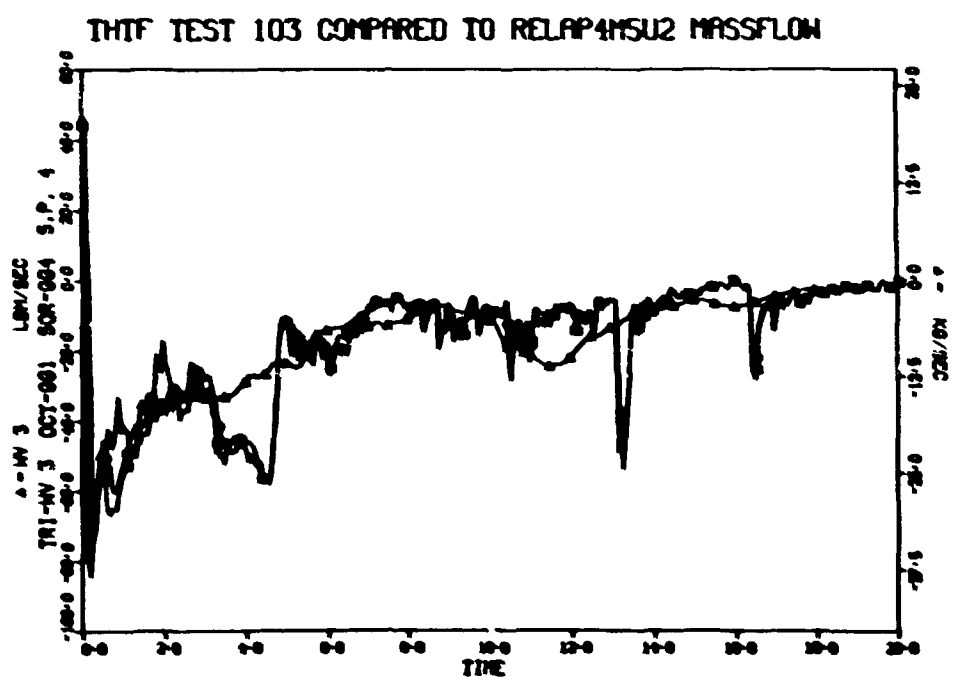

Fig. V.14. Horizontal outlet spool piece mass flow.

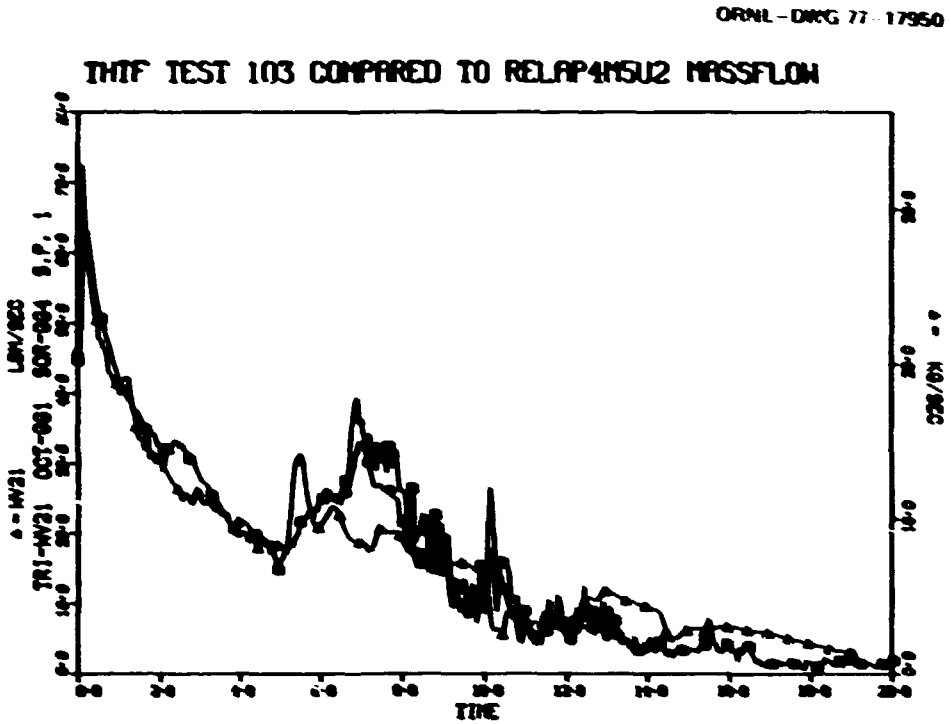

Fig. V.15. Horizontal inlet spool piece mass flow.

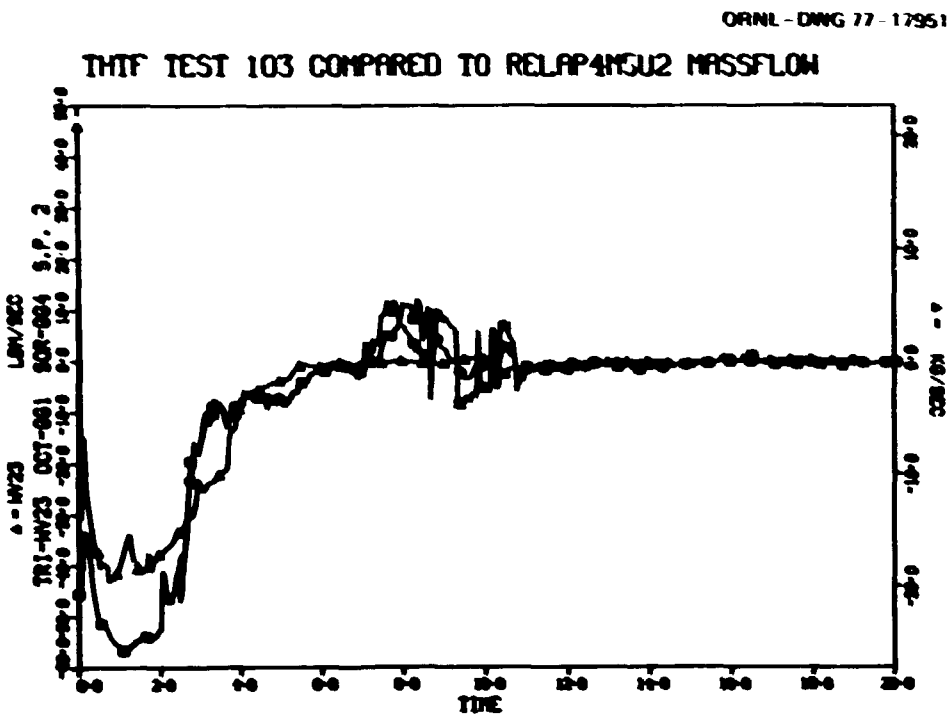

Fig. V.16. Vertical inlet spool piece mass flow.

disks in the calculation. As with the volumetric flow comparisons, RELAP's predicted mass flows are not in close agreement with calculated ones. Once again, the uncertainties in the calculated numbers must be considered (see Chapter I). The vertical outlet mass flow calculation (Fig. V.13) drops to, and oscillates about, zero in the period from 3 to 5 sec, corresponding to the arrival of the subcooled block of fluid at the horizontal outlet spool piece. At 5 sec, as the subcooled fluid is expelled, saturated pressurizer fluid begins to flow through the horizontal outlet piping and the calculated mass flow there sharply decreases (Fig. V.14). The mass flow at the horizontal inlet spool piece increases from 5 to 7 sec with the flow reversal occurring in the vertical inlet piping and decreases after 7 sec with saturation (Fig. V.15). The vertical inlet mass flow shows a marked decrease between 2 and 3 sec, coinciding with saturation.

Finally, comparisons between the predicted and measured rod and fluid behavior in the core are presented. Since detailed analysis of core phenomena and RELAP's ability to predict them will be provided in a subsequent report, only a portion of the data is presented here. There are four thermocouples in the lower plenum. Two of these four, located 90° to the left and right of the direction from which the water enters the test section, show a period of superheat from 2 to 6 sec (Fig. V.17). The remaining two thermocouples, located at 0 and 180° from the direction of the water entering the test section, do not show this superheat, but rather decrease smoothly with depressurization after an initial temperature rise at 1 sec, similarly to that shown in the figure. This initial rise shown by all four thermocouples is due to the passage of water from the core region toward the inlet break. At the opposite end of the test section, numerous subchannel thermocouples have been placed between the rods above the heated zone. Eight of these thermocouples are compared with RELAP's predicted fluid temperature for the top of the core in Fig. V.18. As well as predicting too much superheat, RELAP also predicts that the superheat peaks at 5 sec instead of at 7 sec, when the maximum peak actually occurs. RELAP's superheat peak occurs during the time when RELAP is predicting the decrease in flow in the vertical inlet and the increase in flow in the vertical outlet. The actual superheat peak occurs

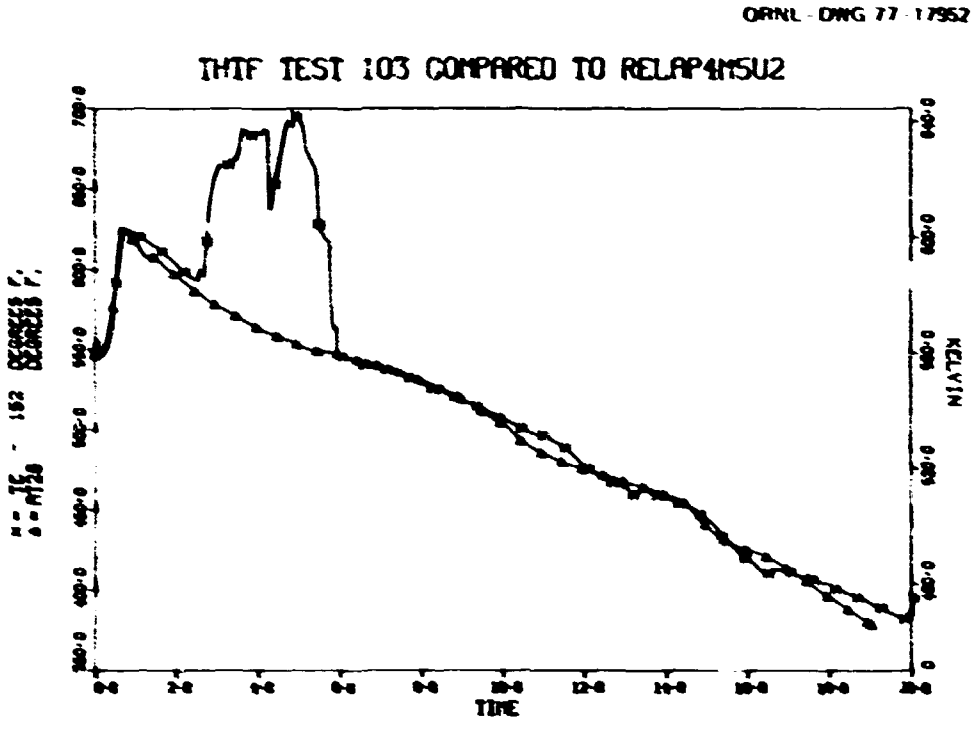

Fig. V.17. Lower plenum temperature.

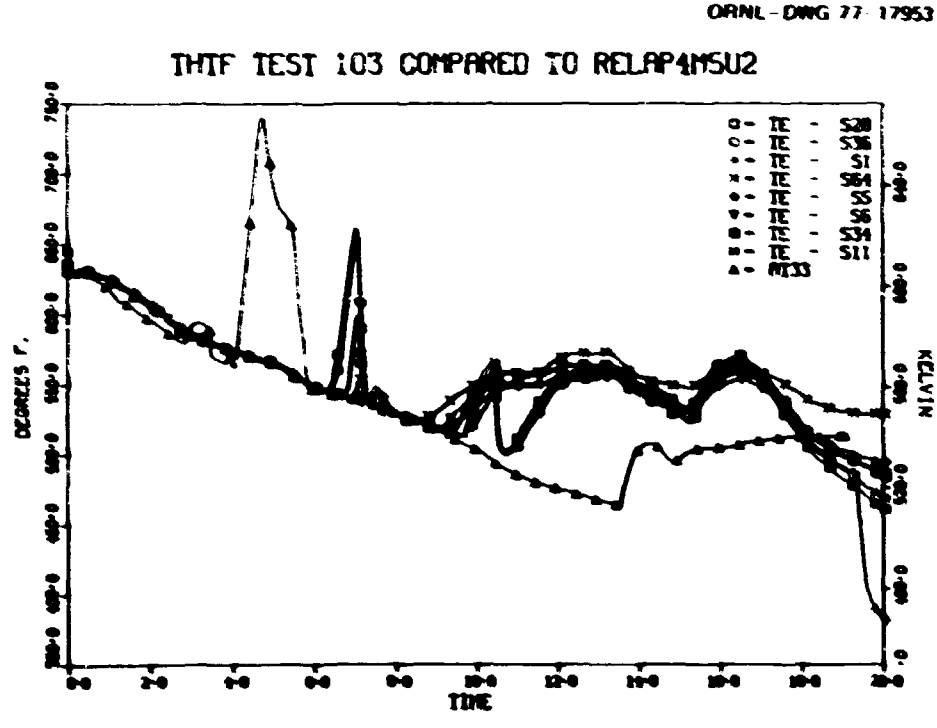

Fig. V.18. Test section subchannel temperatures.

during the actual flow reversal in the vertical inlet and increase in flow in the vertical outlet. This suggests that RELAP's early prediction of the flow change leads to the early prediction of the peak. The thermocouples with the larger peaks at 7 sec are near the center of the bundle and those with the smaller or nonexistent peaks are near the shroud box walls (Fig. I.4). All data channels show a return to superheat between 9 and 10 sec, presumably due to lack of water remaining in the core. RELAP predicts this phenomenon 4 sec late. The central subchannels show a dip in temperature at 11 sec, which is suggestive of a rewetting that the outside subchannels do not experience.

When considering the behavior of the rods themselves, the quantities of primary interest are the surface temperatures and surface heat fluxes. Temperatures and fluxes calculated from experimental data are compared to RELAP's predicted temperatures and fluxes in Figs. V.19 to V.24 for three different heights in the bundle for a typical rod. RELAP's predictions of surface temperature for positions high in the bundle are much worse than

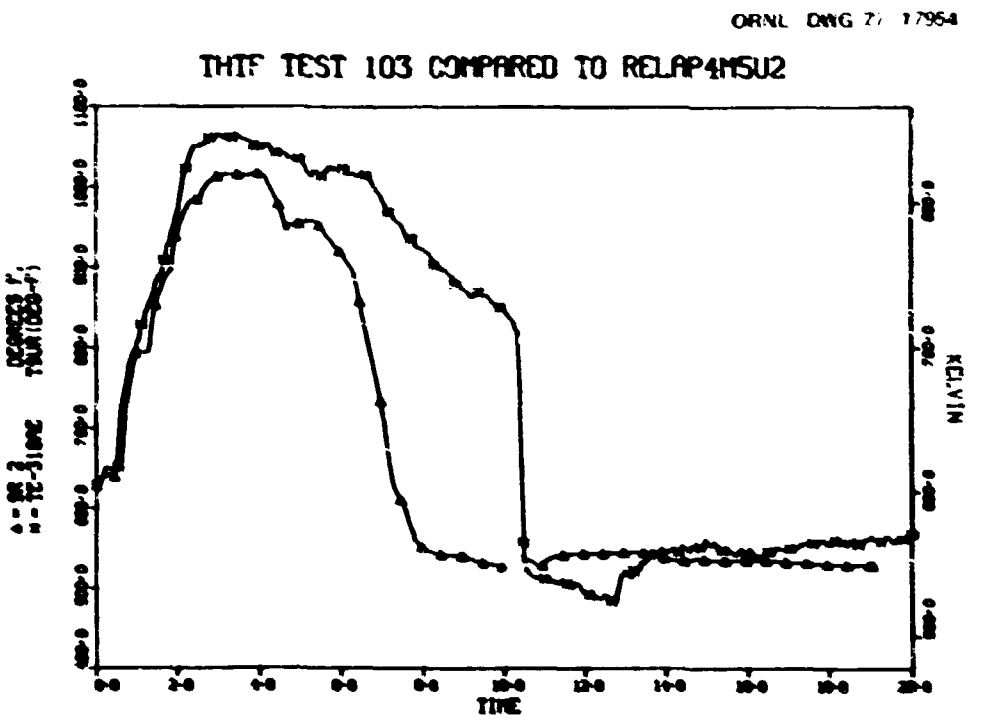

Fig. V.19. Surface temperature, rod 18, level E.

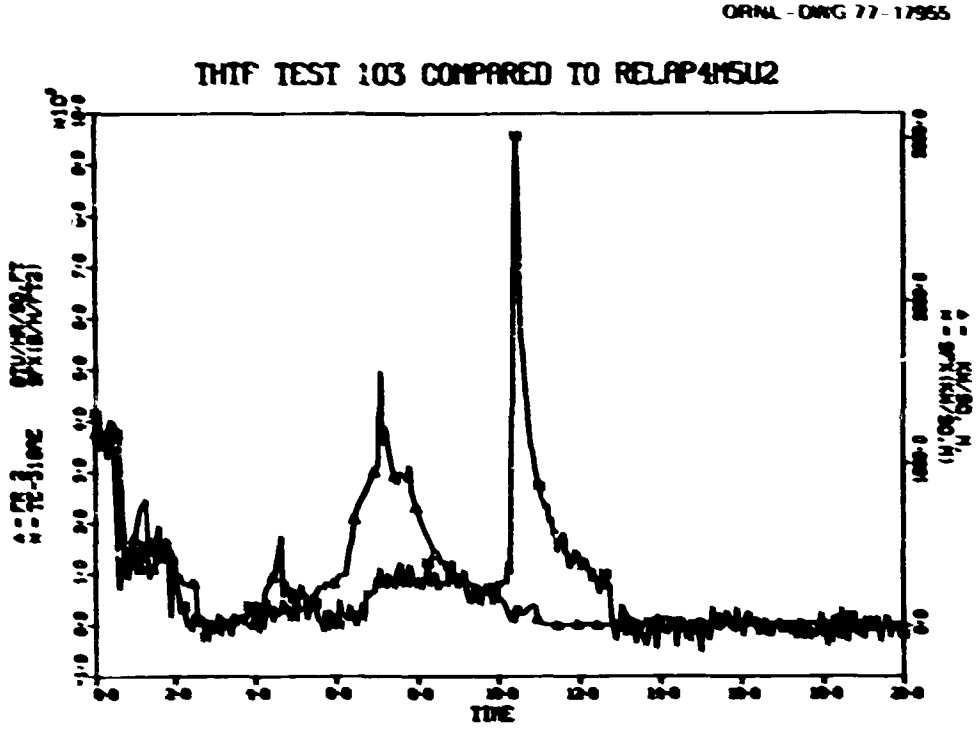

Fig. V.20. Surface heat flux, rod 18, level E.

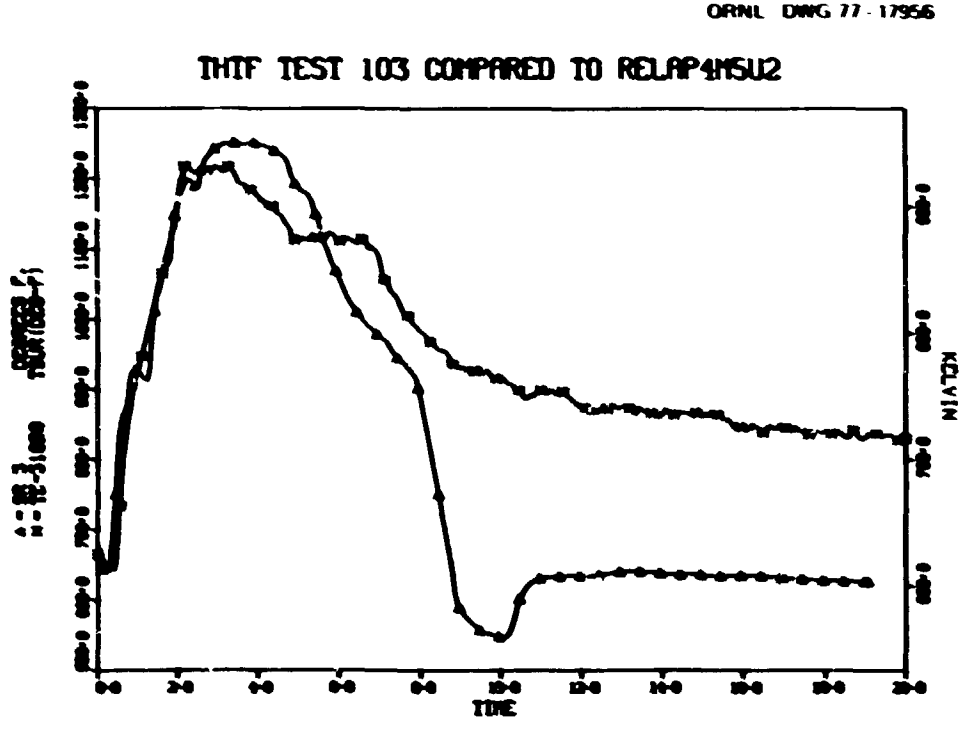

Fig. V.21. Surface temperature, rod 18, level G.

ORNL-DWG 77-17957

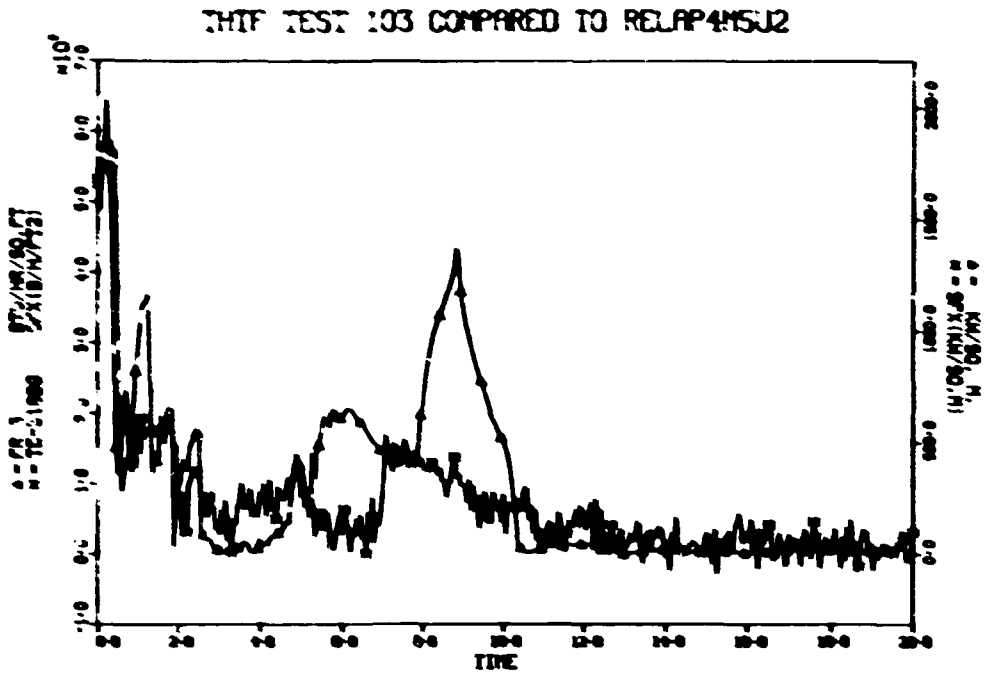

Fig. V.22. Surface heat flux, rod 18, level G.

ORNL DWG 77 17958

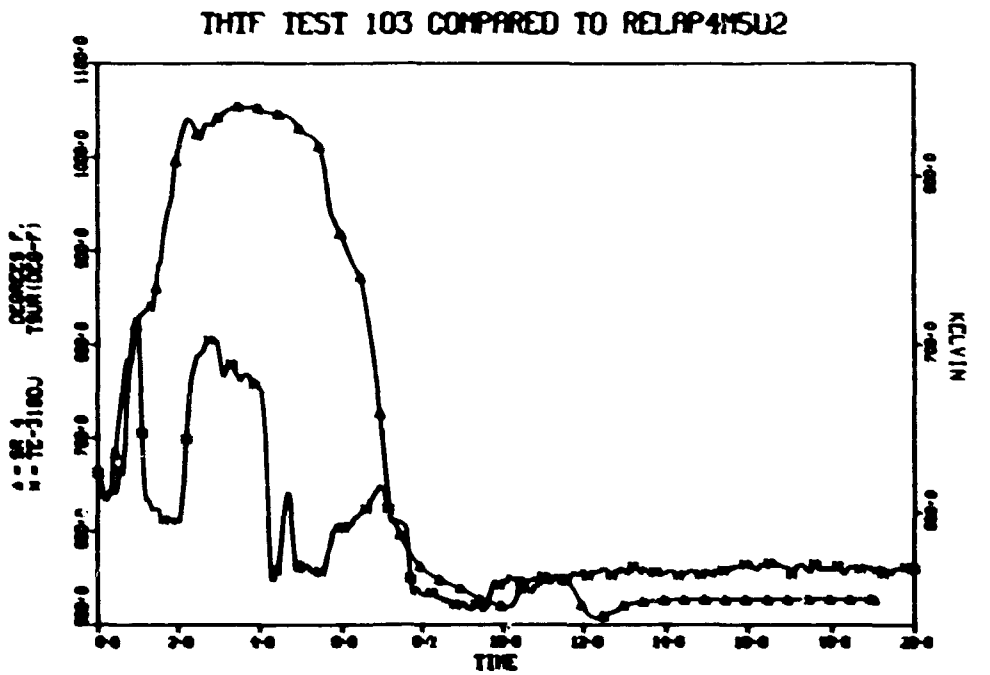

Fig. V.23. Surface temperature, rod 18, level J.

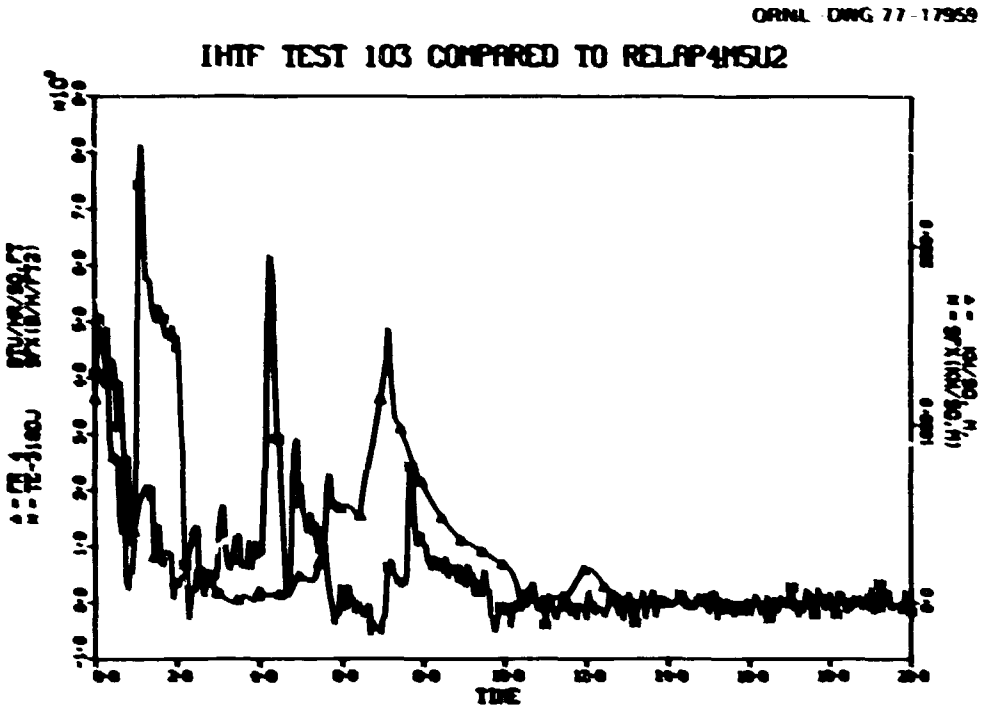

Fig. V.24. Surface heat flux, rod 18, level J.

those for lower in the bundle. The flux predictions follow the same pattern. The data used for these comparisons were taken from sheath thermocouples located near the axial centers of the rod sections modeled in RELAP. Since RELAP predicts a single set of average properties for the entire length of each modeled rod section, the comparisons vary somewhat from those shown when RELAP's prediction is compared to data taken from thermocouples at the ends of the modeled rod sections.

VI. TEST 104

VI.1. Description

Test 104, the fourth test with bundle 1 in place,[5] was conducted on July 8, 1976, to obtain CHF in bundle 1 under blowdown conditions. The break configuration was a 50% inlet–50% outlet break with a total area of 12.54 cm^2 (0.0135 ft^2). To produce CHF, the electric core was maintained at full power (122 kW/rod) for 2 sec into the transient. The primary coolant pump was tripped coincident with rupture, and closure of the main heat exchanger secondary side valves was initiated at power trip. The THTF fluid conditions immediately preceding rupture are presented in Tables VI.1 and VI.2.

Test 104 provided the first CHF and post-CHF heat transfer data in bundle 1. The transient data also provided the thermal-hydraulic response of the THTF under blowdown conditions with delayed power trip. Extensive steady-state data were taken to expand the bundle thermocouple and flow instrumentation calibration data base.

VI.2. Thermal Hydraulics

There are many similarities in the comparisons between the experimental data and RELAP predictions for tests 104 and 103. Since these common characteristics are detailed in Section V, the focus here will be on the differences between the two comparisons. Because the pressure comparisons for test 104 are similar to those for test 103, they are not presented in this section.

In test 104, all the densitometers except the vertical outlet spool piece densitometer failed at 15.5 sec. The measured and predicted density comparisons for the outlet spool pieces for test 104 (Figs. VI.1 and VI.2) are much like those for test 103. The arrival at the outlet of the block of subcooled fluid caused a greater surge upward into the vertical spool piece in test 104 than in test 103, but since test 104 had a smaller outlet break area, this is not surprising. The occurrence of several sharp density changes later in the transient is somewhat different in test 104

Table VI.1. Desired vs actual prerupture conditions - test 104

Parameters	Desired[a]	Actual[b]
System pressure (PE-201)	15.513 MN/m² (2250 psig)	15.586 MN/m² (2260 psig)
Core power (EHE-9, EHE-10, EHE-11, EHE-12, EIE-9, EIE-10, EIE- , EIE-12)	5.978 MW	5.975 MW
Voltage decay constant	0	0
Core volumetric flow rate (FE-19)	0.0283 m³/sec (420 gpm)	0.027 m³/sec (~25 gpm)
Test section inlet temperature (TE-162)	559.3 K (547°F)	559.8 K (548°F)
Test section outlet temperature (TE-212)	610.4 K (639°F)	606.5 K (632°F)
Pressurizer		
Pressure (PE-.06)	15.031 MN/m² (2180 psig)	15.210 MN/m² (2206 psig)
Mass liquid water (LT-100)	63.50 kg (140 lb_m)	55.88 kg (123.43 lb_m)
Coolant pump		
Speed (SE-72)	59.67 rps (3580 rpm)	59.68 rps (3581 rpm)
Pressure differential (P_dE-78)	.421 MN/m² (460 psid)	.482 MN/m² (450 psid)
Pressure between HCV-2 and FCV-18 (PE-16)	16.996 MN/m² (2465 psig)	17.037 MN/m² (2471 psig)
Pressure differential across main heat exchangers (P_dE-46)	0.172 MN/m² (25 psid)	0.186 MN/m² (27 psid)

[a] Desired prerupture conditions are based on programmatic requirements.

[b] Actual prerupture conditions are based on instrument signals recorded within 10 sec of primary system rupture.

Table VI.2. Prerupture primary coolant temperature and pressure distribution[a] - test 104

Location	Instrument	Temperature [K (°F)]	Pressure [MN/m² (psig)]
Vertical inlet spool piece	TE-172	559.3 (547)	
Vertical inlet spool piece	PE-174		15.686 (2275)
Test section inlet	TE-162	559.8 (548)	
Lower plenum	TE-150	560.9 (550)	
Lower plenum	PE-156		15.686 (2275)
Upper plenum	PE-201		15.586 (2249)
Test section outlet	TE-212	606.5 (632)	
Vertical outlet spool piece	TE-222	606.5 (632)	
Vertical outlet spool piece	PE-224		15.368 (2229)
Heat exchanger inlet header	PE-44		15.293 (2218)
Mixed mean temperature downstream heat exchangers	TE-208	561.5 (551)	
Pressurizer surge line	TE-2	615.9 (649)	
Pressurizer	PE-106		15.210 (2206)
Primary pump suction	PE-76		15.148 (2197)
Between main control valves HCV-2, FCV-18	TE-48	555.9 (541)	
Between main control valves HCV-2, FCV-18	PE-16		17.037 (2471)

[a] Prerupture distribution is based on instrument signals recorded within 10 sec of primary system rupture.

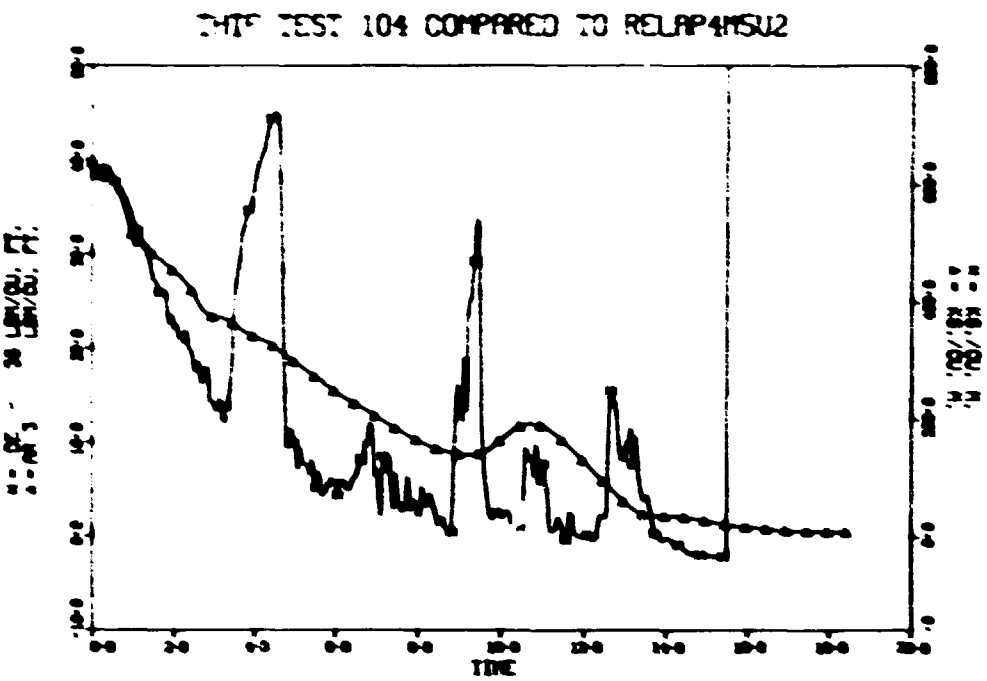

Fig. VI.1. Horizontal outlet spool piece density.

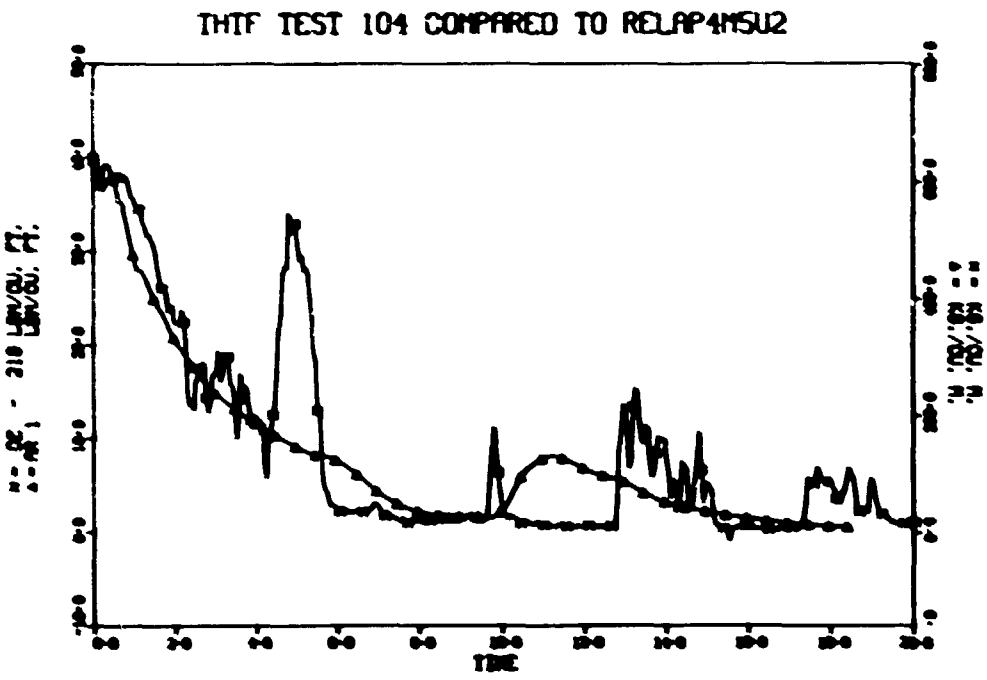

Fig. VI.2. Vertical outlet spool piece density.

than in test 103 for a reason we have not yet determined. As in test 103, RELAP's prediction smooths and spreads the sharp density shifts into smaller, longer density changes. The inlet density comparisons are so much like those of test 103 that they are not included.

The similarity of predicted and measured quantities extends to the temperatures outside the core. Once again, no plots are included. The occasion when superheat was shown in the response of the vertical outlet spool piece thermocouple for test 103 (Fig. V.8) does not appear in test 104; that thermocouple displays saturated temperatures throughout the transient.

Although the volumetric flow comparisons show some differences between the two tests, none are of particular significance. The mass flow comparisons show the same differences, so these are presented instead of the volumetric flows (Figs. VI.3 to VI.6).

The RELAP-predicted and the measured core temperatures show the same qualitative relationship for tests 103 and 104, but there is a marked difference in magnitudes. The two lower-plenum thermocouples show less

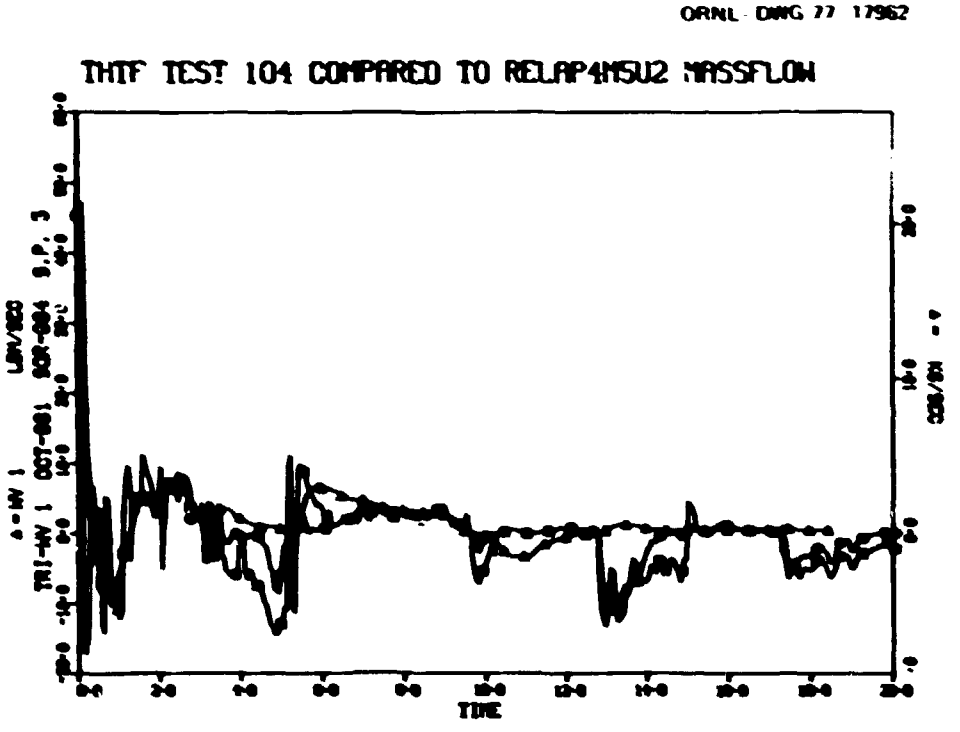

Fig. VI.3. Vertical outlet spool piece mass flow.

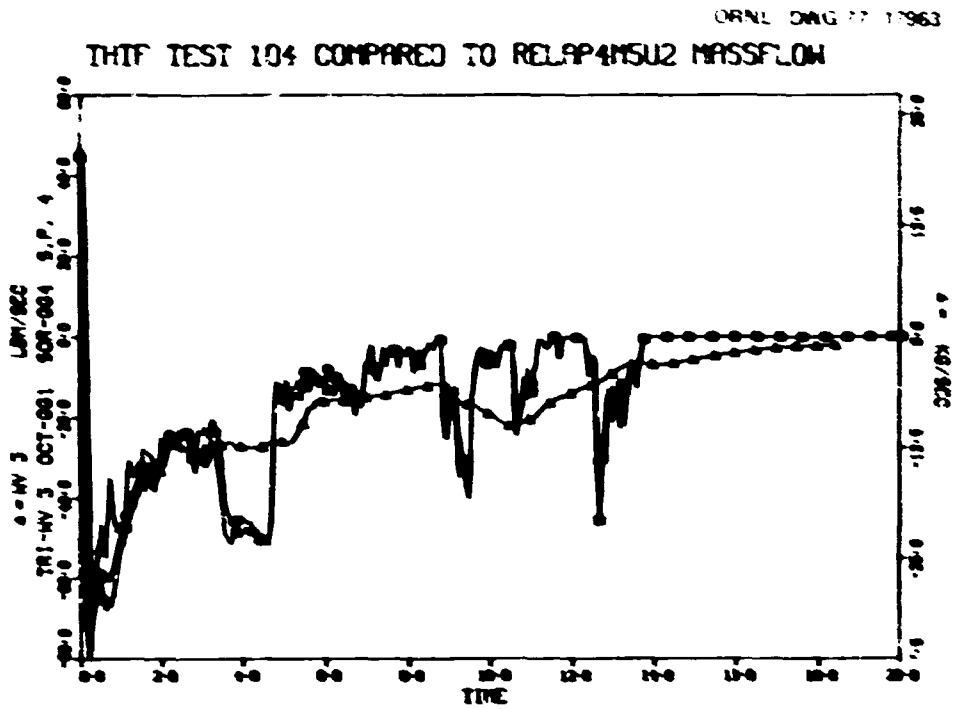

Fig. VI.4. Horizontal outlet spool piece mass flow.

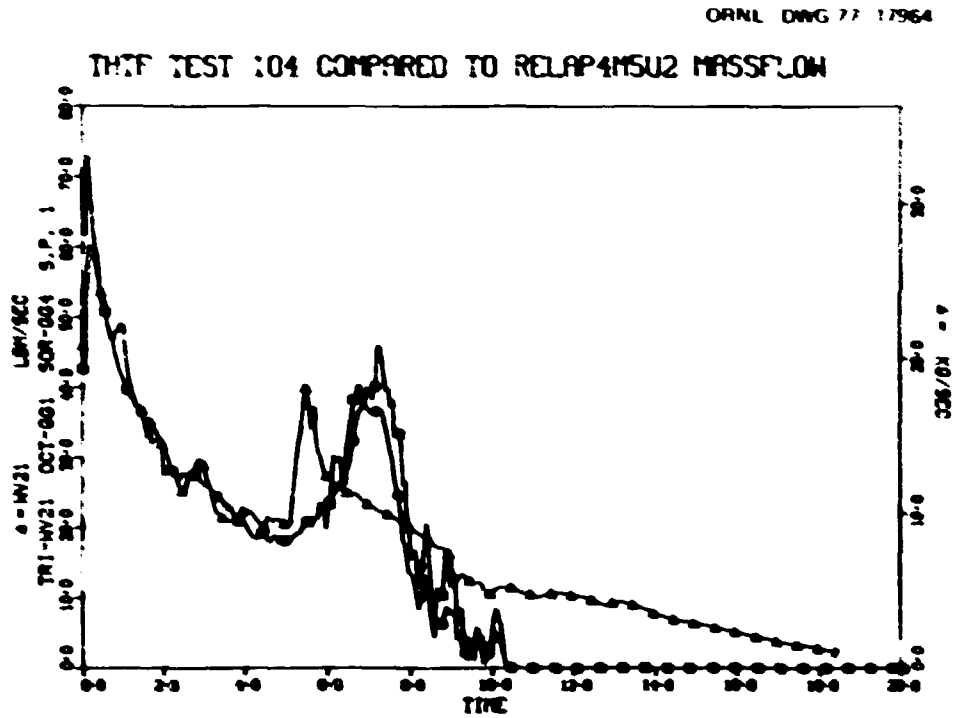

Fig. VI.5. Horizontal inlet spool piece mass flow.

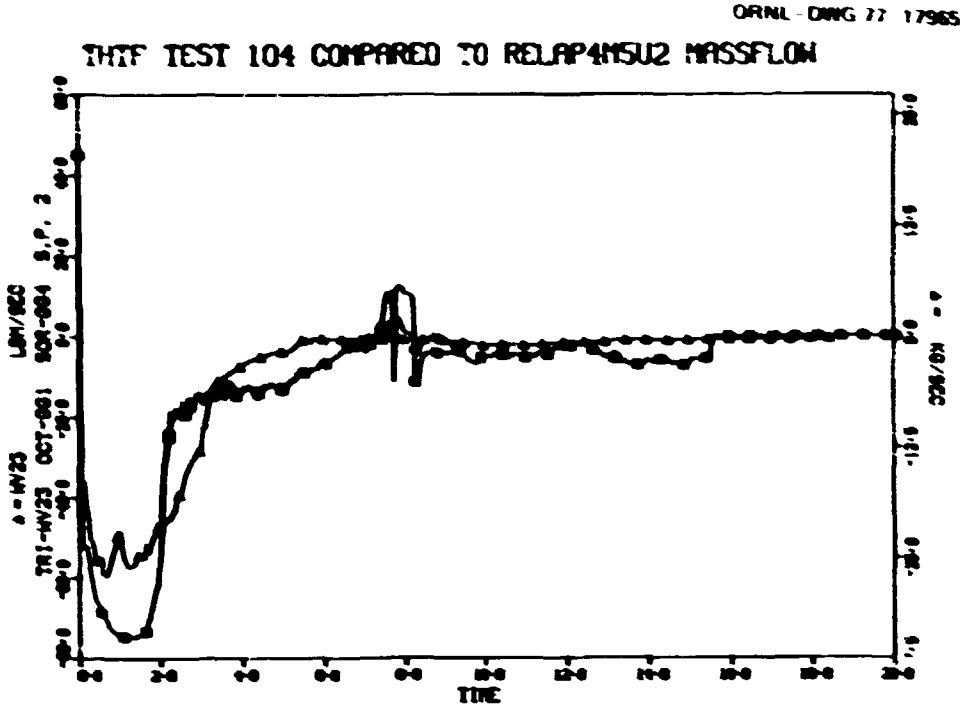

Fig. VI.6. Vertical inlet spacer piece mass flow.

superheat in test 104 than in test 103. The differences can also be seen in the subchannel thermocouple plot (Fig. VI.7). The spike that occurs in a few output signals just after 2 sec is thought to be an extraneous input in the data acquisition system. Note that, as in test 103, RELAP's predicted superheat is too high and occurs too soon. Test 104 does not exhibit the general occurrence of superheat at the subchannel thermocouples late in the transient seen in test 103; however, RELAP predicts such a phenomenon at 17 sec. The rod surface temperatures and heat fluxes (Figs. VI.8 to VI.13) show a marked difference in RELAP's predictions for tests 103 and 104. RELAP's predictions for rod surface temperatures and fluxes for test 104 are uniformly poor with our model, much worse than for test 103.

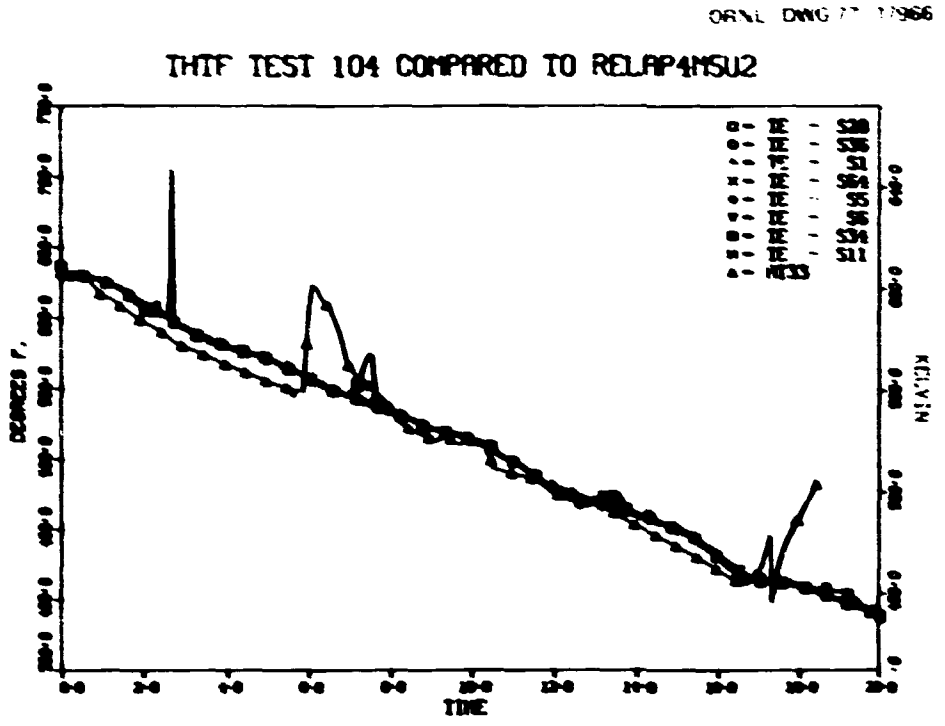

Fig. VI.7. Test section subchannel temperatures.

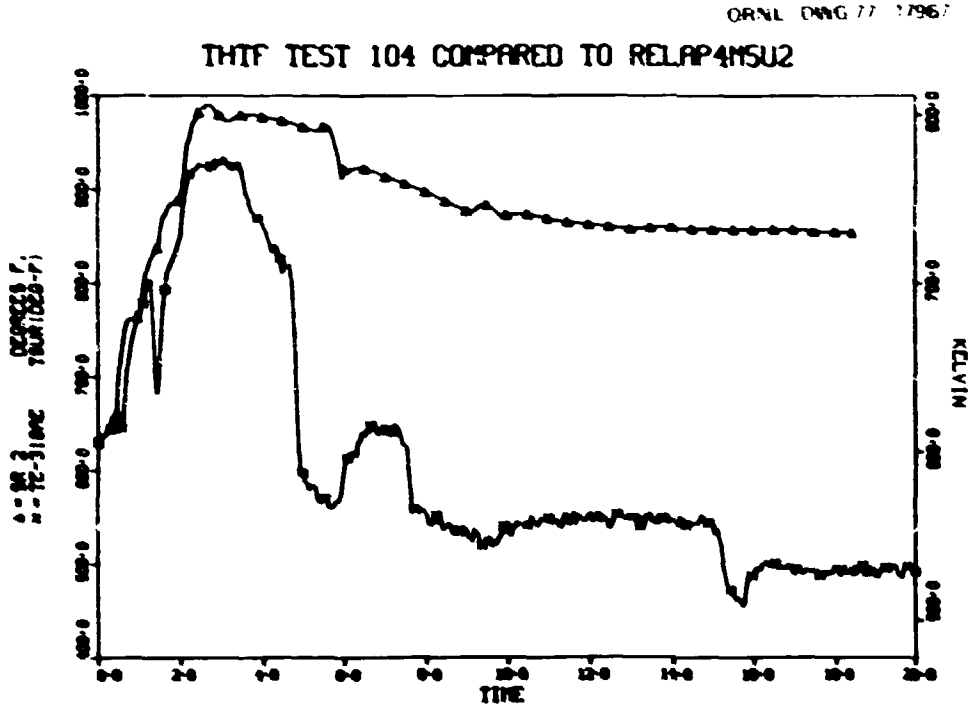

Fig. VI.8. Surface temperature, rod 18, level E.

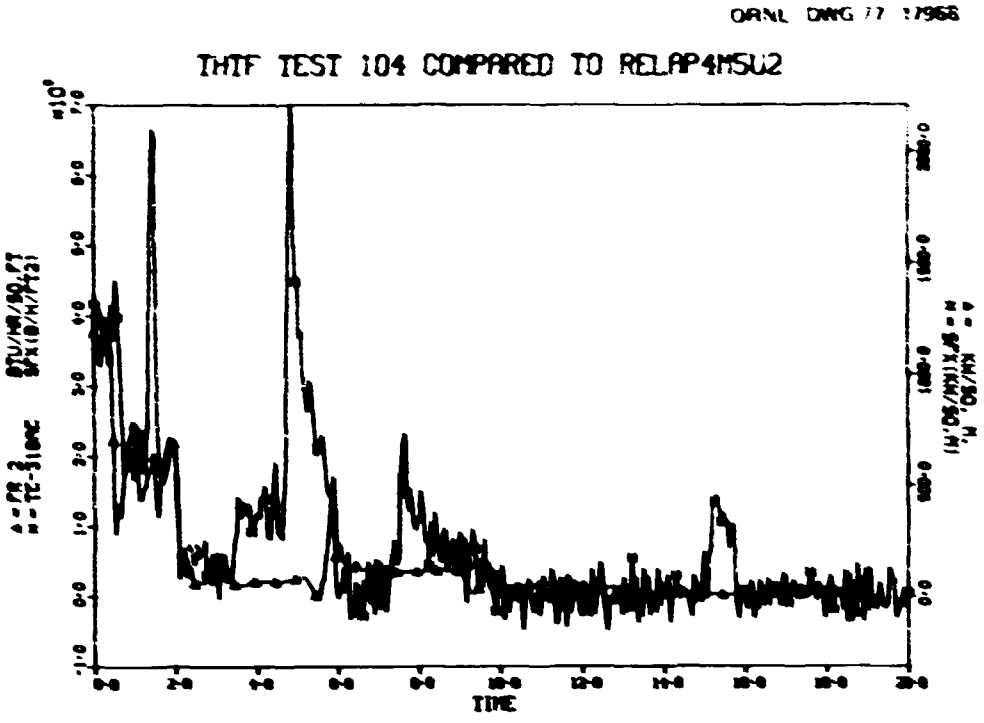

Fig. VI.9. Surface heat flux, rod 18, level E.

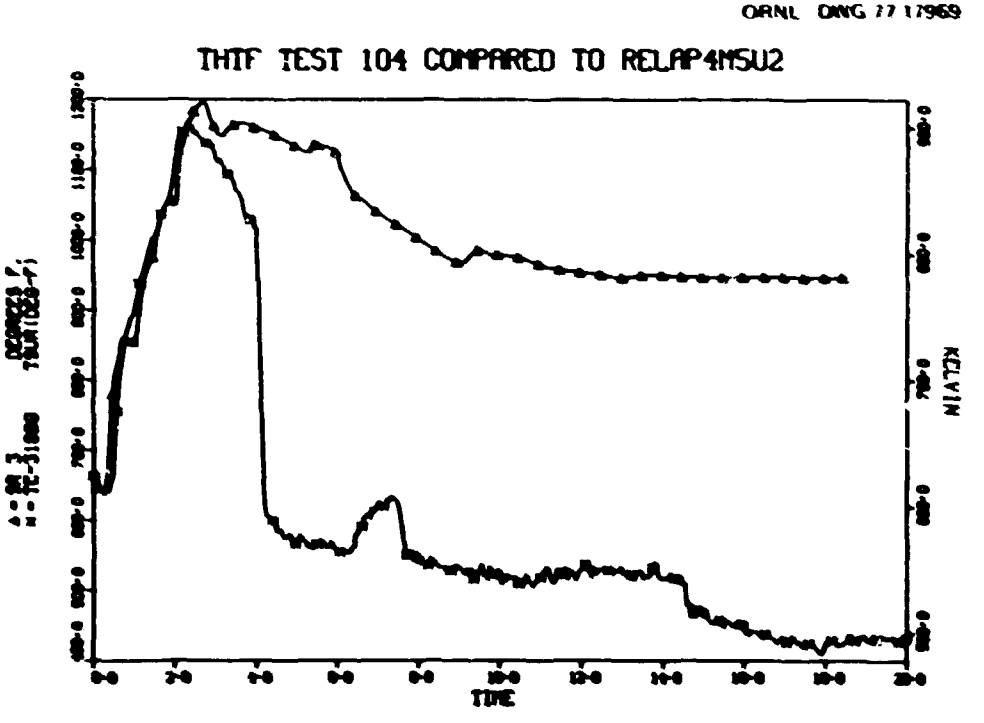

Fig. VI.10. Surface temperature, rod 18, level G.

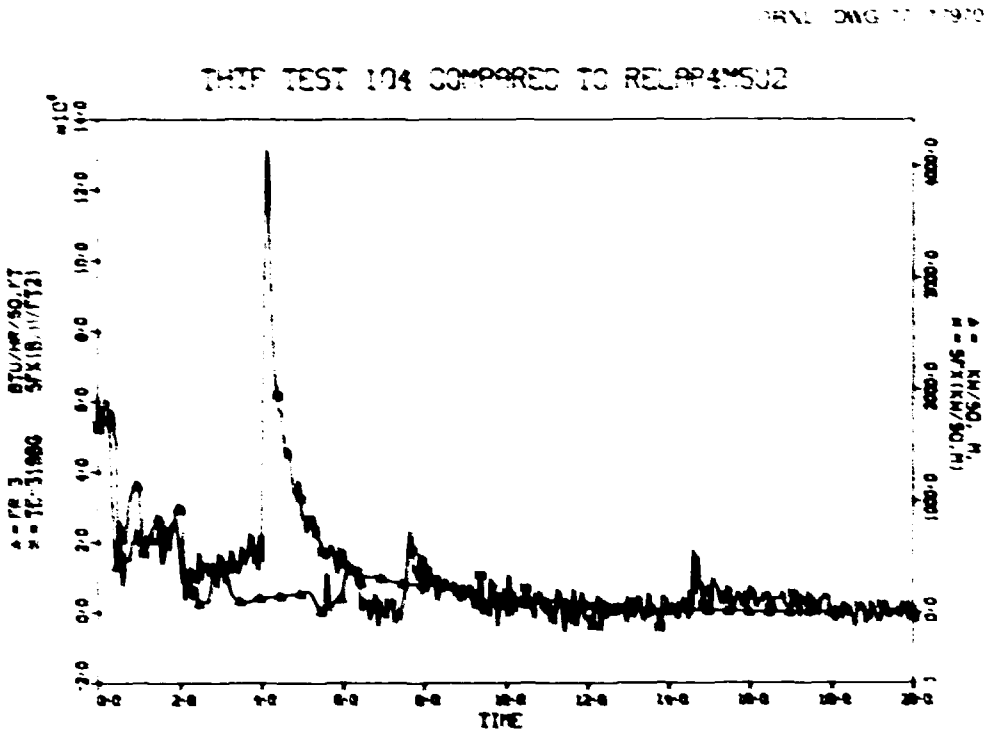

Fig. VI.11. Surface heat flux, rod 18, level G.

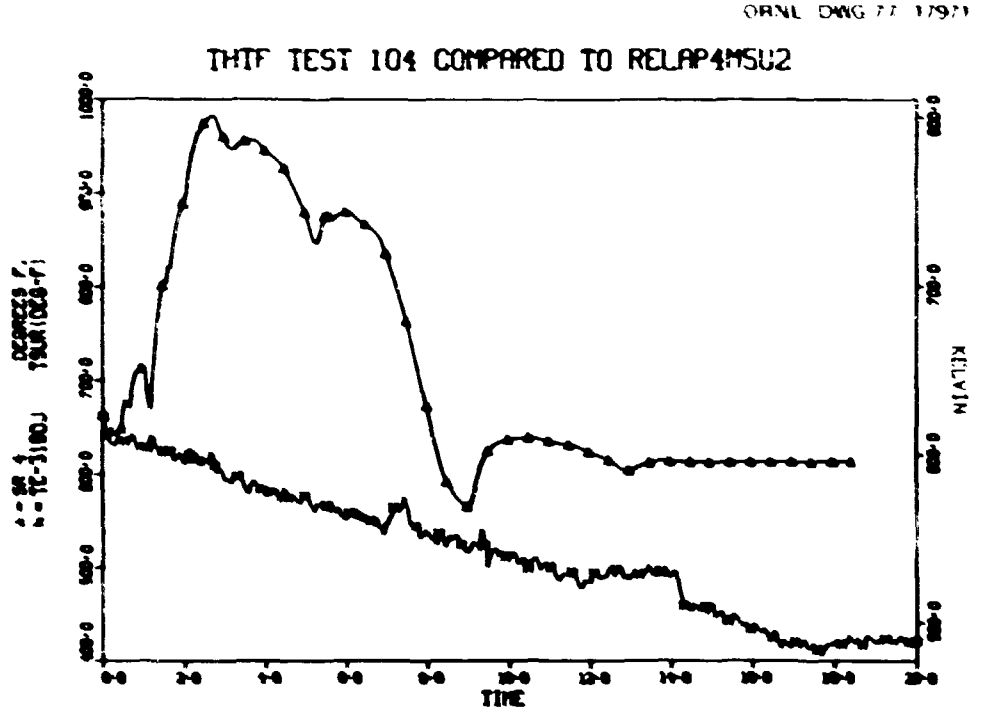

Fig. VI.12. Surface temperature, rod 18, level J.

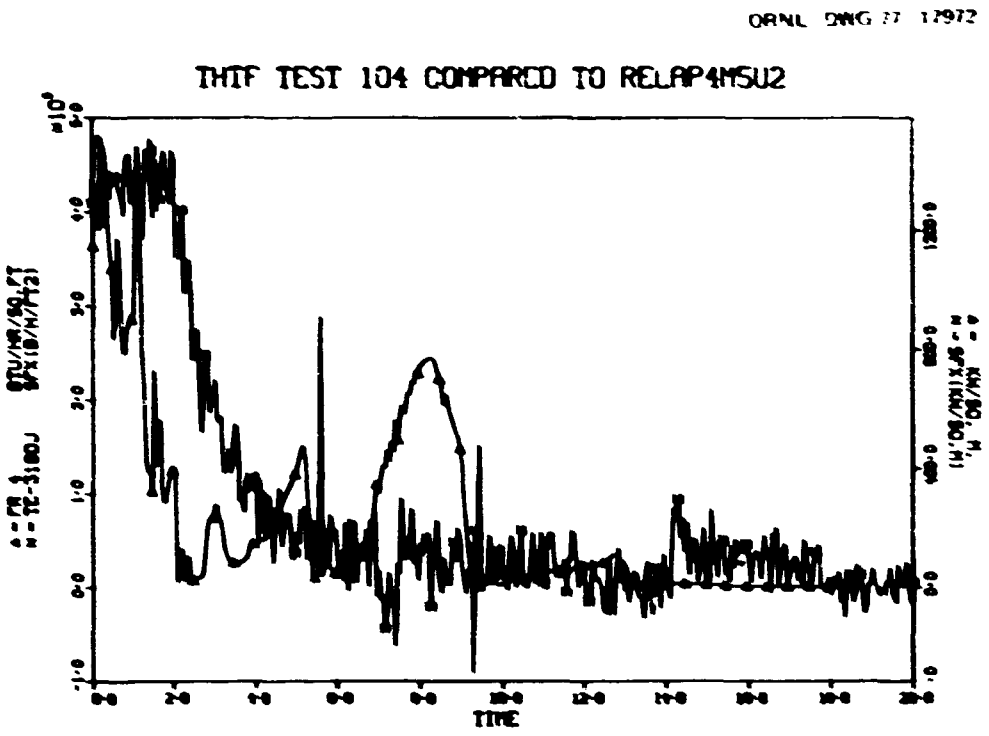

Fig. VI.13. Surface heat flux, rod 18, level J.

VII. TEST 105

VII.1. Description

Test 105, the sixth test in the THTF with bundle 1 in place, was conducted on August 19, 1976, to obtain CHF in a prescribed flow and power transient. The break configuration was a 40% inlet–60% outlet break with a total area of 12.54 cm^2 (0.0135 ft^2). The electric core was maintained at full power for 2 sec into the transient and then the power was decayed with a time constant of 0.45 sec. The primary coolant pump was tripped coincident with rupture, and closure of the main heat exchanger secondary side valves was initiated at trip from full power. The THTF fluid conditions immediately preceding rupture are presented in Tables VII.1 and VII.2.

Test 105 provided core flows which best approximated those from an NRC-supplied PWR double-ended guillotine break study. This was also the first test which incorporated power decay after 2 sec. These two conditions made test 105 the "reactor" case of this test series.

VII.2. Thermal Hydraulics

The two break orifices and the hot- and cold-leg fluid temperatures in test 105 were very similar to those in test 103; therefore, the observed hydraulic instrument response was also similar. System pressures, fluid temperatures, densities, and volumetric and mass flows for test 105 were predicted by RELAP with the same areas of agreement and disagreement as for test 103.

In all the blowdown tests in this series, power to the primary circulation pump was tripped by 0.1 sec after rupture. Relatively high pump speed was maintained throughout the blowdown by the inertia of the pump impellers, shaft, and rotor windings. The resulting pressure rise across the pump is shown in Fig. VII.1. Saturation of the fluid at the pump suction apparently occurs at 4 sec, as evidenced by continued degradation of the pump head and a reduction in the pump speed deceleration due to a drop in hydraulic torque on the impellers (Fig. VII.2). An orifice meter

Table VII.1. Desired vs actual prerupture conditions - test 105

Parameters	Desired[a]	Actual[b]
System pressure (PE-201)	15.513 MN/m² (2250 psig)	15.458 MN/m² (2242 psig)
Core power (EEE-9, EEE-10, EEE-11, EEE-12, EIE-9, EIE-10, EIE-11, EIE-12)	5.978 MW	5.973 MW
Voltage decay constant	1.35 sec	0.90 sec
Core volumetric flow rate (FE-19)	0.0265 m³/sec (420 gpm)	0.027 m³/sec (425 gpm)
Test section inlet temperature (TE-162)	559.3 K (547°F)	558.2 K (545°F)
Test section outlet temperature (TE-212)	610.4 K (639°F)	606.5 K (632°F)
Pressurizer		
Pressure (PE-108)	15.031 MN/m² (2180 psig)	15.189 MN/m² (2203 psig)
Mass liquid water (LT-108)	63.50 kg (140 lb_m)	59.84 kg (131.93 lb_m)
Coolant pump		
Speed (SE-72)	59.67 rps (3580 rpm)	59.65 rps (3579 rpm)
Pressure differential (P_dE-78)	4.413 MN/m² (640 psid)	4.306 MN/m² (639 psid)
Pressure between HCV-2 and FCV-18 (PE-16)	16.996 MN/m² (2465 psig)	16.809 MN/m² (2438 psig)
Pressure differential across main heat exchangers (P_dE-46)	0.172 MN/m² (25 psid)	0.172 MN/m² (25 psid)

[a]Desired prerupture conditions are based on programmatic requirements.

[b]Actual prerupture conditions are based on instrument signals recorded within 10 sec of primary system rupture.

Table VII.2. Prerupture primary coolant temperature and pressure distribution[a] - test 105

Location	Instrument	Temperature [K (°F)]	Pressure [MN/m² (psig)]
Vertical inlet spool piece	TE-172	558.2 (545)	
Vertical inlet spool piece	PE-174		15.644 (2269)
Test section inlet	TE-162	558.2 (545)	
Lower plenum	TE-150	559.8 (548)	
Lower plenum	PE-156		15.630 (2267)
Upper plenum	PE-201		15.458 (2242)
Test section outlet	TE-212	606.5 (632)	
Vertical outlet spool piece	TE-222	606.5 (632)	
Vertical outlet spool piece	PE-224		15.368 (2229)
Heat exchanger inlet header	PE-44		15.237 (2210)
Mixed mean temperature downstream heat exchangers	TE-208	564.8 (557)	
Pressurizer surge line	TE-2	615.9 (649)	
Pressurizer	PE-108		15.189 (2203)
Primary pump suction	PE-76		15.072 (2186)
Between main control valves HCV-2, FCV-18	TE-48	555.9 (541)	
Between main control valves HCV-2, FCV-18	PE-16		16.809 (2438)

[a]Prerupture distribution is based on instrument signals recorded within 10 sec of primary system rupture.

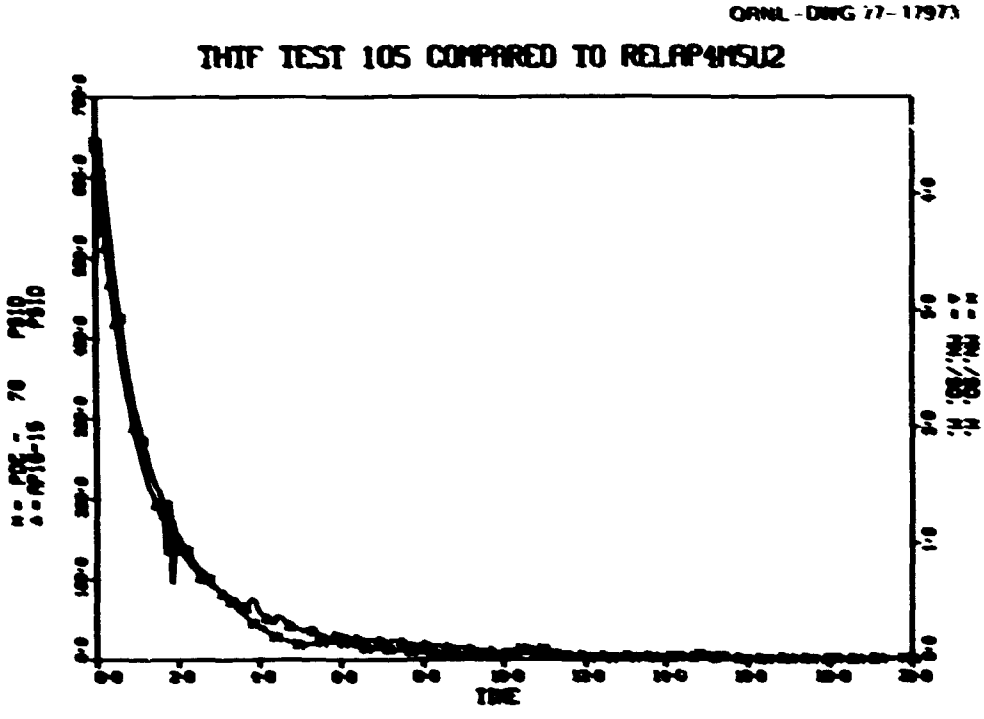

Fig. VII.1. THTF primary pump pressure difference.

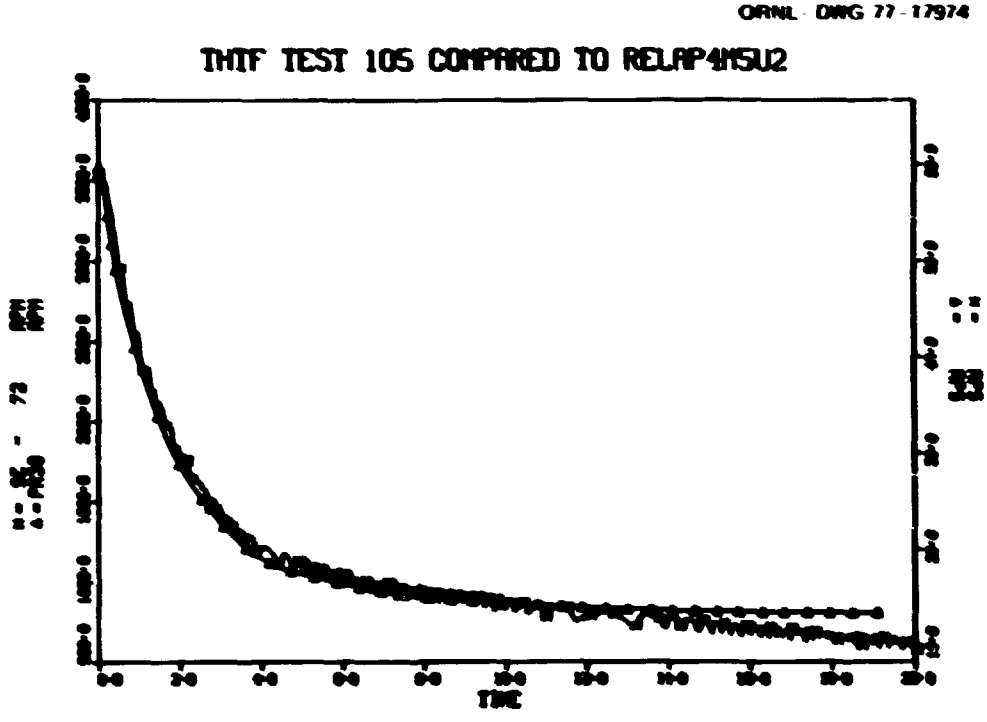

Fig. VII.2. THTF primary pump speed.

near the pump discharge indicates probable flashing at 5 sec (Fig. VII.3); flows indicated by this meter are not reliable after that time. RELAP calculations of pump behavior were generally good except for overprediction of the pump head when two-phase conditions existed. No density measurements were available at the pump suction for development of two-phase pump head multipliers for RELAP. Errors in the pump speed calculation after 14 sec are not significant since the pump head is negligible by that time.

Better insight into the accuracy of RELAP and the THTF model in the calculation of early-blowdown flows may be gained by comparison of the RELAP-calculated flows and analog turbine meter data. Figures VII.4 and VII.5, respectively, show unprocessed signals from FE-19 at the horizontal inlet and from FE-34 at the horizontal outlet for test 105. The processed flows for FE-19 (Fig. VII.6) include a peak before 0.05 sec which was not discernible in the raw data. RELAP's calculated flow had several peaks during this interval. At the outlet, comparison shows that RELAP-calculated flow reverses much more rapidly than the processed data indicate (Fig. VII.7).

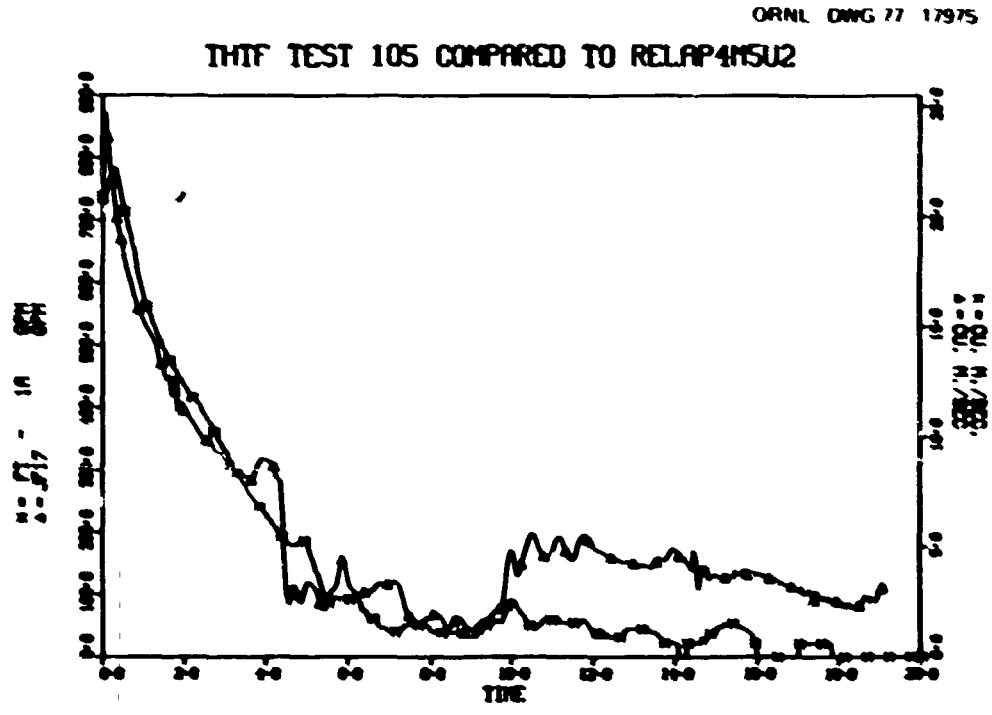

Fig. VII.3. Primary pump outlet volumetric flow.

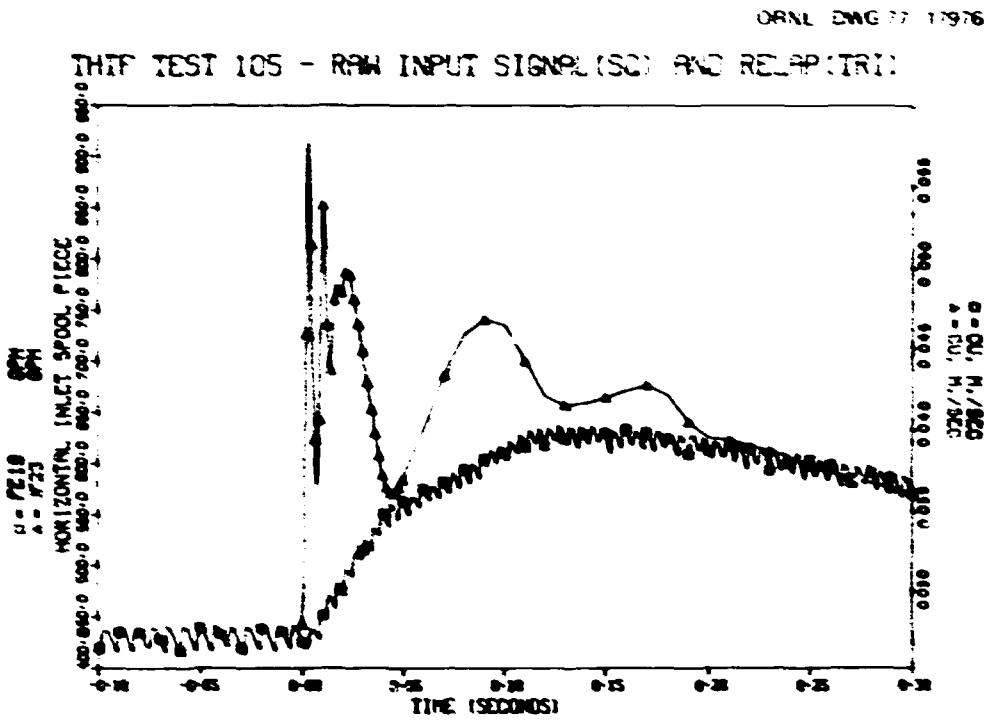

Fig. VII.4. Volumetric flow at horizontal inlet unprocessed analog signal.

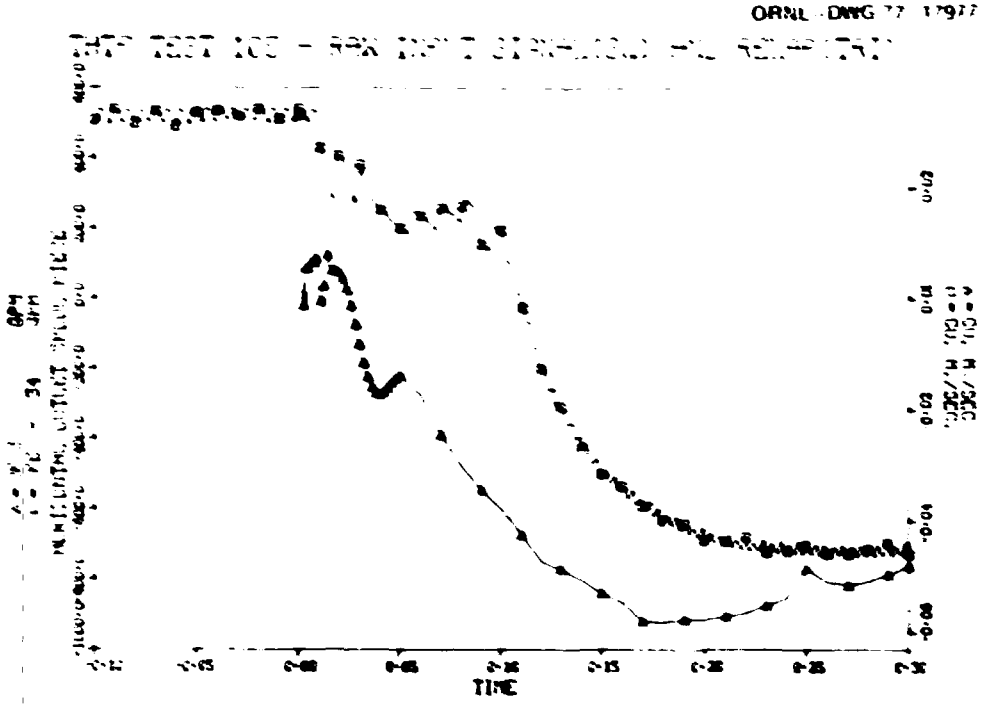

Fig. VII.5. Volumetric flow at horizontal outlet unprocessed analog signal.

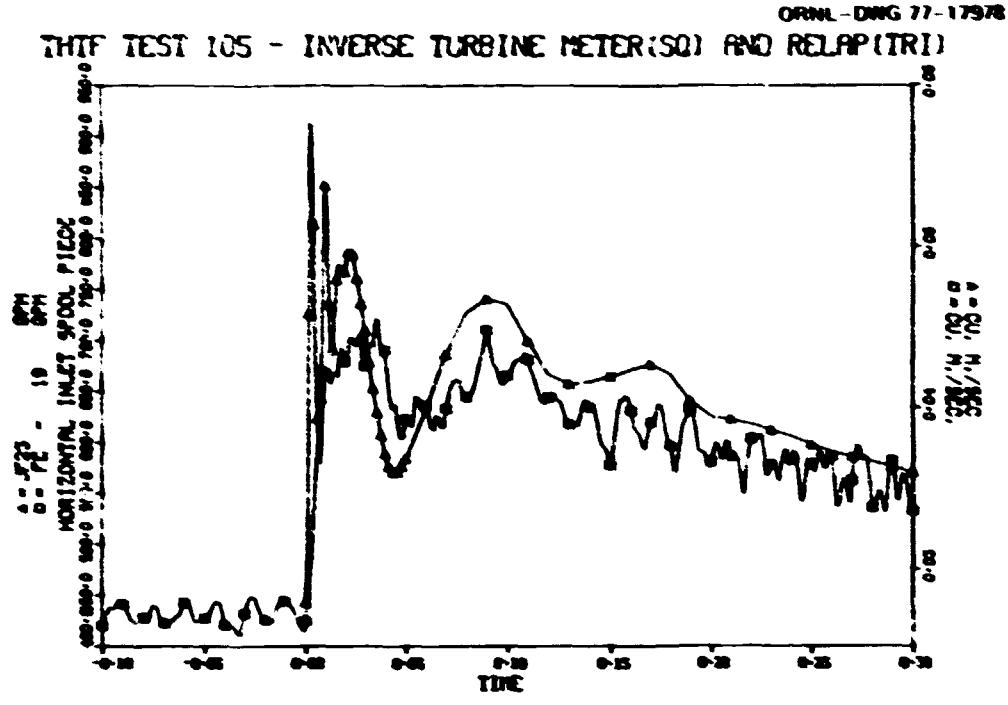

Fig. VII.6. Volumetric flow at horizontal inlet processed analog signal.

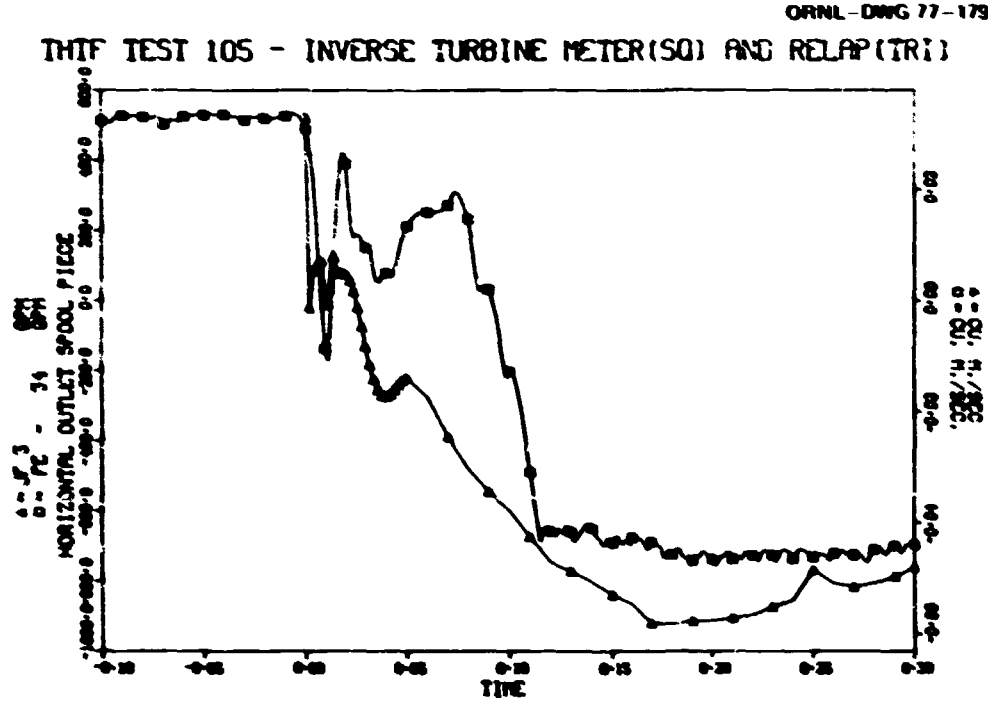

Fig. VII.7. Volumetric flow at horizontal outlet processed analog signal.

Because of the exponential decay of the bundle power beginning 2 sec after initiation of blowdown, heater rod temperatures and resulting test section fluid temperatures were higher for test 105 than for any previous test. Figure VII.8 shows a comparison of the fluid temperatures measured by several THTF subchannel thermocouples with the temperature calculated by RELAP for the uppermost heated control volume. Comparison of this plot with Fig. V.18 for test 103 shows that the time of fluid temperature peaks is virtually identical for the two tests, which implies similar flow response in the test section. The maximum values of both calculated and measured fluid temperatures for test 105 are greater than for test 103 as a result of the longer period during which the rod power was on. Radial flow effects inferred from the subchannel thermocouples for test 103 are also in evidence for test 105. RELAP's early prediction of the negative-to-positive core flow reversal is again reflected in its calculation of the superheat peak at the upper end of the bundle (Fig. VII.8).

During the first 2 sec after initiation of blowdown, flow is negative through the test section. The heater rods rapidly reach critical heat

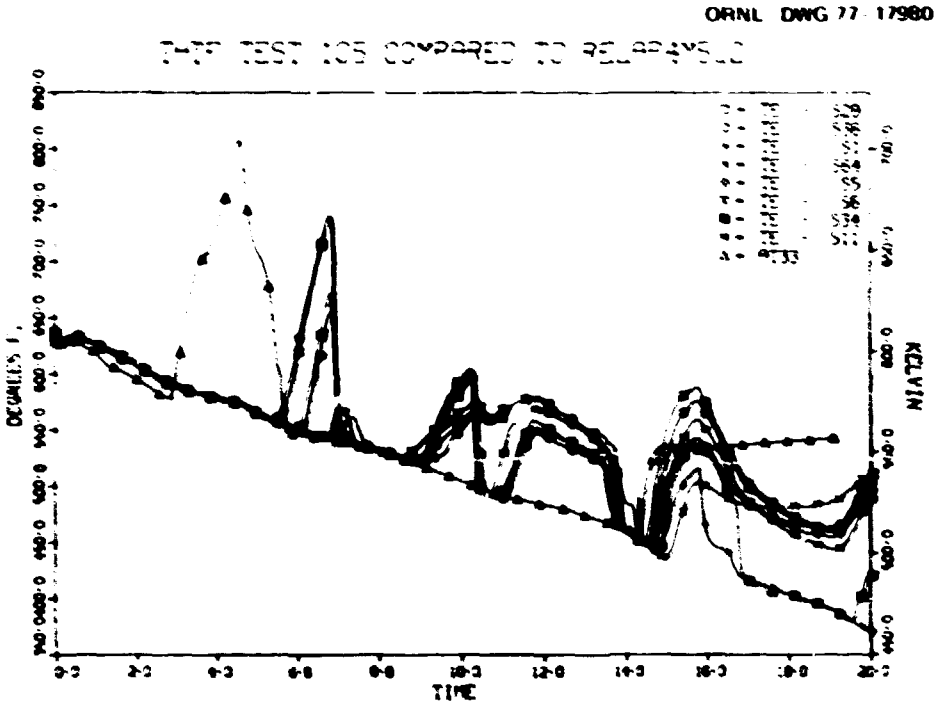

Fig. VII.8. Test section subchannel temperatures.

flux below the midplane of the bundle [e.g., rod 18, level E (Fig. VII.9)]. Some fluid becomes superheated and is detected at 4 sec by TE-178 (Fig. VII.10), which is located in the lowest RELAP heated zone; RELAP predicts a similar peak slightly earlier. Three of the four lower-plenum fluid thermocouples indicated superheat between 2 and 5 sec; TE-151 was the exception. RELAP calculations for test 105 show no superheat in the lower plenum.

The vertical inlet turbine meter, FE-166, reversed polarity three times during test 105 at approximately 0.1, 3.0, and 4.2 sec; the inverted signal is presented in Fig. VII.11. The signal from FE-34 (Fig. VII.12) at the horizontal outlet had the wrong sign between 2 and 4 sec. The volumetric flow at the vertical outlet has a strongly positive acceleration at 5 sec, as in test 103, and the flow at the inlet vertical spool becomes positive at 7 or 8 sec. Between 5 and 8 sec, the stagnation point of flow moves downward through the test section, resulting in a superheat spike indicated by the subchannel thermocouples and rewetting of thermocouples in the lower plenum and at level D in the rod bundle.

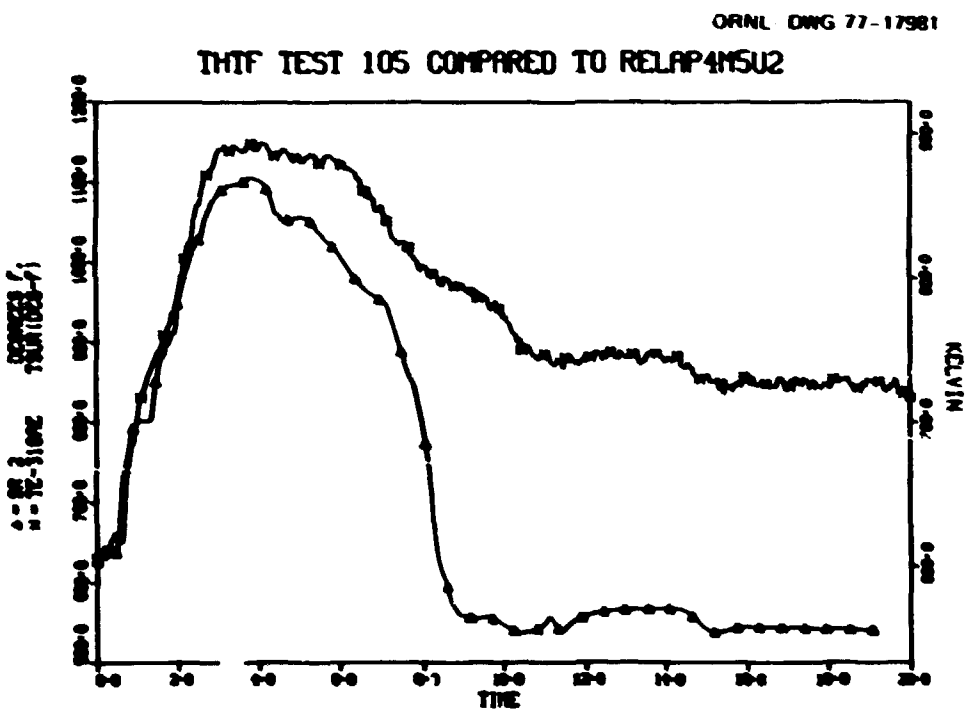

Fig. VII.9. Surface temperature, rod 18, level E.

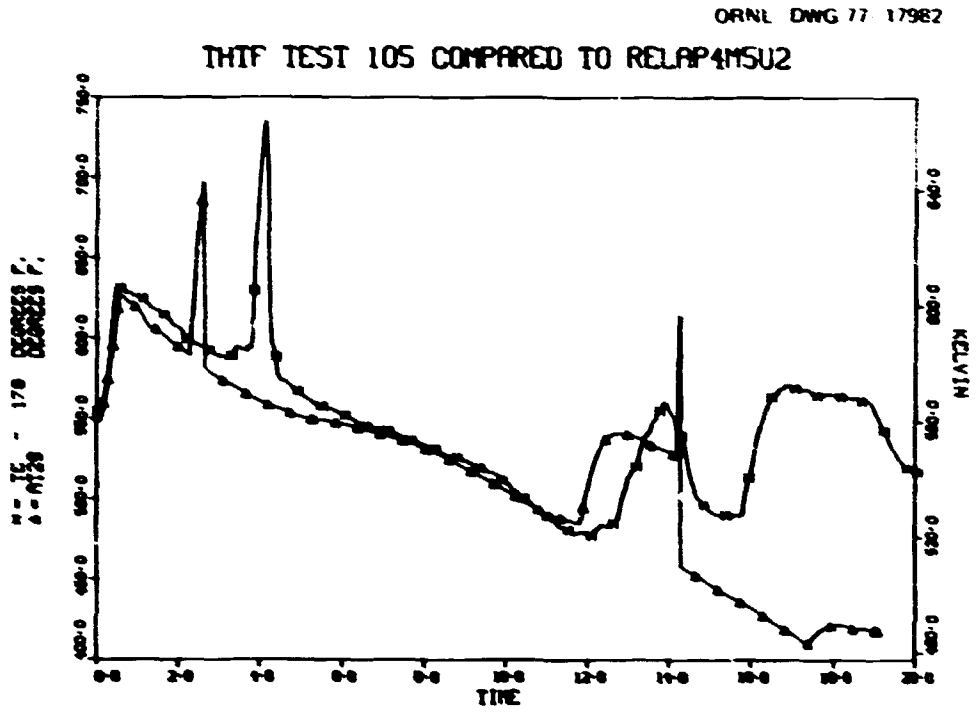

Fig. VII.10. Bundle fluid temperature near bottom of bundle.

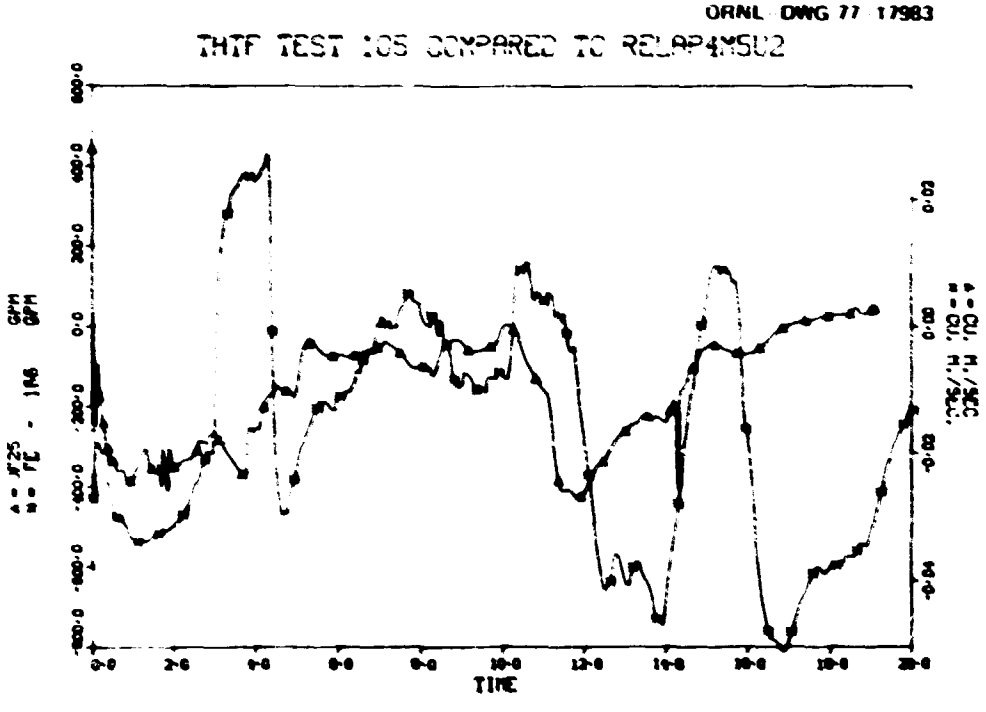

Fig. VII.11. Vertical inlet spool piece volumetric flow (corrected).

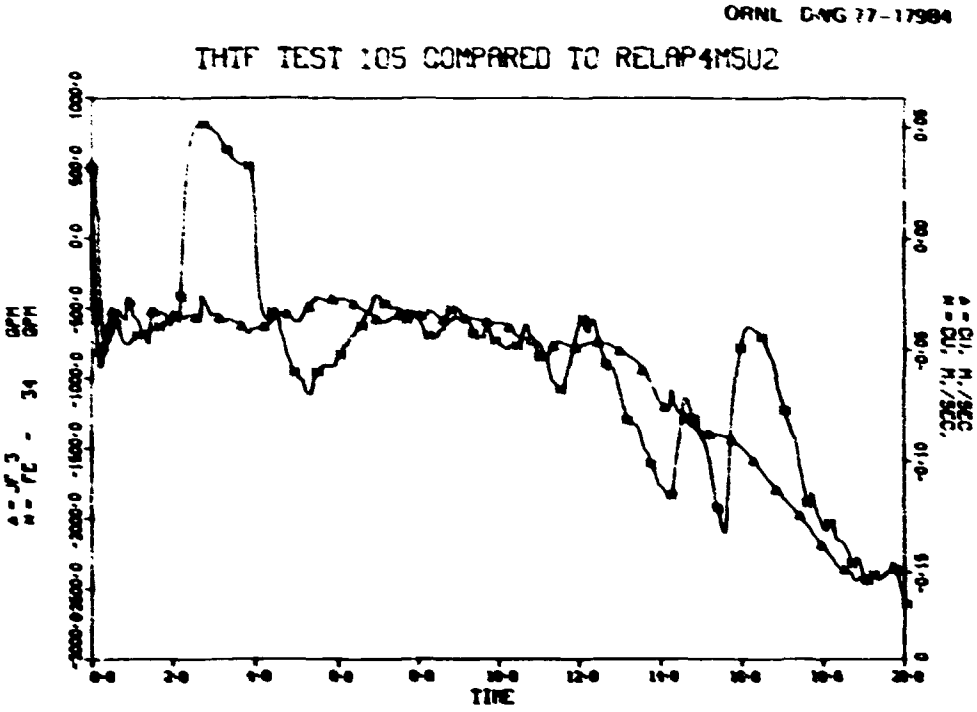

Fig. VII.12. Horizontal outlet spool piece volumetric flow.

Overlay plots of the RELAP-predicted and ORINC-calculated surface temperatures for test 105 at three axial levels appear in Figs. VII.9, VII.13, and VII.14. Comparison with Figs. V.19 and V.21 for test 103 shows that the exponential decay of the power to the heater rods after 2 sec in test 105 results in higher maximum surface temperatures at levels E and G. At level E, a maximum temperature of 895 K (1150°F) was reached, compared to an 850 K (1070°F) maximum in test 103 (Fig. (V.19). RELAP calculations underpredict the temperatures at level E and incorrectly predict a rewetting at 8 sec at level E. Such a rewetting did occur at level D, near the bottom of RELAP slab 2. A maximum surface temperature of over 975 K (1300°F) occurred at approximately 3.5 sec at level G, near the core midplane (Fig. VII.13). In test 103, the maximum at level G of about 920 K (1200°F) occurred at approximately 2.2 sec. There are discrepancies between predicted and observed surface temperatures and fluxes at level G, specifically, RELAP's overprediction of the heat flux between 4 and 7 sec (Fig. VII.15) followed by its incorrect calculation of rewet at 8 sec. At level J, RELAP obviously overpredicts the rod surface temperatures for rod

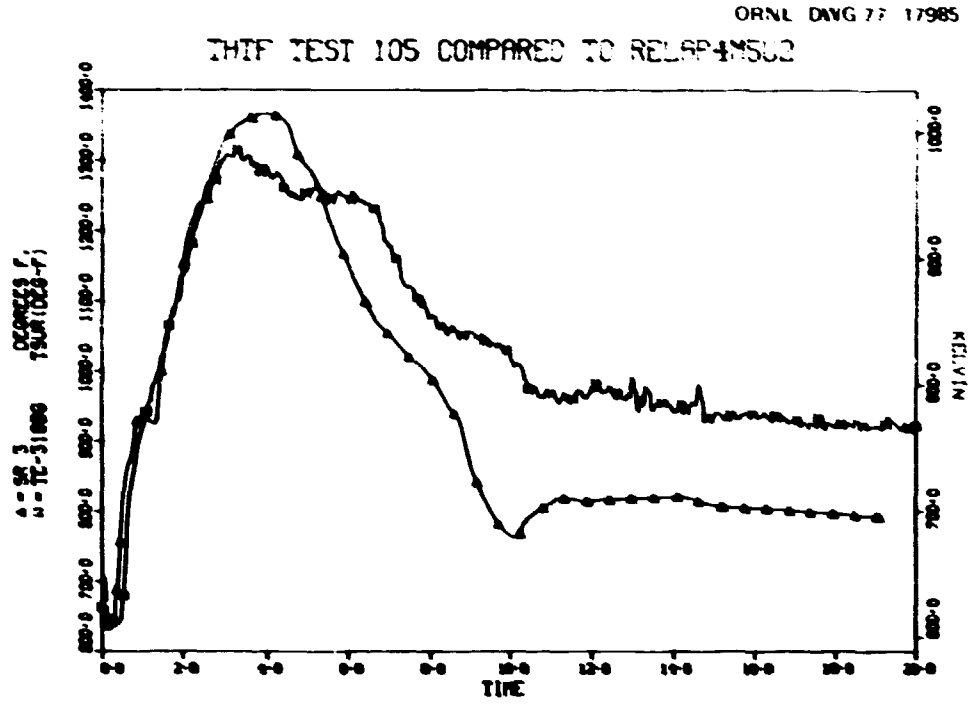

Fig. VII.13. Surface temperature, rod 18, level G.

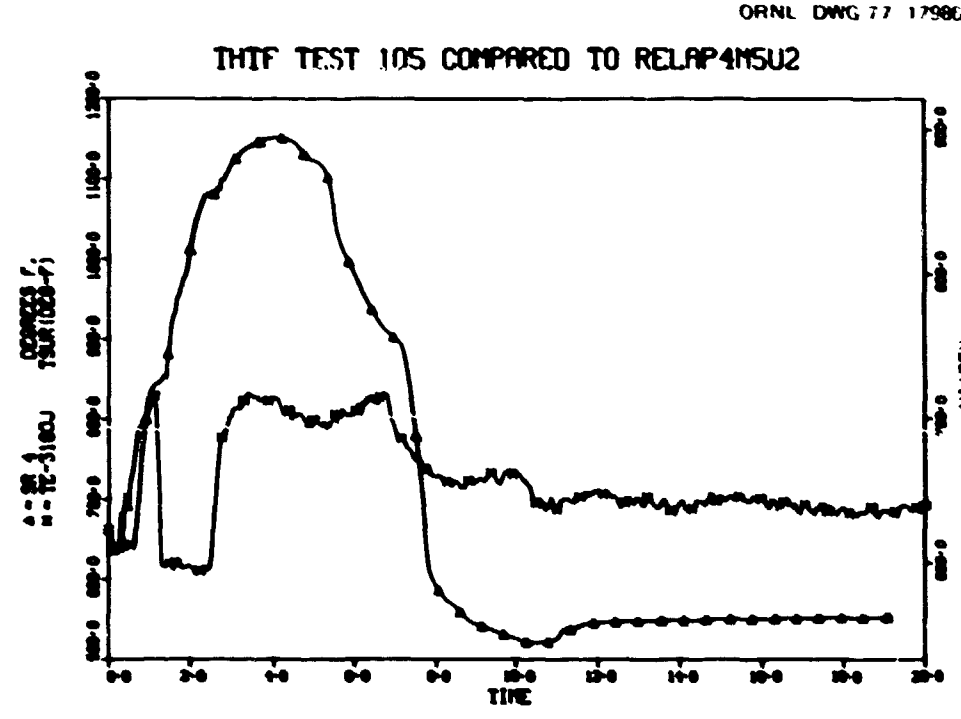

Fig. VII.14. Surface temperature, rod 18, level J.

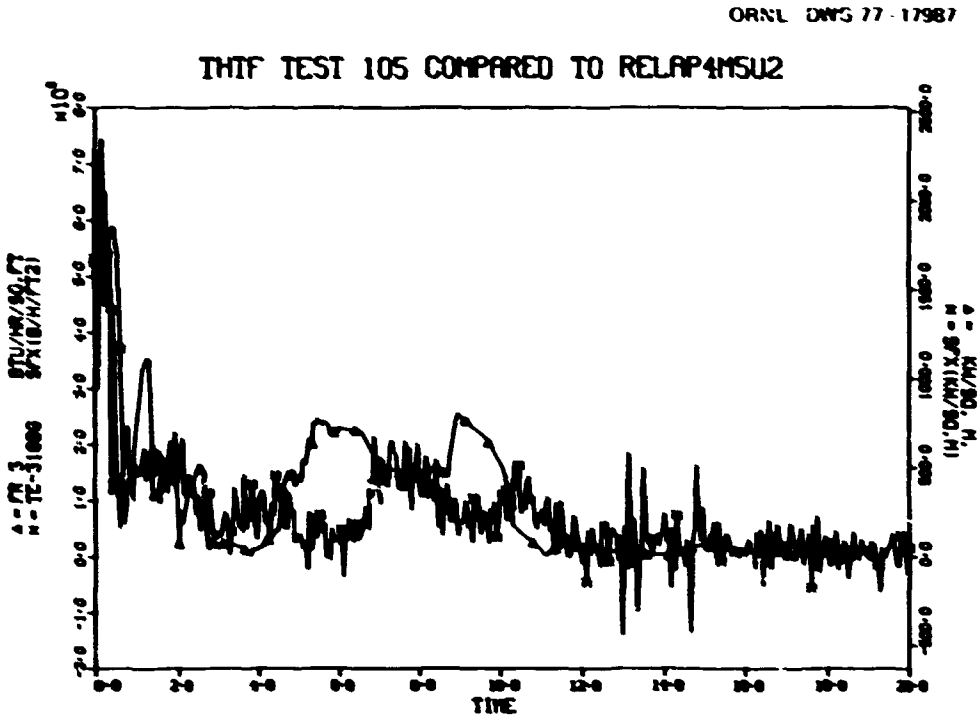

Fig. VII.15. Surface heat flux, rod 18, level G.

18 (Fig. VII.14). For the first 8 sec, cooling conditions in the upper half of the rod bundle were generally better for these tests than calculations implied.

VIII. RELAP CODE VERIFICATION

In analyzing how well RELAP models blowdown in the THTF, judgments of the relative significance of the differences between RELAP predictions and the experimental data must be made. Since this report is concerned with RELAP's hydraulic prediction capability, those hydraulic parameters which will have the greatest impact on the core, specifically errors in pressure and density, have been given the most attention.

An incorrect system pressure prediction will cause a correct critical flow model to predict incorrect mass flow through the breaks, thus producing errors in the system mass inventory. It will alter the calculated effectiveness of heat transfer, particularly nucleate boiling heat transfer, and the times at which a heat transfer regime change is predicted.

Errors in the prediction of the second important parameter, density, also affect system response. The existence of the solid plug of very low (or zero) quality fluid at the outlet break from 3 to 5 sec in tests 102 through 105 keeps flow in the vertical outlet piping near zero. When the plug is expelled, vertical outlet flow toward the break resumes and flow reversal in the core is permitted. RELAP's error in density prediction at the horizontal outlet spool piece contributed to its early prediction of this phenomenon. The time and extent to which flow reversals occur produce periods of low or zero flow at changing positions in the core, which result in major changes in the fluid and rod temperatures. Reversals also determine the source of fluid surrounding the rods, resulting in heat transfer to hotter or colder fluid and attendant changes in rod temperatures. Density errors cause incorrect enthalpies to be used in the critical flow models and can cause poor convective heat transfer predictions and incorrect selection of heat transfer regimes. Errors in quality prediction are reflected in density prediction errors.

Before discussing the primary sources of RELAP's inaccuracies in detail, input parameters found to have little impact on code predictions are mentioned. Here, little impact means the effect of variations in the parameter are small compared to the existing discrepancies between our RELAP model predictions and the THTF instrument responses as presented previously in the report. A 10% variation in the rated flow and rated head

input for the pump had little effect. A 20% change in the initial pressurizer mixture level did not significantly change the prediction, and use of the bubble rise option in the pressurizer only slightly improved it. When modeling heater rods, failure to include an air gap when one exists will have a significant effect, but whether a mean or variable gap model is used is not important if gap variations are not of extreme size. (This will be discussed in more detail in the subsequent report investigating RELAP's heat transfer capabilities.) RELAP's predictions are not sensitive to variations in the total loop volume until such variations approach 10%. Hydraulic resistance in the pressurizer surge line is relatively small. An increase of 100% or more in the input value for this resistance does not appreciably affect RELAP's prediction of too much pressure resurgence. Comparisons of RELAP predictions using two different fluid-flow equations show little difference. The two equations are for compressible single-stream flow with momentum flux and for incompressible single stream flow without momentum flux.[9]

The choice of choking model and multiplier has a significant effect on RELAP's pressure prediction. Of the 25 combinations of models available in RELAP, three were selected for investigation: the Homogeneous Equilbrium Model (HEM),[9] the Henry-Fauske/HEM[9] (HF/HEM), and the Modified Momentum/HEM[9] (MM/HEM). Each of these uses HEM choking in the two-phase region but a different model in the subcooled region. The three subcooled models produced different pressure predictions early in the transient during the resurgence. The subcooled portion of the transient is so brief, however, that the different subcooled choking models do not change the total mass inventory sufficiently to make a significant difference in the pressure prediction during the rest of the transient. Differences between the models after saturation are further decreased by feedback from the pressure; a model which predicts lower critical flow slows the decrease of the pressure, which tends to produce a higher critical flow and increases the rate of depressurization. A 10% change in the choked flow multiplier makes a significant difference in the pressure in spite of this feedback. The HF/HEM and MM/HEM models provide for a transition region in which the choked flow is interpolated between the subcooled and

the saturated values. This transition region extends from the saturation point to a quality specified by the user. The width of this region did not appreciably affect THTF predictions except when it was made so narrow as to induce numerical oscillations due to the abrupt change in choked flow. Oscillations were produced when the transition region was ended at a quality of 0.0001 but were avoided with an end point of 0.01.

In all the powered tests, the relative positions of RELAP's predicted pressures and the measured pressures were similar throughout the system except for the period of pressure resurgence. For the first 6 sec, the predicted pressure was below the experimental data throughout the system, with the discrepancy slightly greater at the pressurizer than at the spool pieces. However, in test 100 the difference was much larger at the pressurizer than at the spool pieces. Since test 100 was performed without rod power, valves in the heat exchangers were adjusted to force 98% of the initial flow through the heat exchanger bypass line. Therefore, in test 100 as compared to the powered tests, such a difference in hydraulic resistance in the heat exchangers would tend to produce greater flow through the bypass line throughout the transient. In test 100, RELAP's prediction for the pressure drop across the main heat exchangers and bypass line was far below that measured for the first 3 sec of the transient (Fig. II.3). For the powered tests, RELAP's predicted pressure drop was closer to the data for this period (Fig. VIII.1). This suggests that an inaccuracy exists in RELAP's calculations for the valve hydraulic resistance in the heat exchanger bypass line. Such an inaccuracy would have a greater effect in test 100 than in the powered tests because of the larger flow through the valve. Inaccuracies in the pressure prediction in the pressurizer are not as important as at the spool pieces, since the spool piece pressures control the break flow and core pressure conditions. Thus, evaluation of RELAP's ability to predict pressures will be based primarily on the spool piece pressures.

All the predictions previously described in this report were made using HF/HEM choking with a multiplier of 0.8 for the HF and 0.9 for the HEM. The pressure calculations using this model, while predicting too much resurgence, were better in the first 10 sec for test 100 than for

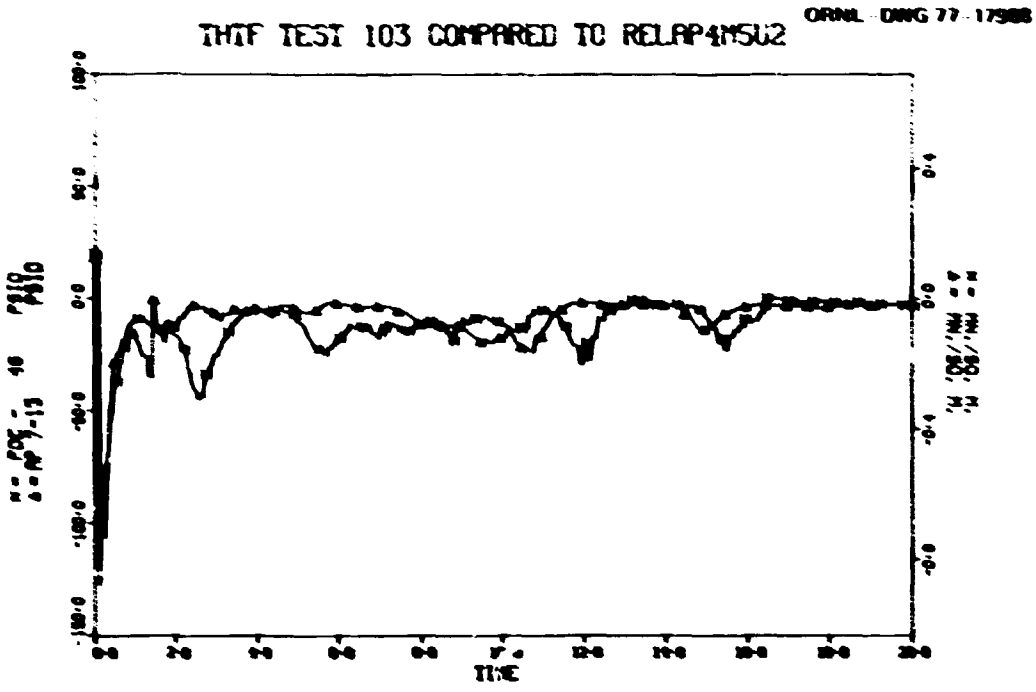

Fig. VIII.1. Main heat exchanger pressure difference.

all the powered tests; the predictions were farther below the data for the powered tests. RELAP closely predicts the pressures after the resurgence for the powered tests using HEM choking with a 0.8 multiplier, but using this same model produces a markedly high pressure prediction for test 100. To investigate this, calculations of the actual break enthalpies were made for tests 100 and 103 and compared with the enthalpies RELAP used to obtain mass flows from its choked-flow tables. The results of the calculations of actual break conditions can only be considered as approximate, since they were obtained from flow and density data which are considered questionable (see Chapter I). The calculations of break enthalpies were sometimes above and below RELAP predictions. But, when enthalpies and pressures determined from the experiment were used with the HEM flow tables to obtain mass flows and the results integrated over a period of time, the result was close to the integrated mass flow predicted by RELAP using HEM. The effects of the high and low enthalpies essentially nullified each other over a period of several seconds. Thus, the fluid conditions used in RELAP to calculate critical flow are close

enough to actual conditions to prevent introducing substantial error in the prediction.

Next, the integrated mass expelled from the break as predicted by RELAP was compared with the actual integrated mass leaked. To approximate the latter quantity, the mass flows calculated for the spool pieces by the Aya method were used to infer a mass flow through each break. The integrated mass flows at 2, 3, and 5 sec in the transient were compared with RELAP's predictions using different choking models. As mentioned previously, RELAP predicts too much pressure for test 100 if HEM choking with a 0.8 multiplier is used, but RELAP's predicted value for the total mass leaked in 5 sec was 20% too low. RELAP's prediction for total mass leakage in test 100 using HF/HEM choking and 0.8 and 0.9 multipliers was only 6% below the amount calculated as the actual mass leaked. For test 103, RELAP's prediction using HEM (0.8) was again markedly low in total mass leaked; the prediction using HF/HEM (0.8/0.9) also was low but not as low as that for HEM even though, in RELAP, HF/HEM was using pressures below the data while HEM was using more correct pressures. The same results were obtained when similar comparisons were made for the total energy leaked through the breaks. Although the calculated values used as the actual mass and energy leaked are not of high accuracy, the differences between the models were large enough to show that HF/HEM (0.8/0.9) is the more correct choking model for our tests. Due to the relatively small effect the model used in the subcooled region has on the prediction through the majority of the transient, this means that HEM with a 0.9 multiplier is more accurate in two-phase conditions than HEM with a 0.8 multiplier. In the subcooled region, HF (0.8) produces a better prediction of the critical flow rate and pressure resurgence than HEM (0.8).

RELAP's low pressure prediction for test 103 and the other powered tests now arouses greater interest since this low pressure prediction is made in spite of RELAP's retention of excessive mass and energy in the system. Given a specified amount of mass and energy within a system, the partitioning of the energy within the mass will affect the pressure throughout the system. For example, a fixed volume divided into two equal parts, one filled with water at 15.17 MN/m^2 (2200 psia) and 561 K (550°F) and the other with water at 15.17 MN/m^2 (2200 psia) and 611 K

(640°F), will remain in pressure equilibrium until the two portions of fluid are permitted to transfer energy. The same amount of mass and energy uniformly distributed throughout the volume will cause the pressure to decrease several meganewtons per square meter (several hundred psi).

To explore the importance of this effect for an open transient system, a special depressurization test model (DTM) was created for RELAP (Fig. VIII.2) and was given the physical characteristics of the THTF pressurizer and piping leading to the outlet break (Appendix C). Five test calculations were conducted using RELAP. The first three used a fill table for junction 14 to insure identical time-dependent boundary conditions. All cases began with the pressurizer saturated and the entire system at a pressure of 15.17 MN/m^2 (2200 psia). The differences in these cases involved the initial temperature distribution (other than the pressurizer); one case, designated HHH, had a temperature of 607 K (633°F), the outlet temperature from the core in most heated THTF tests, in all volumes; another, HCH, had a temperature of 559 K (547°F) in volumes 2–5 and 607 K (633°F) in the rest. The third case, HCC, had a temperature of 559 K (547°F) in all volumes except the pressurizer. Thus, the HHH test had one interface between fluids having a temperature difference of 9.4 K (17°F). Test HCC, like test 100, had one interface between fluids having a temperature difference of 56.7 K (102°F). Test HCH, like test 103, had the same interface as test HCC and a second interface between fluids having a temperature difference of 47.8 K (86°F).

The fill table supplying the boundary conditions removed fluid at the rate and enthalpy expected for the HCH test. If RELAP did not mix the different temperature fluids, the 607 to 559 K (633 to 547°F) interface in the HCH test would arrive at the end of volume 14 in approximately 2 sec. During this period, the fill table specified the removal of fluid at approximately the correct enthalpy for both the HHH and HCH tests. Since the depressurization rate is expected to be proportional to the time rate of change of the total mass and total energy of the system, any pressure differences in the first 2 sec of the HCH and HHH tests can be attributed to RELAP's assumption of homogeneous fluid within each of its volumes, thus mixing the different temperature waters. In Fig. VIII.3, at 2 sec, the pressure in the HCH test is 0.52 MN/m^2 (75 psi) below that in the HHH test. The relative positions of the pressure predictions are

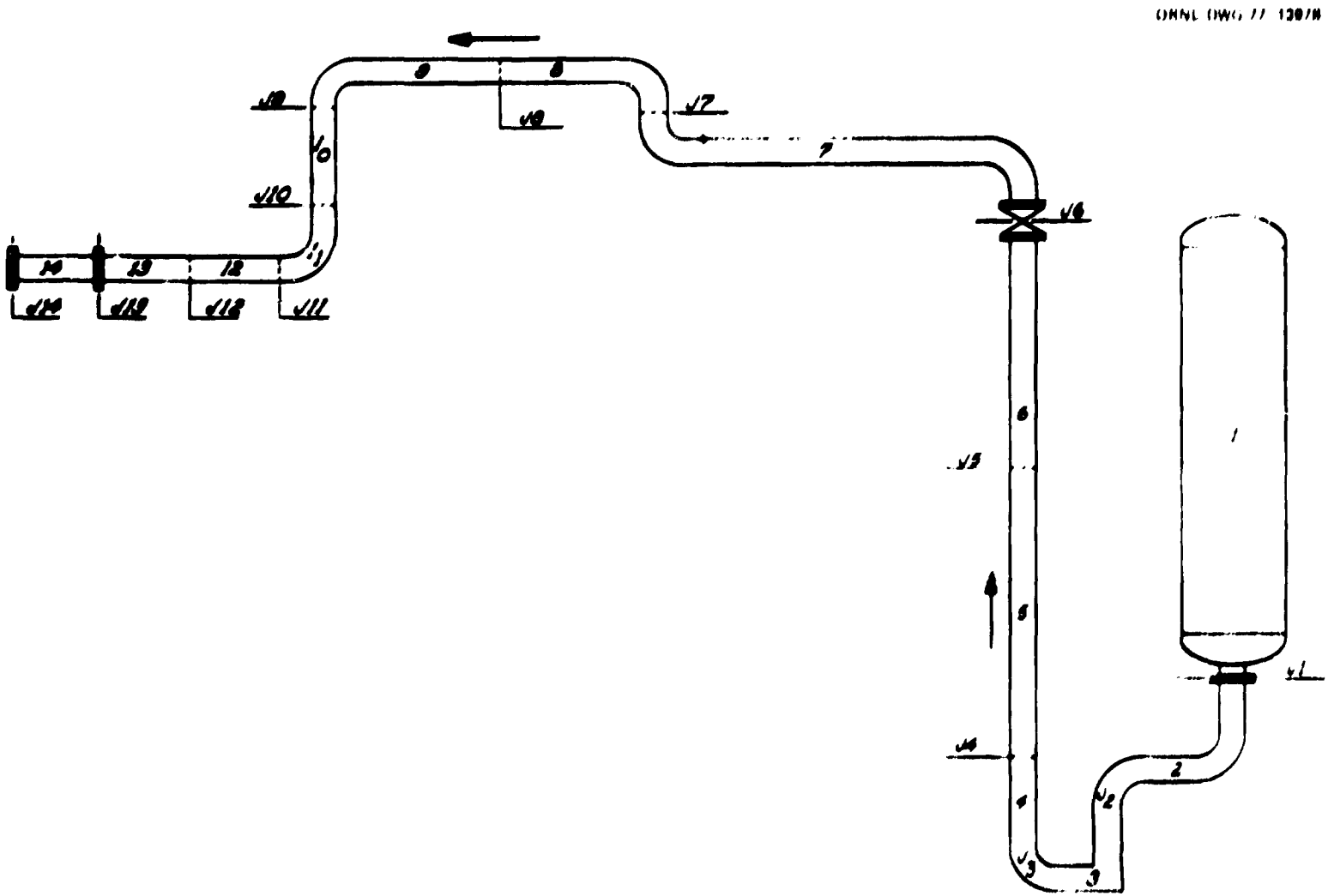

Fig. VIII.2. Depressurization test model node diagram.

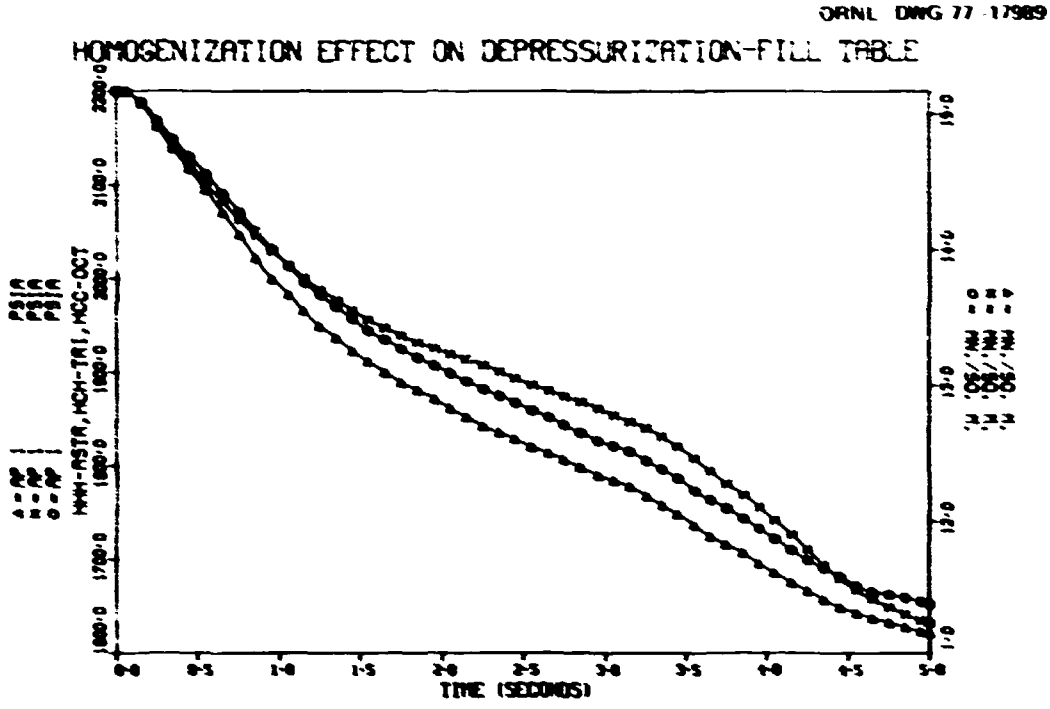

Fig. VIII.3. Depressurization test model; pressure in pressurizer when model is bounded by a fill table.

the same throughout the system. This demonstrates that RELAP's homogenization of fluid can significantly depress the predicted system pressure.

After 2 sec in the HHH test and through most of the HCC test, the difference between the fill table's specified enthalpy and that of the fluid arriving in volume 14 will increase. We do not believe this introduces significant error, so comparisons between all runs for the entire 5 sec will reflect the effects of fluid homogenization. The HCH test pressure is substantially below that for the HCC test. Note that the magnitude of the pressure depression caused by the addition of the 607 to 559 K (633 to 547°F) interface is comparable to the amount that RELAP's predicted pressure for test 103 is below the measured data. The HHH and HCH tests were also calculated by RELAP with the fill table replaced by a leak junction with HF/HEM (0.8/0.9) choking. The pressure feedback has only a marginal effect (Fig. VIII.4).

In test 103, the 566.5 K (560°F) water initially between the heat exchanger and the pressurizer had remained essentially intact when it reached the outlet break. In RELAP, this water was incorrectly mixed

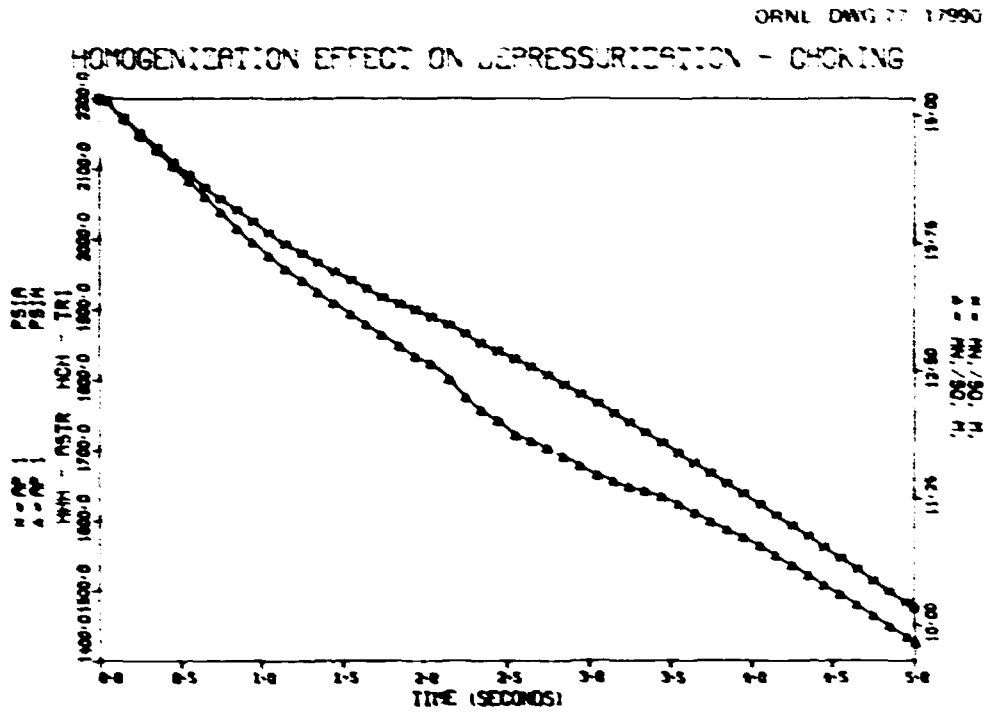

Fig. VIII.4. Depressurization test model; pressure in pressurizer when model is bounded by a leak junction.

with the 607 K (633°F) water of the outlet piping, thus lowering its pressure prediction below the data. In test 100, such an interface did not exist, and RELAP closely predicted the pressure. In test 101, where the outlet piping temperature difference is smaller [572 to 559 K (570 to 547°F)], RELAP's prediction was not as far below the data as in test 103. All THTF tests share a temperature interface at the pressurizer surge line where the saturated fluid contacts the cold water downstream of the heat exchangers. RELAP will homogenize this interface as well, but the extent of error introduced by this depends on the extent to which the interface is maintained in the actual test. If the fluids had been thoroughly mixed, RELAP's homogenization would have been correct. Unrealistic mixing at this second interface would tend to incorrectly depress the pressure prediction, but, as previously mentioned, HF/HEM (0.8/0.9) retains too much mass in the system and these effects may compensate for each other to produce the better pressure prediction for test 100.

Based on the preceding work, the most correct choking model used thus far for the THTF is HF/HEM (0.8/0.9). It produces a better prediction of

the resurgence and more correct break flows. A model of the THTF with a larger number of smaller volumes has been created (Fig. VIII.5), but it does not significantly reduce the depression of pressure. A model with very small volumes may ameliorate this effect to a noticeable degree; this possibility is currently being investigated. The enthalpy transport option[9] does not operate as intended in RELAP4/MOD5 (update 2) and was not used. A properly operating enthalpy transport option might reduce the pressure depression. RELAP's homogeneous assumption is the major cause of the errors in pressure seen in the powered tests.

In addition to directly altering the system pressure by homogenizing mass and energy variations, mixing has had other deleterious effects on RELAP calculations. A marked slowing of the depressurization rate in the THTF in full-power tests, believed to be due to passage of the low-quality plug at the outlet break, was not calculated by RELAP. For example, in the vertical outlet spool piece pressure comparison for test 102 (Fig. IV.1), the pressure error of about 0.34 MN/m^2 (50 psi) existing at 2 sec is probably due to mixing which occurred from 0.5 to 1.5 sec in the hot-leg piping. The divergence in the two pressures from 2 until 4 sec occurs because RELAP has no concentrated liquid to be blown through the outlet break during that period; its pressure curve continues to rapidly decay while the actual pressure decays at a slower rate. Thus, the calculated pressure at 4.5 sec is in error by 0.69 MN/m^2 (100 psi).

As a result of a too-rapid transport of energy, calculated enthalpies will sometimes be in error in the control volume upstream of a junction where a critical flow rate is being calculated. This results in erroneous input data for the critical flow model in RELAP, and incorrect mass fluxes are returned. If the starting system inventory is correctly modeled, this effect tends to cancel itself later in the transient, since an overprediction of the enthalpy at this point will probably result in an underprediction later.

In the simulation of a blowdown experiment, RELAP tends to "wash out" temperature interfaces in subcooled fluids, possibly resulting in calculation of premature or tardy times of saturation. At the horizontal inlet spool piece (Fig. VIII.6), the leading edge of hot fluid from the pressurizer was predicted to arrive too soon, causing calculated saturation times

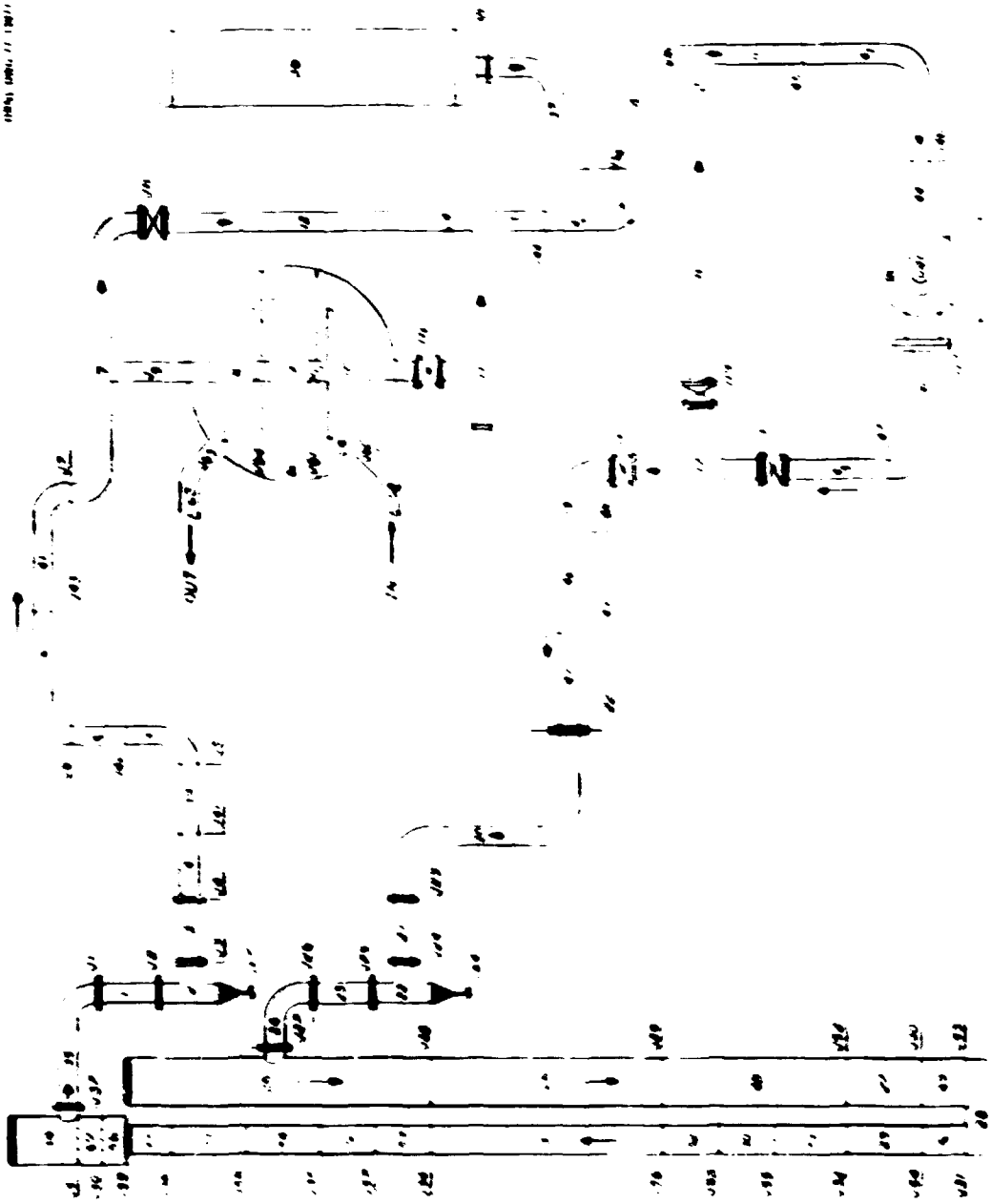

FIG. VIII.5. RELAP renoded model of THTF.

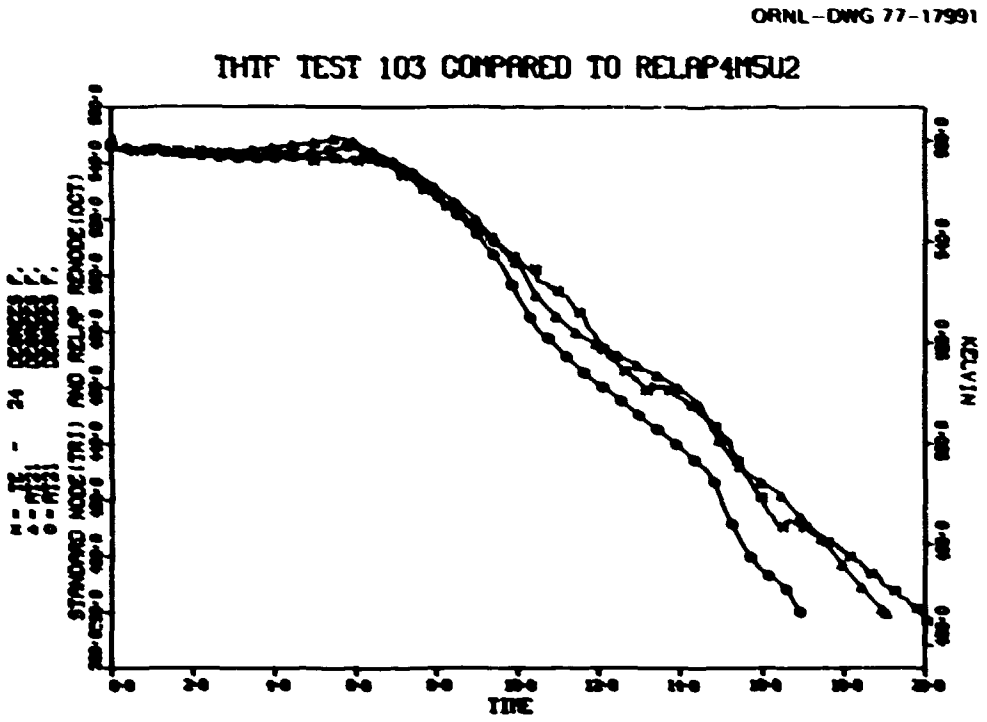

Fig. VIII.6. Horizontal inlet spool piece temperature; system model and renoded model vs experimental data for test 103.

to be early by at least 1 sec in the six THTF tests analyzed. For some calculations, time-dependent fluid conditions were specified in the pressurizer, resulting in calculation of correct or slightly high pressures at the horizontal inlet spool piece; saturation was still predicted to occur approximately 0.6 sec early. At a temperature of 560 K (548°F), only a 3.3 K (6°F) temperature rise is required to offset a 0.34-MN/m^2 (50-psi) pressure excess. At the vertical inlet spool piece (Fig. V.6), a 25 K (45°F) rise actually occurred by 2 sec and flashing occurred at a pressure of 9.65 MN/m^2 (1400 psi). In RELAP calculations, the temperature front was broad, and only a 16.7 K (30°F) rise could be realized before the saturation curve was reached. If the calculated pressure had been correct, RELAP's saturation time would have been even later at the vertical inlet. The pressure differential across the test section may be poorly simulated when such problems occur in the predicted densities. In the hydraulics section of the RELAP version used, mixing may well be the single largest source of inaccuracy, considering its influence on errors in calculated densities and pressures.

The renoded THTF system model shown in Fig. VIII.5 was produced during these studies (Appendix C). Its main purpose was to explore the effect of additional detail on RELAP's energy transport problems. The renoded test section also allowed definition of a small node, number 55, for use in comparing calculated fluid temperatures with subchannel thermocouple data. The improvement observed in calculated fluid temperatures and densities was not dramatic. The density predicted for the horizontal outlet was perhaps more like the recorded data (Fig. VIII.7), but the resulting presure flattening effect was still not predicted. Fluid temperatures before saturation at the horizontal inlet were definitely improved (Fig. VIII.6), but the temperature in the special subchannel node was nearly identical to that in the uppermost node in the standard model. RELAP still predicted too much superheat. Some improvement in the calculation of volumetric flow rates was also noted, mostly between 10 and 20 sec.

THTF pressures calculated with the renoded model were generally lower than either the standard model or the recorded data, especially late in

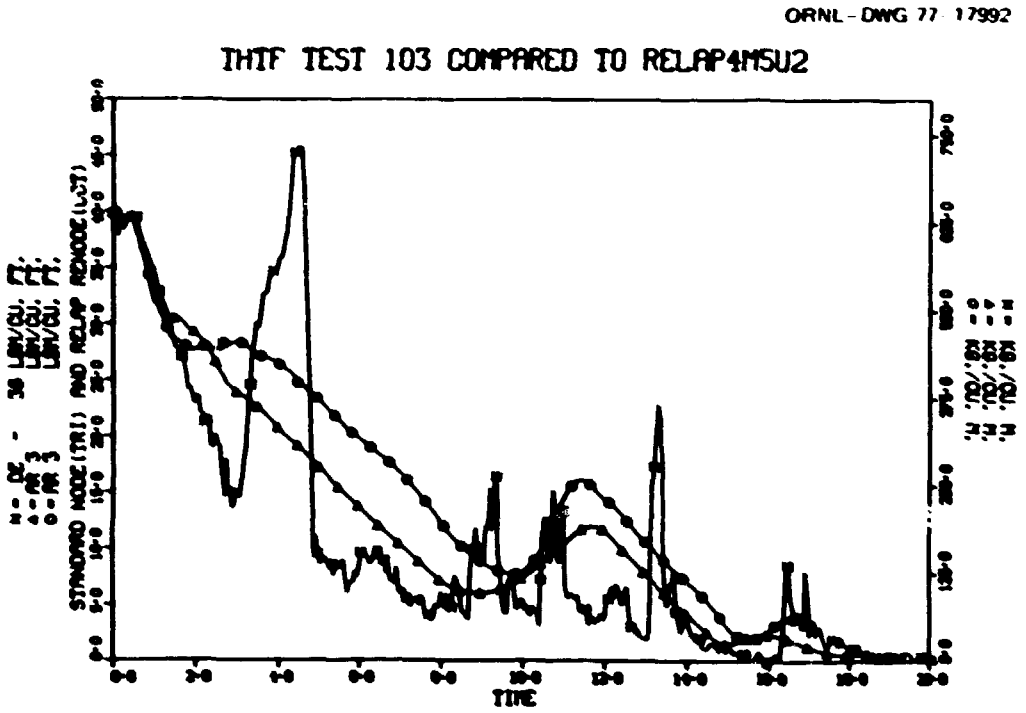

Fig. VIII.7. Horizontal outlet spool piece density; system model and renoded model vs experimental data for test 103.

the transient. Figure VIII.8 illustrates that this was due to omission of piping heat transfer from the renoded model. The standard model without piping heat slabs produces the low pressures, while addition of the piping slabs restores the pressure to a more correct level. Inclusion of one slab for each piping node was not possible in the renoded model concurrent with the more detailed modeling of the test section. Therefore, we chose to use the standard nodalization for the final analysis, trading additional detail for a smaller number of piping nodes with heat transfer. The maximum of 50 heat slabs currently available in RELAP requires continuation of the practice of supplying boundary conditions for a detailed test section model from a system model having a minimum number of test section heat slabs. The system model should, however, have as much detail in loop piping as possible, still allowing one piping heat slab per node.

Use of the vertical slip option in RELAP is appropriate when low mass fluxes are calculated to occur in vertical stacks of nodes. Predictions of volumetric flows at the test section outlet were improved

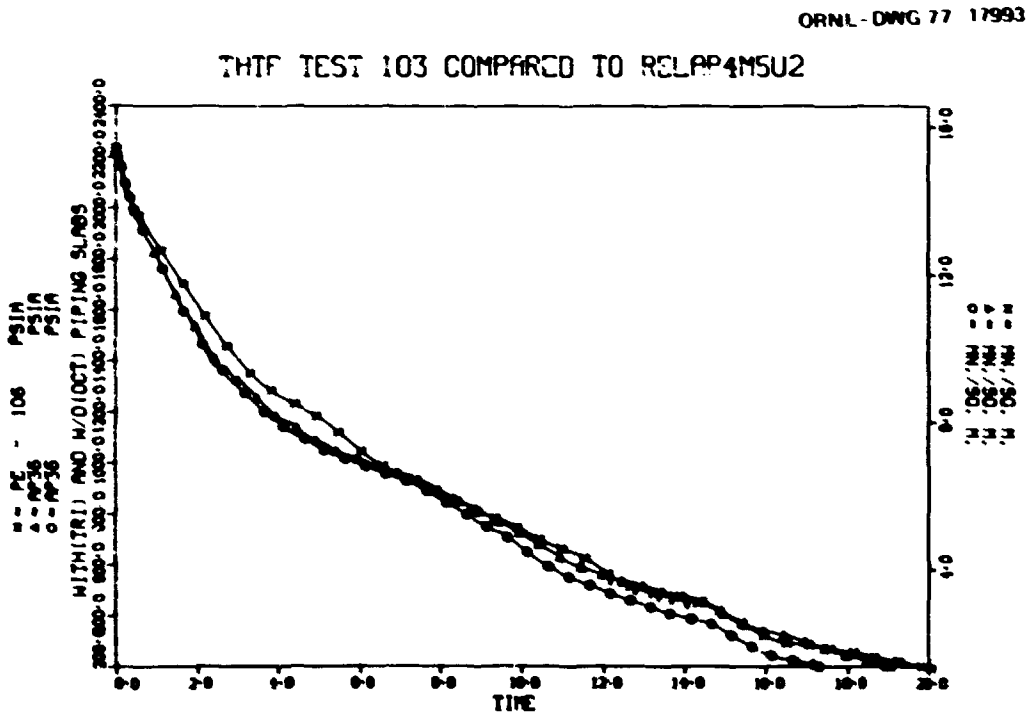

Fig. VIII.8. Pressurizer pressure; system model with and without piping heat slabs vs experimental data for test 103.

when vertical slip was used in downcomer junctions 28, 29, and 30. The most improvement was in test 101, where the transient was relatively slow due to a smaller break area and gravitational forces had greater effect. When a negative-to-positive flow reversal was indicated by the vertical inlet turbine, a sharp density increase was also recorded. Without slip in the downcomer, RELAP predicted the flow reversal and density rise; with slip, the predicted flow was slightly different such that positive flow was not realized and no density increase occurred. The vertical slip model allows more steam to flow upward out of the downcomer and toward the inlet break, while the net mass flow rate near the lower plenum remains positive. Calculated flow through the vertical inlet spool becomes negative due to steam exiting the test section. Conditions in the test section itself are probably better modeled with vertical slip in the downcomer, though core instrumentation is presently inadequate for a firm conclusion to be reached.

IX. CONCLUSIONS

IX.1. Experimental

The experimental data presented in this report represent the most significant aspects of the overall system response for THTF tests 100 through 105. These tests encompass the experimental checkout of the facility and its ability to produce the transient data required. They also include baseline tests for determining the input parameters necessary for the verification of large digital simulators such as RELAP4/MOD5 (update 2). Tests 103, 104, and 105 provide a significant data base for use in investigating thermal-hydraulic phenomena associated with loss-of-coolant accidents.

Test 100 was designed to investigate the ability of the THTF to withstand blowdown forces, to provide flow and pressure drop data for improvement of the RELAP4 model, and to check the computer-controlled data acquisition system with approximately 550 rod bundle thermocouples being monitored. All of these objectives were met. Test 101 operated with a 100% (nominal size) outlet break and 25% of full power. The data acquired provided a case with a small core temperature differential and no core flow reversal. Test 102 was the first test at full power and design fluid temperatures. Comparison of the responses from tests 102 and 100 shows the effects of initial hot-leg to cold-leg temperature differential with the 50% inlet–50% outlet break configuration. In test 104, which was performed next in the series, the first measurements of departure from nucleate boiling and post-critical heat flux heat transfer were made. The electric core in this test was operated at 100% full power for 2 sec into the transient. The indicated flows at the spool pieces were very similar to those observed in test 102, but the measured fluid temperatures were higher during the transient due to the longer operation of the electric core at full power. Test 103 was performed to verify RELAP calculations which indicated that the core flows in an NRC PWR double-ended guillotine break study could be approximated in the THTF with a 60% outlet–40% inlet break configuration. Test 105 was performed with this same break configuration, and the electric core power was decayed with a 0.45-sec

time constant after 2 sec of full power in the transient. The desired flows coupled with the power transient made test 105 the "reactor case" of this series. The power decay resulted in higher core fluid and rod sheath temperatures.

In this test series, the fluid in the pressurizer represented a large portion of the total system mass and had the highest average specific internal energy. With the pressurizer discharging into the primary system downstream of the main heat exchangers, its surge during the early portion of the blowdown retarded or completely stopped the flow from the test section outlet. Thus, the performance of the primary pump and heat exchangers and the energy deposition from the electric core and primary loop piping had secondary influence on the observed hydraulic response at the spool pieces during the first 10 sec of the tests. The critical flow rates at the breaks and the pressurizer fluid discharge and subsequent redistribution were the dominant forcing functions during that time period.

The reduced spool piece instrument responses allowed valuable comparisons to the predictions from the RELAP system model of the THTF. Although two-phase flow instrumentation problems existed, an understanding of the overall hydraulic response of the THTF with bundle 1 has been gained. Core flows similar to those of the NRC PWR double-ended guillotine break study have been achieved, but obtaining other desired flows will require moving and isolating the pressurizer. A detailed discussion of the core heat transfer phenomena and the calculation of transient heat transfer coefficients will be presented in a separate report.

IX.2. RELAP

Hydraulic phenomena observed in THTF tests 100 through 105 were analyzed, and the ability of the minimum controls version of RELAP4/MOD5 (update 2) to predict the phenomena was evaluated. Comparisons of predicted and recorded pressures, densities, and fluid temperatures at the spool pieces were emphasized, since those properties were most reliably measured and since they directly influence test section fluid conditions.

Variation of some RELAP input parameters was found to have little effect on calculated system response, but choice of critical flow models

and their multipliers strongly influenced the predictions. Differences between the accuracy of calculated system pressures for test 100 and for the tests with rod power led to investigation of the effects of integral averaging of fluid properties in RELAP. Predictions of the total leaked mass and energy were found to be in better agreement with estimates of the actual system losses for calculations using the Extended-Henry (0.8 multiplier, subcooled)-Homogeneous Equilibrium Model (0.9 multiplier, two phase) critical flow tables than for those using the HEM (0.8 multiplier) alone. The underprediction of pressures with the HF-HEM option is primarily the result of the mixing by RELAP of fluid energy fronts. The initial temperature differential across interfaces, the number of interfaces, and the degree of actual mixing in the system affect the severity of errors in predicted pressures.

In addition to pressure depression, mixing also caused errors in density and fluid temperature predictions. Density errors at leak junctions produced errors in critical flow calculations and depressurization rates and contributed to poorly predicted times of flow reversals at the spool pieces and in the test section. Temperature errors due to mixing and too-rapid transport of energy contribute to incorrect predictions of calculated fluid saturation times.

In studies made thus far, more detailed nodalization of the THTF has not significantly improved low pressure predictions, although some improvement was seen in calculated transport of energy fronts. Heat slabs representing system piping are required for accurate calculation of late transient pressures, but only 50 heat slabs are allowed in RELAP. Therefore, a system model with a simple test section nodalization should be used to supply boundary conditions for a component model of the test section.

With the current configuration of the THTF (i.e., the pressurizer, without an orifice, located downstream of the main heat exchangers), the effects of fluid homogenization in RELAP are particularly in evidence. In spite of this, some observed trends are generally well predicted although those of in-core flow response are difficult to evaluate at present. Some existing spool piece instrumentation needs refinement for more useful modeling comparisons. Improvement in the existing system model may be possible with finer nodalization outside the test section and/or incorporation of the enthalpy transport option when it is corrected.

REFERENCES

1. *Project Description ORNL PWR Blowdown Heat Transfer Separate-Effects Program — Thermal-Hydraulic Test Facility (THTF)*, ORNL/NUREG/TM-2 (February 1976).

2. M. D. White and R. A. Hedrick, *PWR Blowdown Heat Transfer Separate-Effects Program — Thermal-Hydraulic Test Facility Experimental Data Report for Test 101*, ORNL/NUREG/TM-114 (August 1977).

3. M. D. White and R. A. Hedrick, *PWR Blowdown Heat Transfer Separate-Effects Program — Thermal-Hydraulic Test Facility Experimental Data Report for Test 101*, ORNL/NUREG/TM-128 (September 1977).

4. R. A. Hedrick et al., *PWR Blowdown Heat Transfer Separate-Effects Program — Thermal-Hydraulic Test Facility Experimental Data Report for Test 102*, ORNL/NUREG/TM- (to be published).

5. R. A. Hedrick et al., *PWR Blowdown Heat Transfer Separate-Effects Program — Thermal-Hydraulic Test Facility Experimental Data Report for Test 103*, ORNL/NUREG/TM- (to be published).

6. R. A. Hedrick et al., *PWR Blowdown Heat Transfer Separate-Effects Program — Thermal-Hydraulic Test Facility Experimental Data Report for Test 104*, ORNL/NUREG/TM- (to be published).

7. R. A. Hedrick et al., *PWR Blowdown Heat Transfer Separate-Effects Program — Thermal-Hydraulic Test Facility Experimental Data Report for Test 105*, ORNL/NUREG/TM-143 (to be published).

8. R. A. Hedrick et al., *Data Evaluation Report — Electric Core Response THTF Test Series 100*, ORNL/NUREG/TM- (to be published).

9. *RELAP4/MOD5: A Computer Program for Transient Thermal-Hydraulic Analysis of Nuclear Reactors and Related Systems Users' Manual*, ANCR/NUREG/1335 (September 1976).

10. R. A. Hedrick et al., *RELAP4 Models of the Thermal-Hydraulic Test Facility*, ORNL/NUREG/TM- (to be published).

11. G. F. Hewitt and P. C. Lovegrove, *Experimental Methods in Two-Phase Flow Studies*, EPRI NP-118 (March 1976).

12. H. Estrada, Jr., and J. D. Sheppard, *Some Aspects of Interpreting Two-Phase Flow Measurements in Instrumented Piping Spool Pieces*, NUREG-0280 (June 1977).

13. Calculational method to be published later.

14. Izuo Aya, *A model to Calculate Mass Flow Rate and Other Quantities of Two-Phase Flow in a Pipe with a Densitometer, a Drag Disk, and a Turbine Meter*, ORNL/TM-4759 (November 1975).

15. L. J. Ott, and R. A. Hedrick, ORINC – A One-Dimensional Implicit Approach to the Inverse Heat Conduction Problem, ORNL/NUREG/TM-117 (to be published).

Appendix A

RELAP THTF STANDARD MODEL LISTING

```
*BE103       BEST EFFORT DECK WITH MEAN GAP FOR TEST 103 - 20 APR 77
*
*   THIS DECK HAS A MODELED SECONDARY SIDE TO THE MAIN HX
*   THIS DECK USES AN APPROXIMATION TO THE ACTUAL INITIAL CONDITIONS
*   FOR TEST 103.  IT HAS INITIAL FLOW DERIVED FROM AN ENERGY BALANCE
*   ON THE CORE USING THERMOCOUPLE AND POWER METER READINGS.  IT DOES NOT
*   HAVE SLIP.  IT HAS A FIXED SIZE (SET AT THE MEAN FOR THAT LEVEL)
*   GAP MODEL IN ALL CORE SLABS - BETWEEN THE SS SHEATHS IN THE
*   INNER CORE SLABS AND BETWEEN THE BN AND SS IN THE OUTER CORE
*   SLABS.  THE PRESSURES HAVE BEEN ADJUSTED TO BE CLOSER TO THE
*   ACTUAL PRESSURES.  THE TEMPERATURES IN THE LOOP HAVE ALSO BEEN
*   ADJUSTED.  THE MIXTURE LEVEL IN THE PRESSURIZER HAS BEEN ADJUSTED.
*   NOTE:  PRESS. MIX LEVEL ADJUSTED AS OF 25 MAR 77
*   THE MATERIAL PROPERTIES HAVE BEEN UPDATED.
*   ENTHALPY TRANSPORT IS NOT USED.
*
*
*
*
*
*
* PROBLEM DIMENSIONS
*
C10001 -2  9  4  5 43  1  2 46  1  0  2  0 45 11  6  5  1  0
C10002    5.9725  1.0
*
* MIMIR EDIT VARIABLES
*
C20000 AP 31 AT 31 TS 31 AM 31 AX 31 FR 3 CR 3 KR 3 SR 3
*
*   ENTHALPY TRANSPORT SHUT OFF
*
C30003  0  0.  0.  .000001
*
* TIME STEP CARDS
*
C30010   500  10  1  0  .0001   .00001       .001
C30020    50  10  1  0  .001    .00001       .01
C30030     5  10  1  0  .01     .00001       .5
C30040     5  10  1  0  .01     .00001  210.
*
* TRIP CARDS
*
C40010  1  1  0  0   20.0    0.0 * TRIP END
C40020  2  1  0  0    0.0    0.0 * TRIP LEAK TO FIRST POWER CURVE
C40030  3  1  0  0    0.0    0.09* TRIP PUMP
C40040  4  1  0  0    0.0    1.965 *TRIP SEC FLOW ON HEAT-X
C40050  1 -4 36  0  200.     0.   * TRIP END BELOW 200 PSI
*
* VOLUME DATA CARDS
*
C50011 0    0 2265.4326 634.2156 -1.000 0.200400   3.0000   3.0000 *S.P.1 OUTLET
C50021 0    0 2257.1453 634.1633 -1.000 0.202600   2.0140   2.0140 *BLOWDOWN TEE
C50031 0    0 2246.4516 634.0959 -1.000 0.200400   0.2920   0.2920 *S.P.2 OUTLET
C50041 0    0 2236.4834 634.0327 -1.000 0.675100   0.2920   0.2920 *HORIZ TO HEX
C50051 0    0 2234.1450 634.0178 -1.000 0.871900  13.2900  13.2900 *VERT TO HEX
C50061 0    0 2232.0383 634.0046 -1.000 0.657900   1.6440   1.6440 *TO HX HEADER
C50071 0    0 2231.9729 634.0042 -1.000 0.233200   0.2920   0.2920 *INLET HEADR
C50081 0    0 2232.4535 562.7591 -1.000 0.591400   4.1000   4.1000 *HEX FIRST PT
C50091 0    0 2233.0513 406.7654 -1.000 0.591400   0.9000   0.9000 *HX SECOND PT
C50101 0    0 2233.4221 279.5674 -1.000 0.591400   2.1500   2.1500 *HX THIRD PT
C50111 0    0 2212.6554 223.9976 -1.000 0.560700   0.2920   0.2920 *OUT HEADER
C50121 0    0 2212.4524 633.8801 -1.000 0.495900   7.0400   7.0400 *HX BYPASS
C50131 0    0 2213.9527 560.3484 -1.000 0.591100   0.4870   0.4870 *VERT TO PRES
C50141 0    0 2215.2236 560.3503 -1.000 0.403000   0.2920   0.2920 *HORZ TO PRES
C50151 0    0 2211.7473 543.4497 -1.000 1.702000   1.1000   1.1000 * TO PUMP IN
C50161 0    0 2856.6955 547.3533 -1.000 0.970000   0.1460   0.1460 *PUMP DISCHARGE
C50171 0    0 2456.0351 547.0427 -1.000 0.196300   0.2920   0.2920 *BYPASS TEE
C50181 0    0 2215.2104 526.2637 -1.000 0.266500   0.4580   0.4580 *BYPASS, HX D
C50191 0    0 2349.8721 546.9497 -1.000 1.386995   0.2920   0.2920 *HORZ TO T.S.
C50201 0    0 2339.1611 546.9402 -1.000 0.373500   2.3330   2.3330 *VERT TO SP11
C50211 0    0 2330.4255 546.934  -1.000 0.200400   0.2920   0.2920 *S.P. 1 INLET
C50221 0    0 2322.9158 546.9255 -1.000 0.267800   1.9140   1.9140 *B.C.TEE INLET
C50231 0    0 2313.1542 546.9167 -1.000 0.200400   3.0000   3.0000 *S.P.2 INLET
C50241 0    0 2304.1514 546.9078 -1.000 0.170200   1.2600   1.2600 *T.S. INLET
C50251 0    0 2304.7765 546.9077 -1.000 0.927800   5.0210   5.0210 *TOP DOWNCOMER
C50261 0    0 2306.0359 546.9092 -1.000 0.525400   2.9500   2.9500 *MID DOWNCOMER
C50271 0    0 2307.2136 546.9104 -1.000 0.834000   4.5130   4.5130 *BOT DOWNCMER
C50281 0    0 2308.0453 546.9114 -1.000 0.236000   0.8740   0.8740 *LOWER PLENUM
C50291 0    0 2302.5462 552.3870 -1.000 0.169000   2.6540   2.6540 *1ST HEATED
C50301 0    0 2297.7075 566.7417 -1.000 0.118400   1.8590   1.8590 *2ND HEATED
C50311 0    0 2291.9441 594.3459 -1.000 0.097900   2.9500   2.9500 *3RD HEATED
C50321 0    0 2285.5524 619.2241 -1.000 0.117900   1.8530   1.8500 *4TH HEATED
C50331 0    0 2280.2668 630.3374 -1.000 0.167000   2.6230   2.6230 *5TH HEATED
C50341 0    0 2277.0000 634.2881 -1.000 0.618000   2.4930   2.4930 *UPPER PLENUM
C50351 0    0 2274.8096 634.2744 -1.000 0.384000   0.8530   0.8500 *OUTLET LINE
C50361 1    0 2211.8083    0.0     0.0  7.450000  12.4000   5.79   *PRESSURIZER
C50371 0    0 2214.3757 560.3489 -1.000 0.658100   6.1000   6.1000 *PRNSS LN
C50381 0    0 2274.5066 545.4102 -1.000 1.490000   2.0000   2.0000 * PUMP
C50391  0  1  250.   70.  -1.0  0.4912  1.25  1.25          *SEC INLET HEADER
C50401  0  0  238.   51.5 -1.0  0.4912  0.95  0.95          *HEX SEC PART ONE
C50411  0  0  236.  143.5 -1.0  0.4912  0.95  0.95          *HEX SEC PART TWO
C50421  0  0  234.0 211.5 -1.0  0.4912  0.95  0.95          *HEX SEC PART THREE
```

```
050431  0   2   232.    250.    -1.0    0.4912   3.1537   3.1537      *HEX SEC OUTLET HDR
050012  0   0.C668100   C.2516959   930.7100   0                       *S.P.1 OUTLET
050022  0   C.11C4000   C.3750000   928.7076   0                       *BLOWDOWN TEE
050032  0   C.C668100   0.2516959   929.7078   0                       *S.P.2 OUTLET
050042  0   C.C668100   C.2516959   929.7078   0                       *HORIZ TO HEX
050052  0   0.C668100   C.2516959   929.8538   0                       *VERT TO HEX
050062  0   C.C668100   C.2516959   941.5000   0                       *TO HX HEADER
050072  0   0.C668100   0.2516959   941.3528   0                       *INLET HEADR
050082  0   0.C573C00   0.0562158   937.2537   0                       *HEX FIRST PT
050092  0   0.C573C00   C.0562158   936.3606   0                       *HX SECOND PT
050102  0   0.C573000   0.0562158   934.2610   0                       *HX THIRD PT
050112  0   C.C668200   C.2516959   934.2620   0                       *OUT HEADER
050122  0   0.C668100   C.2516959   934.4170   0                       *HX BYPASS
050132  0   C.C668100   C.2516959   924.9380   0                       *VERT TO PRES
050142  0   C.C668100   C.2516959   924.7920   0                       *HORZ TO PRES
050152  0   0.C668100   0.2516959   923.8825   0                       * TO PUMP IN
050162  0   0.C668100   0.2516959   924.(750   0                       *PUMP DISCHARGE
050172  0   C.C668100   0.2516959   923.9368   0                       *BYPASS TEE
050182  0   0.C2C5000   0.1619959   923.4886   0                       *BYPASS, HX O
050192  0   C.C668100   C.2516959   923.9368   0                       *HORZ TO T.S.
050202  0   C.C668100   C.2516959   924.0828   0                       *VERT TO SPII
050212  0   0.C668100   C.2516959   926.2710   0                       *S.P. 1 INLET
050222  0   C.1 C4000   C.3750000   925.2710   0                       *B.D.TEE INLET
050232  0   0.C668100   0.2516959   927.1089   0                       *S.P.2 INLET
050242  0   C.C668100   C.2516959   930.1050   0                       *T.S. INLET
050252  0   0.1848000   0.1750000   927.7317   0                       *TOP DOWNCOMER
050262  0   C.1848000   C.1750000   924.7830   0                       *MID DOWNCOMER
050272  0   C.1848000   C.1750000   920.2737   0                       *BOT DOWNCMER
050282  0   0.3C19000   C.1750000   919.4500   0                       *LOWER PLENUM
050292  0   C.C634800   0.0197321   920.2698   0                       *1ST HEATED
050302  0   0.C634800   0.0197321   922.9197   0                       *2ND HEATED
050312  0   0.C634800   0.0197321   924.7747   0                       *3RD HEATED
050322  0   C.C634800   C.0197321   927.7205   0                       *4TH HEATED
050332  0   C.C634800   C.0197321   929.5669   0                       *5TH HEATED
050342  0   C.2520000   C.3150000   932.1858   0                       *UPPER PLENUM
050352  0   0.C668100   0.2520000   933.7000   0                       *OUTLET LINE
050362  0   0.6C1C000   0.6750000   930.9397   0                       *PRESSURIZER
050372  1   0.C668100   0.2516959   924.8997   0                       *PRNSS LN
050382  0   C.C668100   C.2516959   922.0999   0                       * PUMP
050392   0   0.C6551   C.0   934.261
050402   0   0.C6551   C.04720   935.4606
050412   0   0.C6551   C.04720   936.3606
050422   0   0.C6551  C.04720   937.2537
050432   0   0.C6551  C.0   938.2
*
* BUBBLE RISE CARD
060011                0.8          3.0
*
*
* TIME DEPENDENT VOLUMES FOR SECONDARY HX SIDE
*
070100  1
070200  6   2.   232.   250.   0.   3.1537
070201      5.   246.2   250.   0.   3.1537
070202      7.   247.5   250.   0.   3.1537
070203     12.   247.8   250.   0.   3.1537
070204     20.   248.0   250.   0.   3.1537
*
* JUNCTION DATA CARDS
*
*THE AREA OF JUNCTIONS WITH ORIFICES OR VALVES IS = ADJACENT VOL CS AREA
*
080011 35  1    C   0 46.035993 0.0668100   933.70459   0.0          7.500       7.500
080021  1  2    C   0 46.039993 0.0668100   930.71094   0.0          7.500       7.500
080031  2  3    C   0 46.035993 0.0668100   929.85375   0.0          7.500       7.500
080041  3  4    C   0 46.039993 0.0668100   929.85375   0.0          7.500       7.500
080051  4  5    C   0 46.035993 0.0668100   929.85474   0.0          0.0         0.0
080061  5  6    C   0 46.039993 0.0668100   943.14258   0.0          0.0         0.0
080071  6  7    C   0 46.035993 0.0668100   941.54932   0.0          0.0         0.0
080081  7 12    C   0 35.638412 0.0668100   941.39966   0.0          0.0         0.0
080091  7  8    C   0 10.401578 0.0573000   941.35303   0.0          0.0         0.0
080101  8  9    C   0 10.401578 0.0573000   937.25977   0.0          0.0         0.0
080111  9 10    C   0 10.401578 0.0573000   936.36084   0.0          0.0         0.0
080121 10 11    C   0 10.401578 0.0573000   934.29932   0.0          0.0         0.0
080131 11 13    C   0 10.401578 0.0668100   934.41797   0.0          0.0         0.0
080141 12 13    C   0 35.638412 0.0668100   934.41968   0.0          0.0         0.0
080151 13 14    C   0 46.039993 0.0668100   924.93973   0.0          0.0         0.0
080161 14 15    C   0 46.035993 0.0668100   924.93973   0.0          0.0         0.0
080171 38 16    1   0 67.355994 0.0668100   924.08252   0.0          0.0         0.0
080181 16 17    C   0 67.355994 0.0668100   924.09961   0.0          0.0         0.0
080191 17 18    C   0 21.360C01 0.0205000   923.93973   0.0          0.0         0.0
080201 18 15    C   0 21.360C01 0.0205000   923.93973   0.0          0.0         0.0
080211 17 19    C   0 46.035993 0.0668100   924.09961   0.0          0.0         0.0
080221 19 20    C   0 46.035993 0.0668100   924.08472   0.0          9.000       9.000
080231 20 21    C   0 46.039993 0.0668100   926.29932   0.0          7.500       7.500
080241 21 22    C   0 46.035993 0.0668100   926.29932   0.0          7.500       7.500
080251 22 23    C   0 46.035993 0.0668100   927.13965   0.0          7.500       7.500
080261 23 24    C   0 46.039993 0.0668100   930.10669   0.0          7.500       7.500
080271 24 25    C   0 46.035993 0.0668100   931.29932   0.0          0.0         0.0
080281 25 26    C   0 46.035993 0.1848000   927.73218   0.0          0.0         0.0
080291 26 27    C   0 46.035993 0.1848000   924.78467   0.0          0.0         0.0
080301 27 28    C   0 46.035993 0.1848000   920.27588   0.0          0.639       0.639
080311 28 29    C   0 46.039993 0.0634800   920.27173   0.0          1.614       1.614
```

```
080321  29  30    C   0 46.035993 0.0634800   922.92182    0.0          1.654      1.654
080331  30  31    C   0 46.035993 0.0634800   924.77686    0.0          1.762      1.762
080341  31  32    C   0 46.035993 0.0634800   927.72266    0.0          1.758      1.758
080351  32  33    C   0 46.035993 0.0634800   929.56885    0.0          1.639      1.639
080361  33  34    C   0 46.035993 0.0634800   932.18799    0.0          1.605      1.605
080371  34  35    C   0 46.035993 0.0668100   934.50000    0.0          0.500      0.500
080381  36  37    C   0   0.0      0.0668100   930.94971    0.0          1.000      1.000
080391  37  14    C   0   0.0      0.0668100   924.91968   90.000000     1.000      1.000
080401  15  38   -1   0 67.355994 0.0668100   924.08252    0.0          0.0        0.0
080411  39  40    C   0  29.31   0.03475   935.4608   10.  8.   8.    *HEX SEC CONTROL VALV
080421  40  41    C   0  29.31   0.06951   936.3608  10.   0.5  0.5
080431  41  42    C   0  29.31   0.06951   937.2539  10.   0.5  0.5
080441  42  43    C   0  29.31   0.06951   938.202  10.   0.5  0.5
080451  22   0    2   0   0.0       0.0135000   925.29932    0.0          0.0        0.0
080461   2   0    1   0   0.0       0.0135000   928.70972    0.0          0.0        0.0
080012 0   C   2   0 0.C       0.600    0 0 0.0       0
080022 0   C   2   0 0.C       0.600    0 0 0.0       0
080032 0   C   2   0 0.C       0.600    0 0 0.0       0
080042 0   C   2   0 0.C       0.600    0 0 0.0       0
080052 0   0   3   C 0.C       0.600    0 0 0.0       0
080062 0   C   3   0 0.C       0.600    0 0 0.0       0
080072 0   C   3   C 0.C       0.600    0 0 0.0       0
080082 0   C   3   C 0.C       0.600    0 0 0.0       0
080092 0   C   3   3 0.C       0.600    0 0 0.0       0
080102 0   C   3   0 0.C       0.600    0 0 0.0       0
080112 0   C   3   0 0.C       0.600    0 0 0.0       0
080122 0   0   3   0 0.C       0.600    0 0 0.0       0
080132 0   C   3   3 0.C       0.600    0 0 0.0       0
080142 0   0   3   C 0.C       0.600    0 0 0.0       0
080152 0   C   3   0 0.C       0.600    0 0 0.0       0
080162 0   C   3   0 0.C       0.600    0 0 0.0       0
080172 0   C   3   C 0.C       0.600    0 0 0.0       0
080182 0   C   3   C 0.C       0.600    0 0 0.0       0
080192 0   C   3   3 0.C       0.600    0 0 0.0       0
080202 0   0   3   3 0.C       0.600    0 0 0.0       0
080212 0   C   3   C 0.C       0.600    0 0 0.0       0
080222 0   C   2   C 0.C       0.600    0 0 0.0       0
080232 0   C   2   0 0.C       0.600    0 0 0.0       0
080242 0   C   2   C 0.C       0.600    0 0 0.0       0
080252 0   C   2   C 0.C       0.600    0 0 0.0       0
080262 0   C   2   0 0.C       0.600    0 0 0.0       0
080272 0   C   3   C 0.C       0.C      0 0 0.0       0
080282 0   C   3   C 0.C       0.0      0 0 1.0       0
080292 0   C   3   0 0.C       C.C      0 0 1.0       0
080302 0   0   2   C 0.C       0.C      0 0 1.0       0
080312 0   C   2   0 0.C       C.C      0 0 0.0       0
080322 0   C   2   0 0.C       C.C      0 0 0.0       0
080332 0   C   2   C 0.C       0.C      0 0 0.0       0
080342 0   C   2   C 0.C       0.C      0 0 0.0       0
080352 0   C   2   C 0.C       C.C      0 0 0.0       0
080362 0   0   2   0 0.C       0.C      0 0 0.0       0
080372 0   0   2   0 0.C       0.C      0 0 0.0       0
080382 0   C   2   0 0.C       C.600    0 0 0.0       0
080392 0   C   0   3 0.C       0.600    0 0 0.0       0
080402 0   0   3   C 0.C       C.600    0 0 0.0       0
080412   0   0   0   3   C.   1.0   0 0
080422   0   0   0   3   C.   1.0   0 0
080432   0   0   0   3   C.   1.0   0 0
080442   0   0   0   3   C.   1.0   0 0
080452 0   S   3   C 0.C       1.000   11 0 0.0       0
080462 0   S   3   C 0.C       1.000   11 0 0.0       0
*
* HENRY-FAUSKE-HEM CRITICAL FLOW MODEL DIALS
*
082003    .5   C.8   0.E   0.C1
*
* PUMP DATA CARDS
*
090011   3 3 C C 0 3580.  1.  640.  1980.0 572.  90.80 47.10
090012   C.000     0.C   00.000   0.000    0.00
*
* PUMP CURVE INPUT INDICATOR
*
100000   0   0   E   0
*
* PUMP CURVES
*
103011   1   1   5     C.C      1.1357   0.2847   1.1253   0.5694   1.0944    *     V/A-LT.1
103012                 0.8541   1.0427   1.0      1.0                         *     HEAD V/A
103021   1   2   7   0.         0.0      0.524    0.1135    0.562    0.1753   *     A/V-LT.1
103022                 0.689     0.3768   0.7024    0.4127    0.8781 0.7324  *     HEAD A/V
103023                 1.       1.
103031   2   1   5     0.C      0.59     0.2857   0.708    0.5714   0.826     *     V/A-LT.1
103032                 0.8571   C.944    1.0      1.0                         *     TORQ V/A
103041   2   2   8     0.      -0.2      0.389    0.25     0.437    0.2933    *     A/V-LT.1
103042                 0.5      0.3538   0.583    0.4415   0.67     0.529     *     TORQ A/V
103043                 0.875    0.8128   1.       1.                          *     TORQ A/V
103051 1 3 3 -1.0 2.C -0.3 1.15 0.0 1.1357
103061 2 3 4 -1.0 1.C -C.7 0.60 -.3 0.5 0.0 0.59
*
```

```
* LEAK JUNCTION CARDS:
*
120100  2  2  14.7  0.0  .6  210.  .6
120200  2  2  14.7  0.0  .4  210.  .4
*
* KINETIC CONSTANTS CARD
*
140000  0  0  0.  0.
*
* SCRAM POWER CARD
*
141001  -4  2  0.  1.0  1.965  1.0  2.025  0.  210.  0.
*
* SLAB CARDS
*
150011   0 29  3 0 0  2  2   0.0          14.4285980  0.12769979  0.0          0.03760000
150021   0 30  2 1 0  2  2   0.0          10.0949984  0.08959997  0.0          0.03760000
150031   0 31  1 1 0  2  2   0.0          16.0529938  0.14199996  0.0          0.03760000
150041   0 32  9 1 0  2  2   0.0          10.0799990  0.08999982  0.0          0.03760000
150051   0 33 10 1 0  2  2   0.0          14.2539988  0.12599999  0.0          0.03760000
150061  23  0  7 0 0  2  2  2.7500000     0.0         0.13089997  0.0          0.0
150071  24  0  7 0 0  2  2  2.3339987     0.0         0.11109996  0.0          0.0
150081  25  0  7 0 0  2  2  3.2089987     0.0         0.15289980  0.0          0.0
150091  26  0  4 0 0  2  2  2.0019999     0.0         0.18579996  0.0          0.0
150101  25  0  4 0 0  2  2 11.5029984     0.0         1.06799984  0.0          0.0
150111  26  0  4 0 0  2  2  6.7579985     0.0         0.62699986  0.0          0.0
150121  27  0  4 0 0  2  2 10.3399992     0.0         0.95999998  0.0          0.0
150131  24  0  4 0 0  2  2  4.1699982     0.0         0.38709980  0.0          0.0
150141  25 27  5 0 0  2  2  1.7689991     2.4329987   0.17509997  0.02760000   0.0
150151  30 27  5 0 0  2  2  1.2399999     1.7039986   0.12259996  0.02760000   0.0
150161  31 26  5 0 0  2  2  1.9679995     2.7039986   0.19459999  0.02760000   0.0
150171  32 25  5 0 0  2  2  1.2339993     1.6959982   0.12199998  0.02760000   0.0
150181  33 25  5 0 0  2  2  1.7490000     2.3999987   0.17299998  0.02760000   0.0
150191  25 27  6 0 0  2  2  1.7689991     2.6539984   0.13799977  0.02760000   0.0
150201  30 27  6 0 0  2  2  1.2359998     1.8589993   0.09679997  0.02760000   0.0
150211  31 26  6 0 0  2  2  1.9679995     2.9499989   0.15359998  0.02760000   0.0
150221  32 25  6 0 0  2  2  1.2339993     1.8499985   0.09639978  0.02760000   0.0
150231  33 25  6 0 0  2  2  1.7490000     2.6229992   0.13659996  0.02760000   0.0
150241   1  0  7 0 0  2  2  2.7500000     0.0         0.13089997  0.0          0.0
150251   3  0  7 0 0  2  2  2.7500000     0.0         0.13089997  0.0          0.0
150261   4  0  7 0 0  2  2  9.4799986     0.0         0.45159996  0.0          0.0
150271   5  0  7 0 0  2  2 12.1899995     0.0         0.58029979  0.0          0.0
150281   6  0  7 0 0  2  2  9.6899996     0.0         0.46099997  0.0          0.0
150291   7  0  7 0 0  2  2  3.2099991     0.0         0.15269995  0.0          0.0
150301  11  0  7 0 0  2  2  7.2159984     0.0         0.34379995  0.0          0.0
150311  12  0  7 0 0  2  2  7.1929989     0.0         0.34249979  0.0          0.0
150321  13  0  7 0 0  2  2  8.6599989     0.0         0.41229981  0.0          0.0
150331  14  0  7 0 0  2  2  5.5299988     0.0         0.26339997  0.0          0.0
150341  15  0  7 0 0  2  2 20.5299988     0.0         0.97700000  0.0          0.0
150351  16  0  7 0 0  2  2 13.8599987     0.0         0.66189981  0.0          0.0
150361  17  0  7 0 0  2  2  2.7500000     0.0         0.13089997  0.0          0.0
150371  18  0  7 0 0  2  2 19.4599915     0.0         0.92679977  0.0          0.0
150381  20  0  7 0 0  2  2  5.3399992     0.0         0.25439996  0.0          0.0
150391  21  0  7 0 0  2  2  2.7500000     0.0         0.13089997  0.0          0.0
150401  38  0  7 0 0  2  2 20.4299927     0.0         0.97289979  0.0          0.0
150411  39  0  8 0 0  2  2 34.0312958     0.0         3.53230000  0.0          0.0
150421  37  0  7 0 0  2  2  7.1931992     0.0         0.34249985  0.0          0.0
150431   8 42 11  0  0  2  2  30.016     41.637   0.14531     0.04392   0.
150441   9 41 11  0  0  2  2  30.016     41.637   0.14531     0.04392   0.
150451  10 40 11  0  0  2  2  30.016     41.637   0.14531     0.04392   0.
150012  0.0          0.0471000   0.0          0.0         0.0          0.0
150022  0.0          0.0471000   0.0          0.0         0.0          0.0
150032  0.0          0.0471000   0.0          0.0         0.0          0.0
150042  0.0          0.0471000   0.0          0.0         0.0          0.0
150052  0.0          0.0471000   0.0          0.0         0.0          0.0
150062  0.0          0.0         3.000000     0.0         0.0          0.0
150072  0.0          0.0         2.549996     0.0         0.0          0.0
150082  0.0          0.0         4.000000     0.0         0.0          0.0
150092  0.0          0.0         0.0          0.0         0.0          0.0
150102  0.0          0.0         0.0          0.0         0.0          0.0
150112  0.0          0.0         0.0          0.0         0.0          0.0
150122  0.0          0.0         0.0          0.0         0.0          0.0
150132  0.0          0.0         0.0          0.0         0.0          0.0
150142  0.0          0.0         0.0          2.653996    0.0          2.653996
150152  0.0          0.0         0.0          1.858996    2.655000     4.509996
150162  0.0          0.0         0.0          2.950000    0.0          0.0
150172  0.0          0.0         0.0          1.849998    0.001000     1.839996
150182  0.0          0.0         0.0          2.622996    1.851000     4.591000
150192  0.0          0.0         0.0          2.653996    0.0          2.653996
150202  0.0          0.0         0.0          1.858996    2.655000     4.511996
150212  0.0          0.0         0.0          2.950000    0.0          0.0
150222  0.0          0.0         0.0          1.849998    0.001000     1.849000
150232  0.0          0.0         0.0          2.622996    1.851000     4.591000
150242  0.0          0.0         3.000000     0.0         0.0          0.0
150252  0.0          0.0         3.000000     0.0         0.0          0.0
150262  0.0          0.0        10.349998     0.0         0.0          0.0
150272  0.0          0.0        13.299996     0.0         0.0          0.0
150282  0.0          0.0        10.570000     0.0         0.0          0.0
150292  0.0          0.0         3.500000     0.0         0.0          0.0
150302  0.0          0.0         7.879996     0.0         0.0          0.0
150312  0.0          0.0         7.849998     0.0         0.0          0.0
150322  0.0          0.0         9.450000     0.0         0.0          0.0
150332  0.0          0.0         6.030000     0.0         0.0          0.0
150342  0.0          0.0        22.399994     0.0         0.0          0.0
```

```
150352 0.0          0.0          15.169996   0.0          0.0          0.0
150362 0.0          0.0           3.000000   0.0          0.0          0.0
150372 0.0          0.0          21.239975   0.0          0.0          0.0
150382 0.0          0.0           5.830000   0.0          0.0          0.0
150392 0.0          0.0           3.000000   0.0          0.0          0.0
150402 0.0          0.0          22.259988   0.0          0.0          0.0
150412 0.0          0.0          12.379997   0.0          0.0          0.0
150422 0.0          0.0           7.849998   0.0          0.0          0.0
150432   0.043S2    0.   6.043   7.067  0.   0.93
150442   0.043S2    0.   6.043   7.---  0.   0.89
150452   0.043S2    0.   6.043   7.067  0.   0.93
*
* CORE CARDS
*
160010  1  5  8  9 0.0        0.1110400 0.0          0.0
160020  2  5 12 13 0.0        0.1858799 0.0          0.0
160030  3  5 12 13 0.0        0.4131899 0.0          0.0
160040  4  5 12 13 0.0        0.1758900 0.0          0.0
160050  5  5  8  9 0.0        0.1100000 0.0          0.0
*
* SLAB GEOMETRY CARDS
*
170101 2 6 3 2 0. .0005067 0.
170102  0      1  2  1.100E-03    1.0
170103  0      4  3  4.167E-03    0.
170104 0   2 4 .0025 0.
170105   0   6   1   7.0042E-6   0.
170106 0   2 2 .000833 0.
170201 2 6 3 2 0. .0005575 0.
170202  0      1  2                1.508E-03     1.0
170203  0      4  3                4.167E-03     0.
170204 0   2 4 .0025 0.
170205  0  6  1  3.7509E-6    0.
170206 0   2 2 .000833 0.
170301 2 6 3 2 0. .0007666 0.
170302  0      1  1                1.783E-03     0.5
170303  0      5  1                7.18E-04      0.5
170304  0      4  3                4.167E-03     0.
170305  0  6  1  1.666E-6     0.
170306 0   2 5 3.333E-3 0.
170401  2  2  2  3  0.365   0.0333      0.
170402  0     2  1           0.05        0.
170501  1  1  2  4  0.       0.08333     0.
170601  1  1  2  4  0.       0.0625      0.
170701  2  2  2  3  0.1459   0.01666     0.
170702  0     2  1           0.025       0.
170801 2 2 2 3 0.4375 0.0375  0.
170802  0  2  2  .05625  0.
170901 2 6 3 2 0. .0005575 0.
170902  0      1  2                1.508E-03     1.0
170903  0      4  3                4.167E-03     0.
170904 0   2 4 .0025 0.
170905  0  6  1  5.7055E-6    0.
170906 0   2 2 .000833 0.
171001 2 6 3 2 0. .0007666 0.
171002  0      1  1                1.783E-03     0.5
171003  0      5  1                7.18E-04      0.5
171004  0      4  3                4.167E-03     0.
171005  0  6  1  3.5204E-6    0.
171006 0   2 5 3.333E-3 0.
171101  2  1  2  4  0.02196  0.004083  0.
*
*   VOLUMETRIC HEAT CAPACITY  BTU/F-FT**3  MATERIAL 1 - INCONNEL
*
190101 20        0.     51.41       200.     57.434       300.     59.527  * INCONNEL
190102          400.    61.167      500.     62.476       600.     63.572  * INCONNEL
190103          700.    64.578      800.     65.612       900.     66.795  * INCONNEL
190104         1000.    68.247     1100.     70.088      1200.     72.439  * INCONNEL
190105         1300.    75.420     1400.     79.150      1500.     83.750  * INCONNEL
190106         1600.    89.341     1700.     96.042      1800.    103.973  * INCONNEL
190107         1900.   113.255     2000.    124.008                        * INCONNEL
*
*   THERMAL CONDUCTIVITY BTU/FT-HR-F   MATERIAL 1 - INCONNEL
*
180101 20        0.      8.4294     200.      9.098       300.      9.495  *9INCONNEL
180102          400.     9.930      500.     10.398       600.     10.896  * INCONNEL
180103          700.    11.420      800.     11.967       900.     12.532  * INCONNEL
180104         1000.    13.113     1100.     13.704      1200.     14.303  * INCONNEL
180105         1300.    14.906     1400.     15.509      1500.     16.109  * INCONNEL
180106         1600.    16.701     1700.     17.282      1800.     17.849  * INCONNEL
180107         1900.    18.397     2000.     18.922                        * INCONNEL
*
*   LINEAR EXPANSION COEFFICIENT   1/F  MATERIAL 1 - INCONNEL
*
*
*   VOLUMETRIC HEAT CAPACITY  BTU/F-FT**3  MATERIAL 2 - 316 SS
*
190201 20        0.     51.68       200.     56.923       300.     59.020  * 316-STST
190202          400.    60.846      500.     62.447       600.     63.865  * 316-STST
190203          700.    65.141      800.     66.308       900.     67.400  * 316-STST
190204         1000.    68.444     1100.     69.463      1200.     70.480  * 316-STST
190205         1300.    71.508     1400.     72.563      1500.     73.652  * 316-STST
190206         1600.    74.782     1700.     75.952      1800.     77.162  * 316-STST
190207         1900.    78.406     2000.     79.672                        * 316-STST
*
```

```
*   THERMAL CONDUCTIVITY BTU/FT-HR-F   MATERIAL 2 - 316 SS
*
180201 20        C.      7.2456      200.      8.225       300.      8.691  * 316-STST
180202          400.     9.144       500.      9.586       600.     10.020  * 316-STST
180203          700.    10.448       800.     10.872       900.     11.294  * 316-STST
180204         1000.    11.718      1100.     12.145      1200.     12.577  * 316-STST
180205         1300.    13.017      1400.     13.467      1500.     13.929  * 316-STST
180206         1600.    14.406      1700.     14.900      1800.     15.414  * 316-STST
180207         1900.    15.948      2000.     16.507                        * 316-STST
*
*   LINEAR EXPANSION COEFFICIENT   1/F   MATERIAL 2 - 316 SS
*
*
*   VOLUMETRIC HEAT CAPACITY  BTU/F-FT**3  MATERIAL 3 - MGO
*
190301 20 C. 47.5516 200. 52.2156 300. 54.2094 400. 55.9468 500. 57.4944
190302 600. 58.8512 700. 60.0384 800. 61.0348 900. 61.9040 1000. 62.6460
190303 1100. 63.2608 1150. 63.5364 1200. 63.7908 1250. 64.0240 1300. 64.2360
190304 1400. 64.5564 1500. 64.9144 1600. 65.1900 1700. 65.4444 1800. 65.9776
*
*   THERMAL CONDUCTIVITY BTU/FT-HR-F   MATERIAL 3 - MGO
*
180301 20 0. 8.4435  200.  6.4805  300.  5.7049   400.  5.0470   500.  4.4937
180302  600.  4.0326  700.  3.6523   800.  3.3423   900.  3.0930
180303  1000.  2.8555  1100.  2.7431  1200.  2.6281  1300.  2.5450
180304  1400.  2.4888  1500.  2.4558  1600.  2.4428  1700.  2.4428
180305 1800.  2.4428  1900.  2.4428  2000.  2.4428
*
*   LINEAR EXPANSION COEFFICIENT   1/F   MATERIAL 3 - MGO
*
*
*   VOLUMETRIC HEAT CAPACITY  BTU/F-FT**3  MATERIAL 4 - BN
*
190401 20        C.     20.58       200.     29.896       300.     33.012  *         BN
190402          400.    36.265      500.     39.178       600.     41.775  *         BN
190403          700.    44.078      800.     46.112       900.     47.900  *         BN
190404         1000.    49.466     1100.     50.834      1200.     52.026  *         BN
190405         1300.    53.067     1400.     53.980      1500.     54.789  *         BN
190406         1600.    55.517     1700.     56.188      1800.     56.826  *         BN
190407         1900.    57.453     2000.     58.094                        *         BN
*
*   THERMAL CONDUCTIVITY BTU/FT-HR-F   MATERIAL 4 - BN
*
180401  20    0.      21.0562  300.   18.5490  500.   17.0927  600.   16.3442
180402        700.    15.6187  750.   15.2654  800.   14.9186  850.   14.5788
180403        900.    14.2463  950.   13.9212  1000.  13.6040  1050.  13.2950
180404        1100.   12.9944  1150.  12.7025  1200.  12.4196  1300.  11.8821
180405        1400.   11.3744  1500.  10.9287  1700.  10.1531  2000.  9.3650
*
*   LINEAR EXPANSION COEFFICIENT   1/F   MATERIAL 4 - BN
*
*
*   VOLUMETRIC HEAT CAPACITY  BTU/F-FT**3  MATERIAL 5 - 70CU30NI
*
190501 20        0.     52.55       200.     55.512       300.     56.817  * 70CU30NI
190502          400.    58.032      500.     59.179       600.     60.260  * 70CU30NI
190503          700.    61.358      800.     62.435       900.     63.532  * 70CU30NI
190504         1000.    64.672     1100.     65.876      1200.     67.167  * 70CU30NI
190505         1300.    68.567     1400.     70.098      1500.     71.782  * 70CU30NI
190506         1600.    73.641     1700.     75.697      1800.     77.973  * 70CU30NI
190507         1900.    80.489     2000.     83.269                        * 70CU30NI
*
*   THERMAL CONDUCTIVITY BTU/FT-HR-F   MATERIAL 5 - 70CU30NI
*
180501 20        C.     16.802      200.     17.972       300.     19.314  * 70CU30NI
180502          400.    20.560      500.     22.833       600.     24.919  * 70CU30NI
180503          700.    27.261      800.     29.964       900.     33.193  * 70CU30NI
180504         1000.    37.174     1100.     42.190      1200.     48.589  * 70CU30NI
180505         1300.    56.774     1400.     67.212      1500.     80.429  * 70CU30NI
180506         1600.    97.010     1700.    117.602      1800.    142.911  * 70CU30NI
180507         1900.   173.704     2000.    210.807                        * 70CU30NI
*
*
*   LINEAR EXPANSION COEFFICIENT   1/F   MATERIAL 5 - 70CU30NI
*
*
*   VOLUMETRIC HEAT CAPACITY  BTU/F-FT**3  MATERIAL 6 - AIR IN GAP
*
190601 20  25. .01573     68. .01812     100. .01708    200. .01449
190602     300. .01258    400. .01131    500. .00995    600. .00901
190603     700. .00824    800. .00758    900. .00702   1000. .00654
190604    1100. .00612   1200. .00575   1300. .00543   1400. .00513
190605    1500. .00487   1600. .00463   1700. .00442   2000. .00388
*
*   THERMAL CONDUCTIVITY BTU/FT-HR-F   MATERIAL 6 - AIR IN GAP
*
180601 20  25. .01354     68. .0144689   100. .01516    200. .01732
180602     300. .01548    400. .02164    500. .02380    600. .02596
180603     700. .02812    800. .03028    900. .03244   1000. .03460
180604    1100. .03676   1200. .03892   1300. .04108   1400. .04324
180605    1500. .04540   1600. .04756   1700. .04972   2000. .05620
*
```

```
*   LINEAR EXPANSION COEFFICIENT   1/F  MATERIAL 6 - AIR IN GAP
*
*
* HEAT EXCHANGER CARDS
*
$1010:   2   4  18    0.C   C.1871  210.00  0.1871
*
```

Appendix B

RELAP DEPRESSURIZATION TEST MODEL LISTING

```
=TEST          TEST MODEL FOR DEPRESSURIZATION STUDIES - 28 MAY 77
*
*   THIS DECK USES A FILL TABLE AND A ..IT-HOT-HOT TEMPERATURE
*   DISTRIBUTION
*
* PROBLEM DIMENSIONS
*
010001 -2 9 4 2 14 1 0 14 0 0 0 1 1 1 1 0 0 0
010002 0. 1.0
*
* MINOR EDIT VARIABLES
*
020000 AP 1 AP 3 AP 5 AP 7 AP 9 AP 11 AP 13 FV 13 JN 13
*
*   ENTHALPY TRANSPORT SHUT DOWN
*
030003  0  0.  0.  .000001
*
*
* TIME STEP CARDS
*
030010  500  10  1  0  .0001  .00001      .001
030020   50  10  1  0  .001   .00001      .05
030030    5  10  1  0  .01    .00001      .5
030040    5  10  1  0  .01    .00001  210.
*
* TRIP CARDS
*
040010  1  1  0  0   5.0   0.0 * TRIP END
040020  2  1  0  0   0.0   0.0 * TRIP LEAK TO FIRST POWER CURVE
*
* VOLUME DATA CARDS
*
050141 0   0 2200.0000 633.0000 -1.000 0.203400  0.2920  0.2920 *S.P.2 OUTLET
050131 0   0 2200.0000 633.0000 -1.000 0.304700  0.2920  0.2920
050111 0   0 2200.0000 633.0000 -1.000 0.436000  6.9000  6.9000
050091 0   0 2200.0000 633.0000 -1.000 0.304500  0.2920  0.2920
050071 0   0 2200.0000 633.0000 -1.000 0.233200  0.2920  0.2920 *INLET HEADR
050061 0   0 2200.0000 633.0000 -1.000 0.495900  7.0400  7.0400 *HX BYPASS
050051 0   0 2200.0000 633.0000 -1.000 0.295600  4.8000  4.8000
050031 0   0 2200.0000 633.0000 -1.000 0.403000  0.2920  0.2920 *HORZ TO PRES
050011 1   0 2200.0000   0.0     0.0   7.450000 12.4000 11.00   *PRESSURIZER
050021 0   0 2200.0000 633.0000 -1.000 0.658100  6.1000  6.1000 *PRNSS LN
050121 0   0 2200.0000 633.0000 -1.000 0.370400  0.2920  0.2920
050101 0   0 2200.0000 633.0000 -1.000 0.436000  6.7000  6.7000
050081 0   0 2200.0000 633.0000 -1.000 0.353300  1.6500  1.6500
050041 0   0 2200.0000 633.0000 -1.000 0.295600  4.8000  4.8000
050142 0  0.0668100   0.2916999  929.7078  0                      *S.P.2 OUTLET
050132 0  0.0668100   0.2916999  929.7078  0
050112 0  0.0668100   0.2916999  929.7078  0
050092 0  0.0668100   0.2916999  943.0999  0
050072 0  0.0668100   0.2916999  941.3529  0                      *INLET HEADR
050062 0  0.0668100   0.2916999  934.4170  0                      *HX BYPASS
050052 0  0.0668100   0.2916999  929.6250  0
050032 0  0.0668100   0.2916999  924.7920  0                      *HORZ TO PRES
050012 0  0.6010000   0.8750000  930.9397  0                      *PRESSURIZER
050022 1  0.0668100   0.2916999  924.8997  0                      *PRNSS LN
050122 0  0.0668100   0.2916999  929.7078  0
050102 0  0.0668100   0.2916999  936.5498  0
050082 0  0.0668100   0.2916999  941.5000  0
050042 0  0.0668100   0.2916999  924.9380  0
*
* BUBBLE RISE CARD
060011              0.          3.0
*
* JUNCTION DATA CARDS
*
*THE AREA OF JUNCTIONS WITH ORIFICES OR VALVES IS = ADJACENT VOL CS AREA
*
080141  0 14   1  1  0.0       0.0381000  929.85376   0.0          7.500      7.5
080131 13 14   0  0  0.0       0.0668100  929.85376   0.0          7.500      7.5
080111 11 12   0  0  0.0       0.0668100  929.85376   0.0          0.0        0.0
080091  9 10   0  0  0.0       0.0668100  943.19995   0.0          0.0        0.0
080071  7  8   0  0  0.0       0.0668100  941.54980   0.0          0.0        0.0
080061  6  7   0  0  0.0       0.0668100  941.39986   0.0          0.0        0.0
080051  5  6   0  0  0.0       0.0668100  934.41968   0.0          0.0        0.0
080031  3  4   0  0  0.0       0.0668100  924.93971   0.0          0.0        0.0
080011  1  2   0  0  0.0       0.0668100  930.94971   0.0          1.000      1.000
080021  2  3   0  0  0.0       0.0668100  924.91968  99.00000      1.000      1.000
080121 12 13   0  0  0.0       0.0668100  929.95376   0.0          0.0        0.0
080101 10 11   0  0  0.0       0.0668100  936.59985   0.0          0.0        0.0
080081  8  9   0  0  0.0       0.0668100  943.14258   0.0          0.0        0.0
080041  4  5   0  0  0.0       0.0668100  929.69995   0.0          0.0        0.0
080142 0  0   2 -2 0.0     1.000    0 0 0.0      0
080132 0  0   2  0 0.0     0.600    0 0 0.0      0
080112 0  0   3  0 0.0     0.600    0 0 0.0      0
080092 0  0   3  0 0.0     0.600    0 0 0.0      0
080072 0  0   3  0 0.0     0.600    0 0 0.0      0
080052 0  0   3  0 0.0     0.600    0 0 0.0      0
080032 0  0   3  0 0.0     0.600    0 0 0.0      0
080012 0  0   2  0 0.0     0.600    0 0 0.0      0
080022 0  0   0  3 0.0     0.600    0 0 0.0      0
```

```
300122 2   0   3   0 0.0       0.600     0 0 0.0       0
080102 0   0   3   0 0.0       0.600     0 0 0.0       0
080082 0   0   3   0 0.0       0.600     0 0 0.0       0
080042 0   0   3   0 0.0       0.600     0 0 0.0       0
150011  1   0   1 0 0   2   2  5.5010996   0.0          0.57099998 0.0          0.0
150012 0.0          0.0          0.0          0.0          0.0          0.0
130100 2 4 13 1 LBS/SEC
130101 0. 0. 661.67 .2 -9148.1 662.89 .4 -7271.6 657.734
130102 .6 -9164.3 661.6 .8 -8116.0 662.3 1.0 -6796. 661.9
130103 1.4 -5650. 663.8 1.8 -4539.5 668.97 2.6 -4072.8 679.5
130104 3.0 -3961.7 683.9 3.4 -6098.8 609.7 4.2 -6450.6 581.7
130105 5.0 -1461.7 729.2
170101 2 3 1 4 .4375 .03125  0.
170102 2 1 4 .03125 0.
170103 2 1 4 .03125 0.
*   VOLUMETRIC HEAT CAPACITY  BTU/F-FT**3  MATERIAL 2 - 316 SS
*
190101 20        0.      51.68        200.      56.923       300.      59.323  * 316-STST
190102          400.     60.846       500.      62.447       600.      63.565  * 316-STST
190103          700.     65.141       800.      66.308       900.      67.400  * 316-STST
190104         1000.     68.444      1100.      69.463      1200.      70.489  * 316-STST
190105         1300.     71.508      1400.      72.563      1500.      73.652  * 316-STST
190106         1600.     74.782      1700.      75.952      1800.      77.162  * 316-STST
190107         1900.     78.406      2000.      79.672                         * 316-STST
*
*   THERMAL CONDUCTIVITY BTU/FT-HR-F   MATERIAL 2 - 316 SS
*
180101 20        0.       7.2458      200.       8.225       300.       8.691  * 316-STST
180102          400.      9.144       500.       9.586       600.      10.020  * 316-STST
180103          700.     10.448       800.      10.972       900.      11.294  * 316-STST
180104         1000.     11.718      1100.      12.145      1200.      12.577  * 316-STST
180105         1300.     13.017      1400.      13.467      1500.      13.929  * 316-STST
180106         1600.     14.406      1700.      14.900      1800.      15.414  * 316-STST
180107         1900.     15.948      2000.      16.507                         * 316-STST
*
```

Appendix C

RELAP THTF RENODED MODEL LISTING

BLANK PAGE

```
=RESTART          RENODE LOOP 123 WITH NEW HX AND OLD PZR - 21 MAY 77
*
*   THIS DECK USES AN APPROXIMATION TO THE ACTUAL INITIAL CONDITIONS
*   FOR TEST 123.  IT WAS INITIAL FLOW DERIVED FROM AN ENERGY BALANCE
*   ON THE CORE USING THERMOCOUPLE AND POWER METER READINGS.  IT
*   HAS SLIP IN THE DOWNCOMER ONLY.  IT HAS A MIXED SIZE
*   GAP MODEL IN ALL CORE SLABS - BETWEEN THE SS SHEATHS IN THE
*   INNER CORE SLABS AND BETWEEN THE BN AND SS IN THE OUTER CORE
*   SLABS.  THE PRESSURES HAVE BEEN ADJUSTED TO BE CLOSER TO THE
*   ACTUAL PRESSURES.  THE TEMPERATURES IN THE LOOP HAVE ALSO BEEN
*   ADJUSTED.  THE MIXTURE LEVEL IN THE PRESSURIZER HAS BEEN ADJUSTED.
*   THE MATERIAL PROPERTIES HAVE BEEN UPDATED.
*
*
*
*
*
*
* PROBLEM DIMENSIONS
*
010001 -2 9 4 5 62 1 2 65 1 0 2 3 40 15 5 9 1 0
010002   5.9725  1.0
*
* MINOR EDIT VARIABLES
*
020000 AM 6 JB 7 AM 7 JB 9 AM 8 JB 10 AM 9 JB 11 AM 10
*
*   ENTHALPY TRANSPORT SHUT DOWN
*
030001  0  0.  0.  .000001
*
*
* TIME STEP CARDS
*
030010  500  10  1  0  .0001  .000001      .001
030020   50  10  1  0  .001   .000001      .05
030030    5  10  1  0  .01    .000001      .5
030040    5  10  1  0  .01    .000001  210.
*
* TRIP CARDS
*
040010  1  1  0  0  20.0   0.0 * TRIP END
040020  2  1  0  0   0.0   0.0 * TRIP LEAK TO FIRST POWER CURVE
040030  3  1  0  0   0.0   0.05* TRIP PUMP
040040  4  1  0  0   0.0   1.965 *TRIP SEC FLOW ON HEAT-X
040050  1  -4 36  0  200.   0.  * TRIP END BELOW 200 PSI
*
* VOLUME DATA CARDS
*
050011 0   0 2265.6868 634.2170 -1.000 0.200400  3.0000  3.0000 *S.P.1 OUTLET
050021 0   0 2257.3994 634.1648 -1.000 0.202600  2.0140  2.0140 *BLOWDOWN TEE
050031 0   0 2246.7463 634.0577 -1.000 0.200400  0.2920  0.2920 *S.P.2 OUTLET
050041 0   0 2236.8594 634.0352 -1.000 0.304700  0.2920  0.2920
050051 0   0 2235.4629 634.0264 -1.000 0.436000  6.9000  6.9000
050061 0   0 2232.1541 634.0054 -1.000 0.304500  0.2920  0.2920
050071 0   0 2232.2271 634.0055 -1.000 0.233200  0.2920  0.2920 *INLET HEADR
050081 0   0 2232.7080 562.7996 -1.000 0.591400  4.1000  4.1000 *HEX FIRST PT
050091 0   0 2233.3054 406.7651 -1.000 0.591400  0.9000  0.9000 *HX SECOND PT
050101 0   0 2233.6763 279.5665 -1.000 0.591400  2.1500  2.1500 *HX THIRD PT
050111 0   0 2213.5786 223.9954 -1.000 0.563700  0.2920  0.2920 *OUT HEADER
050121 0   0 2213.3716 631.8860 -1.000 0.495900  7.0400  7.0400 *HX BYPASS
050131 0   0 2214.2469 560.3496 -1.000 0.295600  4.8000  4.8000
050141 0   0 2216.1433 560.3518 -1.000 0.403000  0.2920  0.2920 *HORZ TO PRES
050151 0   0 2213.2090 543.4507 -1.000 0.481300  0.2920  0.2920
050161 0   0 2858.5786 547.3542 -1.000 0.490500  4.2000  4.2000
050171 0   0 2456.9690 547.0432 -1.000 0.196300  0.2920  0.2920 *BYPASS TEE
050181 0   0 2215.9902 526.2637 -1.000 0.266500  1.3500  1.3500 *BYPASS, HX O
050191 0   0 2352.8049 546.9515 -1.000 0.462300  0.2920  0.2920
050201 0   0 2341.8308 546.9421 -1.000 0.373500  2.3339  2.3339 *VERT TO SPLI
050211 0   0 2333.0955 546.9343 -1.000 0.200430  0.2920  0.2920 *S.P. 1 INLET
050221 0   0 2325.5859 546.9275 -1.000 0.267800  1.9140  1.9140 *B.D.TEE INLET
050231 0   0 2315.8555 546.9187 -1.000 0.203400  3.0000  3.0000 *S.P.2 INLET
050241 0   0 2306.8623 546.9097 -1.000 0.170200  1.2600  1.2600 *T.S. INLET
050251 0   0 2307.4336 546.9104 -1.000 0.945060  5.0210  5.0210 *1ST DOWNCOMER
050261 0   0 2308.7014 546.9119 -1.000 0.565260  3.0000  3.0000 *2ND DOWNCOMER
050271 0   0 2310.3625 546.9138 -1.000 0.282630  1.5000  1.5000 *4TH DOWNCOMER
050281 0   0 2310.7449 546.9141 -1.000 0.057509  0.1560  0.1560 *LOWER PLENUM
050291 0   0 2305.4138 549.5778 -1.000 0.395276  1.5000  1.5000 *1ST HEATED CORE
050301 0   0 2300.3950 561.5466 -1.000 0.355578  0.8750  0.8750 *3RD HEATED CORE
050311 0   0 2293.6719 594.3528 -1.000 0.190353  3.0000  3.0000 *5TH HEATED CORE
050321 0   0 2286.8789 623.3257 -1.000 0.355578  0.8750  0.8750 *7TH HEATED CORE
050331 0   0 2281.5421 632.3718 -1.000 0.095276  1.5000  1.5000 *9TH HEATED CORE
050341 0   0 2276.9980 634.2881 -1.000 0.338100  1.1578  1.1578 *3RD UPPER PLEN.
050351 0   0 2275.0635 634.2755 -1.000 0.384000  0.8500  0.8500 *OUTLET LINE
050361 1   0 2212.7000   0.0     0.0   7.450000 12.4000  5.79   *PRESSURIZER
050371 0   0 2215.2949 560.3506 -1.000 0.658100  6.1000  6.1000 *PRNSS LN
050381 0   0 2536.7783 545.4116 -1.000 1.493000  2.0000  2.0000 * PUMP
050391 0   0 2236.6379 634.0337 -1.000 0.370400  0.2920  0.2920
050401 0   0 2233.3191 634.0127 -1.000 0.436000  6.7000  6.7000
050411 0   0 2232.1919 634.0056 -1.000 6.353300  1.6500  1.6500
050421 0   0 2215.5771 560.3511 -1.000 0.295600  4.8000  4.8000
050431 0   0 2212.7508 543.4504 -1.000 0.704000  1.0300  1.0300
050441 0   0 2212.7358 543.4504 -1.000 0.543000  3.8100  3.8100
```

```
050451  0    0  2857.3743  547.3535  -1.000  0.479933   0.2933   0.2933
050461  0    0  2352.5410  546.9517  -1.000  0.462330   0.2920   0.2920
050471  0    0  2352.2771  546.9514  -1.000  0.462330   0.2920   0.2920
050481  0    0  2309.6506  546.9181  -1.000  0.565262   3.0000   3.0000  *3RD DOWNCOMER
050491  0    0  2310.5786  546.9141  -1.000  0.102110   0.7188   0.7188  *5TH DOWNCOMER
050501  0    0  2306.3469  546.9114  -1.000  0.345656   0.7188   0.7188  *UNHTD BOT. CORE
050511  0    0  2304.5762  555.2471  -1.000  0.371457   1.1250   1.1250  *2ND HEATED CORE
050521  0    0  2294.3235  570.3935  -1.000  0.363518   1.0000   1.0000  *4TH HEATED CORE
050531  0    0  2289.1025  618.2671  -1.000  0.363518   1.0000   1.0000  *6TH HEATED CORE
050541  0    0  2294.4978  629.3992  -1.000  0.371457   1.1250   1.1250  *8TH HEATED CORE
050551  0    0  2277.5382  634.2910  -1.000  0.339519   0.6875   0.6875  *UNHTD TOP CORE
050561  0    0  2277.3516  634.2903  -1.000  0.382000   0.2740   0.2740  *1ST UPPER PLEN.
050571  0    0  2277.2363  634.2956  -1.000  0.162000   0.5479   0.5479  *2ND UPPER PLEN.
050581  0    1   250.    70.    -1.0   0.4912   1.25   1.25              *SEC INLET HEADER
050591  0    0   238.    91.9   -1.0   0.4912   0.95   0.95              *HEX SEC PART ONE
050601  0    0   236.   143.5   -1.0   0.4912   0.95   0.95              *HEX SEC PART TWO
050611  0    0   234.0  211.5   -1.0   0.4912   0.95   0.95              *HEX SEC PART THREE
050621  0    2   232.   250.    -1.0   0.4912   3.1537   3.1537          *HEX SEC OUTLET HDR
050712  0  0.0668100   0.2916999   930.7103  0                           *S.P.1 OUTLET
050722  0  0.1104000   0.3750000   929.7079  0                           *BLOWDOWN TEE
050732  0  0.0668100   0.2916999   929.7079  0                           *S.P.2 OUTLET
050742  0  0.0668100   0.2916999   929.7079  0
050752  0  0.0668100   0.2916999   929.7078  0
050762  0  0.0668100   0.2916999   943.3999  0
050772  0  0.0668100   0.2916999   941.3528  0                           *INLET HEADR
050782  0  0.0573000   0.0562158   937.2537  0                           *HX FIRST PT
050792  0  0.0573000   0.0562158   936.3636  0                           *HX SECOND PT
050802  0  0.0573000   0.0562158   934.2610  0                           *HX THIRD PT
050812  0  0.0668200   0.2916999   934.2620  0                           *OUT HEADER
050822  0  0.0668100   0.2916999   934.4170  0                           *HX BYPASS
050832  0  0.0668100   0.2916999   929.6253  0
050842  0  0.0668100   0.2916999   924.7922  0                           *NOZZ TO PRES
050852  0  0.0668100   0.2916999   924.7922  0
050862  0  0.0668100   0.2916999   919.9902  0
050872  0  0.0668100   0.2916999   923.9369  0                           *BYPASS TEE
050882  0  0.0235000   0.1615000   923.4289  0                           *BYPASS, HX 0
050892  0  0.0668100   0.2916999   923.9369  0
050902  0  0.0668100   0.2916999   924.3929  0                           *VENT TO SPIT
050912  0  0.0668100   0.2916999   926.2710  0                           *S.P. 1 INLET
050922  0  0.1104000   0.3750000   925.2710  0                           *BLOWDOWN TEE INLET
050932  0  0.0668100   0.2916999   927.1099  0                           *S.P.2 INLET
050942  0  0.0668100   0.2916999   930.1350  0                           *T.S. INLET
050952  0  0.1884200   0.1791300   927.7669  0                           *1ST DOWNCOMER
050962  0  0.1884200   0.1791300   924.7679  0                           *2ND DOWNCOMER
050972  0  0.1884200   0.1791300   920.2698  0                           *4TH DOWNCOMER
050982  0  0.3019000   0.1720000   916.3999  0                           *LOWER PLENUM
050992  0  0.0635175   0.0197321   920.2699  0                           *1ST HEATED CORE
051002  0  0.0635175   0.0197321   922.9929  0                           *3RD HEATED CORE
051012  0  0.0635175   0.0197321   924.7659  0                           *5TH HEATED CORE
051022  0  0.0635175   0.0197321   928.7639  0                           *7TH HEATED CORE
051032  0  0.0635175   0.0197321   930.7629  0                           *9TH HEATED CORE
051042  0  0.2920000   0.3150000   933.7665  0                           *3RD UPPER PLEN.
051052  0  0.0668100   0.2920000   933.7003  0                           *OUTLET LINE
051062  0  0.6010000   0.4750000   930.9397  0                           *PRESSURIZER
051072  1  0.0668100   0.2916999   924.9997  0                           *PRNSS LN
051082  0  0.0668100   0.2916999   918.0000  0                           * PUMP
051092  0  0.0668100   0.2916999   929.7079  0
051102  0  0.0668100   0.2916999   936.5498  0
051112  0  0.0668100   0.2916999   941.5000  0
051122  0  0.0668100   0.2916999   924.9353  0
051132  0  0.0668100   0.2916999   923.7998  0
051142  0  0.0668100   0.2916999   919.9900  0
051152  0  0.0668100   0.2916999   923.9369  0
051162  0  0.0668100   0.2916999   923.9369  0
051172  0  0.0668100   0.2916999   923.9368  0
051182  0  0.1884200   0.1791300   921.7689  0                           *3RD DOWNCOMER
051192  0  0.1420600   0.1393900   919.5518  0                           *5TH DOWNCOMER
051202  0  0.0635175   0.0197321   919.5519  0                           *UNHTD BOT. CORE
051212  0  0.0635175   0.0197321   921.7698  0                           *2ND HEATED CORE
051222  0  0.0635175   0.0197321   923.7668  0                           *4TH HEATED CORE
051232  0  0.0635175   0.0197321   927.7649  0                           *6TH HEATED CORE
051242  0  0.0635175   0.0197321   929.6379  0                           *8TH HEATED CORE
051252  0  0.0580634   0.0137648   932.2610  0                           *UNHTD TOP CORE
051262  0  0.2920000   0.3150000   932.9468  0                           *1ST UPPER PLEN.
051272  0  0.2920000   0.3150000   933.2200  0                           *2ND UPPER PLEN.
051282   0  0.06951   0.0  934.261
051292   0  0.06951   0.04720   935.4606
051302   0  0.06951   0.04720   936.3606
051312   0  0.06951 0.04720   937.2537
051322   0  0.06951 0.0  938.2
*
* BUBBLE RISE CARD
060111            0.          3.0
*
070100  1
070200  6  2.  232.  250.  0.  3.1537
070201     5.  246.2  250.  0.  3.1537
070202     7.  247.5  250.  0.  3.1537
070203    12.  247.8  250.  0.  3.1537
070204    20.  248.0  250.  0.  3.1537
* JUNCTION DATA CARDS
*
```

```
*THE AREA OF JUNCTIONS WITH ORIFICES OR VALVES IS = ADJACENT VOLUMES AREA
*
080011 35  1    0  0  46.039993  0.0668100   933.70459   0.0          7.500       7.500
080021  1  2    0  0  46.039993  0.0668100   930.71094   0.0          7.500       7.500
080031  2  3    0  0  46.039993  0.0668100   929.95376   0.0          7.500       7.500
080041  3  4    0  0  46.039993  0.0668100   929.95376   0.0          7.500       7.500
080051 39  5    0  0  46.039993  0.0668100   929.95376   0.0          0.0         0.0
080061 40  6    0  0  46.039993  0.0668100   943.19995   0.0          0.0         0.0
080071 41  7    0  0  46.039993  0.0668100   941.54980   0.0          0.0         0.0
080081  7 12    0  0  35.639412  0.0668100   941.39966   0.0          0.0         0.0
080091  7  8    0  0  10.401578  0.0573000   941.35303   0.0          0.0         0.0
080101  8  9    0  0  10.401578  0.0573000   937.25977   0.0          0.0         0.0
080111  9 10    0  0  10.401578  0.0573000   936.36094   0.0          0.0         0.0
080121 10 11    0  0  10.401578  0.0573000   934.29932   0.0          0.0         0.0
080131 11 13    0  0  10.401578  0.0668100   934.41797   0.0          0.0         0.0
080141 12 13    0  0  35.639412  0.0668100   934.41968   0.0          0.0         0.0
080151 42 14    0  0  46.039993  0.0668100   924.93970   0.0          0.0         0.0
080161 14 15    0  0  46.039993  0.0668100   924.93970   0.0          0.0         0.0
080171 38 16    1  0  67.399994  0.0668100   919.99487   0.0          0.0         0.0
080181 45 17    0  0  67.399994  0.0668100   924.39961   0.0          0.0         0.0
080191 17 18    0  0  21.360001  0.0205300   924.93970   0.0          0.0         0.0
080201 18 15    0  0  21.360001  0.0205300   924.79980   0.0          0.0         0.0
080211 17 19    0  0  46.039993  0.0668100   924.39961   0.0          0.0         0.0
080221 47 20    0  0  46.039993  0.0668100   924.39472   0.0          0.0000      0.0000
080231 20 21    0  0  46.039993  0.0668100   926.29932   0.0          7.500       7.500
080241 21 22    0  0  46.039993  0.0668100   926.29932   0.0          7.500       7.500
080251 22 23    0  0  46.039993  0.0668100   927.13965   0.0          7.500       7.500
080261 23 24    0  0  46.039993  0.0668100   930.10669   0.0          7.500       7.500
080271 24 25    0  0  46.039993  0.0668100   921.29932   0.0          0.0         0.0
080281 25 26    0  0  46.039993  0.1848900   927.7675    0.0          0.0         0.0
080291 26 48    0  0  46.039993  0.1884200   924.76931   0.0          0.0         0.0
080301 27 49    0  0  46.039993  0.1420600   923.27026   0.0          0.0         0.0
080311 28 50    0  0  46.039993  0.0635180   919.55249   0.0          0.6600      0.0
080321 29 51    0  0  46.039993  0.0635180   921.76929   0.0          0.917       0.0
080331 30 52    0  0  46.039993  0.0635180   923.76733   0.0          0.584       0.0
080341 31 53    0  0  46.039993  0.0635180   927.76538   0.0          1.245       0.0
080351 32 54    0  0  46.039993  0.0635180   929.63843   0.0          0.623       0.0
080361 33 55    0  0  46.039993  0.0580634   932.26147   0.0          1.146       0.0
080371 34 35    0  0  46.039993  0.0668100   934.50000   0.0          0.500       0.500
080381 36 37    0  0    0.0      0.0668100   937.94971   0.0          1.000       1.000
080391 37 14    0  0    0.0      0.0668100   924.91969   90.00000     1.000       1.000
080401 44 38   -1  0  67.399994  0.0668100   919.99487   0.0          0.0         0.0
080411  4 39    0  0  46.039993  0.0668100   929.95376   0.0          0.0         0.0
080421  5 40    0  0  46.039993  0.0668100   916.59995   0.0          0.0         0.0
080431  6 41    0  0  46.039993  0.0668100   943.14258   0.0          0.0         0.0
080441 13 42    0  0  46.039993  0.0668100   929.59995   0.0          0.0         0.0
080451 15 43    0  0  67.399994  0.0668100   924.79980   0.0          0.0         0.0
080461 43 44    0  0  67.399994  0.0668100   923.79492   0.0          0.0         0.0
080471 16 45    0  0  67.399994  0.0668100   924.08276   0.0          0.0         0.0
080481 19 46    0  0  46.039993  0.0668100   924.39961   0.0          0.0         0.0
080491 46 47    0  0  46.039993  0.0668100   924.39951   0.0          0.0         0.0
080501 56 57    0  0  46.039993  0.2920300   933.22046   0.0          0.0         0.0
080511 57 24    0  0  46.039993  0.2920300   931.76733   0.0          0.0         0.0
080521 48 27    0  0  46.039993  0.1884200   921.76929   0.0          0.0         0.0
080531 49 28    0  0  46.039993  0.1420600   919.55249   0.0          0.439       0.0
080541 50 29    0  0  46.039993  0.0635180   923.27026   0.0          1.146       0.0
080551 51 30    0  0  46.039993  0.0635180   923.39331   0.0          0.623       0.0
080561 52 31    0  0  46.039993  0.0635180   924.79636   0.0          1.245       0.0
080571 53 32    0  0  46.039993  0.0635180   928.76440   0.0          0.584       0.0
080581 54 33    0  0  46.039993  0.0635180   930.76245   0.0          0.917       0.0
080591 55 56    0  0  46.039993  0.0580634   932.34727   0.0          0.600       0.0
080601 58 59    0  0  29.31    0.03475    935.4608   10.   0.    0.   *MEA SEC CONTROL  VALV
080611 59 60    0  0  29.31    0.06951    936.3608 10.   0.5   0.5
080621 60 61    0  0  29.31    0.06951    937.3539 10.   0.5   0.5
080631 61 62    0  0  29.31    0.06951    938.202 10.   0.5   0.5
080641 22  0    2  0   0.0       0.3135000   925.29932   0.0          0.0         0.0
080651  2  0    1  0   0.0       0.3135000   928.70972   0.0          0.0         0.0
0800 2  0  0  2   0 0.0       0.600    0 0 0.0       0
080022  0  0  2   0 0.0       0.600    0 0 0.0       0
080032  0  0  2   0 0.0       0.600    0 0 0.0       0
080042  0  0  2   0 0.0       0.600    0 0 0.0       0
080052  0  0  3   0 0.0       0.600    0 0 0.0       0
080062  0  0  3   0 0.0       0.600    0 0 0.0       0
080072  0  0  3   0 0.0       0.600    0 0 0.0       0
080082  0  0  3   0 0.0       0.600    0 0 0.0       0
080092  0  0  3   3 0.0       0.600    0 2 0.0       0
080102  0  0  3   0 0.0       0.600    0 3 0.0       0
080112  0  0  3   0 0.0       0.600    0 3 0.0       0
080122  0  0  3   0 0.0       0.600    0 1 0.0       0
080132  0  0  3   3 0.0       0.600    0 0 0.0       0
080142  0  0  3   0 0.0       0.600    0 0 0.0       0
080152  0  0  3   0 0.0       0.600    0 0 0.0       0
080162  0  0  3   0 0.0       0.600    0 0 0.0       0
080172  0  0  3   0 0.0       0.600    0 0 0.0       0
080182  0  0  3   0 0.0       0.600    0 0 0.0       0
080192  0  0  3   3 0.0       0.600    0 0 0.0       0
080202  0  0  3   3 0.0       0.600    0 0 0.0       0
080212  0  0  3   0 0.0       0.600    0 0 0.0       0
080222  0  0  2   0 0.0       0.600    0 0 0.0       0
080232  0  0  2   0 0.0       0.600    0 0 0.0       0
080242  0  0  2   0 0.0       0.600    0 0 0.0       0
080252  0  0  2   0 0.0       0.600    0 0 0.0       0
080262  0  0  2   0 0.0       0.600    0 0 0.0       0
```

```
080272  0  0  3  0 0.0       0.0       0  0  0.0
080282  0  0  3  0 0.0       0.0       0  0  0.0
080292  0  0  3  0 0.0       0.0       0  0  0.0
080302  0  0  3  0 0.0       0.0       0  0  0.0
080312  0  0  3  0 0.0       0.0       0  0  0.0
080322  0  0  3  0 0.0       0.0       0  0  0.0
080332  0  0  3  0 0.0       0.0       0  0  0.0
080342  0  0  3  0 0.0       0.0       0  0  0.0
080352  0  0  3  0 0.0       0.0       0  0  0.0
080362  0  0  3  0 0.0       0.0       0  0  0.0
080372  0  0  3  0 0.0       0.0       0  0  0.0
080382  0  0  3  0 0.0       0.600
080392  0  0  3  0 0.0       0.600     0  0  0.0
080402  0  0  3  0 0.0       0.600     0  0  0.0
080412  0  0  3  0 0.0       0.600     0  0  0.0
080422  0  0  3  0 0.0       0.600     0  0  0.0
080432  0  0  3  0 0.0       0.600     0  0  0.0
080442  0  0  3  0 0.0       0.600     0  0  0.0
080452  0  0  3  0 0.0       0.600     0  0  0.0
080462  0  0  3  0 0.0       0.600     0  0  0.0
080472  0  0  3  0 0.0       0.600     0  0  0.0
080482  0  0  3  0 0.0       0.600     0  0  0.0
080492  0  0  3  0 0.0       0.600     0  0  0.0
080502  0  0  3  0 0.0       0.0       0  0  0.0
080512  0  0  3  0 0.0       0.0       0  0  0.0
080522  0  0  3  0 0.0       0.0       0  0  1.0
080532  0  0  2  0 0.0       0.0       0  0  1.0
080542  0  0  2  0 0.0       0.0       0  0  0.0
080552  0  0  2  0 0.0       0.0       0  0  0.0
080562  0  0  2  0 0.0       0.0       0  0  0.0
080572  0  0  2  0 0.0       0.0       0  0  0.0
080582  0  0  2  0 0.0       0.0       0  0  0.0
080592  0  0  2  0 0.0       0.0       0  0  0.0
080602  0  0  0  3  0.  1.0  0 2
080612  0  0  0  3  0.  1.0  0 3
080622  0  0  0  3  0.  1.0  0 3
080632  0  0  0  3  0.  1.0  0 1
080642  0  5  3  0 0.0       1.000  11 0 0.0       0
080652  0  5  3  0 0.0       1.000  11 3 0.0       0
*
* HF-HEM CRITICAL FLOW MODEL DIALS
*
082003   .9 .8 .8 .01
*
* PUMP DATA CARDS
*
090011  3 3 0 0 0.3580. 1. 640. 1980.0 572. 90.80 47.10
090012  0.000    0.0  00.000  0.000   0.00
*
* PUMP CURVE INPUT INDICATOR
*
100000  0  0  0  0
*
* PUMP CURVES
*
103011  1  1  5   0.0      1.1357   0.2947   1.1353   0.5694   1.3944   *    V/A.LT.1
103012              0.8541   1.0427   1.0      1.0                       *    HEAD V/A
103021  1  2  7  0.      0.0      0.524    0.1135   0.562    0.1753   *    A/V.LT.1
103022              0.689    0.3769   0.7324   0.4127   0.8781 0.7324 *    HEAD A/V
103023              1.       1.
103031  2  1  5   0.0      0.59     0.2857   0.738    0.5714   0.826    *    V/A.LT.1
103032              0.8571   0.944    1.0      1.0                       *    TORQ V/A
103041  2  2  8   0.      -0.2      0.359    0.25     0.437    0.2933   *    A/V.LT.1
103042              0.5      0.3538   0.593    0.4415   0.67     0.529    *    TORQ A/V
103043              0.875    0.8128   1.       1.                        *    TORQ A/V
103051 1 3 3 -1.0 2.0 -0.3 1.15 0.0 1.1357
103061 2 3 4 -1.0 1.0 -0.7 0.60 -.3 0.5 0.0 0.59
*
* LEAK JUNCTION CARDS:
*
120100  2  2  14.7  0.0  .6  210.  .5
120200  2  2  14.7  0.0  .4  210.  .4
*
* KINETIC CONSTANTS CARD
*
140000  0  0  0.  0.
*
* SCRAM POWER CARD
*
141001  -4  2  0.  1.0  1.965  1.0  2.925  0.  210.  0.
*
* SLAB CARDS
*
150011  0 29  1 0 0  2  2  0.0        8.1202497 0.07138997 0.0        0.03766000
150021  0 51  8 0 0  2  2  0.0        6.0901599 0.05354000 0.0        0.03766000
150031  0 30  9 0 0  2  2  0.0        4.7368097 0.04164000 0.0        0.03766000
150041  0 52  6 0 0  2  2  0.0        5.4134998 0.04759000 0.0        0.03766000
150051  0 31  7 0 0  2  2  0.0       16.2404938 0.14276699 0.0        0.03766000
150061  0 53 10 0 0  2  2  0.0        5.4134998 0.04759000 0.0        0.03766000
150071  0 32 11 0 0  2  2  0.0        4.7368097 0.04164000 0.0        0.03766000
150081  0 54 12 0 0  2  2  0.0        6.0901599 0.05354000 0.0        0.03766000
150091  0 33 13 0 0  2  2  0.0        8.1202497 0.07138997 0.0        0.03766000
150101  0 55 13 0 0  2  2  0.0        3.7217798 0.03272000 0.0        0.02626900
```

```
150111 56  2  3 0 0  2  2  0.5771500  0.0        0.05359000 0.0        0.0
150121 57  0  3 0 0  2  2  1.1540959  0.0        0.10712999 0.0        0.0
150131 34  0  3 0 0  2  2  2.4387693  0.0        0.22638994 0.0        0.0
150141 35  2  4 0 0  2  2  3.2099996  0.0        0.15299998 0.0        0.0
150151  1  0  4 0 0  2  2  2.7500000  0.0        0.13089997 0.0        0.0
150161 23  1  4 0 0  2  2  2.7500000  0.0        0.13089997 0.0        0.0
150171 24  1  4 0 0  2  2  2.3339966  0.0        0.11109996 0.0        0.0
150181 25  2  2 0 0  2  2 11.5019291  0.0        1.06904772 0.0        0.0
150191 26  2  2 0 0  2  2  6.9722391  0.0         .63815156 0.0        0.0
150201 48  2  2 0 0  2  2  6.9722391  0.0         .63815156 0.0        0.0
150211 27  2  2 0 0  2  2  3.4361191  0.0         .31909141 0.0        0.0
150221 49  2  3 0 0  2  2  1.5524893  0.0        0.52225399 0.0        0.0
150231  0 28  1 0 0  2  2  0.0        0.9022530  0.00793000 0.0        0.0
150241  0 50  1 0 0  2  2  0.0        3.8312191  0.03421000 0.0        0.03766000
150251 29 27  5 0 0  2  2  2.0000000  2.8750030  0.17707998 0.03766000 0.17912894
150261 51 48  5 0 0  2  2  1.5000000  2.1562500  0.13281000 0.03766000 0.17912894
150271 30 48  5 0 0  2  2  1.1666699  1.6770792  0.10329998 0.03766000 0.17912894
150281 52 48  5 0 0  2  2  1.3332956  1.9166699  0.11805999 0.03766000 0.17912894
150291 31 26  5 0 0  2  2  4.0000000  5.7500000  0.35416996 0.03766000 0.17912894
150301 53 25  5 0 0  2  2  1.3332996  1.9166698  0.11805999 0.03766000 0.17912894
150311 32 25  5 0 0  2  2  1.1666658  1.6770792  0.10329998 0.03766000 0.17912894
150321 54 25  5 0 0  2  2  1.5000000  2.1562500  0.13281000 0.03766000 0.17912894
150331 33 25  5 0 0  2  2  2.0000000  2.8750030  0.17707998 0.03766000 0.17912894
150341 55 25  5 0 0  2  2  0.9166700  1.3177999  0.08115995 0.03766000 0.17912894
150351 50 49  5 0 0  2  2  0.9584000  1.3776999  0.08485997 0.03766000 0.17912894
150361 28  0  3 0 0  2  2  0.9732700  0.0        1.84527995 0.0        0.0
150371 36  0 14 0 0  2  2 34.0312958  0.0        3.53230000 0.0        0.0
150381  8 61 15  0  0  2  2  30.016   41.637   0.14531    0.04392   0.
150391  9 62 15  0  0  2  2  30.016   41.637   0.14531    0.04392   0.
150401 10 59 15  0  0  2  2  30.016   41.637   0.14531    0.04392   0.
150012 0.0        0.0469300  0.0        0.0        0.0        0.0
150022 0.0        0.0469300  0.0        0.0        0.0        0.0
150032 0.0        0.0469300  0.0        0.0        0.0        0.0
150042 0.0        0.0469300  0.0        0.0        0.0        0.0
150052 0.0        0.0469300  0.0        0.0        0.0        0.0
150062 0.0        0.0469300  0.0        0.0        0.0        0.0
150072 0.0        0.0469300  0.0        0.0        0.0        0.0
150082 0.0        0.0469300  0.0        0.0        0.0        0.0
150092 0.0        0.0469300  0.0        0.0        0.0        0.0
150102 0.0        0.0        0.0        0.0        0.0        0.0
150112 0.0        0.0        0.0        0.0        0.0        0.0
150122 0.0        0.0        0.0        0.0        0.0        0.0
150132 0.0        0.0        0.0        0.0        0.0        0.0
150142 0.0        0.0        4.0000000  0.0        0.0        0.0
150152 0.0        0.0        3.0000000  0.0        0.0        0.0
150162 0.0        0.0        3.0000000  0.0        0.0        0.0
150172 0.0        0.0        2.5499999  0.0        0.0        0.0
150182 0.0        0.0        0.0        0.0        0.0        0.0
150192 0.0        0.0        0.0        0.0        0.0        0.0
150202 0.0        0.0        0.0        0.0        0.0        0.0
150212 0.0        0.0        0.0        0.0        0.0        0.0
150222 0.0        0.0        0.0        0.0        0.0        0.0
150232 0.0        0.0        0.0        0.0        0.0        0.0
150242 0.0        0.0        0.0        0.0        0.0        0.0
150252 0.0        0.0        0.0        0.0        0.0        0.0
150262 0.0        0.0        0.0        0.0        0.0        1.124000
150272 0.0        0.0        0.0        0.0        1.125000   1.999000
150282 0.0        0.0        0.0        0.0        2.000000   2.999000
150292 0.0        0.0        0.0        0.0        0.0        0.0
150302 0.0        0.0        0.0        0.0        0.0        0.999000
150312 0.0        0.0        0.0        0.0        1.000000   1.574000
150322 0.0        0.0        0.0        0.0        1.875000   2.999000
150332 0.0        0.0        0.0        0.0        3.000000   4.499000
150342 0.0        0.0        0.0        0.0        4.299999   5.000000
150352 0.0        0.0        0.0        0.0        0.0        0.0
150362 0.0        0.0        0.0        0.0        0.0        0.0
150372 0.0        0.0        0.0        0.0        0.0        0.0
150382  0.04392   0.   6.043   7.067   0.   0.93
150392  0.04392   0.   6.043   7.067   0.   0.89
150402  0.04392   0.   6.043   7.067   0.   0.93
*
* CORE CARDS
*
160010  1  5  8  9 0.0      0.0540350 0.0        0.0
160020  2  5  8  9 0.0      0.0570030 0.0        0.0
160030  3  5 12 13 0.0      0.0767930 0.0        0.0
160040  4  5 12 13 0.0      0.1089540 0.0        0.0
160050  5  5 12 13 0.0      0.4135399 0.0        0.0
160060  6  5 12 13 0.0      0.1041970 0.0        0.0
160070  7  5 12 13 0.0      0.0757070 0.0        0.0
160080  8  5  8  9 0.0      0.0557380 0.0        0.0
160090  9  5  8  9 0.0      0.0540330 0.0        0.0
*
* SLAB GEOMETRY CARDS
*
170101  2  6  3  2  0.          7.467E-03  0.
170102     0  1  1             1.783E-03  0.402283
170103     0  5  1             9.170E-04  0.597717
170104     0  4  3             4.167E-03  0.
170105 0 6 1 1.6667E-6  0.
170106 0 2 5 3.333E-3 0.
170201 2 3 2 4 .36458 .02777 0.
170202 0 2 4 .02777  0.
```

```
170203  0  2  4  .02777   0.
170301  2  3  2  4  .04375  .02778  0.
170302  0  2  4  .02778  0.
170303  0  2  4  .02778  0.
170401  2  2  2  3  .1459  .01666  0.
170402  0  2  1  .025  0.
170501  1  3  2  4  0.  .024306  0.
170502  0  2  4  .024306  0.
170503  0  2  4  .024306  0.
170601   2   6   3   2   0.          8.725E-03   0.
170602       0   1   2               1.442E-03   1.0
170603       0   4   3               4.167E-03   0.
170604  0  2  4  2.49975E-3  0.
170605  0  6  1  4.1842E-6  0.
170606  0  2  2  8.3325E-4  0.
170701   2   6   3   2   0.          9.067E-03   0.
170702       0   1   2               1.133E-03   1.
170703       0   4   3               4.167E-03   0.
170704  0  2  4  2.49975E-3  0.
170705  0  6  1  7.0042E-6  0.
170706  0  2  2  8.3325E-4  0.
170801   2   6   3   2   0.          7.925E-03   0.
170802       0   1   1               1.783E-03   0.573754
170803       0   5   1               4.580E-04   0.426246
170804       0   4   3               4.167E-03   0.
170805  0  6  1  1.6667E-6   0.
170806  0  2  5  3.333E-3  0.
170901   2   6   3   2   0.          8.408E-03   0.
17   02      0   1   2               1.758E-03   1.0
170903       0   4   3               4.167E-03   0.
170904  0  2  4  2.49975E-3  0.
170905  0  6  1  3.3175E-6  0.
170906  0  2  2  8.3325E-4  0.
171001   2   6   3   2   0.          8.725E-03   0.
171002       0   1   2               1.442E-03   1.0
171003       0   4   3               4.167E-03   0.
171004  0  2  4  2.49975E-3  0.
171005  0  6  1  6.1067E-6  0.
171006  0  2  2  8.3325E-4  0.
171101   2   6   3   2   0.          8.408E-03   0.
171102       0   1   2               1.758E-03   1.0
171103       0   4   3               4.167E-03   0.
171104  0  2  4  2.49975E-3  0.
171105  0  6  1  5.3042E-6  0.
171106  0  2  2  8.3325E-4  0.
171201   2   6   3   2   0.          7.925E-03   0.
171202       0   1   1               1.783E-03   0.573754
171203       0   5   1               4.580E-04   0.426246
171204       0   4   3               4.167E-03   0.
171205  0  6  1  4.1408E-6  0.
171206  0  2  5  3.333E-3  0.
171301   2   6   3   2   0.          7.467E-03   0.
171302       0   1   1               1.783E-03   0.402283
171303       0   5   1               5.170E-04   0.597717
171304       0   4   3               4.167E-03   0.
171305  0  6  1  3.100E-6   0.
171306  0  2  5  3.333E-3  0.
171401  2  3  2  4  .4375  .03125  0.
171402  0  2  4  .03125  0.
171403  0  2  4  .03125  0.
171501   2   1   2   4   0.02196   0.004083   0.
*
*    VOLUMETRIC HEAT CAPACITY  BTU/F-FT**3   MATERIAL 1 - INCONNEL
*
190101 20        0.      51.41        200.      57.434       300.      59.527   * INCONNEL
190102          400.     61.167        500.      62.476       600.      63.572   * INCONNEL
190103          700.     64.579        800.      65.612       900.      66.795   * INCONNEL
190104         1000.     68.247       1100.      70.088      1200.      72.439   * INCONNEL
190105         1300.     75.420       1400.      79.150      1500.      83.750   * INCONNEL
190106         1600.     89.341       1700.      96.042      1800.     103.973   * INCONNEL
190107         1900.    113.255       2000.     124.008                          * INCONNEL
*
*    THERMAL CONDUCTIVITY BTU/F-HR-F    MATERIAL 1 - INCONNEL
*
180101 20        0.      8.4294        200.      9.098       300.      9.495   **INCONNEL
180102          400.      9.930        500.     10.398       600.     10.996   * INCONNEL
180103          700.     11.420        800.     11.967       900.     12.532   * INCONNEL
180104         1000.     13.113       1100.     13.774      1200.     14.303   * INCONNEL
180105         1300.     14.906       1400.     15.509      1500.     16.109   * INCONNEL
180106         1600.     16.701       1700.     17.282      1800.     17.949   * INCONNEL
180107         1900.     18.357       2000.     19.022                          * INCONNEL
*
*    LINEAR EXPANSION COEFFICIENT   1/F   MATERIAL 1 - INCONNEL
*
*
*    VOLUMETRIC HEAT CAPACITY  BTU/F-FT**3   MATERIAL 2 - 316 SS
*
190201 20        0.      51.68        200.      56.923       300.      59.020   * 316-STST
190202          400.     60.846        500.      62.447       600.      63.965   * 316-STST
190203          700.     65.141        800.      66.308       900.      67.400   * 316-STST
190204         1000.     68.444       1100.      69.463      1200.      70.490   * 316-STST
190205         1300.     71.508       1400.      72.563      1500.      73.652   * 316-STST
190206         1600.     74.782       1700.      75.952      1800.      77.162   * 316-STST
190207         1900.     78.406       2000.      79.672                          * 316-STST
*
```

```
*   THERMAL CONDUCTIVITY BTU/FT-HR-F   MATERIAL 2 - 316 SS
*
190201 20        0.      7.2458      200.      8.225       300.      8.691   * 316-STST
190202          400.      9.144      500.      9.596       600.     10.020   * 316-STST
190203          700.     10.448      800.     10.872       900.     11.294   * 316-STST
190204         1000.     11.719     1100.     12.145      1200.     12.577   * 316-STST
190205         1300.     13.017     1400.     13.467      1500.     13.929   * 316-STST
190206         1600.     14.406     1700.     14.900      1800.     15.414   * 316-STST
190207         1900.     15.949     2000.     16.507                         * 316-STST
*
*   LINEAR EXPANSION COEFFICIENT   1/F   MATERIAL 2 - 316 SS
*
*
*   VOLUMETRIC HEAT CAPACITY  BTU/F-FT**3  MATERIAL 3 - MGO
*
190301 20 0. 47.5515 200. 52.2156 300. 54.2084 400. 55.9468 500. 57.4944
190302 600. 58.8512 700. 60.0384 800. 61.0349 900. 61.9040 1000. 62.6462
190303 1100. 63.2609 1150. 63.5364 1200. 63.7909 1250. 64.0240 1300. 64.2360
190304 1400. 64.5964 1500. 64.9144 1600. 65.1930 1700. 65.4444 1800. 65.9776
*
*   THERMAL CONDUCTIVITY BTU/FT-HR-F   MATERIAL 3 - MGO
*
190301 20 0. 8.4435 200. 6.4805 300. 5.7049 400. 5.2470 500. 4.4937
190302 600. 4.0325 700. 3.6523 800. 3.3423 900. 3.0930
190303 1000. 2.8959 1100. 2.7431 1200. 2.6281 1300. 2.5450
190304 1400. 2.4898 1500. 2.4559 1600. 2.4428 1700. 2.4428
190305 1800. 2.4429 1900. 2.4428 2000. 2.4428
*
*   LINEAR EXPANSION COEFFICIENT   1/F   MATERIAL 3 - MGO
*
*
*   VOLUMETRIC HEAT CAPACITY  BTU/F-FT**3  MATERIAL 4 - BN
*
190401 20        0.     20.98       200.     29.896       300.     33.012   *        BN
190402          400.     36.265      500.     39.178       600.     41.775   *        BN
190403          700.     44.078      800.     46.112       900.     47.900   *        BN
190404         1000.     49.466     1100.     50.834      1200.     52.026   *        BN
190405         1300.     53.067     1400.     53.980      1500.     54.789   *        BN
190406         1600.     55.517     1700.     56.188      1800.     56.926   *        BN
190407         1900.     57.453     2000.     58.094                         *        BN
*
*   THERMAL CONDUCTIVITY BTU/FT-HR-F   MATERIAL 4 - BN
*
190401  20    0.      21.0962  300.    18.6490  500.    17.0927  600.    16.3442
190402        700.    15.6197  750.    15.2654  800.    14.9186  850.    14.5788
190403        900.    14.2463  950.    13.9212  1000.   13.6040  1050.   13.2950
190404       1100.    12.9944  1150.   12.7025  1200.   12.4196  1300.   11.9821
190405       1400.    11.3844  1500.   10.9297  1700.   10.1531  2000.    9.3650
*
*   LINEAR EXPANSION COEFFICIENT   1/F   MATERIAL 4 - BN
*
*
*   VOLUMETRIC HEAT CAPACITY  BTU/F-FT**3  MATERIAL 5 - 70CU30NI
*
190501 20        0.     52.55       200.     55.512       300.     56.817   * 70CU30NI
190502          400.     58.032      500.     59.179       600.     60.280   * 70CU30NI
190503          700.     61.358      800.     62.435       900.     63.532   * 70CU30NI
190504         1000.     64.672     1100.     65.876      1200.     67.167   * 70CU30NI
190505         1300.     68.567     1400.     70.098      1500.     71.792   * 70CU30NI
190506         1600.     73.641     1700.     75.697      1800.     77.973   * 70CU30NI
190507         1900.     80.489     2000.     83.269                         * 70CU30NI
*
*   THERMAL CONDUCTIVITY BTU/FT-HR-F   MATERIAL 5 - 70CU30NI
*
190501 20        0.     16.802      200.     17.972       300.     19.314   * 70CU30NI
190502          400.     20.960     500.     22.833       600.     24.919   * 70CU30NI
190503          700.     27.261     800.     29.964       900.     33.193   * 70CU30NI
190504         1000.     37.174     1100.     42.190      1200.     48.589   * 70CU30NI
190505         1300.     56.774     1400.     67.212      1500.     80.429   * 70CU30NI
190506         1600.     97.010     1700.    117.602      1800.    142.911   * 70CU30NI
190507         1900.    173.704     2000.    210.807                         * 70CU30NI
*
*
*   LINEAR EXPANSION COEFFICIENT   1/F   MATERIAL 5 - 70CU30NI
*
*
*   VOLUMETRIC HEAT CAPACITY  BTU/F-FT**3  MATERIAL 6 - AIR IN GAP
*
190601 20  25. .01973    60. .01812    100. .01708    200. .01449
190602     300. .01258    400. .01111    500. .00995    600. .00901
190603     700. .00824    800. .00758    900. .00702   1000. .00654
190604    1100. .00612   1200. .00575   1300. .00543   1400. .00513
190605    1500. .00487   1600. .00463   1700. .00442   2000. .00388
*
*   THERMAL CONDUCTIVITY BTU/FT-HR-F   MATERIAL 6 - AIR IN GAP
*
180601 20  25. .01354    60. .0144688   100. .01516    200. .01732
180602     300. .01948    400. .02181    500. .02380    600. .02596
180603     700. .02812    800. .03028    900. .03244   1000. .03460
180604    1100. .03676   1200. .03892   1300. .04108   1400. .04324
180605    1500. .04540   1600. .04756   1700. .04972   2000. .05620
*
```

```
*   LINEAR EXPANSION COEFFICIENT   1/F  MATERIAL 6 - AIR IN GAP
*
*
* HEAT EXCHANGER CARDS
*
213101   2   4  18    0.0    0.1871  213.00  0.1871
*
```